Table 4.8 (Continued)

Survey No.	Film Positive No.	Time GMT	Altitude ft	Photo Scale in.:ft	Quality Rating	Remarks
242B	51	23:50:48	4775	1:54000	X	--
	52	23:50:57	4775	1:54000	X	--
	53	23:55:55	4800	1:55200	X	--
	54	23:56:04	4825	1:55200	X	--
	55	00:00:54	4825	1:55200	X	--
	56	00:01:03	4825	1:55200	X	--
	57	00:04:22	4800	1:55200	X	--
	58	00:04:32	4850	1:55200	X	--
243A	--	--	--	--	X	--
	2	16:02:29	1125	--	X	--
	3	18:03:12	1075	1:12000	M	Sediment plume
	4	18:03:20	1075	1:12000	H	Plume, *R/V Pelican*, tug and barge track
	5	18:10:20	4700	1:54000	M	Plume, *R/V Pelican*, tug and barge track
	6	18:10:29	4700	1:54000	M	Plume, *R/V Pelican*, tug and barge track
	7	18:16:02	5475	1:64800	H	Plume and *R/V Pelican*
	8	18:16:07	5450	1:64800	H	
	9	18:19:55	5600	1:66000	H	
	10	18:20:04	5600	1:66000	H	
	11	18:25:20	5600	1:66000	H	
	12	18:25:27	5600	1:66000	H	
	13	18:29:12	5600	1:66000	H	
	14	18:29:12	5600	1:66000	M	
	15	18:34:38	5575	1:66000	M	
	16	18:34:45	5575	1:66000	H	
	17	18:40:42	5600	1:66000	H	
	18	18:40:47	5600	1:66000	M	
	19	18:45:40	5675	1:66000	M	
	20	18:45:46	5675	1:66000	M	
	21	18:50:42	5625	1:66000	M	
	22	18:50:48	5625	1:66000	L	
	23	18:55:29	5675	1:66000	M	
	24	18:55:35	5675	1:66000	M	
	25	19:00:19	5650	1:66000	L	
	26	19:00:26	5650	1:66000	L	

(Continued)

Table 4.8 (Concluded)

Survey No.	Film Positive No.	Time GMT	Altitude ft	Photo Scale in.:ft	Quality Rating	Remarks
243A	27	19:04:58	5600	1:66000	M	Plume and *R/V Pelican*
	28	19:05:03	5600	1:66000	M	
	29	19:09:35	5600	1:66000	M	
	30	19:09:41	5600	1:66000	L	
	31	19:14:21	5575	1:66000	M	
	32	19:14:26	5575	1:66000	L	
	33	19:21:30	6125	1:72000	M	
	34	19:21:37	6125	1:72000	L	
	35	19:24:59	6150	1:72000	M	
	36	19:25:05	6150	1:72000	L	Sediment plume
	37	19:29:42	6200	1:72000	M	
	38	19:29:46	6200	1:72000	L	
	39	19:35:58	6600	1:78000	L	
	40	19:36:08	6600	1:78000	L	
	41	19:39:59	6625	1:78000	M	
	42	19:40:05	6625	1:78000	L	
	43	19:45:14	6625	1:78000	M	
	44	19:45:20	6625	1:78000	L	
	45	19:50:26	6650	1:78000	M	
	46	19:50:31	6625	1:78000	L	
	47	19:56:34	6600	1:78000	M	
	48	19:56:41	6600	1:78000	L	
	49	20:00:40	6675	1:78000	M	
	50	20:00:45	6650	1:78000	L	
	51	20:05:09	6675	1:78000	M	
	52	20:05:17	6675	1:78000	L	
	53	20:10:57	6700	1:78000	M	
	54	20:11:01	6700	1:78000	L	
	55	20:15:17	6625	1:78000	L	
	56	20:15:23	6625	1:78000	L	
	57	20:20:46	6625	1:78000	L	
	58	20:20:51	6625	1:78000	X	--

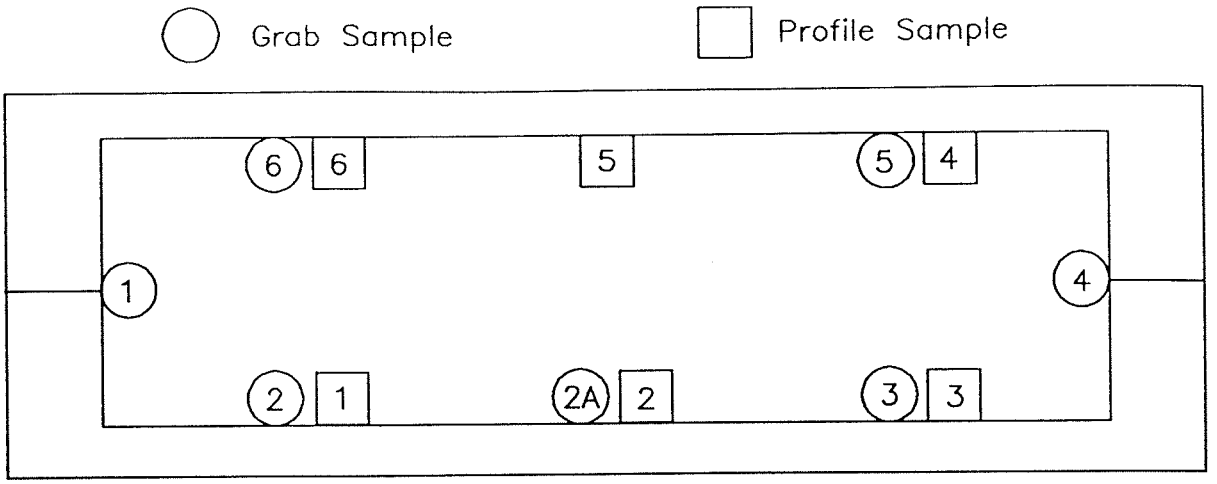

Figure 4.1. Locations of sediment grab samples and sediment profile samples. Numbers are used for sample identification.

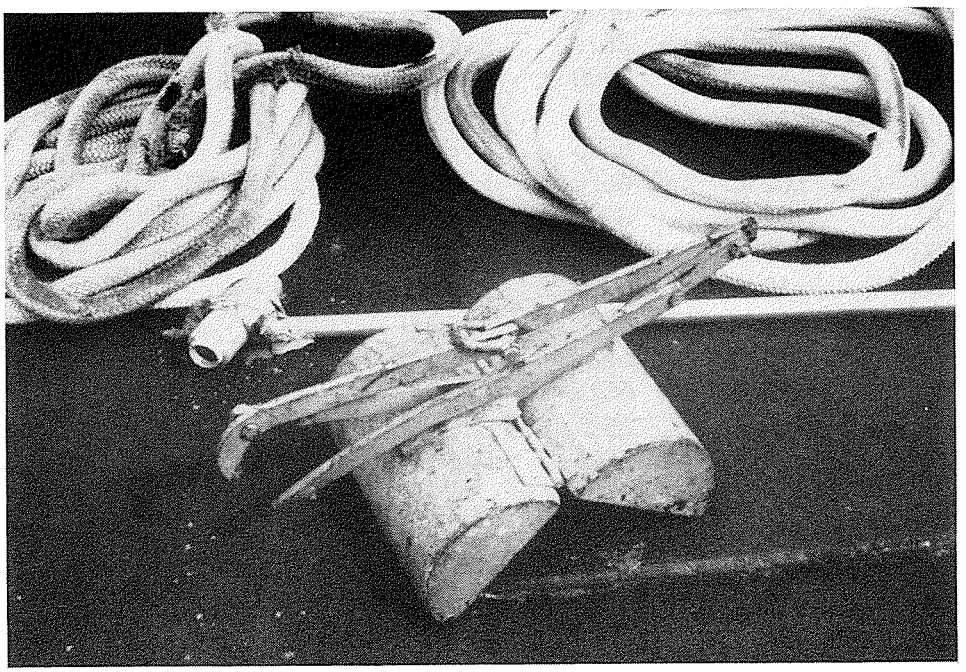

Figure 4.2. Clamshell grab sampler used to sample dredged material in the hopper barge.

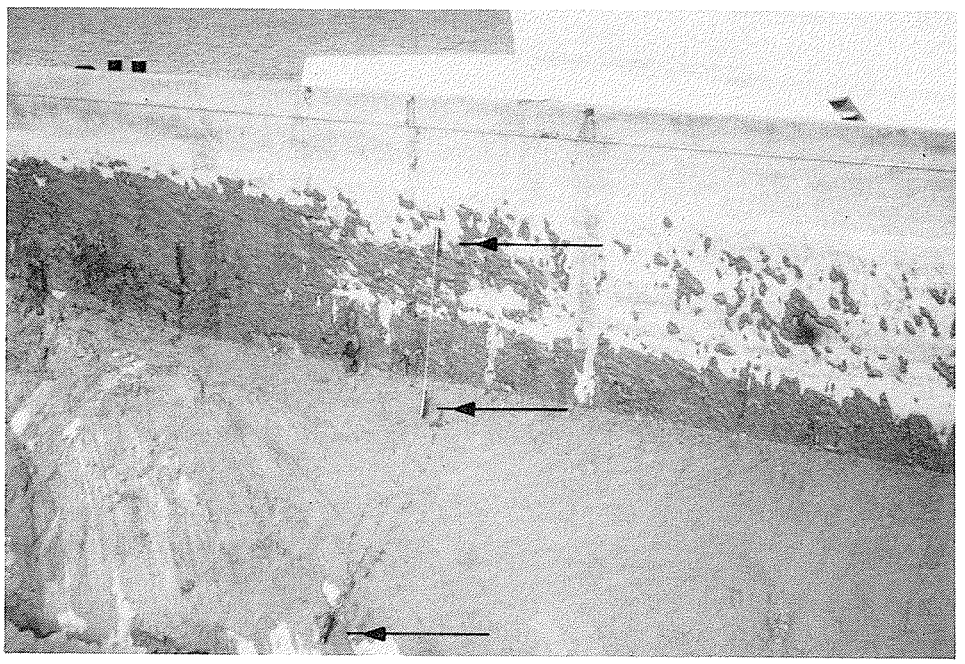

Figure 4.3. Sediment profile samplers used to collect representative sediment samples from the hopper barge. The plugs in the foreground were used to extrude the sample from the container.

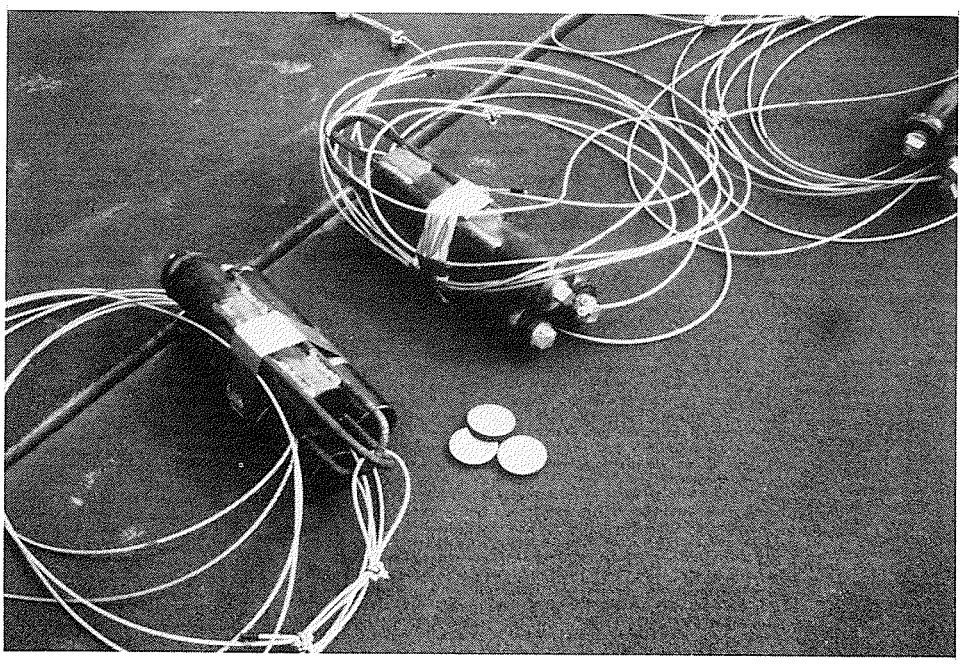

Figure 4.4. Sediment profile samplers positioned in hopper barge.

Appendix 4A: Depth Profiles of Temperature, Salinity, Sigma-Theta, Velocity of Sound, Light Transmission, and Brunt-Väisälä Frequency

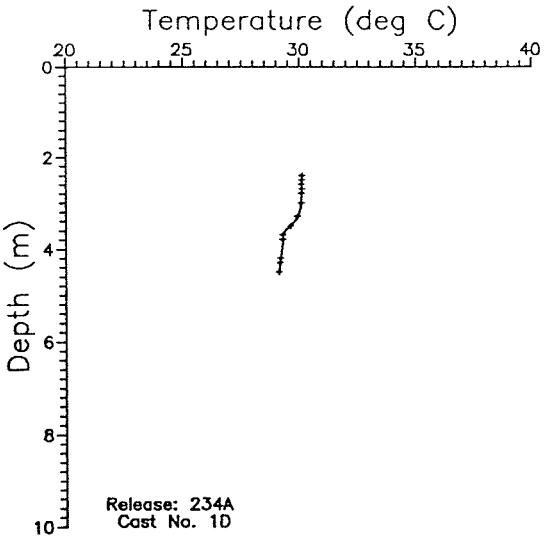
Temperature (deg C)
20
25
30
35
40
Depth (m)
0
2
4
6
8
10
Release: 234A
Cast No. 1D

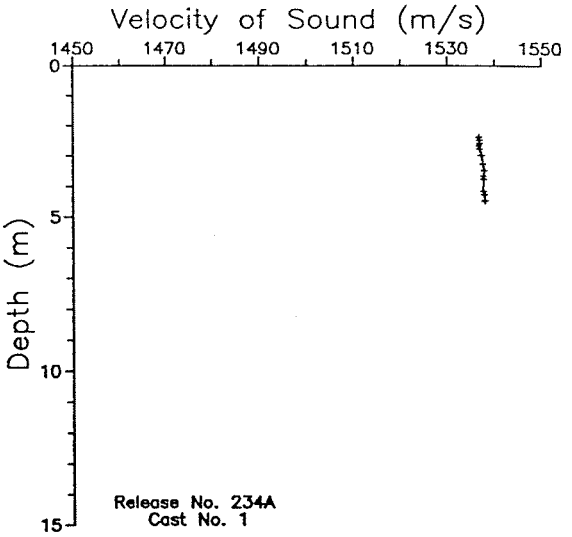
Velocity of Sound (m/s)
1450
1470
1490
1510
1530
1550
Depth (m)
0
5
10
15
Release No. 234A
Cast No. 1

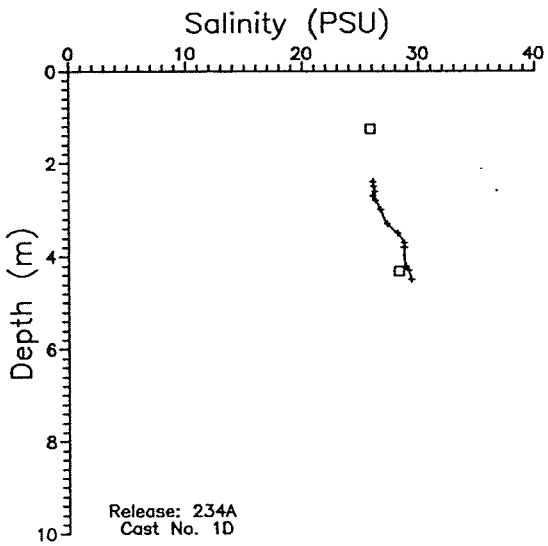
Salinity (PSU)
0
10
20
30
40
Depth (m)
0
2
4
6
8
10
Release: 234A
Cast No. 1D

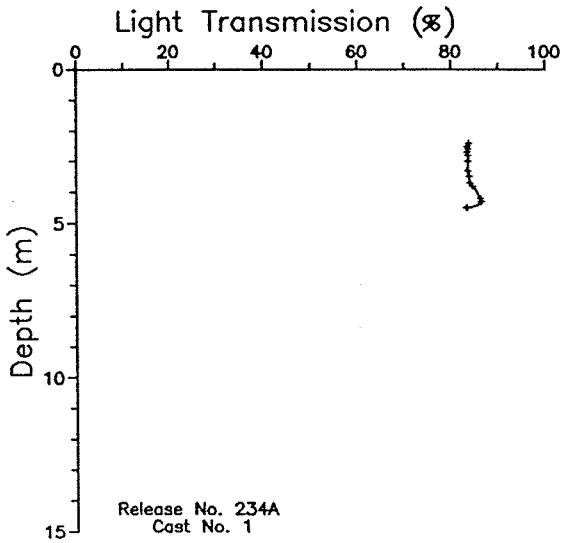
Light Transmission (%)
0
20
40
60
80
100
Depth (m)
0
5
10
15
Release No. 234A
Cast No. 1

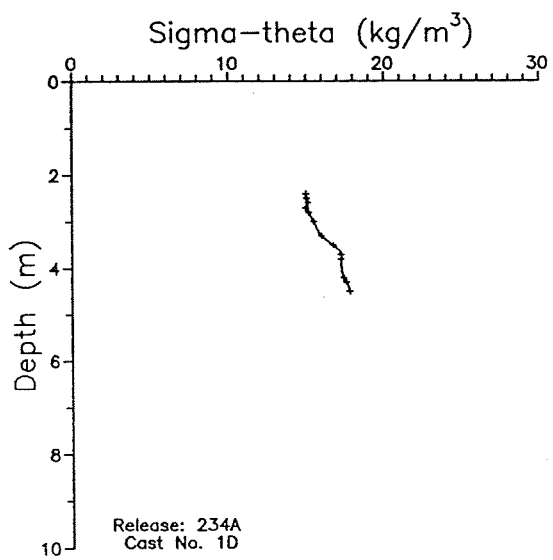
Sigma-theta (kg/m3)
0
10
20
30
Depth (m)
0
2
4
6
8
10
Release: 234A
Cast No. 1D

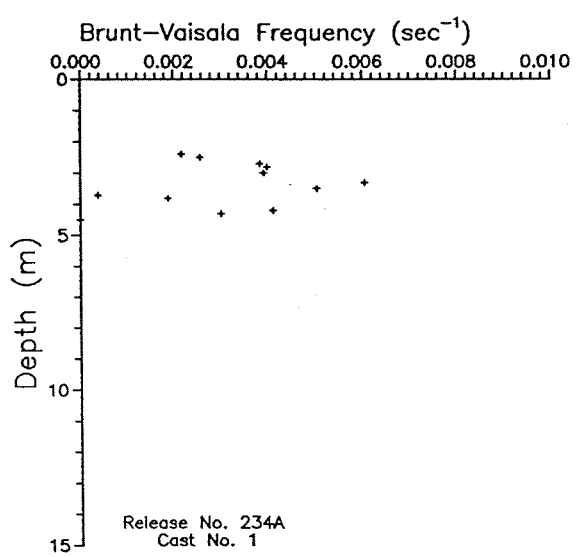
Brunt-Vaisala Frequency (sec-1)
0.000
0.002
0.004
0.006
0.008
0.010
Depth (m)
0
5
10
15
Release No. 234A
Cast No. 1

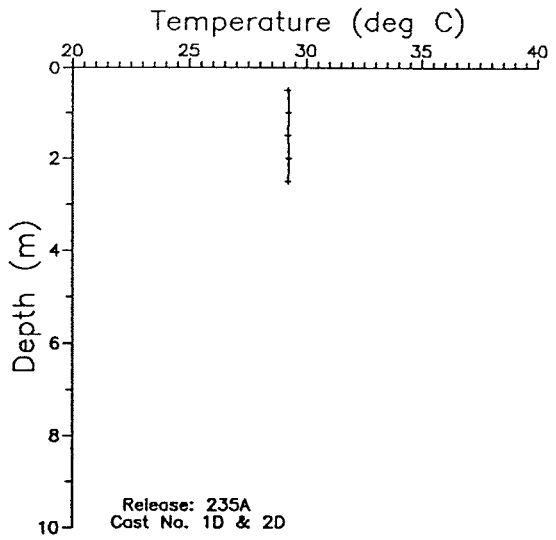
Temperature (deg C)
20
25
30
35
40
Depth (m)
0
2
4
6
8
10
Release: 235A
Cast No. 1D & 2D

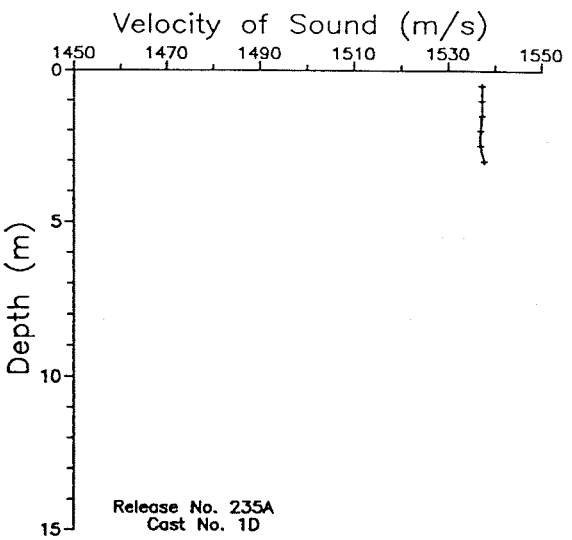
Velocity of Sound (m/s)
1450
1470
1490
1510
1530
1550
Depth (m)
0
5
10
15
Release No. 235A
Cast No. 1D

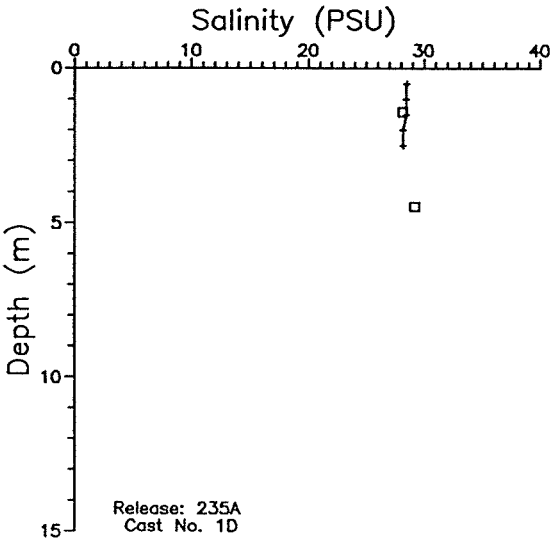
Salinity (PSU)
0
10
20
30
40
Depth (m)
0
5
10
15
Release: 235A
Cast No. 1D

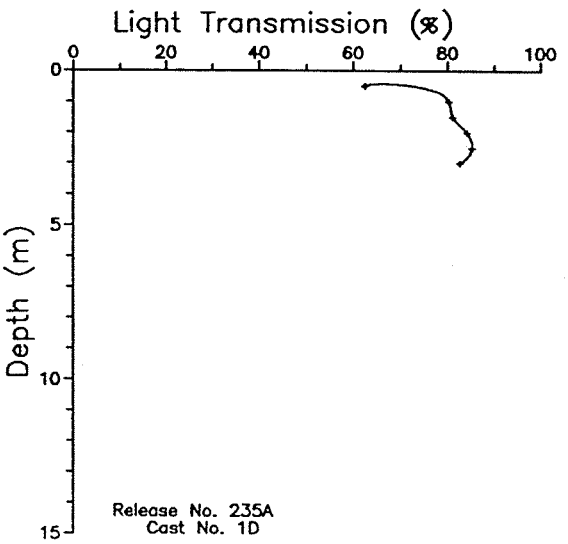
Light Transmission (%)
0
20
40
60
80
100
Depth (m)
0
5
10
15
Release No. 235A
Cast No. 1D

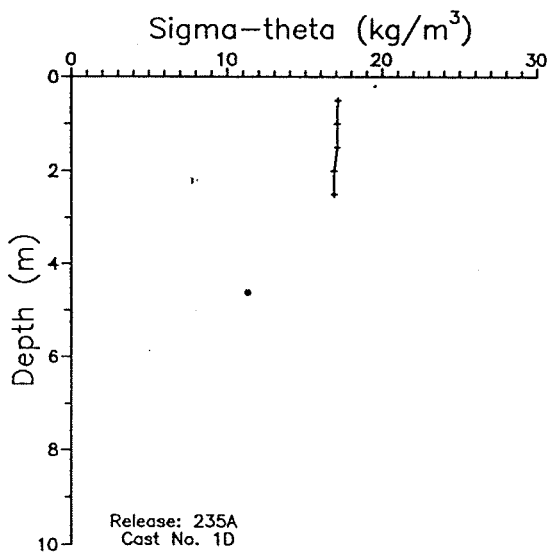
Sigma–theta (kg/m3)
0
10
20
30
Depth (m)
0
2
4
6
8
10
Release: 235A
Cast No. 1D

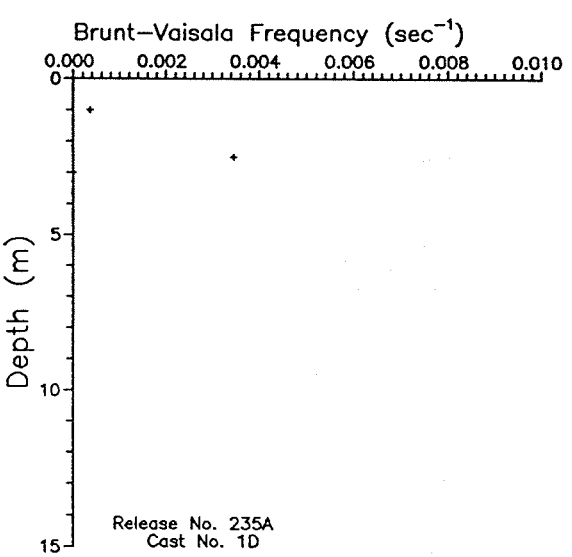
Brunt–Vaisala Frequency (sec-1)
0.000
0.002
0.004
0.006
0.008
0.010
Depth (m)
0
5
10
15
Release No. 235A
Cast No. 1D

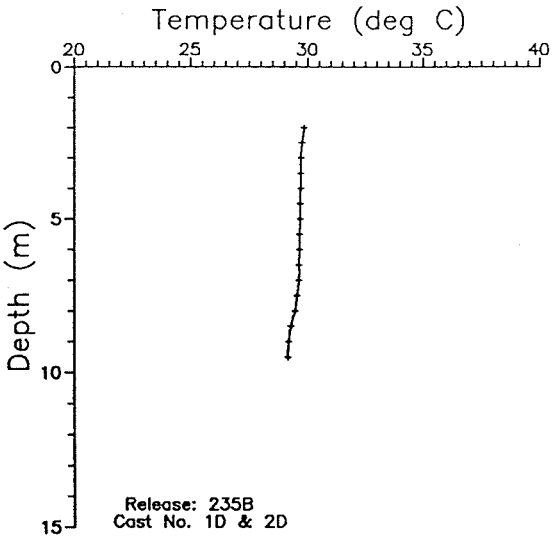
Temperature (deg C)
20
25
30
35
40
Depth (m)
0
5
10
15
Release: 235B
Cast No. 1D & 2D

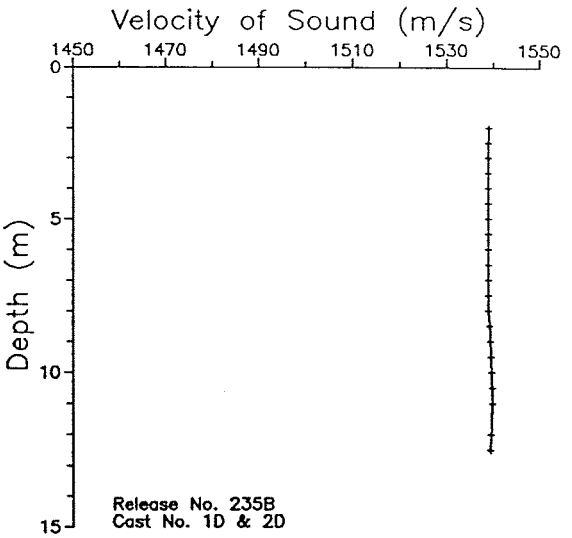
Velocity of Sound (m/s)
1450
1470
1490
1510
1530
1550
Depth (m)
0
5
10
15
Release No. 235B
Cast No. 1D & 2D

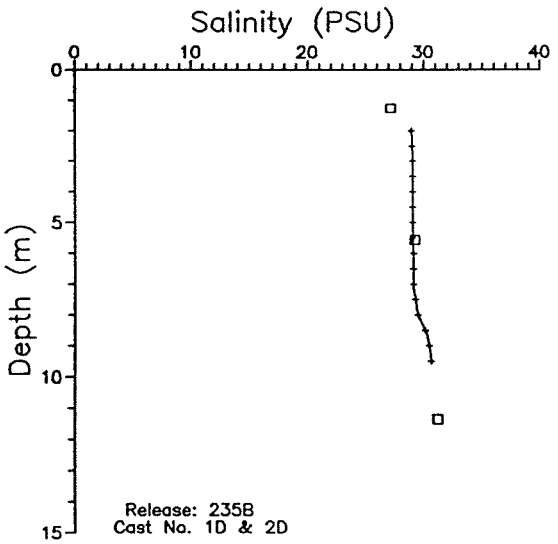
Salinity (PSU)
0
10
20
30
40
Depth (m)
0
5
10
15
Release: 235B
Cast No. 1D & 2D

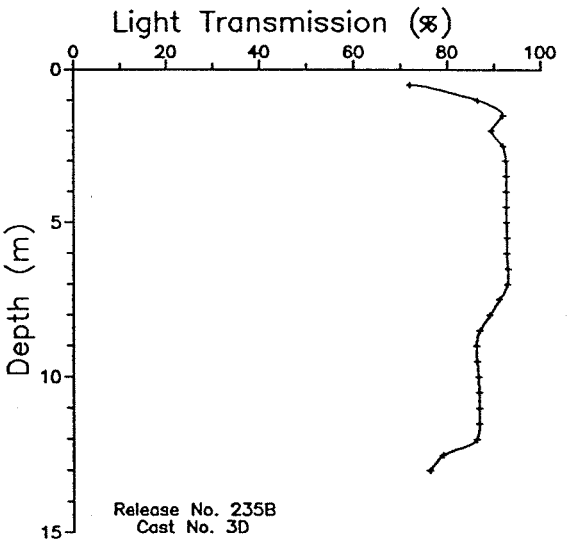
Light Transmission (%)
0
20
40
60
80
100
Depth (m)
0
5
10
15
Release No. 235B
Cast No. 3D

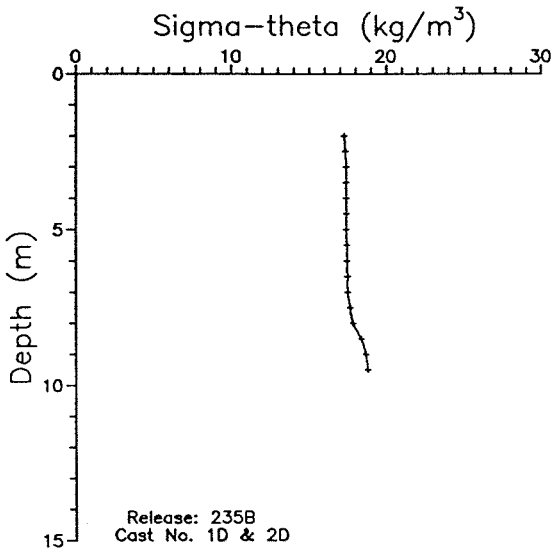
Sigma-theta (kg/m3)
0
10
20
30
Depth (m)
0
5
10
15
Release: 235B
Cast No. 1D & 2D

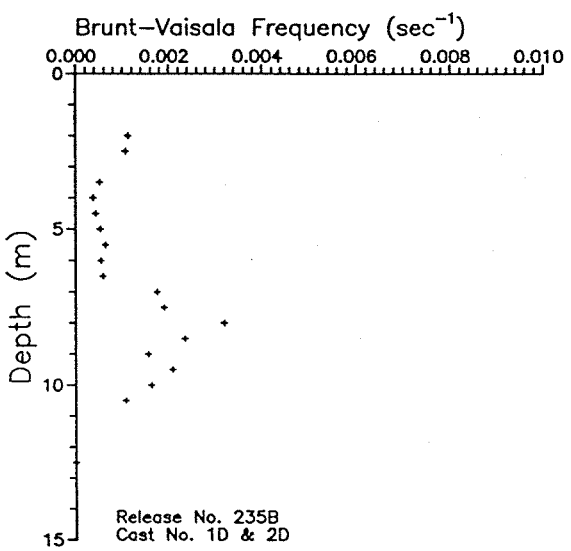
Brunt-Vaisala Frequency (sec-1)
0.000
0.002
0.004
0.006
0.008
0.010
Depth (m)
0
5
10
15
Release No. 235B
Cast No. 1D & 2D

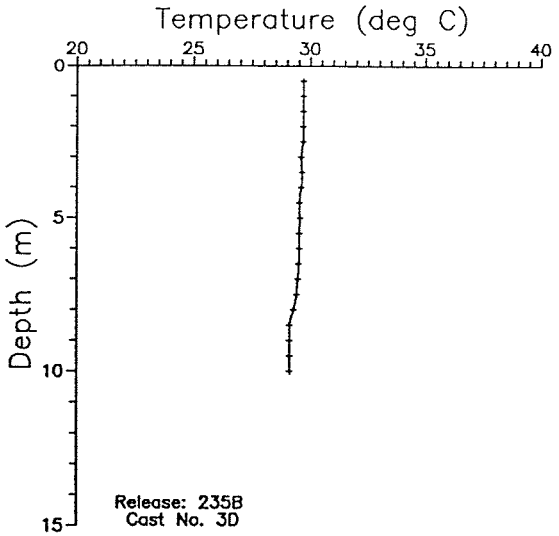
Temperature (deg C)
20
25
30
35
40
0
5
10
15
Depth (m)
Release: 235B
Cast No. 3D

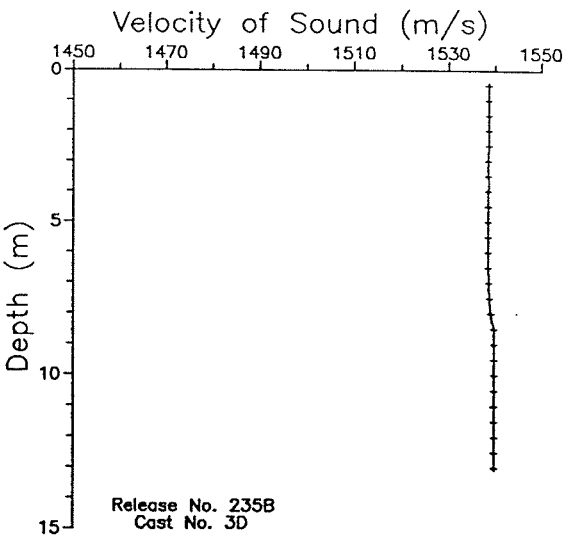
Velocity of Sound (m/s)
1450
1470
1490
1510
1530
1550
0
5
10
15
Depth (m)
Release No. 235B
Cast No. 3D

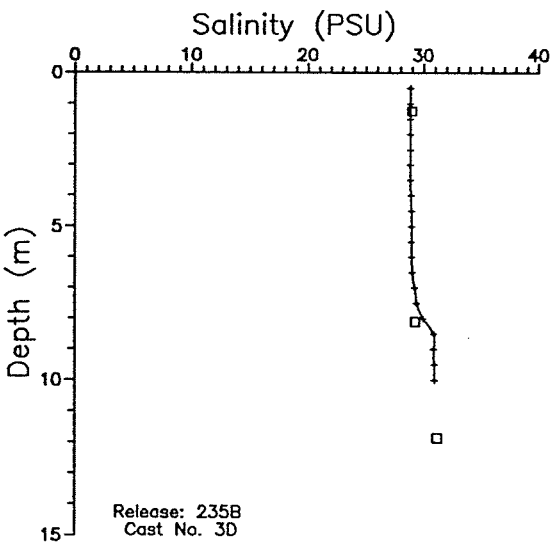
Salinity (PSU)
0
10
20
30
40
0
5
10
15
Depth (m)
Release: 235B
Cast No. 3D

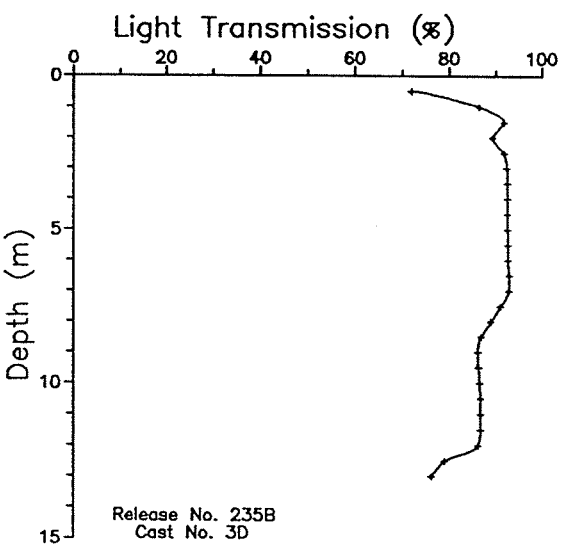
Light Transmission (%)
0
20
40
60
80
100
0
5
10
15
Depth (m)
Release No. 235B
Cast No. 3D

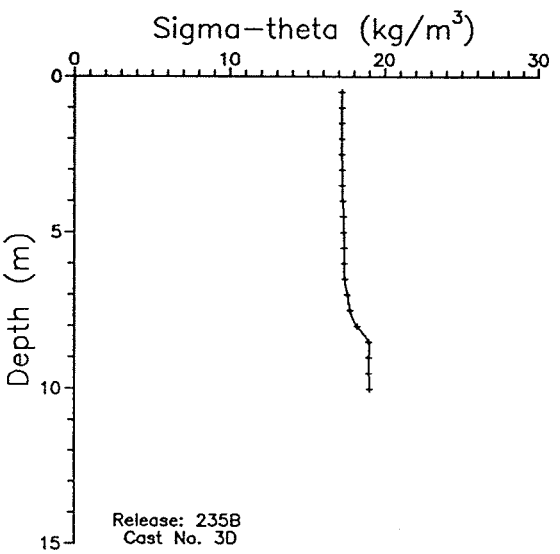
Sigma–theta (kg/m3)
0
10
20
30
0
5
10
15
Depth (m)
Release: 235B
Cast No. 3D

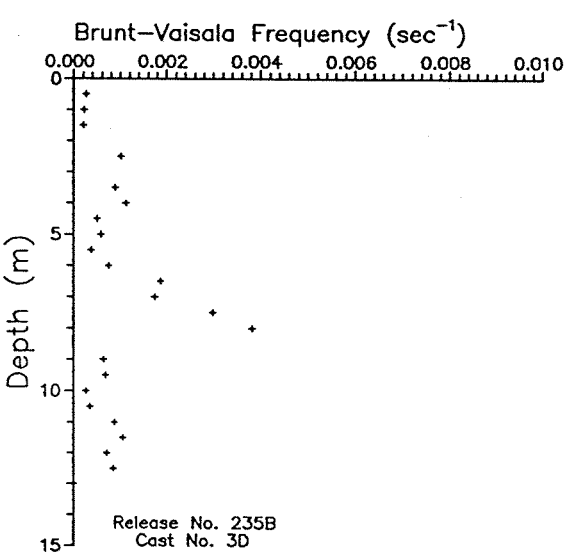
Brunt–Vaisala Frequency (sec-1)
0.000
0.002
0.004
0.006
0.008
0.010
0
5
10
15
Depth (m)
Release No. 235B
Cast No. 3D

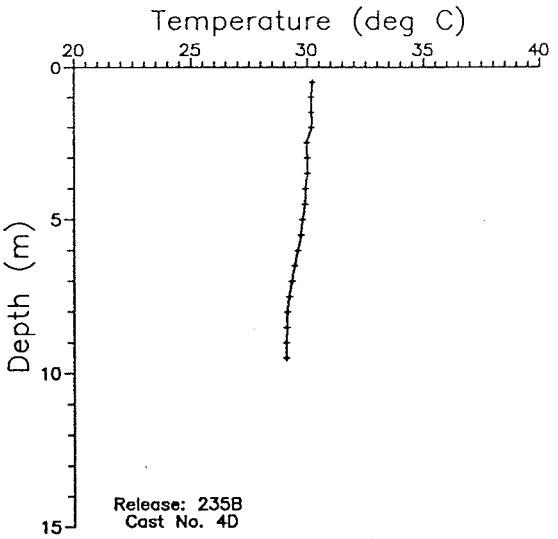
Temperature (deg C)
20
25
30
35
40
0
5
10
15
Depth (m)
Release: 235B
Cast No. 4D

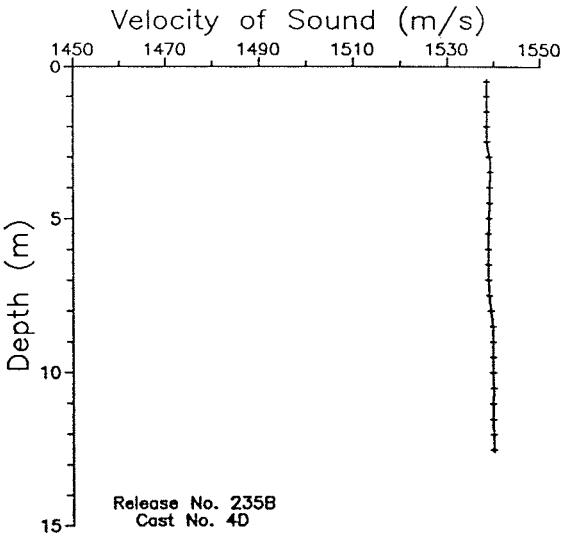
Velocity of Sound (m/s)
1450
1470
1490
1510
1530
1550
0
5
10
15
Depth (m)
Release No. 235B
Cast No. 4D

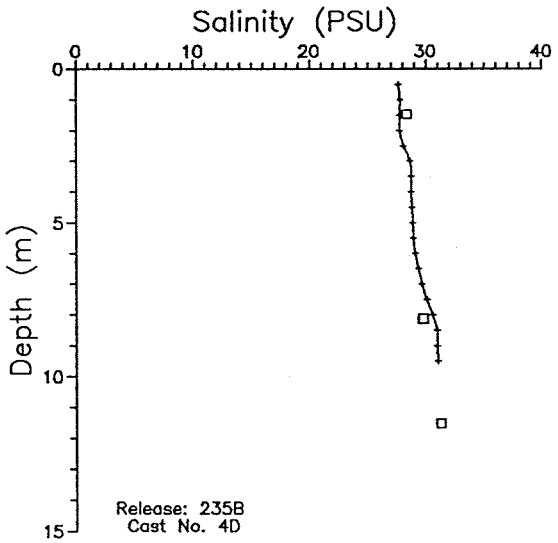
Salinity (PSU)
0
10
20
30
40
0
5
10
15
Depth (m)
Release: 235B
Cast No. 4D

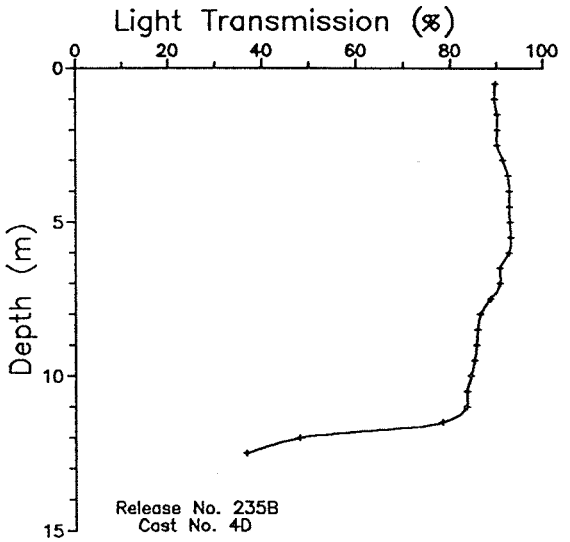
Light Transmission (%)
0
20
40
60
80
100
0
5
10
15
Depth (m)
Release No. 235B
Cast No. 4D

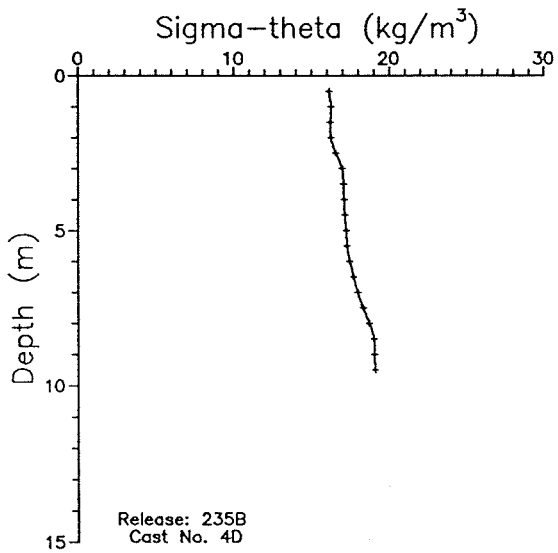
Sigma-theta (kg/m3)
0
10
20
30
0
5
10
15
Depth (m)
Release: 235B
Cast No. 4D

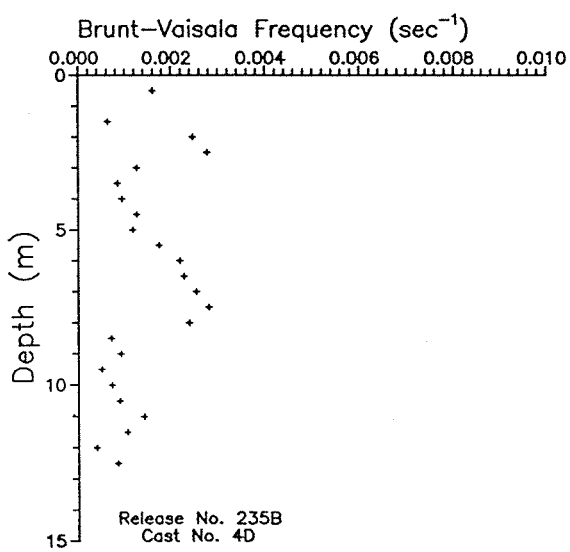
Brunt-Vaisala Frequency (sec-1)
0.000
0.002
0.004
0.006
0.008
0.010
0
5
10
15
Depth (m)
Release No. 235B
Cast No. 4D

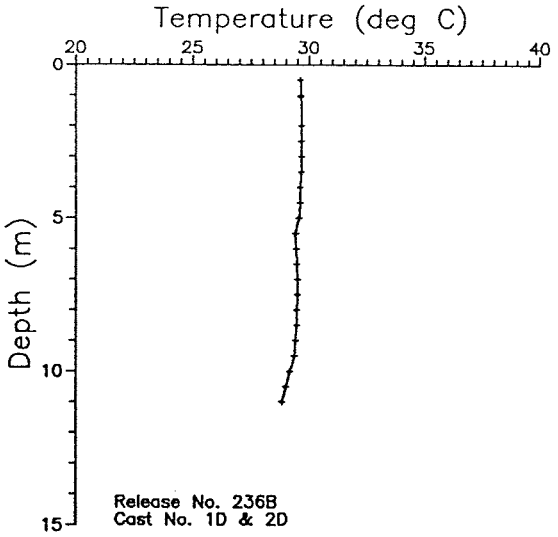
Temperature (deg C)
20
25
30
35
40
0
5
10
15
Depth (m)
Release No. 236B
Cast No. 1D & 2D

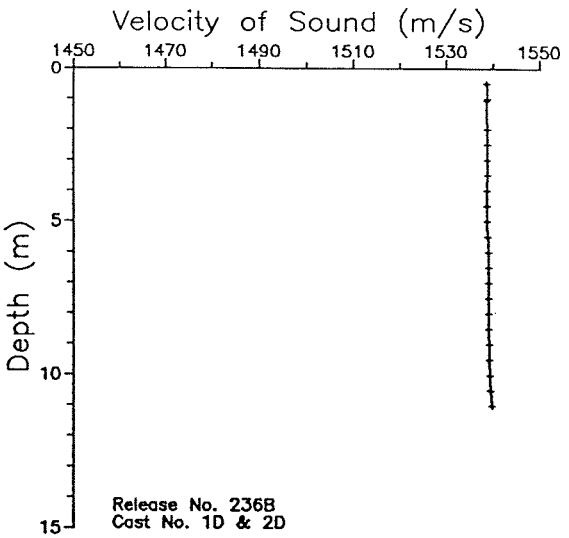
Velocity of Sound (m/s)
1450
1470
1490
1510
1530
1550
0
5
10
15
Depth (m)
Release No. 236B
Cast No. 1D & 2D

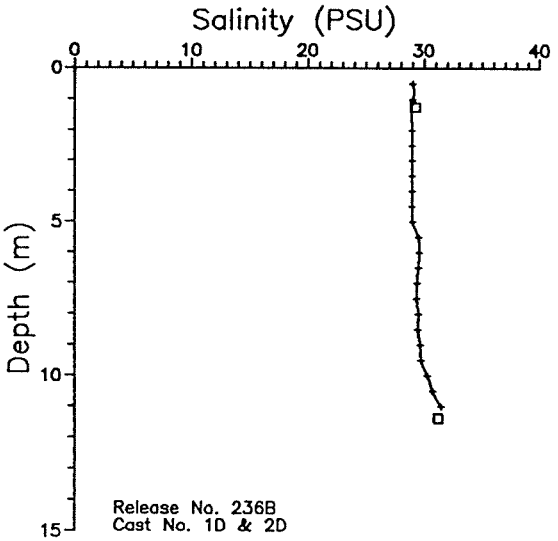
Salinity (PSU)
0
10
20
30
40
0
5
10
15
Depth (m)
Release No. 236B
Cast No. 1D & 2D

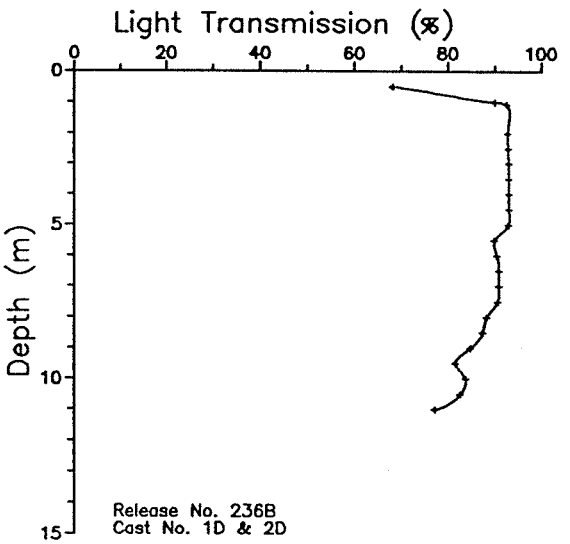
Light Transmission (%)
0
20
40
60
80
100
0
5
10
15
Depth (m)
Release No. 236B
Cast No. 1D & 2D

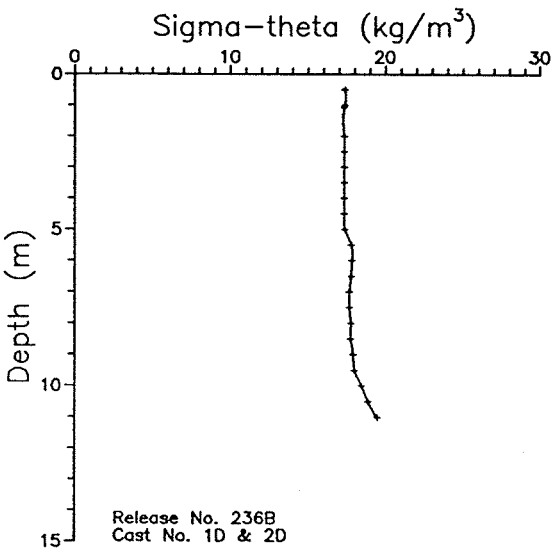
Sigma-theta (kg/m3)
0
10
20
30
0
5
10
15
Depth (m)
Release No. 236B
Cast No. 1D & 2D

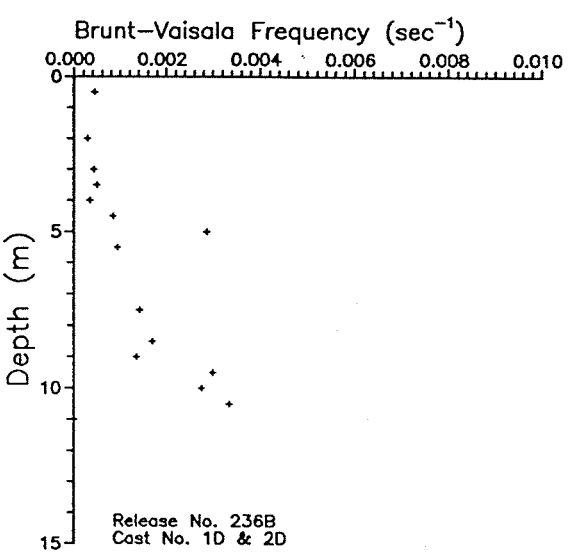
Brunt-Vaisala Frequency (sec-1)
0.000
0.002
0.004
0.006
0.008
0.010
0
5
10
15
Depth (m)
Release No. 236B
Cast No. 1D & 2D

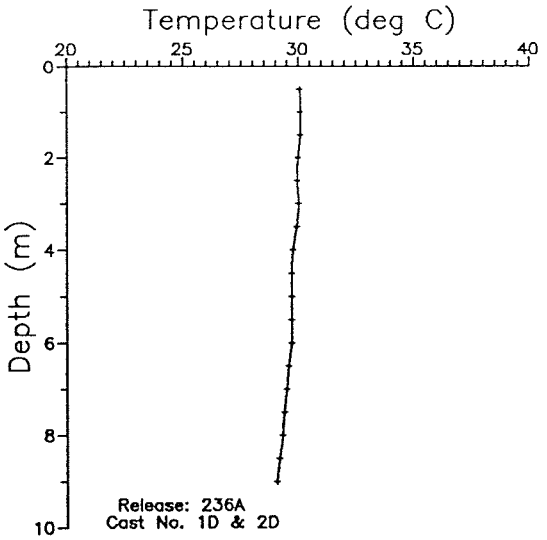
Temperature (deg C)
20
25
30
35
40
Depth (m)
0
2
4
6
8
10
Release: 236A
Cast No. 1D & 2D

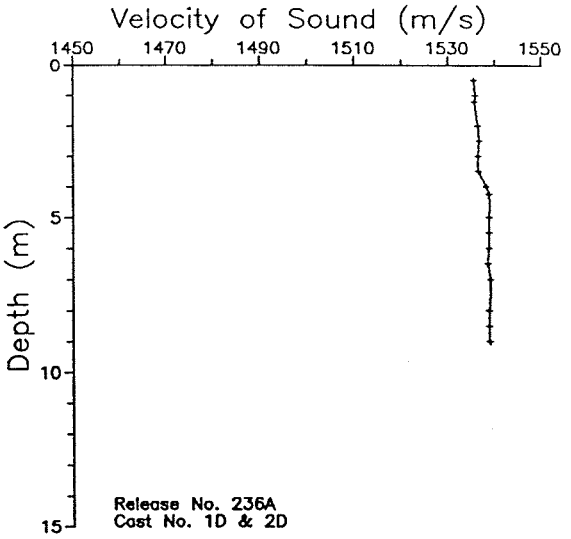
Velocity of Sound (m/s)
1450
1470
1490
1510
1530
1550
Depth (m)
0
5
10
15
Release No. 236A
Cast No. 1D & 2D

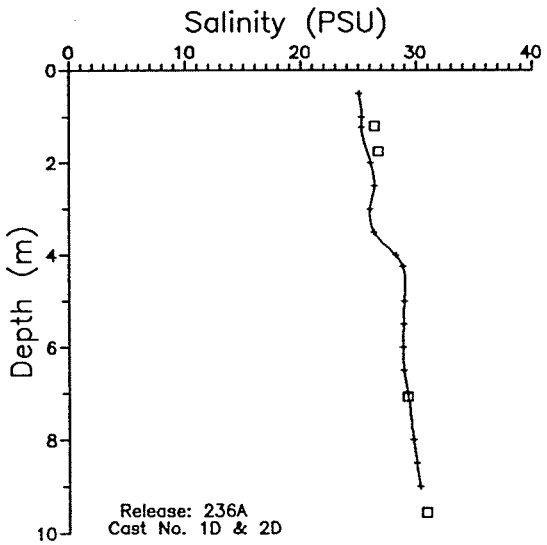
Salinity (PSU)
0
10
20
30
40
Depth (m)
0
2
4
6
8
10
Release: 236A
Cast No. 1D & 2D

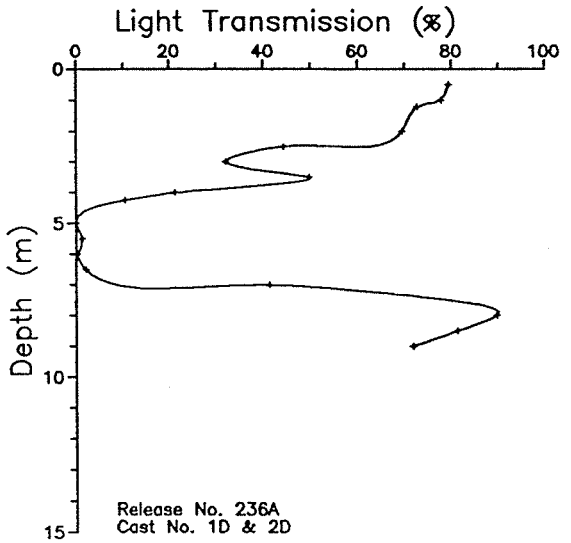
Light Transmission (%)
0
20
40
60
80
100
Depth (m)
0
5
10
15
Release No. 236A
Cast No. 1D & 2D

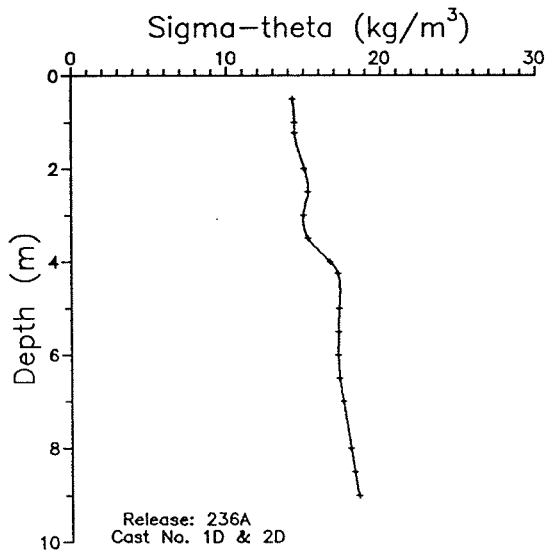
Sigma-theta (kg/m3)
0
10
20
30
Depth (m)
0
2
4
6
8
10
Release: 236A
Cast No. 1D & 2D

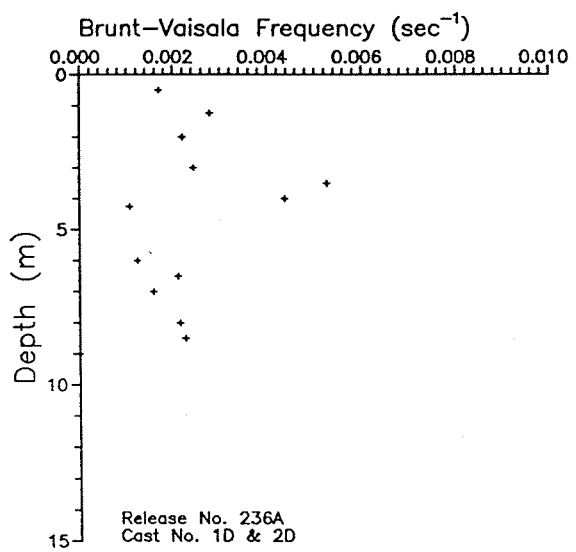
Brunt-Vaisala Frequency (sec-1)
0.000
0.002
0.004
0.006
0.008
0.010
Depth (m)
0
5
10
15
Release No. 236A
Cast No. 1D & 2D

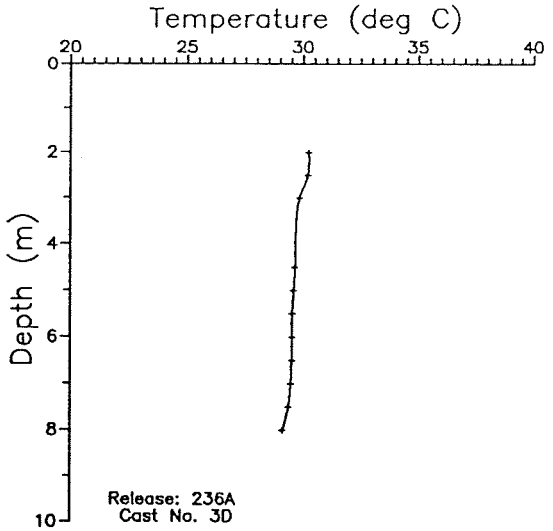
Temperature (deg C)
20
25
30
35
40
Depth (m)
0
2
4
6
8
10
Release: 236A
Cast No. 3D

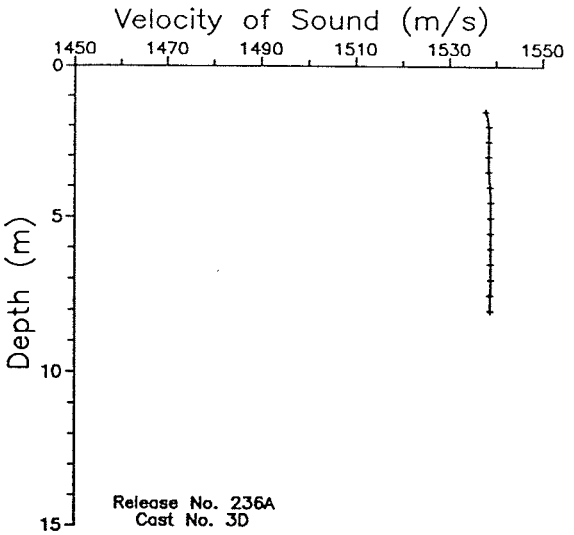
Velocity of Sound (m/s)
1450
1470
1490
1510
1530
1550
Depth (m)
0
5
10
15
Release No. 236A
Cast No. 3D

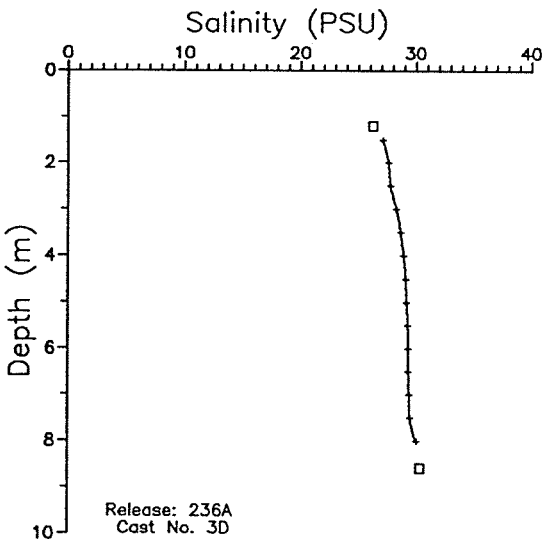
Salinity (PSU)
0
10
20
30
40
Depth (m)
0
2
4
6
8
10
Release: 236A
Cast No. 3D

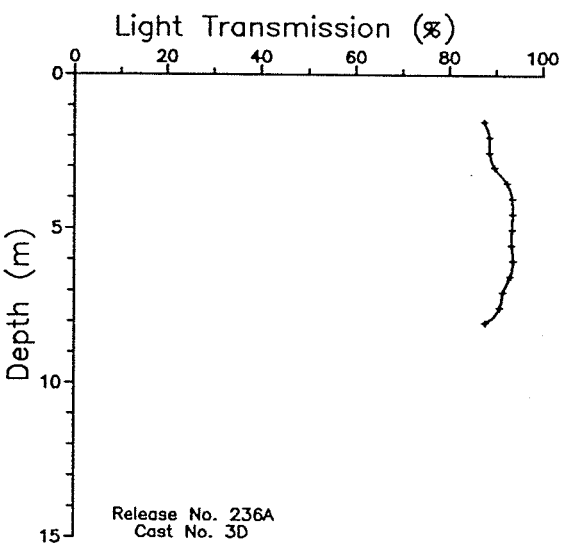
Light Transmission (%)
0
20
40
60
80
100
Depth (m)
0
5
10
15
Release No. 236A
Cast No. 3D

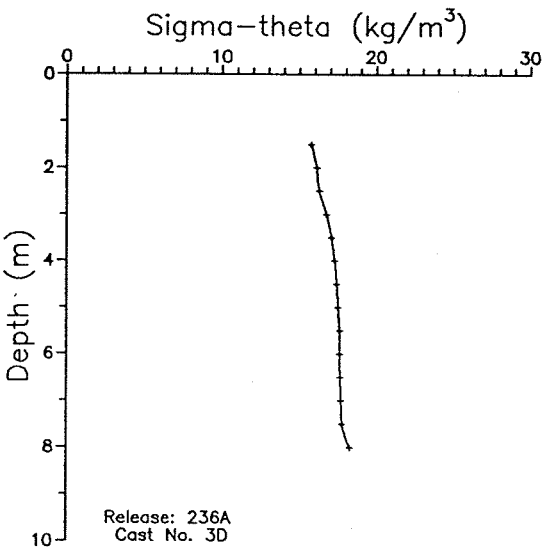
Sigma–theta (kg/m3)
0
10
20
30
Depth (m)
0
2
4
6
8
10
Release: 236A
Cast No. 3D

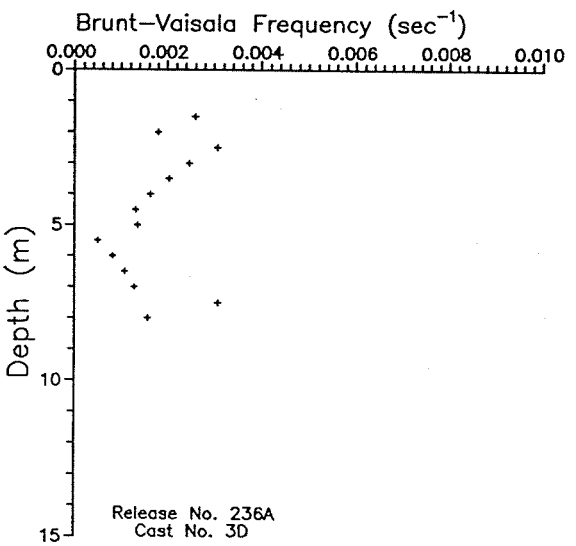
Brunt–Vaisala Frequency (sec-1)
0.000
0.002
0.004
0.006
0.008
0.010
Depth (m)
0
5
10
15
Release No. 236A
Cast No. 3D

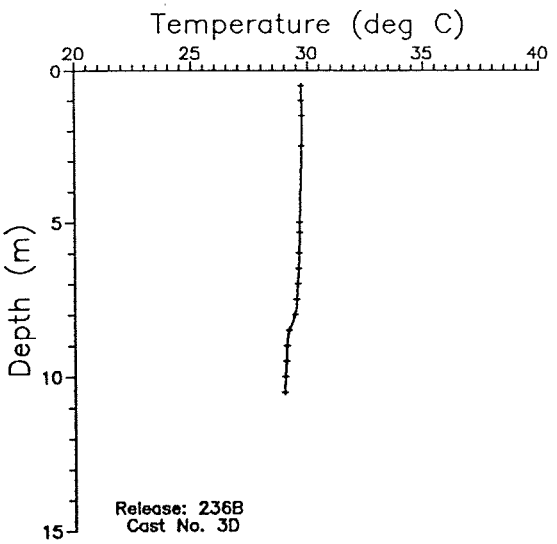
Temperature (deg C)
20
25
30
35
40
Depth (m)
0
5
10
15
Release: 236B
Cast No. 3D

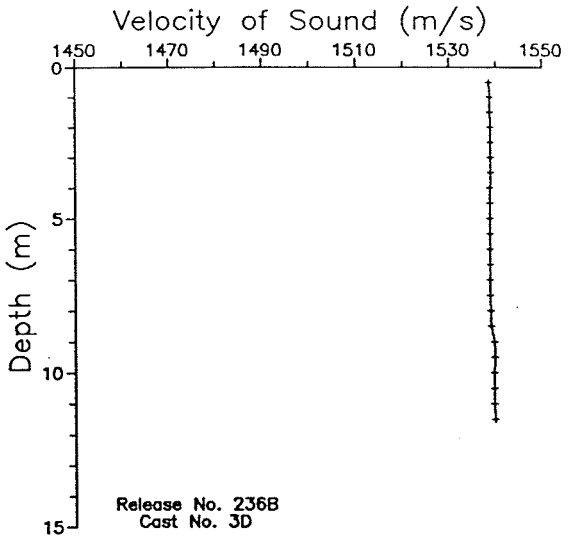
Velocity of Sound (m/s)
1450
1470
1490
1510
1530
1550
Depth (m)
0
5
10
15
Release No. 236B
Cast No. 3D

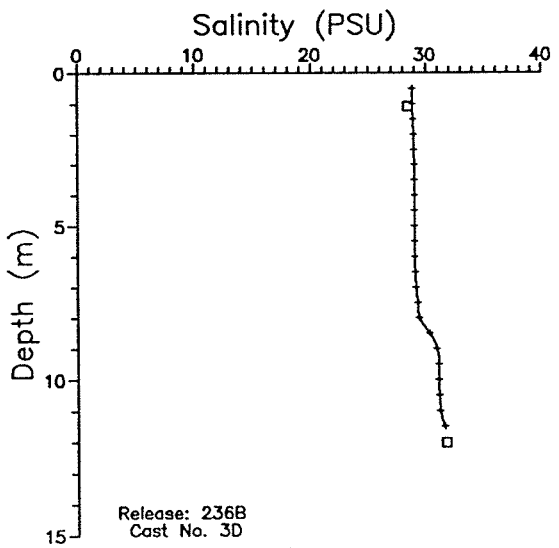
Salinity (PSU)
0
10
20
30
40
Depth (m)
0
5
10
15
Release: 236B
Cast No. 3D

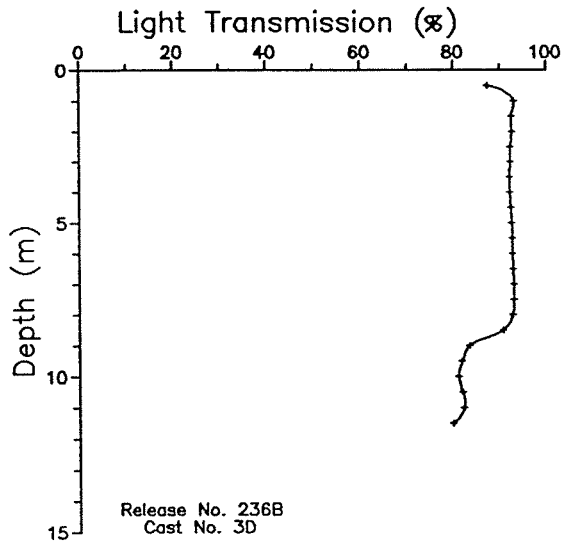
Light Transmission (%)
0
20
40
60
80
100
Depth (m)
0
5
10
15
Release No. 236B
Cast No. 3D

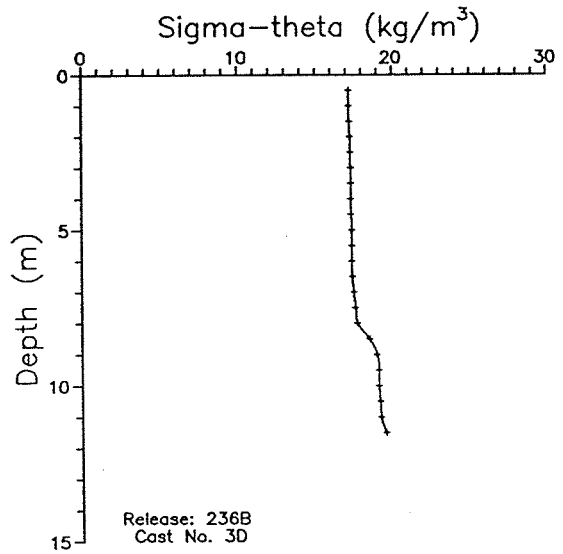
Sigma-theta (kg/m3)
0
10
20
30
Depth (m)
0
5
10
15
Release: 236B
Cast No. 3D

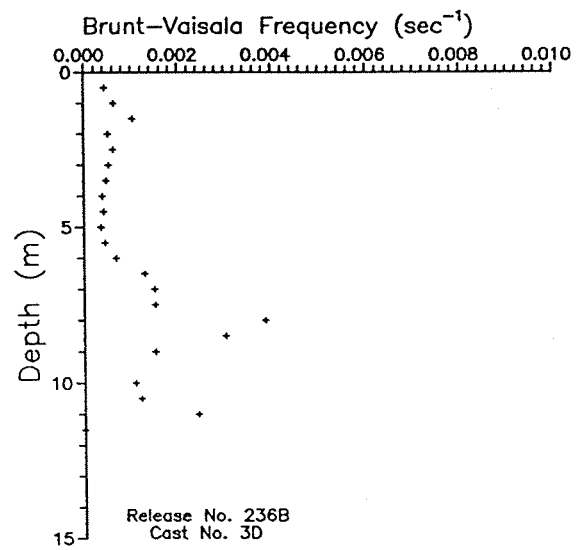
Brunt-Vaisala Frequency (sec-1)
0.000
0.002
0.004
0.006
0.008
0.010
Depth (m)
0
5
10
15
Release No. 236B
Cast No. 3D

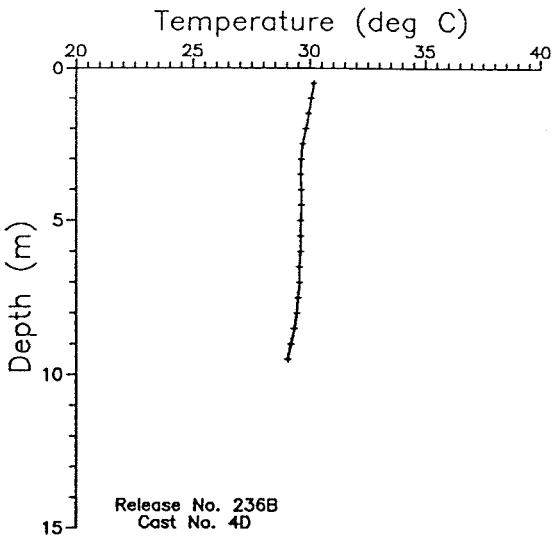
Temperature (deg C)
20
25
30
35
40
0
5
10
15
Depth (m)
Release No. 236B
Cast No. 4D

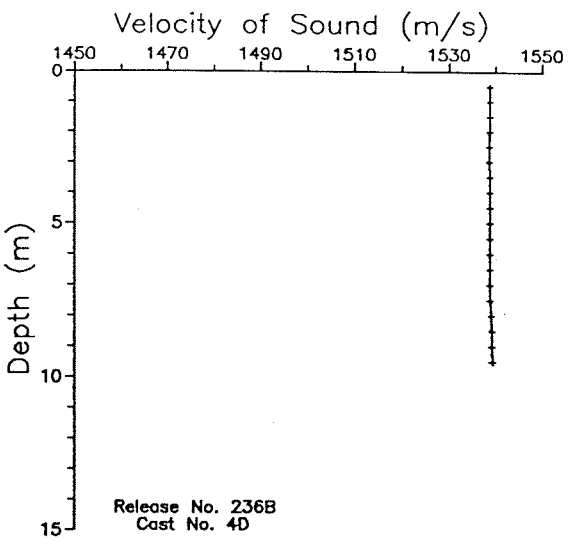
Velocity of Sound (m/s)
1450
1470
1490
1510
1530
1550
0
5
10
15
Depth (m)
Release No. 236B
Cast No. 4D

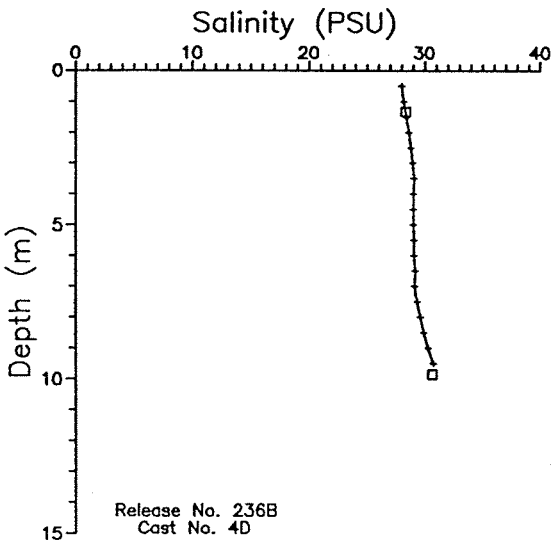
Salinity (PSU)
0
10
20
30
40
0
5
10
15
Depth (m)
Release No. 236B
Cast No. 4D

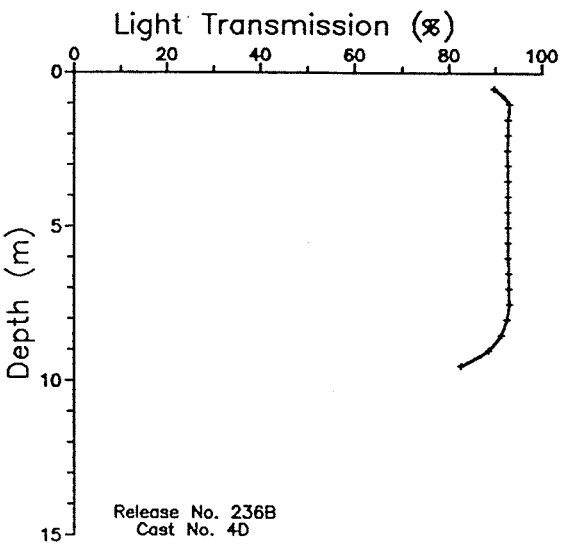
Light Transmission (%)
0
20
40
60
80
100
0
5
10
15
Depth (m)
Release No. 236B
Cast No. 4D

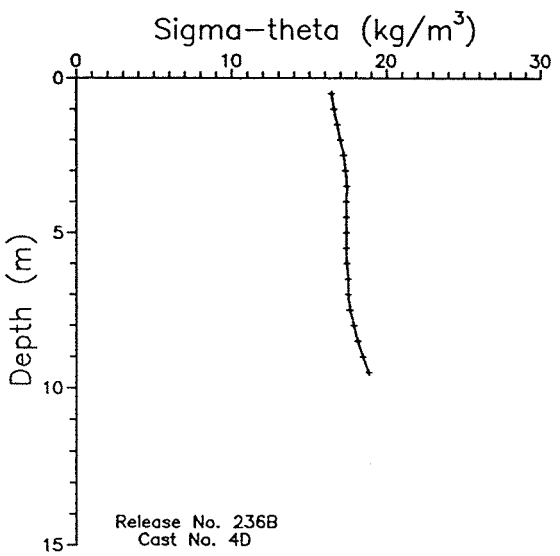
Sigma-theta (kg/m3)
0
10
20
30
0
5
10
15
Depth (m)
Release No. 236B
Cast No. 4D

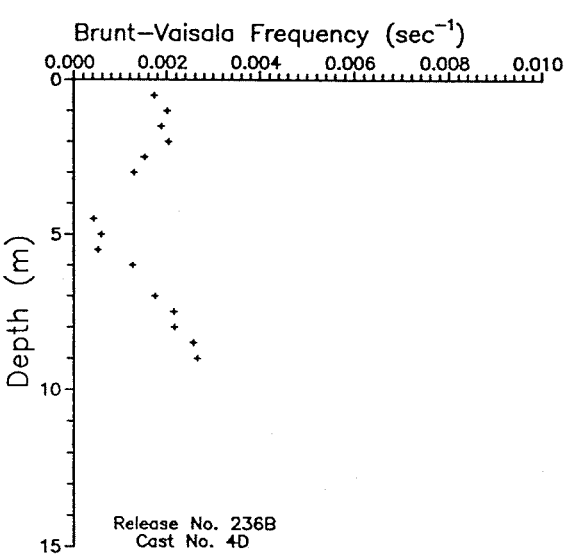
Brunt-Vaisala Frequency (sec-1)
0.000
0.002
0.004
0.006
0.008
0.010
0
5
10
15
Depth (m)
Release No. 236B
Cast No. 4D

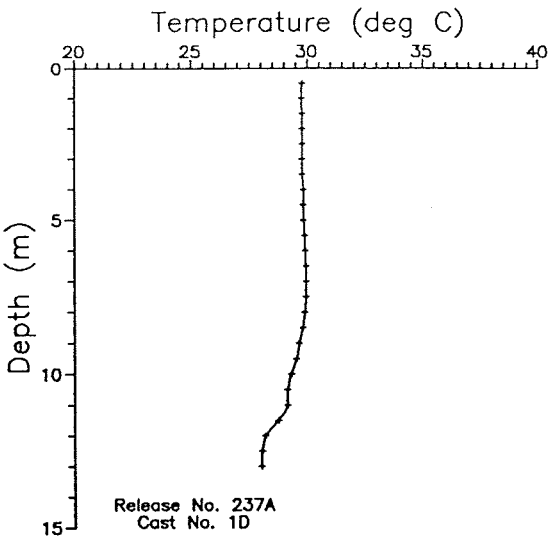
Temperature (deg C)
20
25
30
35
40
0
5
10
15
Depth (m)
Release No. 237A
Cast No. 1D

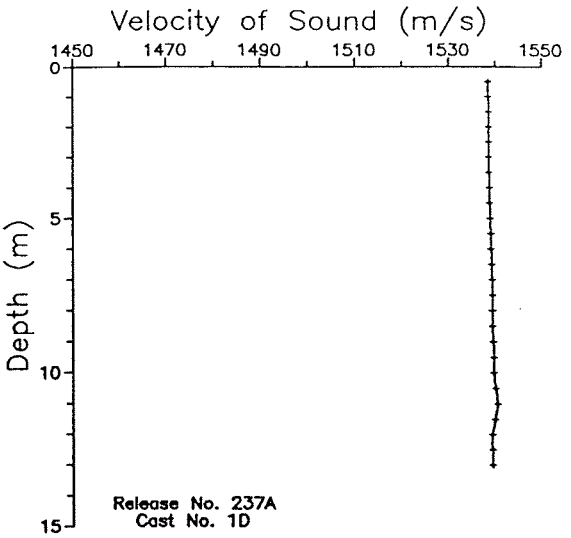
Velocity of Sound (m/s)
1450
1470
1490
1510
1530
1550
0
5
10
15
Depth (m)
Release No. 237A
Cast No. 1D

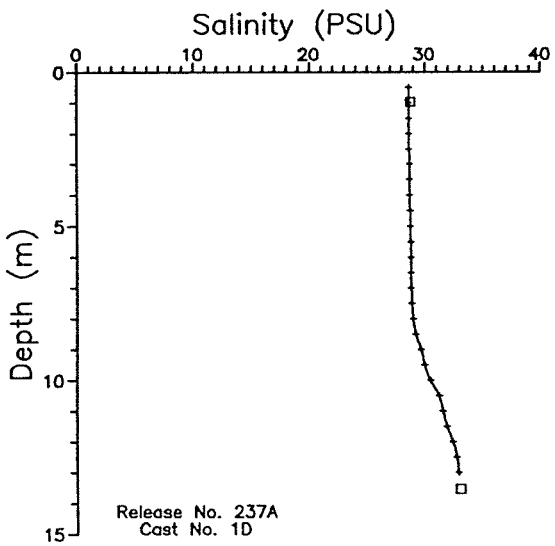
Salinity (PSU)
0
10
20
30
40
0
5
10
15
Depth (m)
Release No. 237A
Cast No. 1D

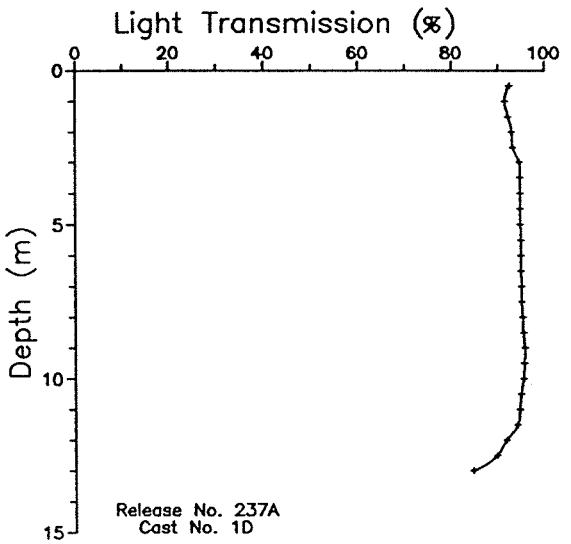
Light Transmission (%)
0
20
40
60
80
100
0
5
10
15
Depth (m)
Release No. 237A
Cast No. 1D

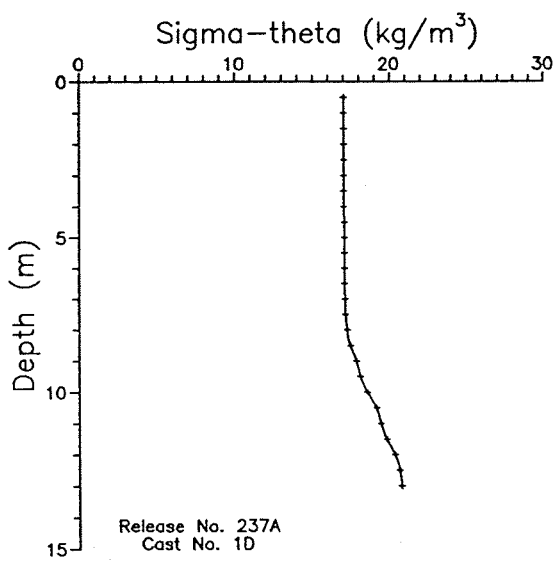
Sigma–theta (kg/m3)
0
10
20
30
0
5
10
15
Depth (m)
Release No. 237A
Cast No. 1D

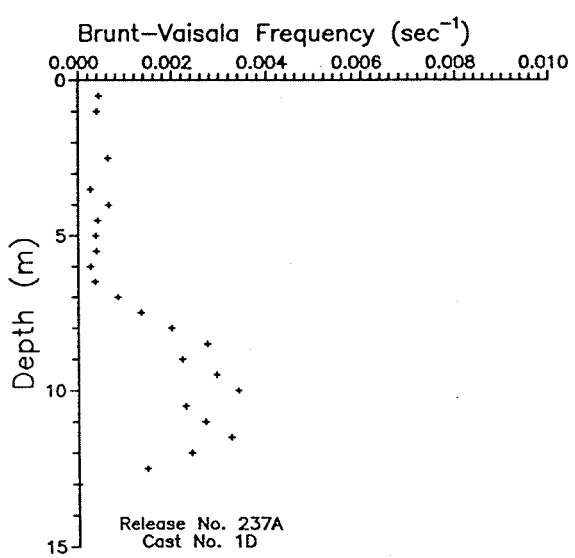
Brunt–Vaisala Frequency (sec-1)
0.000
0.002
0.004
0.006
0.008
0.010
0
5
10
15
Depth (m)
Release No. 237A
Cast No. 1D

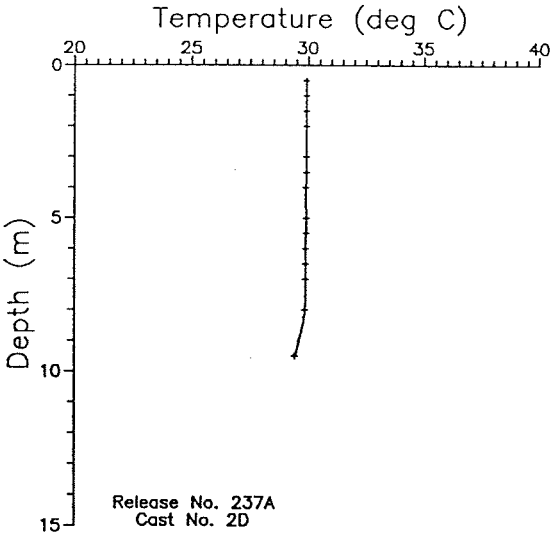
Temperature (deg C)
20
25
30
35
40
0
5
10
15
Depth (m)
Release No. 237A
Cast No. 2D

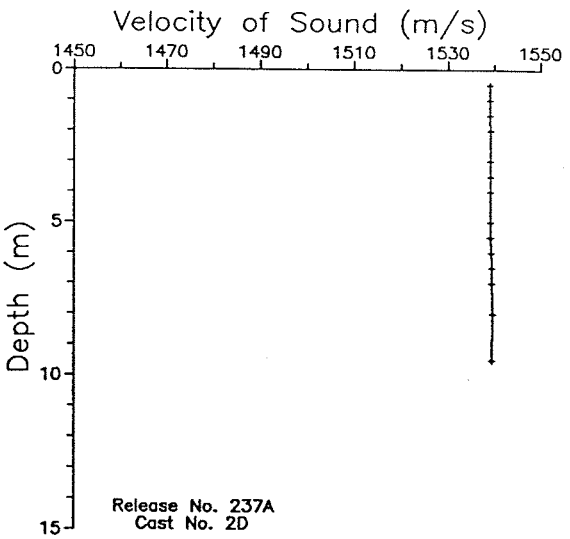
Velocity of Sound (m/s)
1450
1470
1490
1510
1530
1550
0
5
10
15
Depth (m)
Release No. 237A
Cast No. 2D

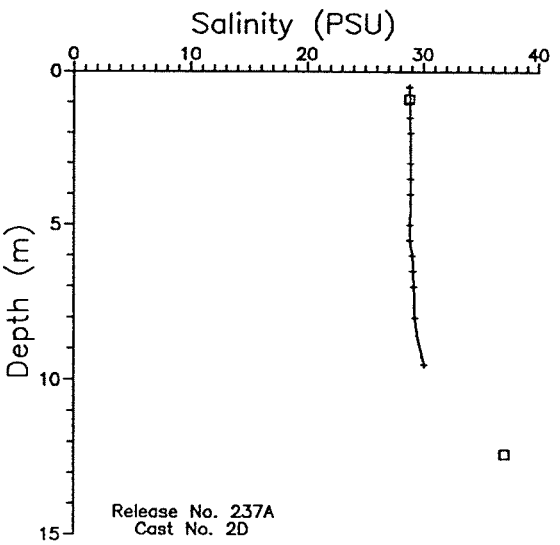
Salinity (PSU)
0
10
20
30
40
0
5
10
15
Depth (m)
Release No. 237A
Cast No. 2D

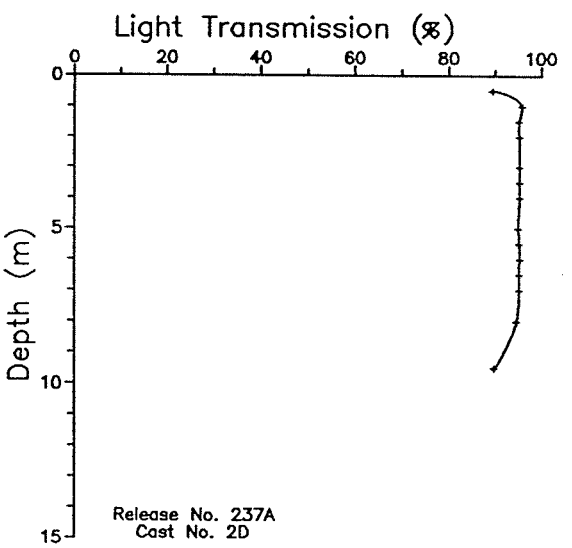
Light Transmission (%)
0
20
40
60
80
100
0
5
10
15
Depth (m)
Release No. 237A
Cast No. 2D

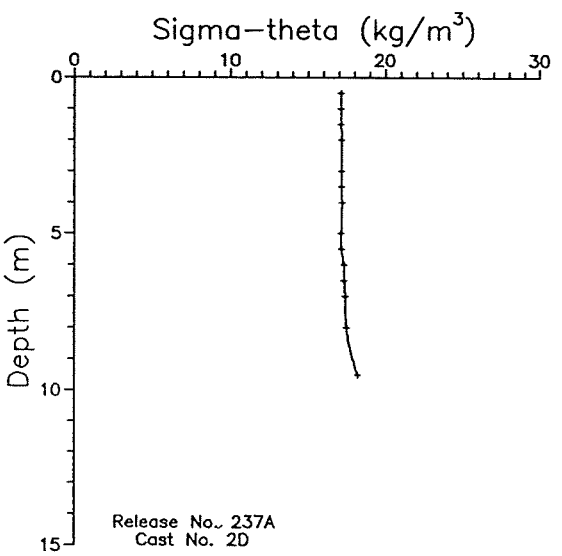
Sigma-theta (kg/m3)
0
10
20
30
0
5
10
15
Depth (m)
Release No. 237A
Cast No. 2D

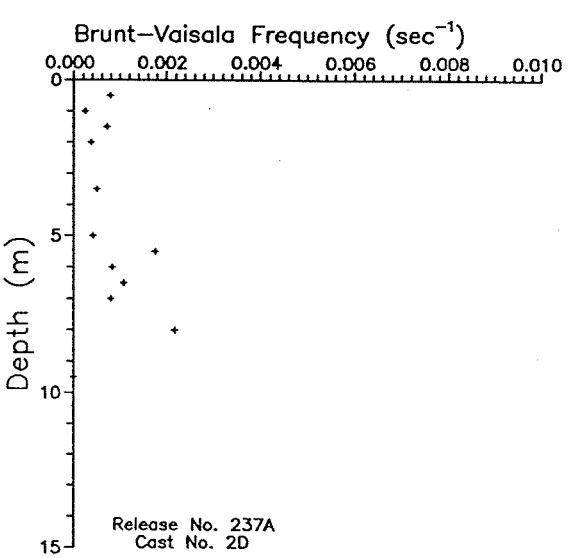
Brunt-Vaisala Frequency (sec-1)
0.000
0.002
0.004
0.006
0.008
0.010
0
5
10
15
Depth (m)
Release No. 237A
Cast No. 2D

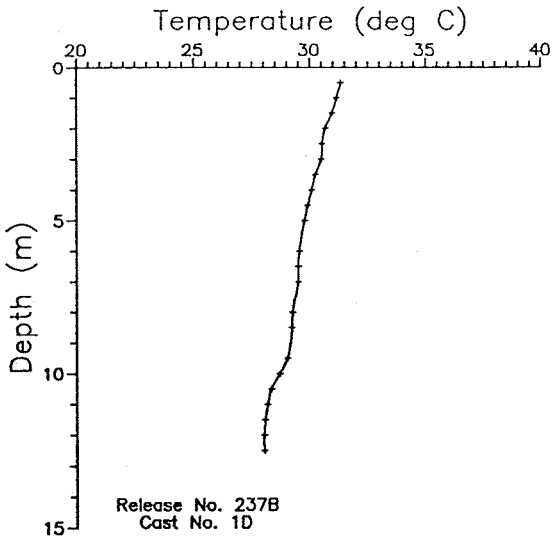
Temperature (deg C)
20
25
30
35
40
0
5
10
15
Depth (m)
Release No. 237B
Cast No. 1D

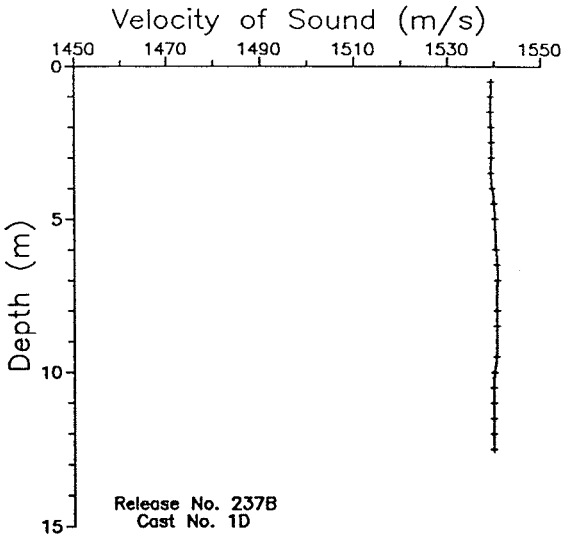
Velocity of Sound (m/s)
1450
1470
1490
1510
1530
1550
0
5
10
15
Depth (m)
Release No. 237B
Cast No. 1D

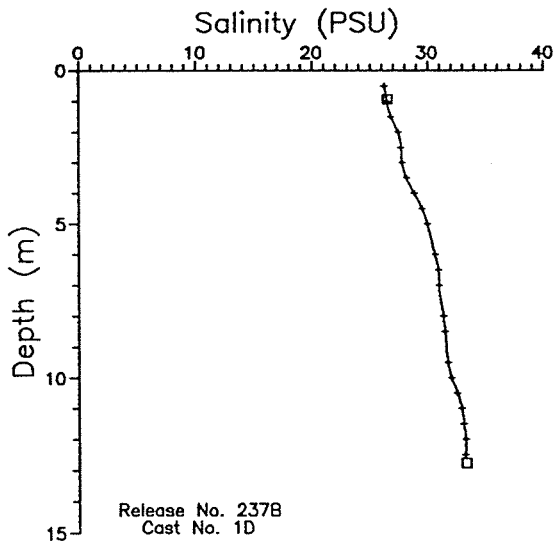
Salinity (PSU)
0
10
20
30
40
0
5
10
15
Depth (m)
Release No. 237B
Cast No. 1D

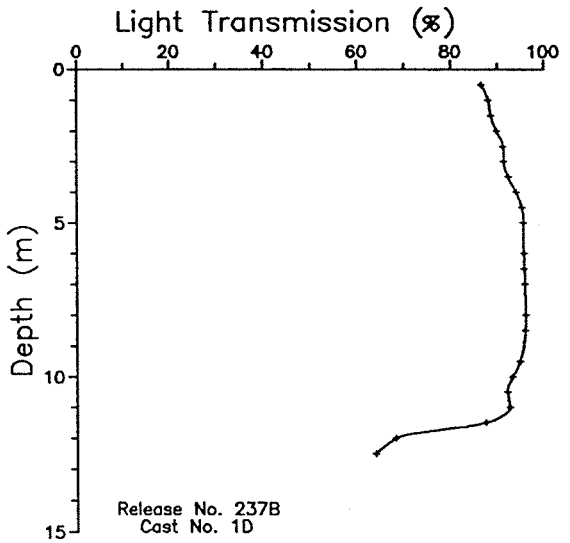
Light Transmission (%)
0
20
40
60
80
100
0
5
10
15
Depth (m)
Release No. 237B
Cast No. 1D

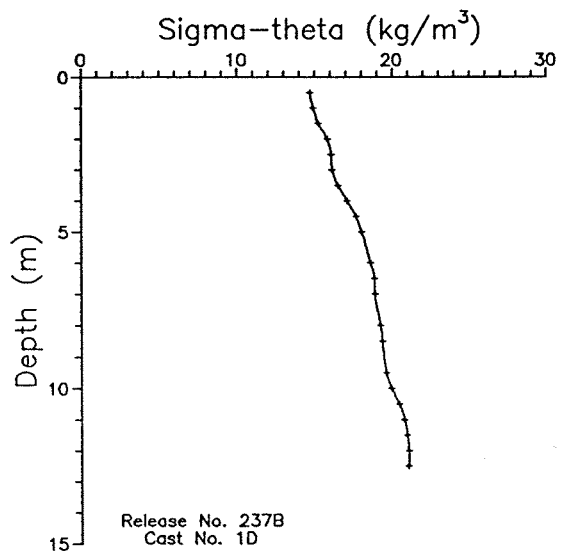
Sigma-theta (kg/m3)
0
10
20
30
0
5
10
15
Depth (m)
Release No. 237B
Cast No. 1D

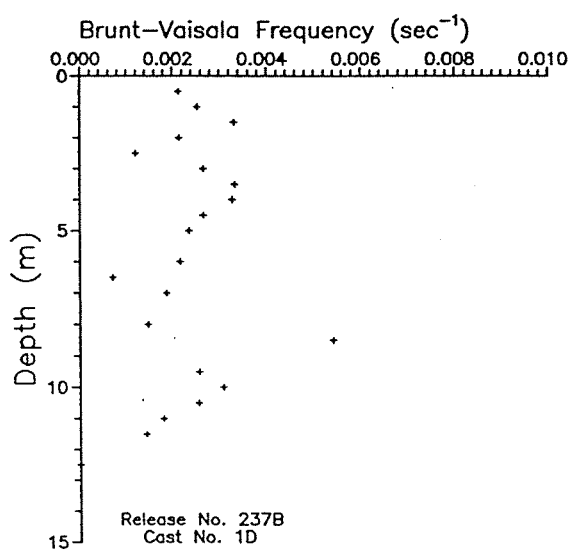
Brunt-Vaisala Frequency (sec-1)
0.000
0.002
0.004
0.006
0.008
0.010
0
5
10
15
Depth (m)
Release No. 237B
Cast No. 1D

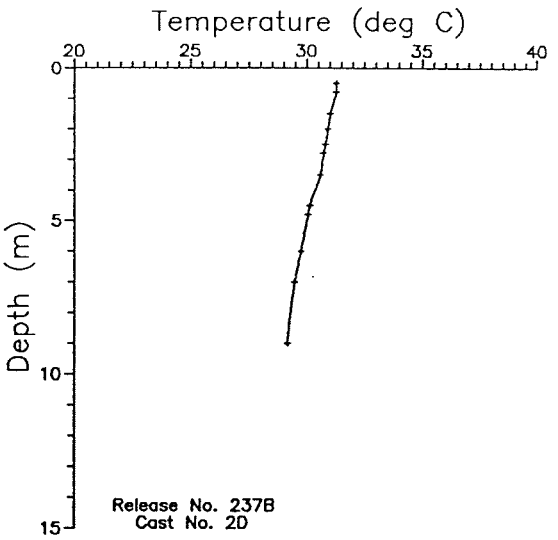
Temperature (deg C)
20
25
30
35
40
Depth (m)
0
5
10
15
Release No. 237B
Cast No. 2D

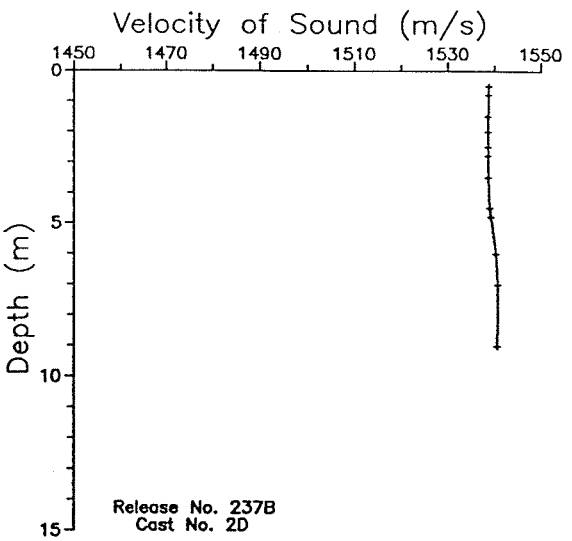
Velocity of Sound (m/s)
1450
1470
1490
1510
1530
1550
Depth (m)
0
5
10
15
Release No. 237B
Cast No. 2D

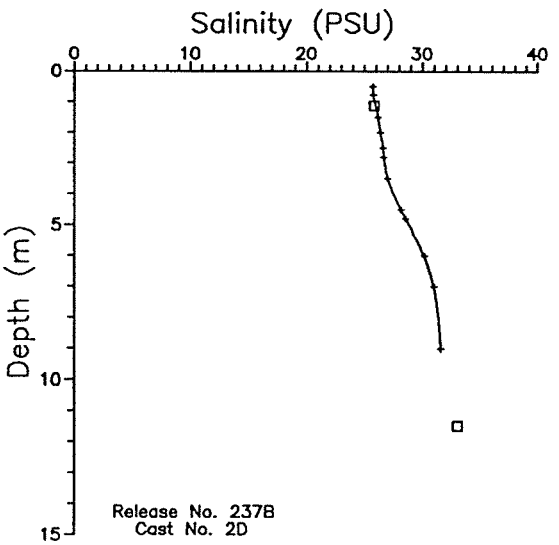
Salinity (PSU)
0
10
20
30
40
Depth (m)
0
5
10
15
Release No. 237B
Cast No. 2D

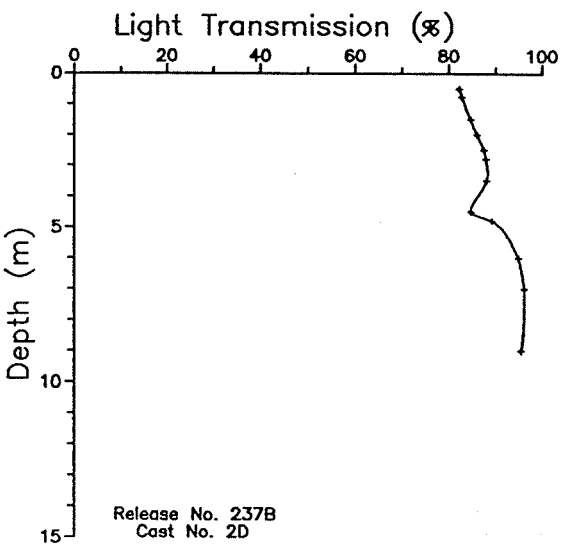
Light Transmission (%)
0
20
40
60
80
100
Depth (m)
0
5
10
15
Release No. 237B
Cast No. 2D

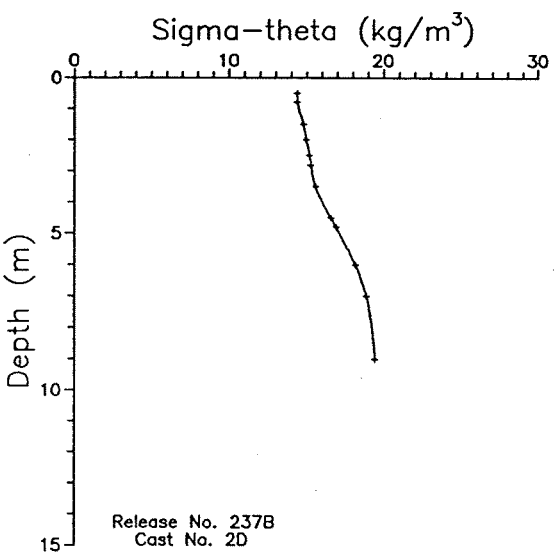
Sigma–theta (kg/m3)
0
10
20
30
Depth (m)
0
5
10
15
Release No. 237B
Cast No. 2D

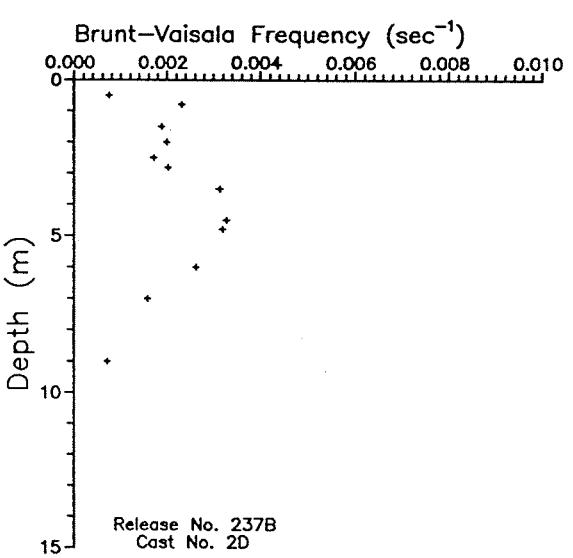
Brunt–Vaisala Frequency (sec-1)
0.000
0.002
0.004
0.006
0.008
0.010
Depth (m)
0
5
10
15
Release No. 237B
Cast No. 2D

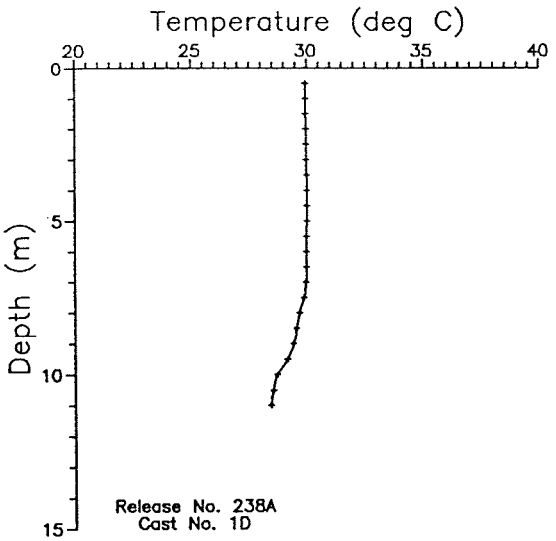
Temperature (deg C)
20
25
30
35
40
0
5
10
15
Depth (m)
Release No. 238A
Cast No. 1D

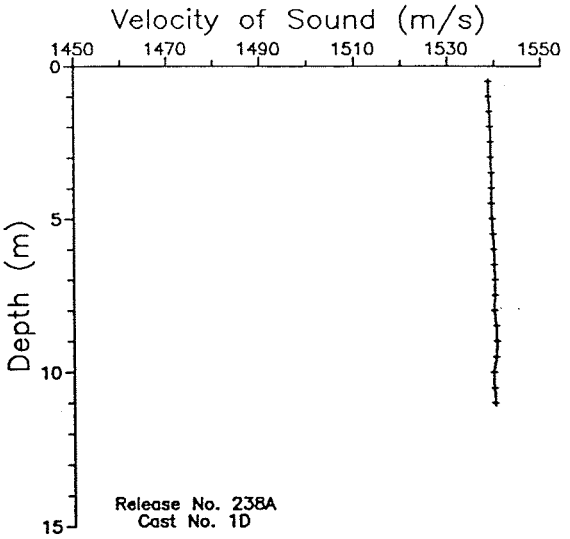
Velocity of Sound (m/s)
1450
1470
1490
1510
1530
1550
0
5
10
15
Depth (m)
Release No. 238A
Cast No. 1D

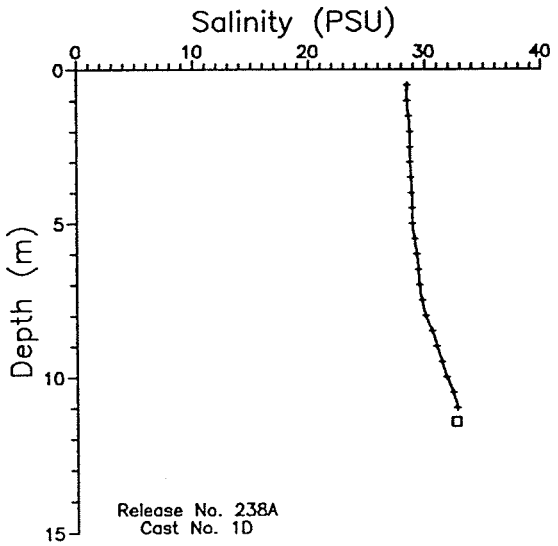
Salinity (PSU)
0
10
20
30
40
0
5
10
15
Depth (m)
Release No. 238A
Cast No. 1D

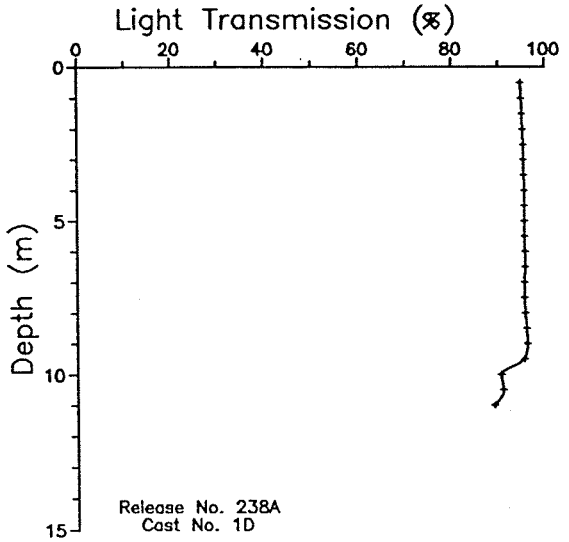
Light Transmission (%)
0
20
40
60
80
100
0
5
10
15
Depth (m)
Release No. 238A
Cast No. 1D

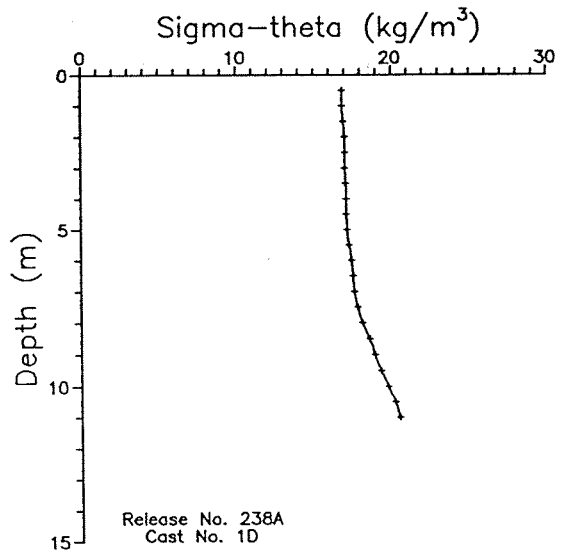
Sigma-theta (kg/m3)
0
10
20
30
0
5
10
15
Depth (m)
Release No. 238A
Cast No. 1D

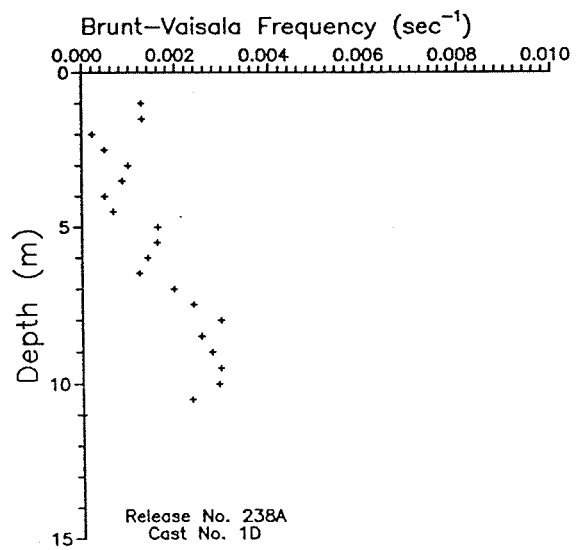
Brunt-Vaisala Frequency (sec-1)
0.000
0.002
0.004
0.006
0.008
0.010
0
5
10
15
Depth (m)
Release No. 238A
Cast No. 1D

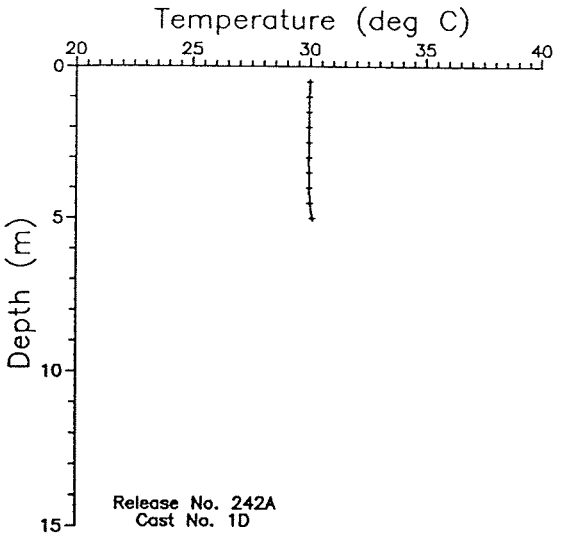
Temperature (deg C)
20
25
30
35
40
0
5
10
15
Depth (m)
Release No. 242A
Cast No. 1D

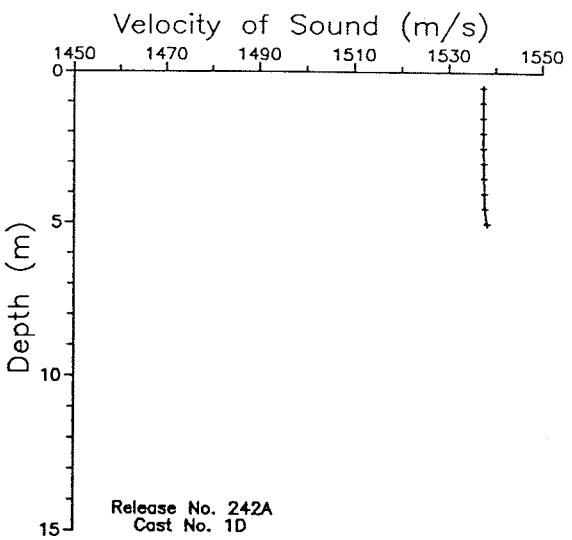
Velocity of Sound (m/s)
1450
1470
1490
1510
1530
1550
0
5
10
15
Depth (m)
Release No. 242A
Cast No. 1D

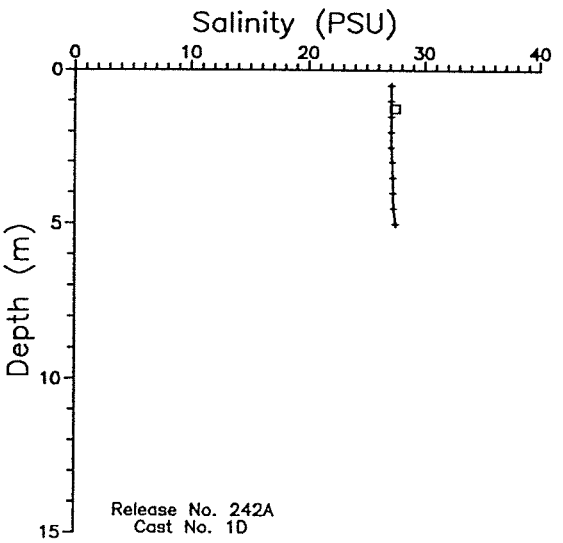
Salinity (PSU)
0
10
20
30
40
0
5
10
15
Depth (m)
Release No. 242A
Cast No. 1D

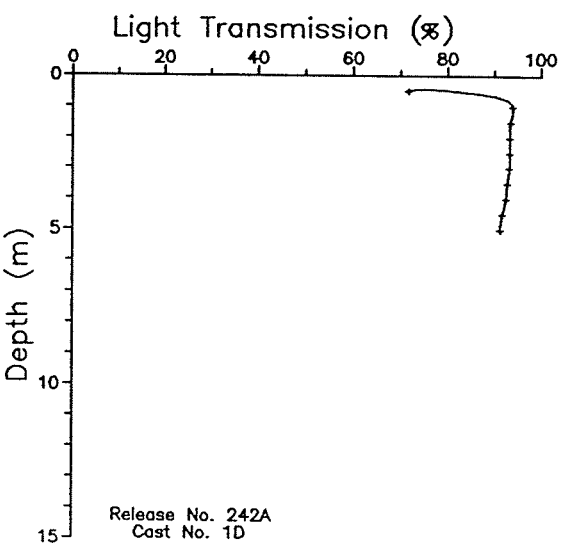
Light Transmission (%)
0
20
40
60
80
100
0
5
10
15
Depth (m)
Release No. 242A
Cast No. 1D

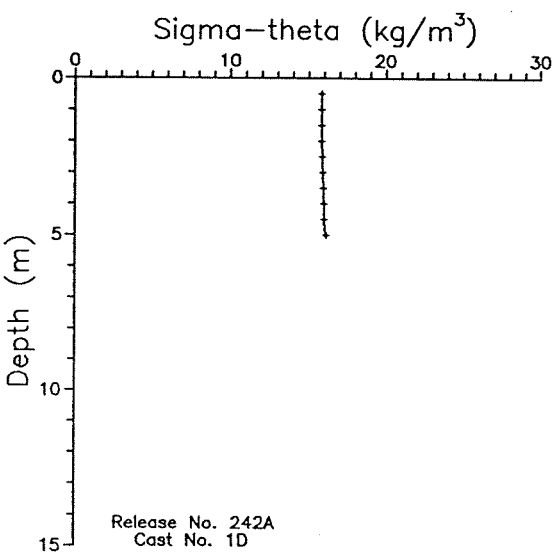
Sigma-theta (kg/m3)
0
10
20
30
0
5
10
15
Depth (m)
Release No. 242A
Cast No. 1D

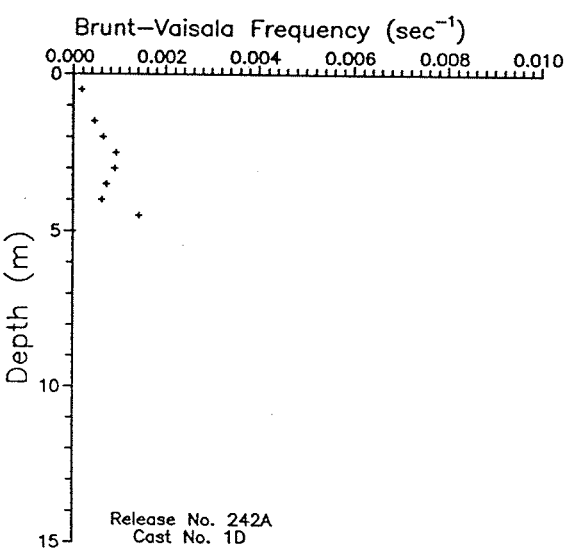
Brunt-Vaisala Frequency (sec-1)
0.000
0.002
0.004
0.006
0.008
0.010
0
5
10
15
Depth (m)
Release No. 242A
Cast No. 1D

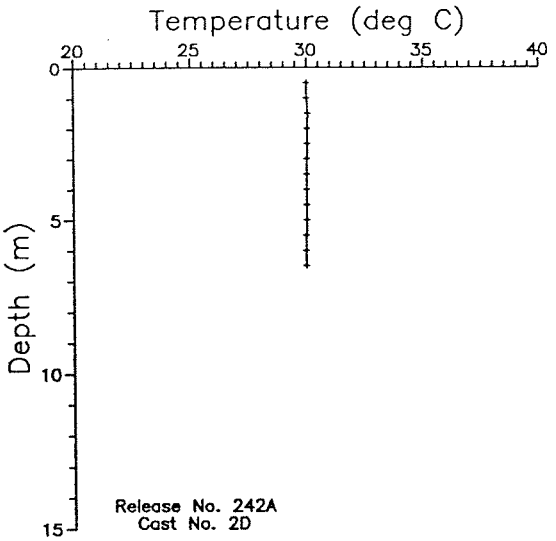
Temperature (deg C)
20
25
30
35
40
0
5
10
15
Depth (m)
Release No. 242A
Cast No. 2D

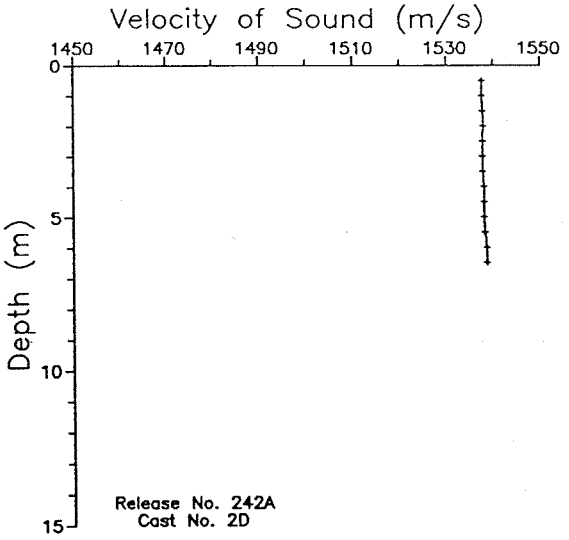
Velocity of Sound (m/s)
1450
1470
1490
1510
1530
1550
0
5
10
15
Depth (m)
Release No. 242A
Cast No. 2D

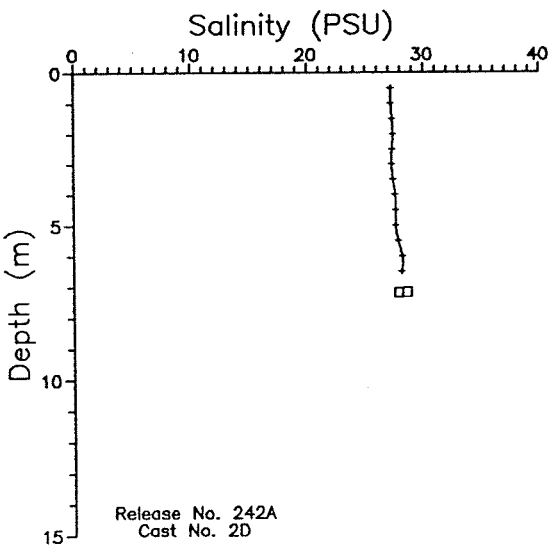
Salinity (PSU)
0
10
20
30
40
0
5
10
15
Depth (m)
Release No. 242A
Cast No. 2D

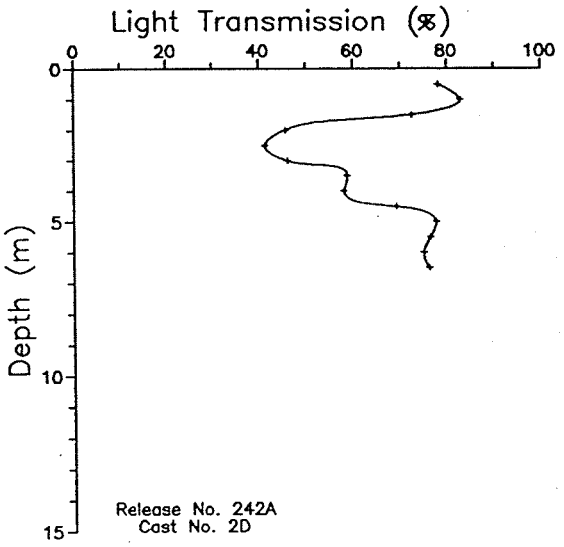
Light Transmission (%)
0
20
40
60
80
100
0
5
10
15
Depth (m)
Release No. 242A
Cast No. 2D

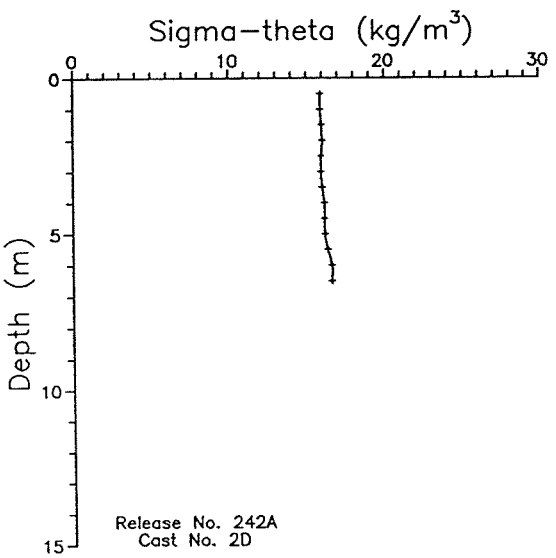
Sigma-theta (kg/m3)
0
10
20
30
0
5
10
15
Depth (m)
Release No. 242A
Cast No. 2D

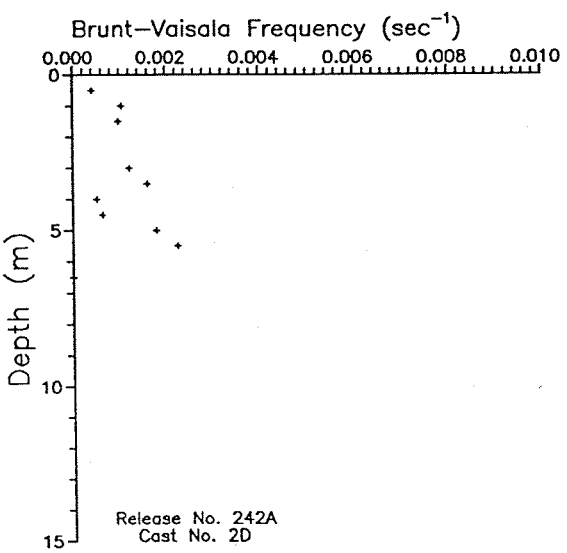
Brunt-Vaisala Frequency (sec-1)
0.000
0.002
0.004
0.006
0.008
0.010
0
5
10
15
Depth (m)
Release No. 242A
Cast No. 2D

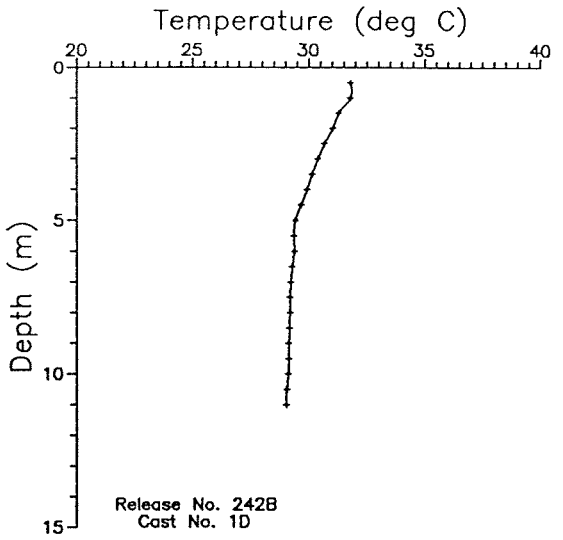
Temperature (deg C)
20
25
30
35
40
0
5
10
15
Depth (m)
Release No. 242B
Cast No. 1D

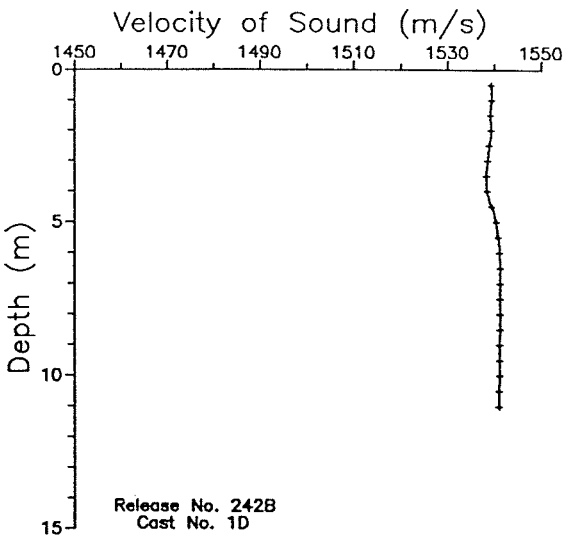
Velocity of Sound (m/s)
1450
1470
1490
1510
1530
1550
0
5
10
15
Depth (m)
Release No. 242B
Cast No. 1D

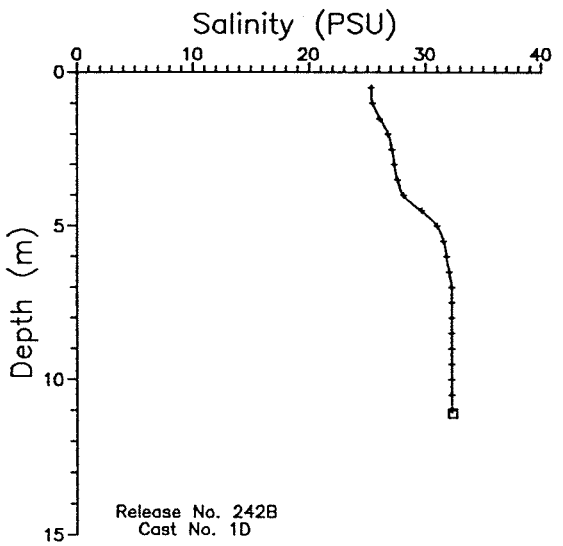
Salinity (PSU)
0
10
20
30
40
0
5
10
15
Depth (m)
Release No. 242B
Cast No. 1D

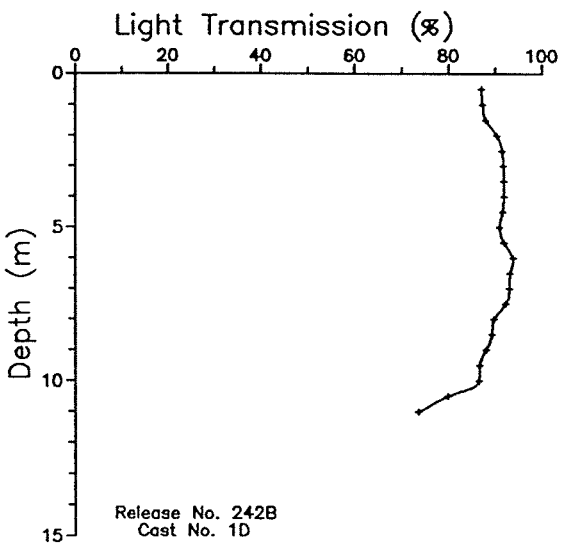
Light Transmission (%)
0
20
40
60
80
100
0
5
10
15
Depth (m)
Release No. 242B
Cast No. 1D

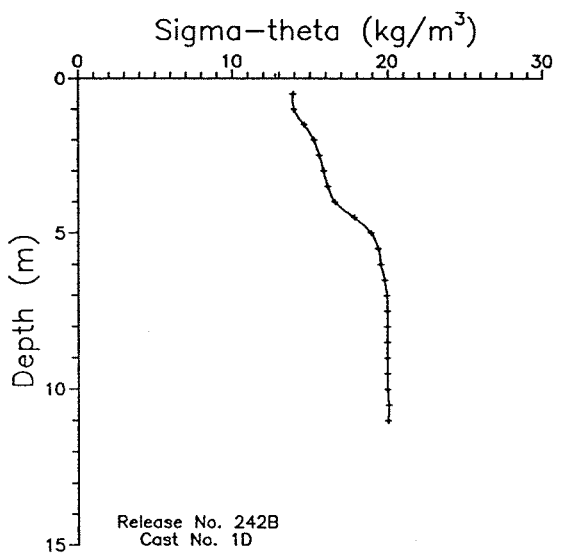
Sigma-theta (kg/m3)
0
10
20
30
0
5
10
15
Depth (m)
Release No. 242B
Cast No. 1D

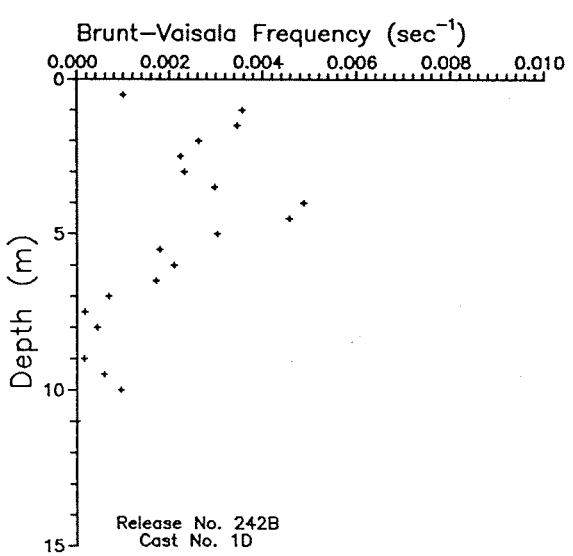
Brunt-Vaisala Frequency (sec-1)
0.000
0.002
0.004
0.006
0.008
0.010
0
5
10
15
Depth (m)
Release No. 242B
Cast No. 1D

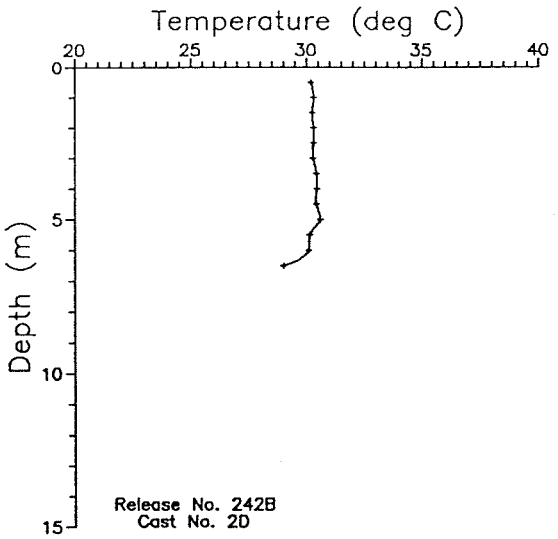
Temperature (deg C)
20
25
30
35
40
0
5
10
15
Depth (m)
Release No. 242B
Cast No. 2D

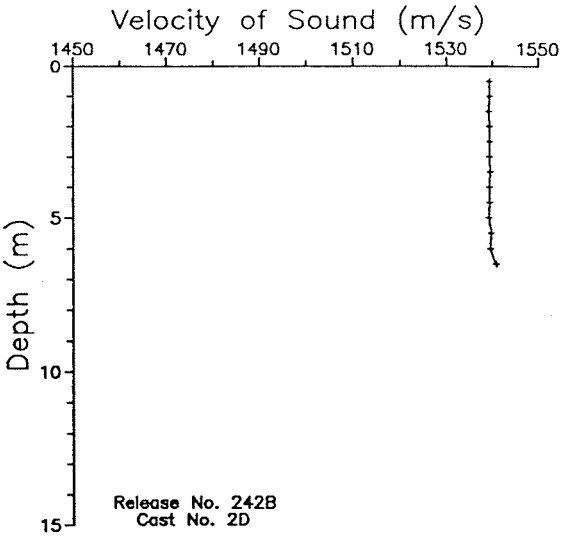
Velocity of Sound (m/s)
1450
1470
1490
1510
1530
1550
0
5
10
15
Depth (m)
Release No. 242B
Cast No. 2D

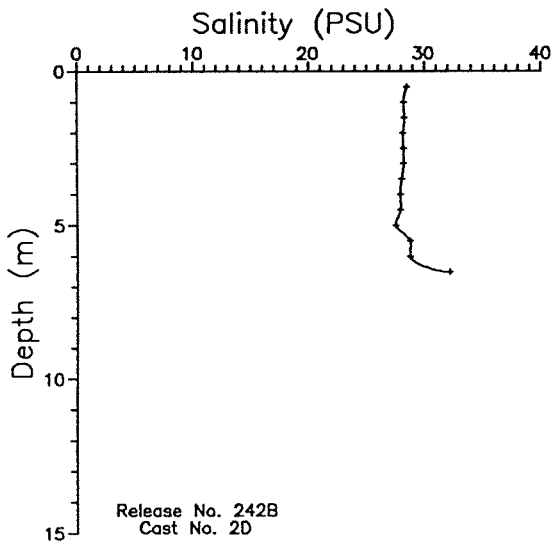
Salinity (PSU)
0
10
20
30
40
0
5
10
15
Depth (m)
Release No. 242B
Cast No. 2D

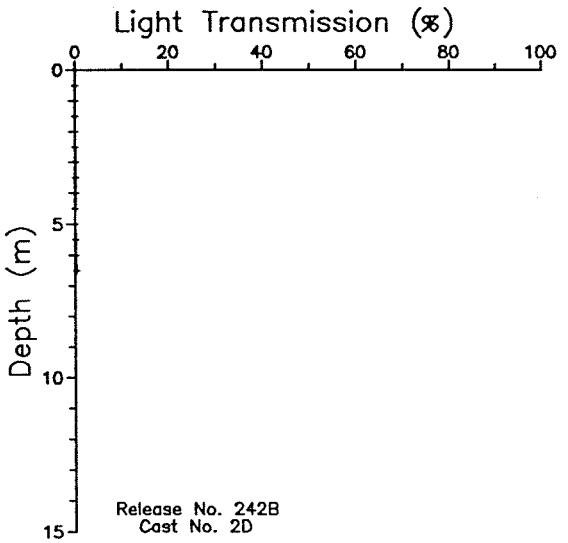
Light Transmission (%)
0
20
40
60
80
100
0
5
10
15
Depth (m)
Release No. 242B
Cast No. 2D

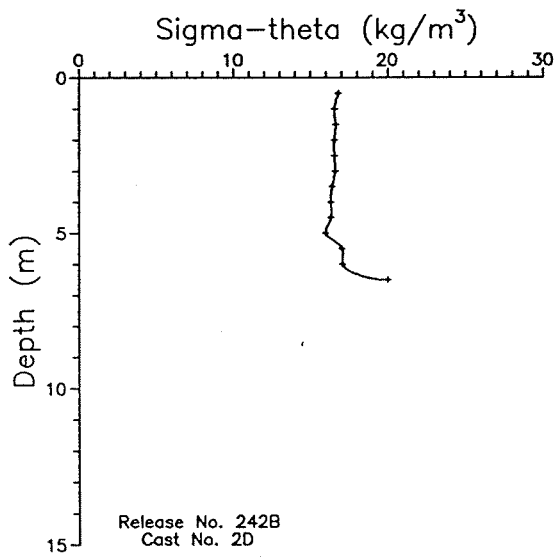
Sigma-theta (kg/m3)
0
10
20
30
0
5
10
15
Depth (m)
Release No. 242B
Cast No. 2D

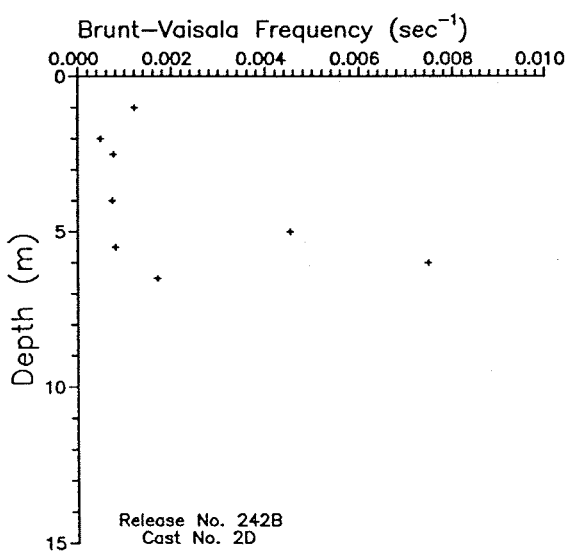
Brunt-Vaisala Frequency (sec-1)
0.000
0.002
0.004
0.006
0.008
0.010
0
5
10
15
Depth (m)
Release No. 242B
Cast No. 2D

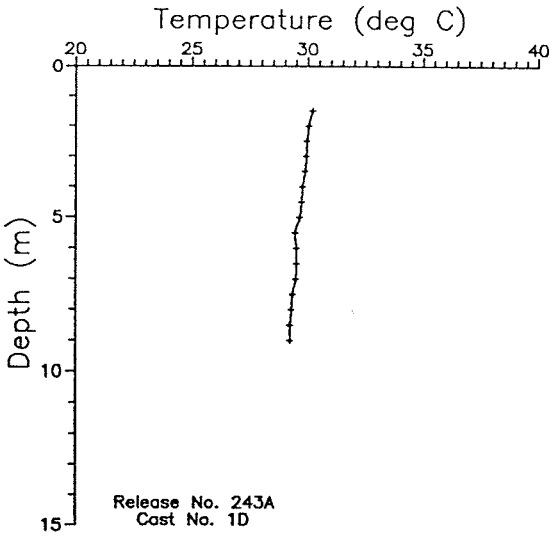
Temperature (deg C)
20
25
30
35
40
0
5
10
15
Depth (m)
Release No. 243A
Cast No. 1D

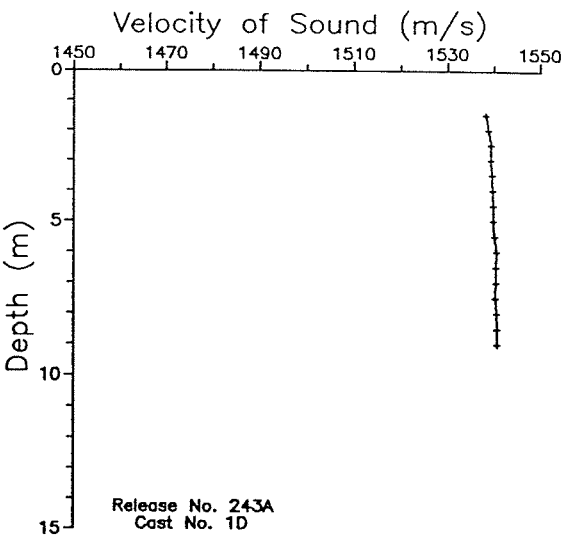
Velocity of Sound (m/s)
1450
1470
1490
1510
1530
1550
0
5
10
15
Depth (m)
Release No. 243A
Cast No. 1D

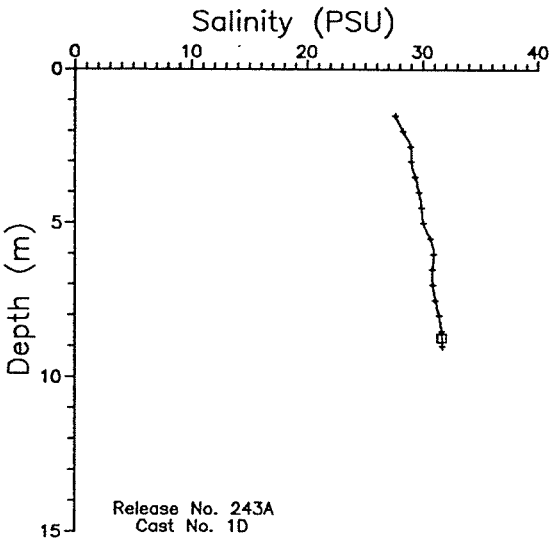
Salinity (PSU)
0
10
20
30
40
0
5
10
15
Depth (m)
Release No. 243A
Cast No. 1D

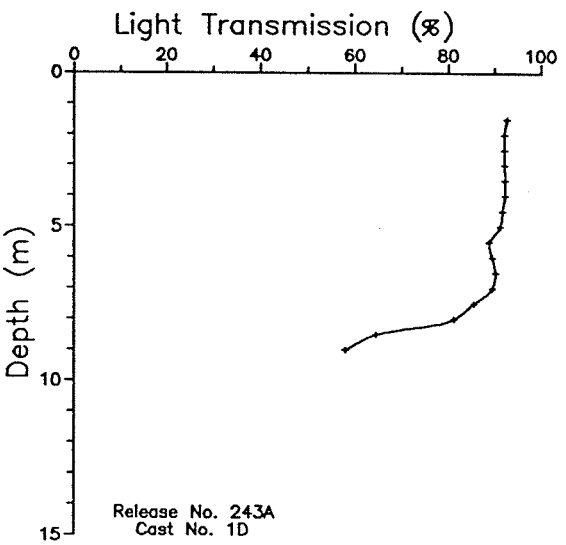
Light Transmission (%)
0
20
40
60
80
100
0
5
10
15
Depth (m)
Release No. 243A
Cast No. 1D

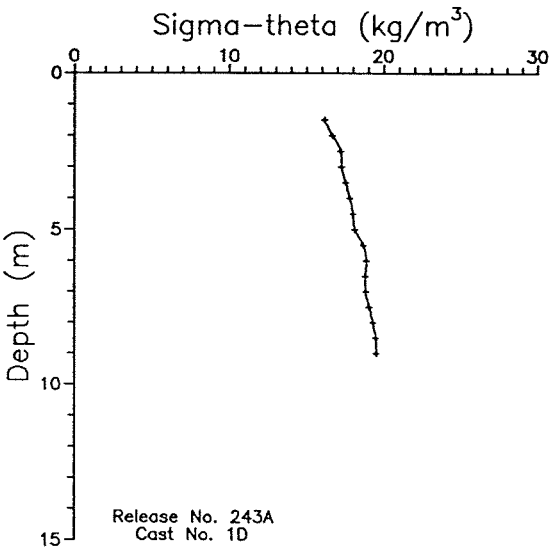
Sigma-theta (kg/m3)
0
10
20
30
0
5
10
15
Depth (m)
Release No. 243A
Cast No. 1D

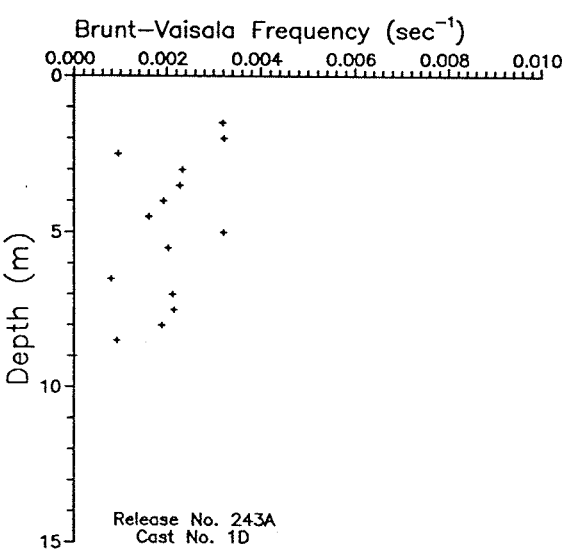
Brunt-Vaisala Frequency (sec-1)
0.000
0.002
0.004
0.006
0.008
0.010
0
5
10
15
Depth (m)
Release No. 243A
Cast No. 1D

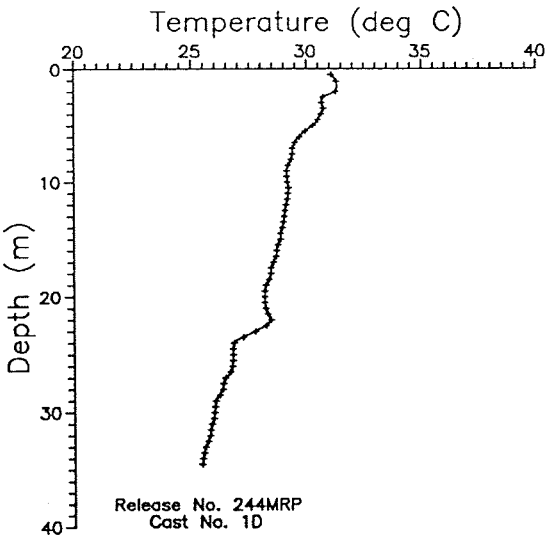
Temperature (deg C)
20
25
30
35
40
0
10
20
30
40
Depth (m)
Release No. 244MRP
Cast No. 1D

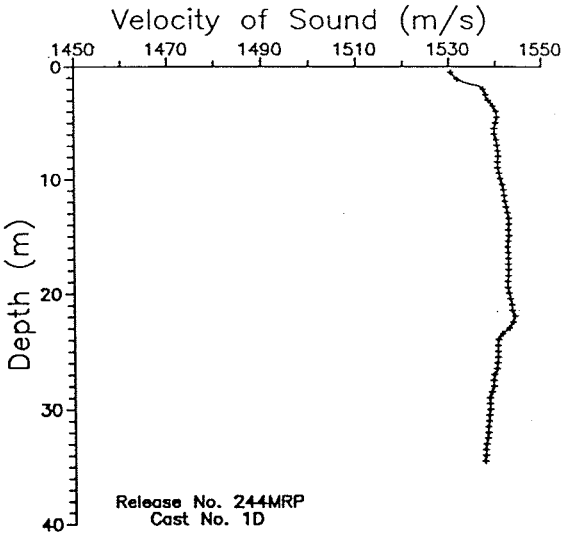
Velocity of Sound (m/s)
1450
1470
1490
1510
1530
1550
0
10
20
30
40
Depth (m)
Release No. 244MRP
Cast No. 1D

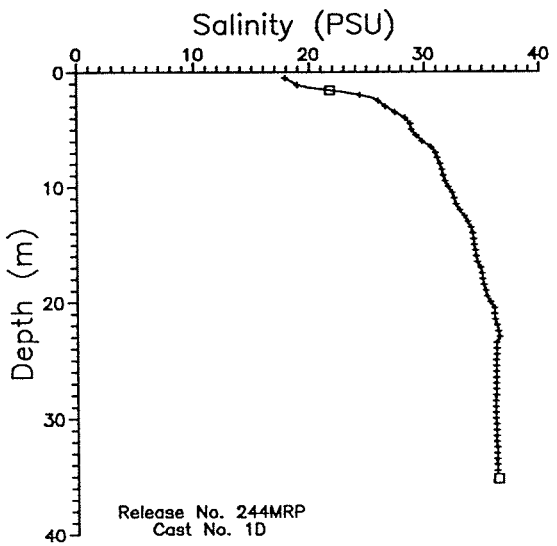
Salinity (PSU)
0
10
20
30
40
0
10
20
30
40
Depth (m)
Release No. 244MRP
Cast No. 1D

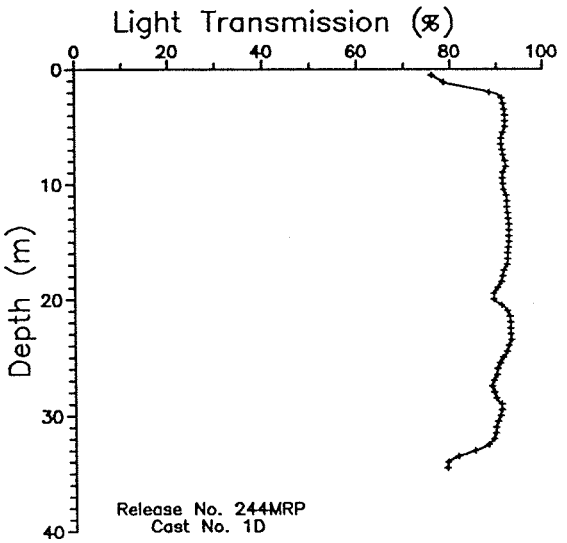
Light Transmission (%)
0
20
40
60
80
100
0
10
20
30
40
Depth (m)
Release No. 244MRP
Cast No. 1D

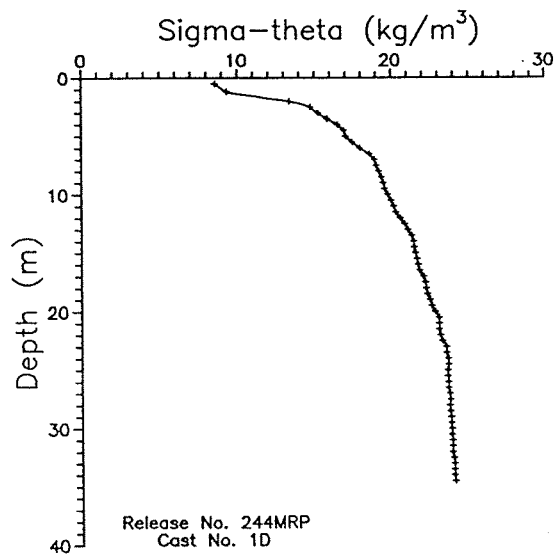
Sigma–theta (kg/m3)
0
10
20
30
0
10
20
30
40
Depth (m)
Release No. 244MRP
Cast No. 1D

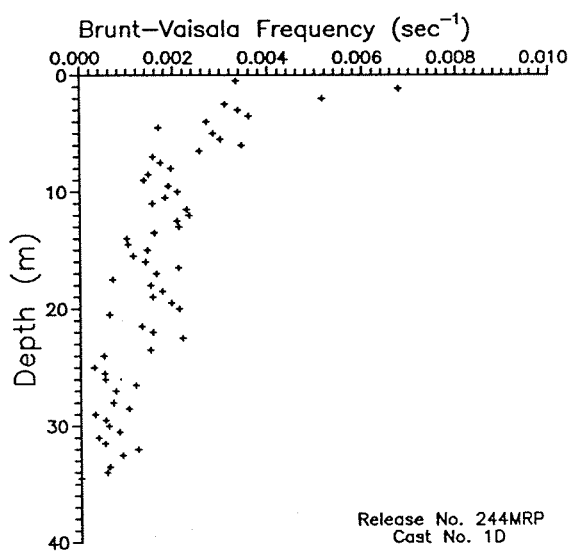
Brunt–Vaisala Frequency (sec-1)
0.000
0.002
0.004
0.006
0.008
0.010
0
10
20
30
40
Depth (m)
Release No. 244MRP
Cast No. 1D

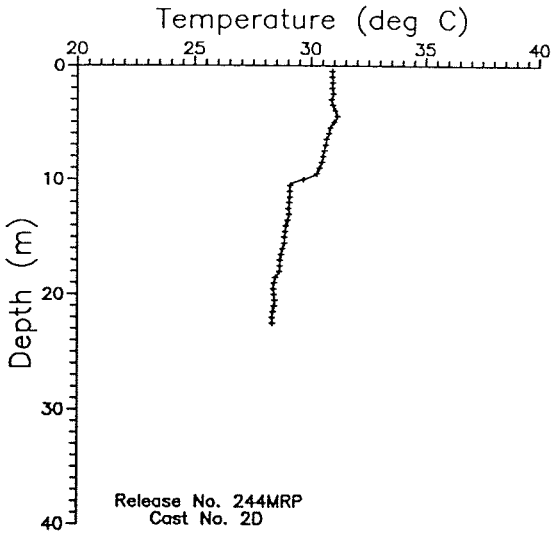
Temperature (deg C)
20
25
30
35
40
0
10
20
30
40
Depth (m)
Release No. 244MRP
Cast No. 2D

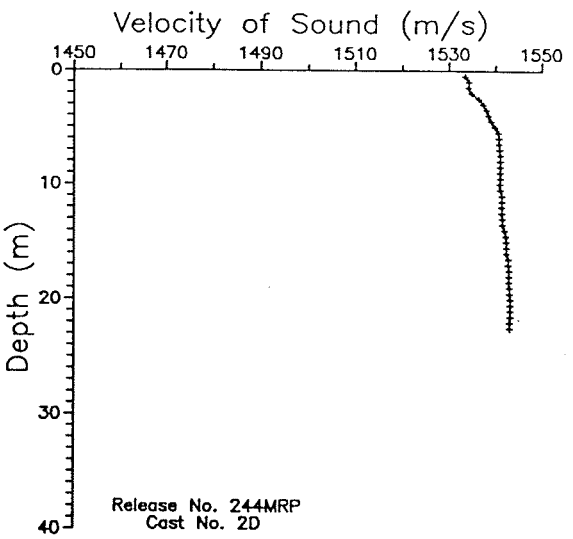
Velocity of Sound (m/s)
1450
1470
1490
1510
1530
1550
0
10
20
30
40
Depth (m)
Release No. 244MRP
Cast No. 2D

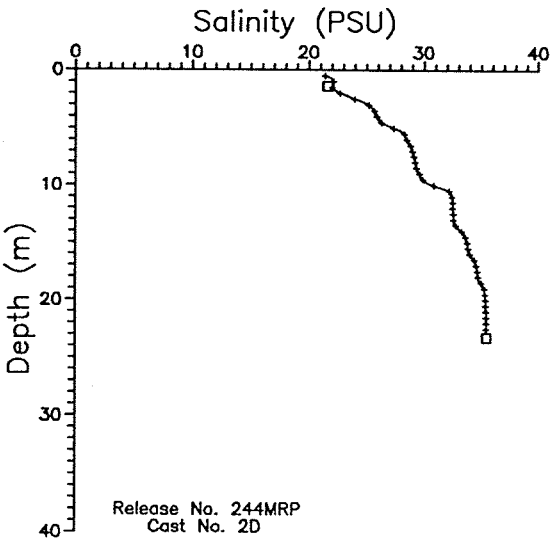
Salinity (PSU)
0
10
20
30
40
0
10
20
30
40
Depth (m)
Release No. 244MRP
Cast No. 2D

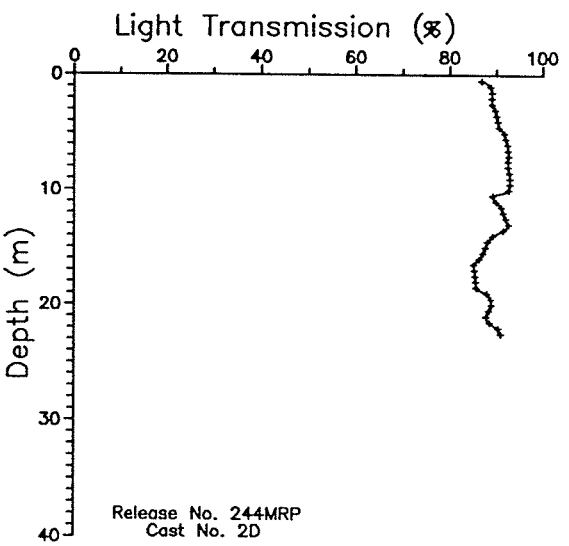
Light Transmission (%)
0
20
40
60
80
100
0
10
20
30
40
Depth (m)
Release No. 244MRP
Cast No. 2D

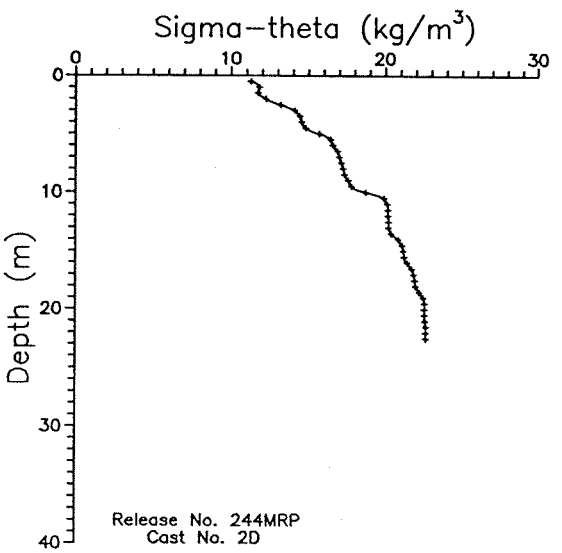
Sigma–theta (kg/m3)
0
10
20
30
0
10
20
30
40
Depth (m)
Release No. 244MRP
Cast No. 2D

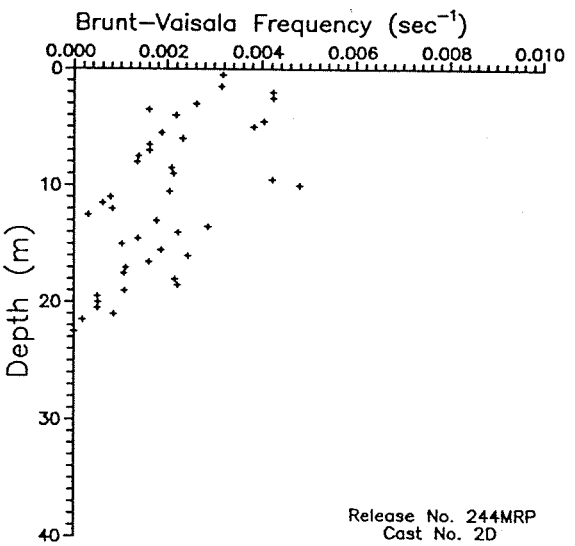
Brunt–Vaisala Frequency (sec-1)
0.000
0.002
0.004
0.006
0.008
0.010
0
10
20
30
40
Depth (m)
Release No. 244MRP
Cast No. 2D

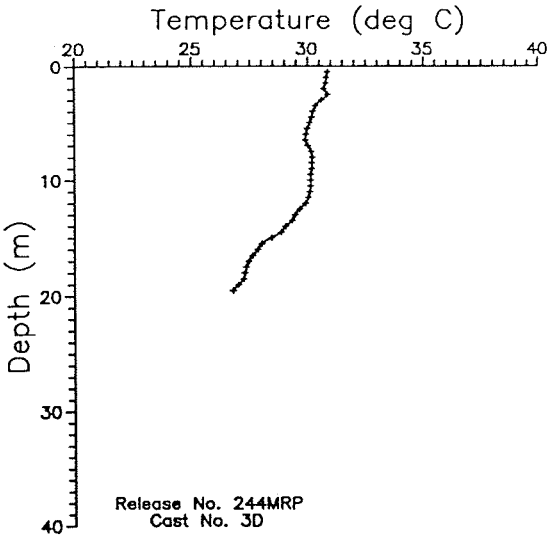
Temperature (deg C)
20
25
30
35
40
0
10
20
30
40
Depth (m)
Release No. 244MRP
Cast No. 3D

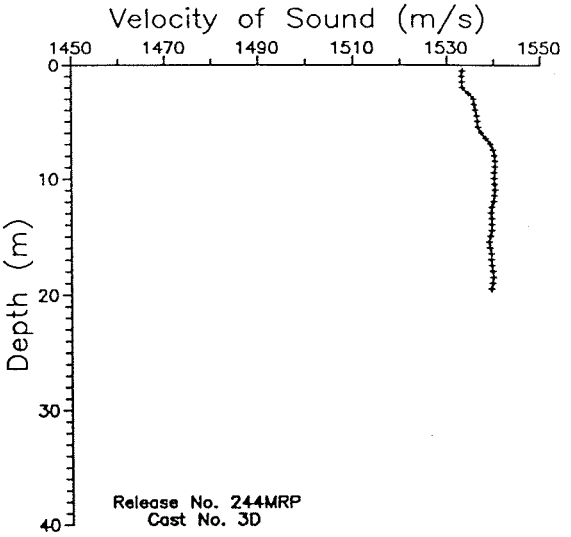
Velocity of Sound (m/s)
1450
1470
1490
1510
1530
1550
0
10
20
30
40
Depth (m)
Release No. 244MRP
Cast No. 3D

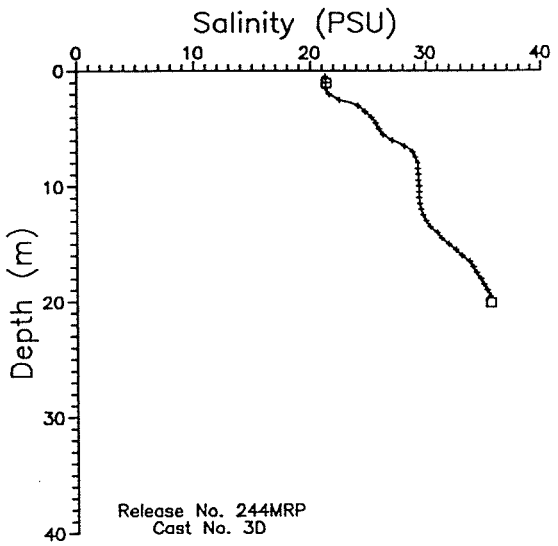
Salinity (PSU)
0
10
20
30
40
0
10
20
30
40
Depth (m)
Release No. 244MRP
Cast No. 3D

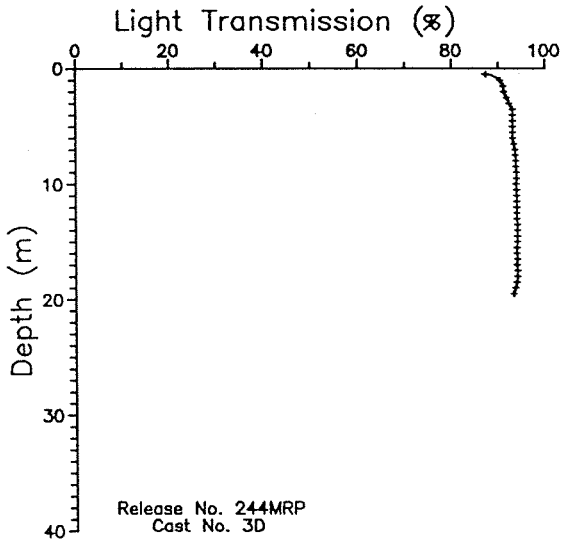
Light Transmission (%)
0
20
40
60
80
100
0
10
20
30
40
Depth (m)
Release No. 244MRP
Cast No. 3D

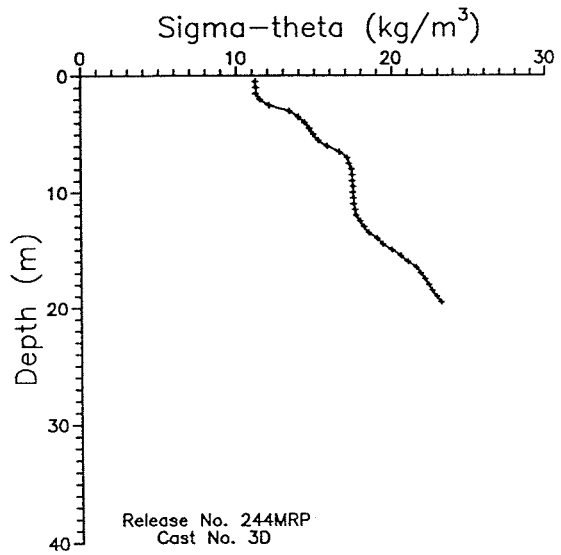
Sigma-theta (kg/m3)
0
10
20
30
0
10
20
30
40
Depth (m)
Release No. 244MRP
Cast No. 3D

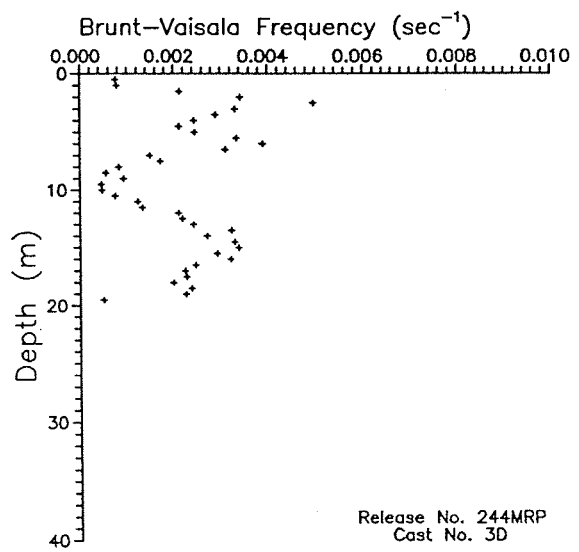
Brunt-Vaisala Frequency (sec-1)
0.000
0.002
0.004
0.006
0.008
0.010
0
10
20
30
40
Depth (m)
Release No. 244MRP
Cast No. 3D

Appendix 4B: Suspended Sediment Sample Grain Size Density Functions

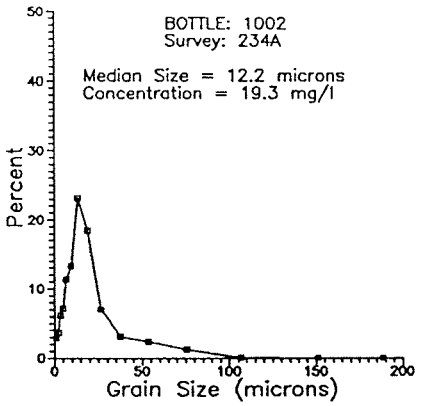
BOTTLE: 1002
Survey: 234A
Median Size = 12.2 microns
Concentration = 19.3 mg/l
Percent
Grain Size (microns)

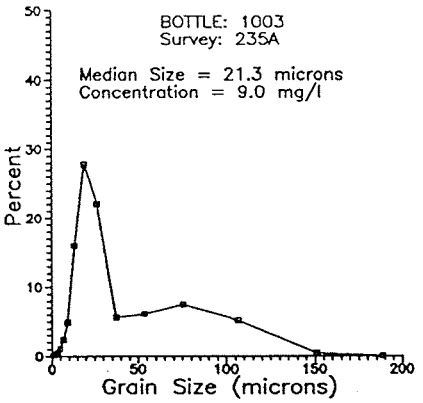
BOTTLE: 1003
Survey: 235A
Median Size = 21.3 microns
Concentration = 9.0 mg/l
Percent
Grain Size (microns)

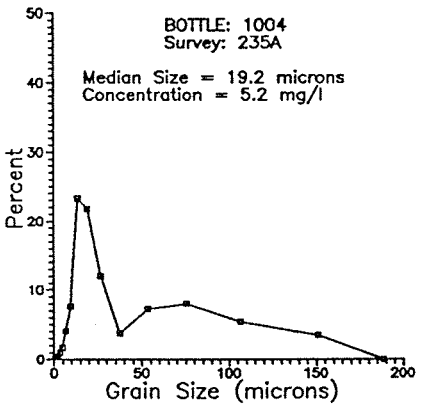
BOTTLE: 1004
Survey: 235A
Median Size = 19.2 microns
Concentration = 5.2 mg/l
Percent
Grain Size (microns)

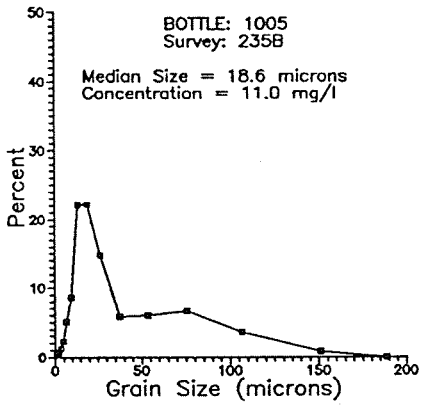
BOTTLE: 1005
Survey: 235B
Median Size = 18.6 microns
Concentration = 11.0 mg/l
Percent
Grain Size (microns)

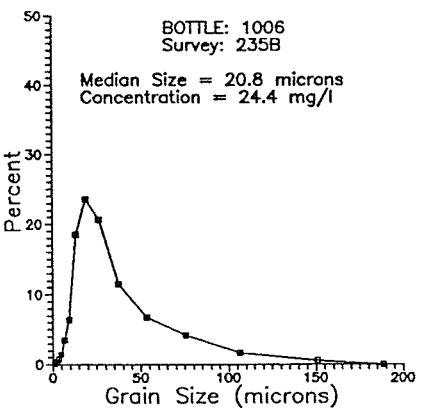
BOTTLE: 1006
Survey: 235B
Median Size = 20.8 microns
Concentration = 24.4 mg/l
Percent
Grain Size (microns)

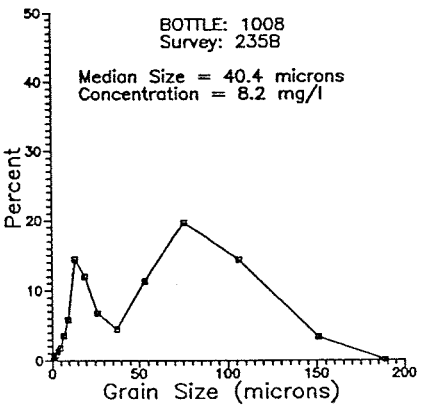
BOTTLE: 1008
Survey: 235B
Median Size = 40.4 microns
Concentration = 8.2 mg/l
Percent
Grain Size (microns)

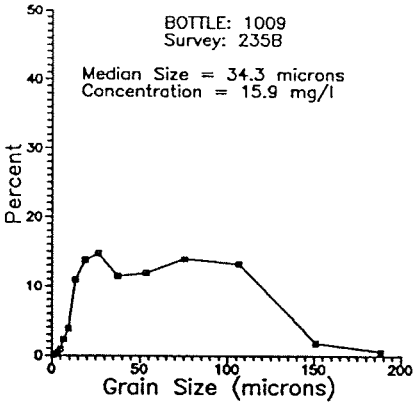
BOTTLE: 1009
Survey: 235B
Median Size = 34.3 microns
Concentration = 15.9 mg/l
Percent
Grain Size (microns)

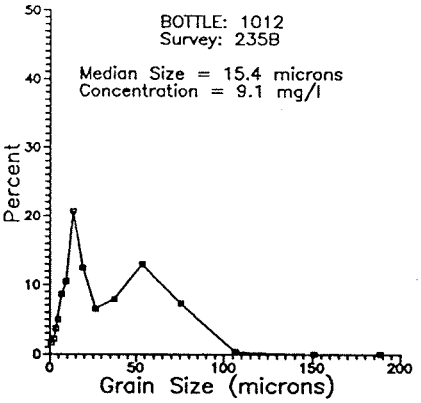
BOTTLE: 1012
Survey: 235B
Median Size = 15.4 microns
Concentration = 9.1 mg/l
Percent
Grain Size (microns)

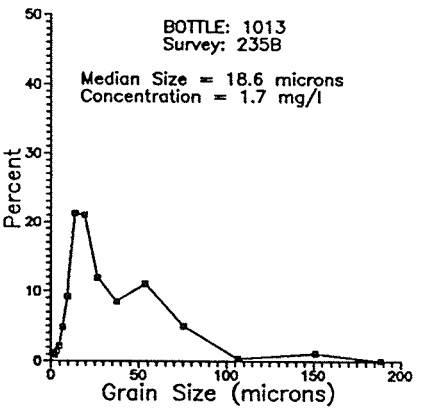
BOTTLE: 1013
Survey: 235B
Median Size = 18.6 microns
Concentration = 1.7 mg/l
Percent
Grain Size (microns)

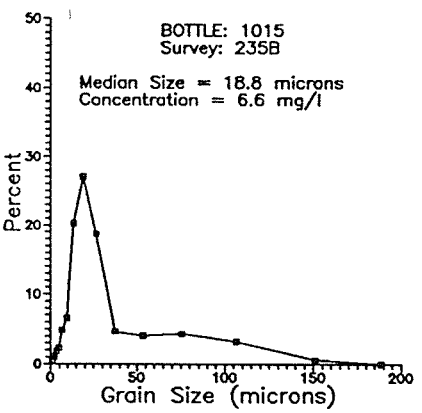
BOTTLE: 1015
Survey: 235B
Median Size = 18.8 microns
Concentration = 6.6 mg/l
Percent
Grain Size (microns)

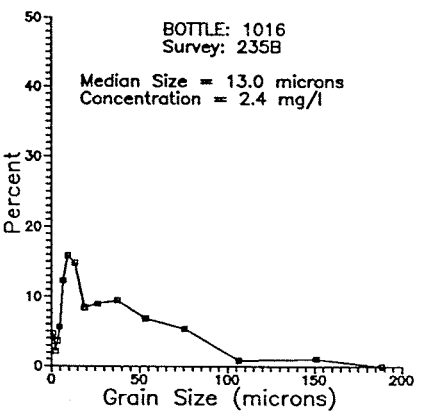
BOTTLE: 1016
Survey: 235B
Median Size = 13.0 microns
Concentration = 2.4 mg/l
Percent
Grain Size (microns)

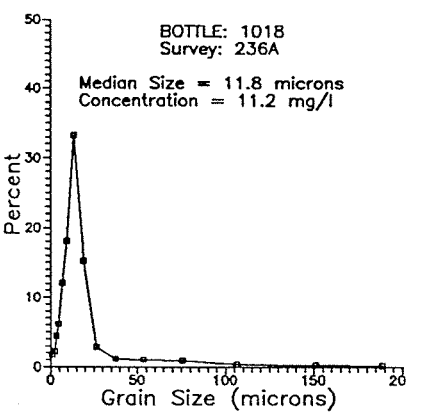
BOTTLE: 1018
Survey: 236A
Median Size = 11.8 microns
Concentration = 11.2 mg/l
Percent
Grain Size (microns)

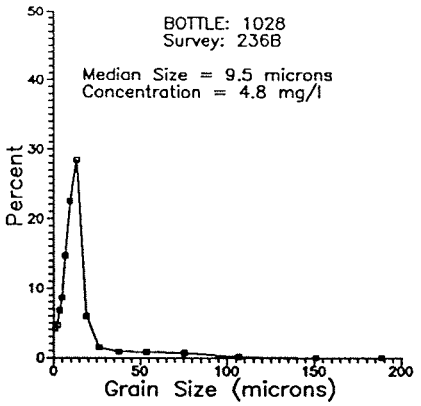
BOTTLE: 1028
Survey: 236B
Median Size = 9.5 microns
Concentration = 4.8 mg/l
Percent
Grain Size (microns)

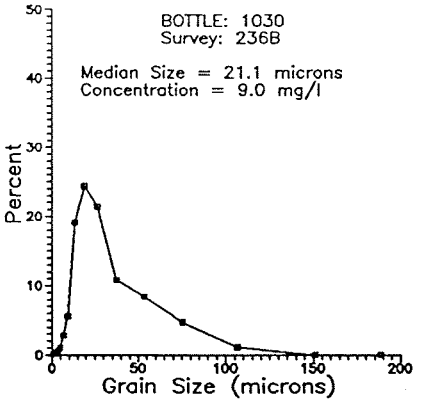
BOTTLE: 1030
Survey: 236B
Median Size = 21.1 microns
Concentration = 9.0 mg/l
Percent
Grain Size (microns)

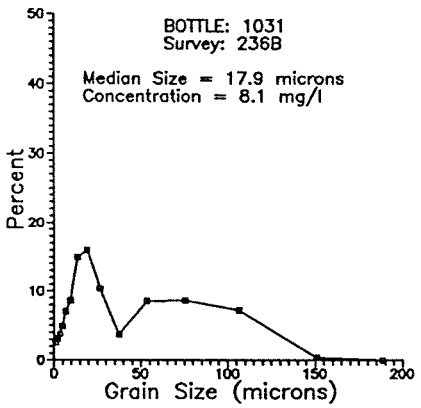
BOTTLE: 1031
Survey: 236B
Median Size = 17.9 microns
Concentration = 8.1 mg/l
Percent
Grain Size (microns)

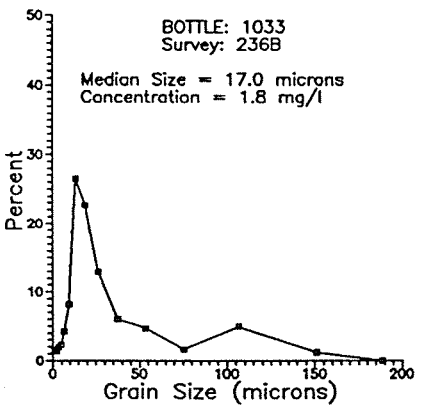
BOTTLE: 1033
Survey: 236B
Median Size = 17.0 microns
Concentration = 1.8 mg/l
Percent
Grain Size (microns)

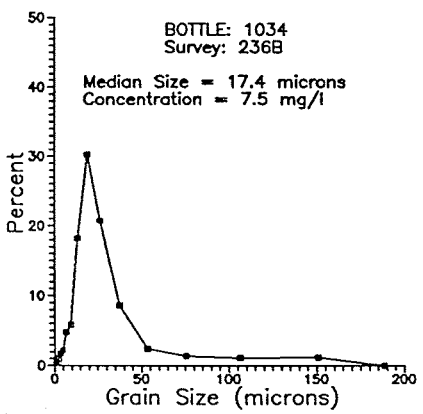
BOTTLE: 1034
Survey: 236B
Median Size = 17.4 microns
Concentration = 7.5 mg/l
Percent
Grain Size (microns)

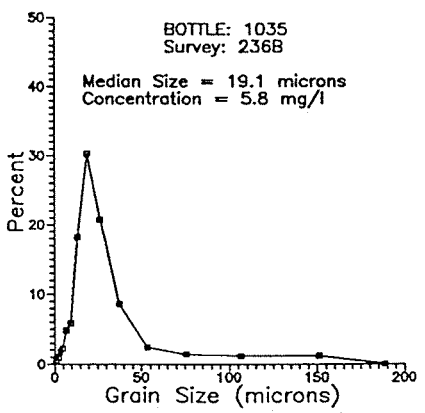
BOTTLE: 1035
Survey: 236B
Median Size = 19.1 microns
Concentration = 5.8 mg/l
Percent
Grain Size (microns)

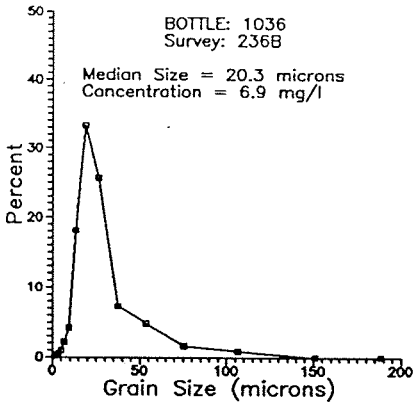
BOTTLE: 1036
Survey: 236B
Median Size = 20.3 microns
Concentration = 6.9 mg/l
Percent
Grain Size (microns)

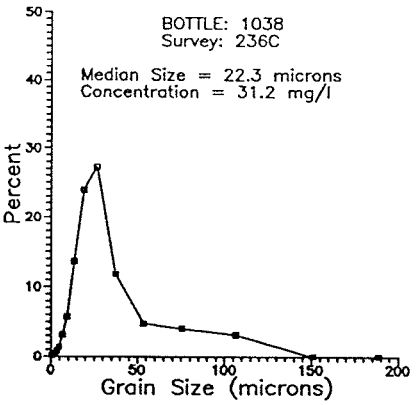
BOTTLE: 1038
Survey: 236C
Median Size = 22.3 microns
Concentration = 31.2 mg/l
Percent
Grain Size (microns)

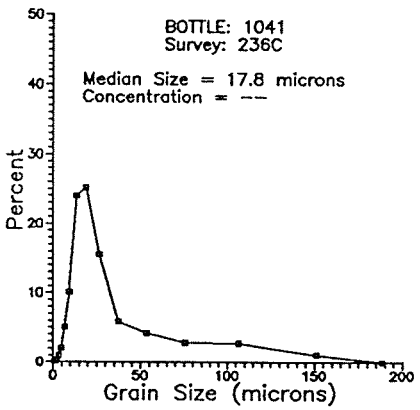
BOTTLE: 1041
Survey: 236C
Median Size = 17.8 microns
Concentration = --
Percent
Grain Size (microns)

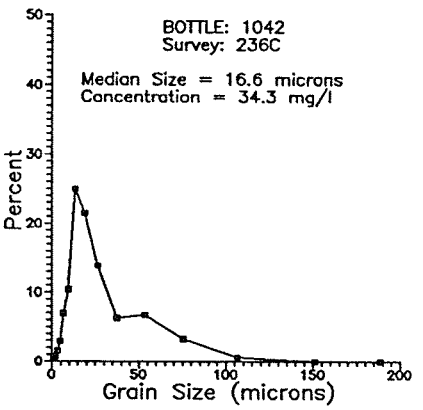
BOTTLE: 1042
Survey: 236C
Median Size = 16.6 microns
Concentration = 34.3 mg/l
Percent
Grain Size (microns)

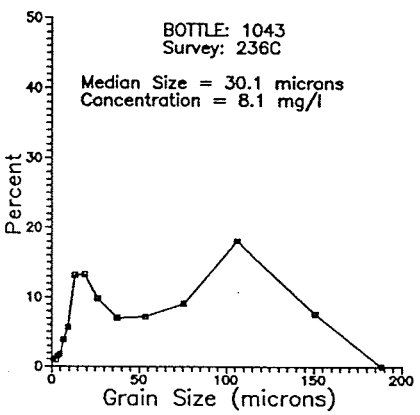
BOTTLE: 1043
Survey: 236C
Median Size = 30.1 microns
Concentration = 8.1 mg/l
Percent
Grain Size (microns)

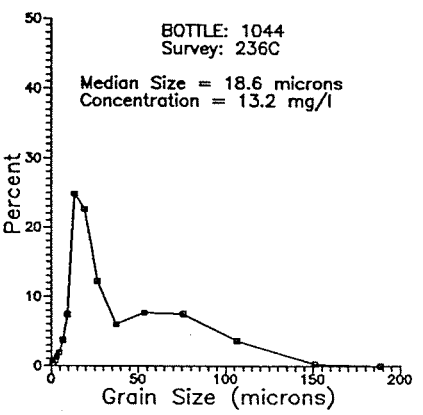
BOTTLE: 1044
Survey: 236C
Median Size = 18.6 microns
Concentration = 13.2 mg/l
Percent
Grain Size (microns)

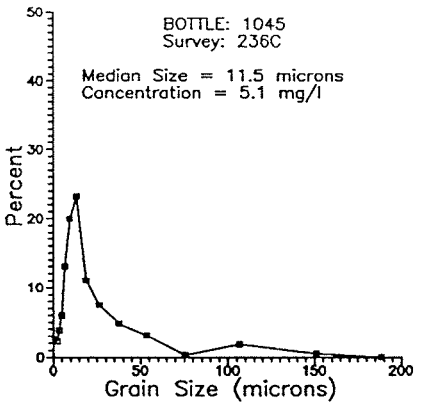
BOTTLE: 1045
Survey: 236C
Median Size = 11.5 microns
Concentration = 5.1 mg/l
Percent
Grain Size (microns)

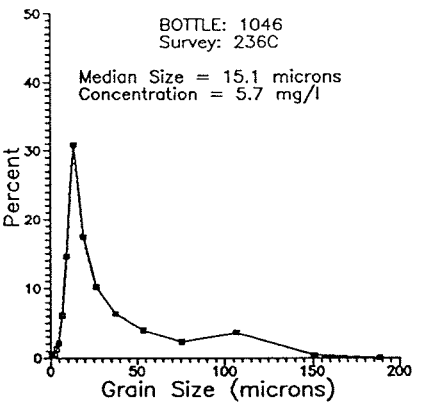
BOTTLE: 1046
Survey: 236C
Median Size = 15.1 microns
Concentration = 5.7 mg/l
Percent
Grain Size (microns)

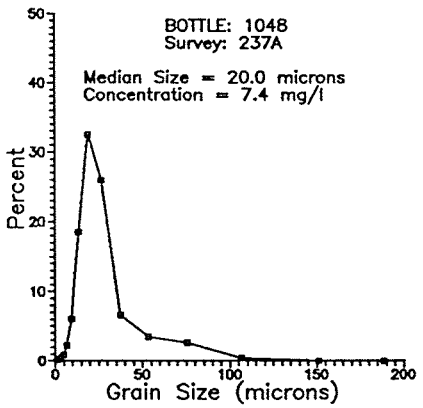
BOTTLE: 1048
Survey: 237A
Median Size = 20.0 microns
Concentration = 7.4 mg/l
Percent
Grain Size (microns)

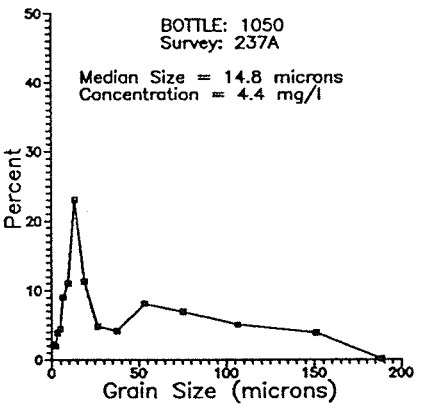
BOTTLE: 1050
Survey: 237A
Median Size = 14.8 microns
Concentration = 4.4 mg/l
Percent
Grain Size (microns)

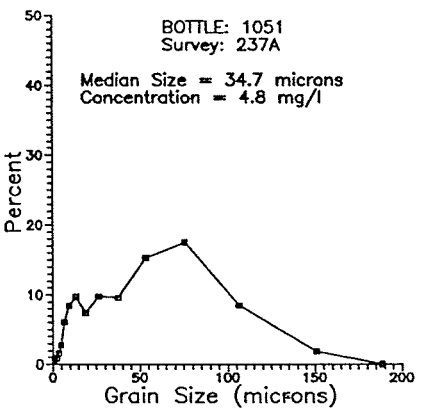
BOTTLE: 1051
Survey: 237A
Median Size = 34.7 microns
Concentration = 4.8 mg/l
Percent
Grain Size (microns)

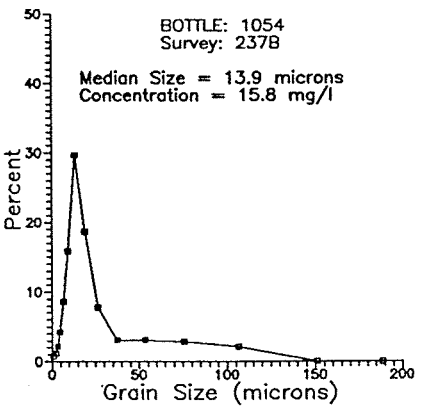
BOTTLE: 1054
Survey: 237B
Median Size = 13.9 microns
Concentration = 15.8 mg/l
Percent
Grain Size (microns)

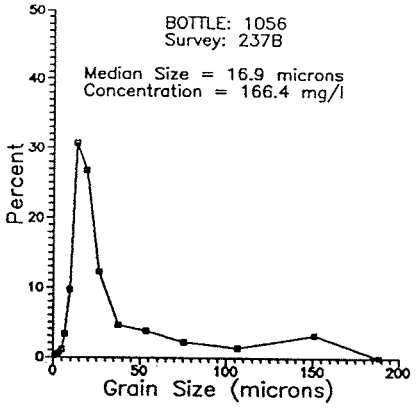
BOTTLE: 1056
Survey: 237B
Median Size = 16.9 microns
Concentration = 166.4 mg/l
Percent
Grain Size (microns)

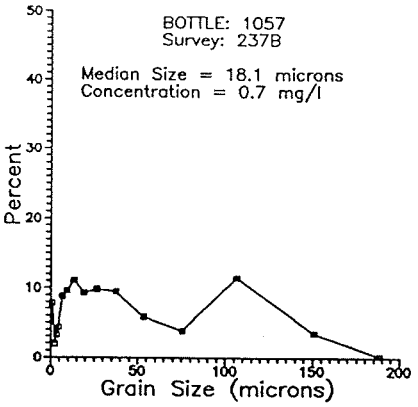
BOTTLE: 1057
Survey: 237B
Median Size = 18.1 microns
Concentration = 0.7 mg/l
Percent
Grain Size (microns)

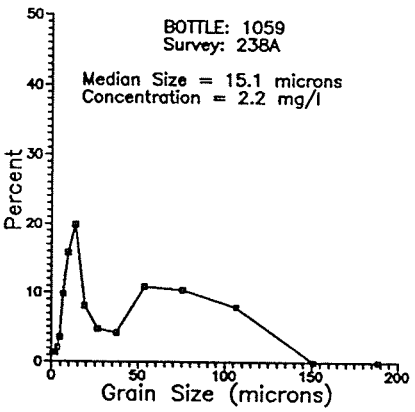
BOTTLE: 1059
Survey: 238A
Median Size = 15.1 microns
Concentration = 2.2 mg/l
Percent
Grain Size (microns)

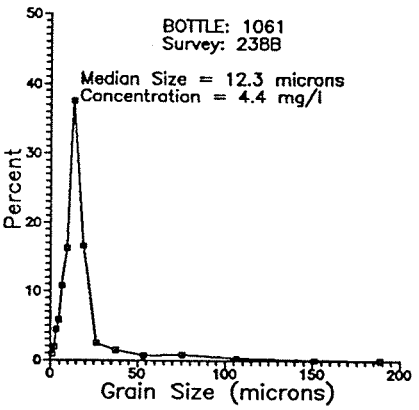
BOTTLE: 1061
Survey: 238B
Median Size = 12.3 microns
Concentration = 4.4 mg/l
Percent
Grain Size (microns)

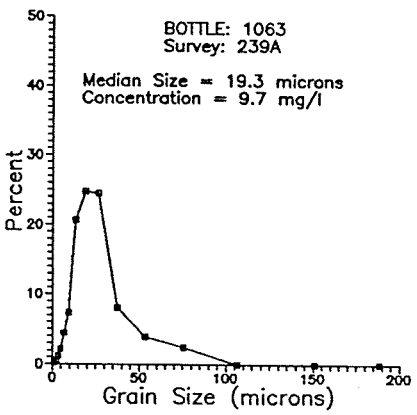
BOTTLE: 1063
Survey: 239A
Median Size = 19.3 microns
Concentration = 9.7 mg/l
Percent
Grain Size (microns)

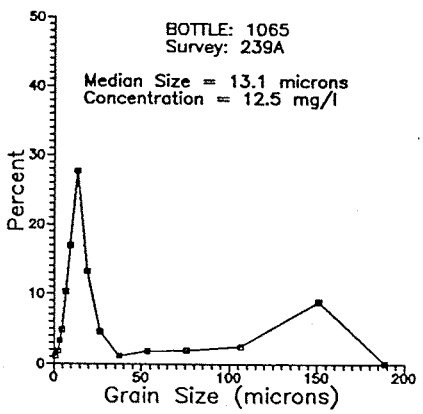
BOTTLE: 1065
Survey: 239A
Median Size = 13.1 microns
Concentration = 12.5 mg/l
Percent
Grain Size (microns)

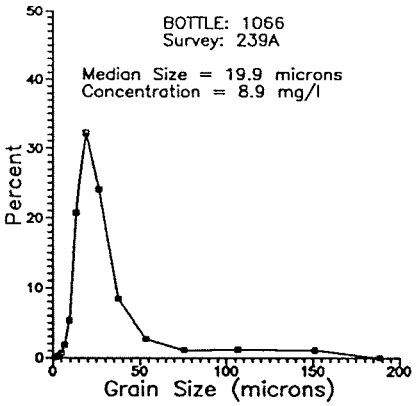
BOTTLE: 1066
Survey: 239A
Median Size = 19.9 microns
Concentration = 8.9 mg/l
Percent
Grain Size (microns)

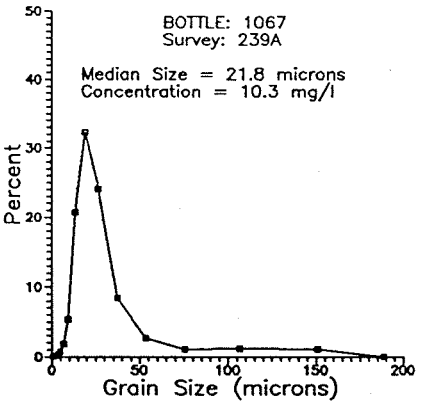
BOTTLE: 1067
Survey: 239A
Median Size = 21.8 microns
Concentration = 10.3 mg/l
Percent
Grain Size (microns)

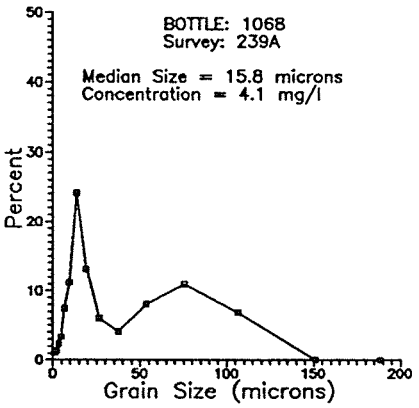
BOTTLE: 1068
Survey: 239A
Median Size = 15.8 microns
Concentration = 4.1 mg/l
Percent
Grain Size (microns)

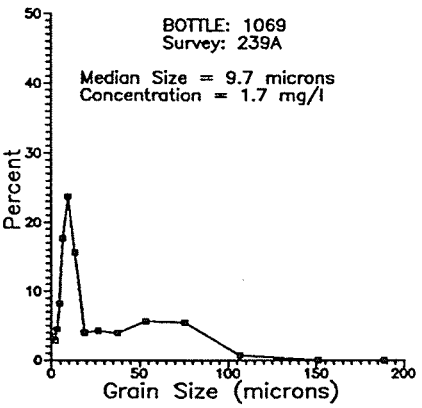
BOTTLE: 1069
Survey: 239A
Median Size = 9.7 microns
Concentration = 1.7 mg/l
Percent
Grain Size (microns)

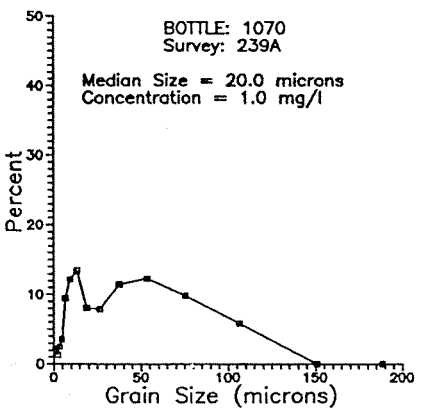
BOTTLE: 1070
Survey: 239A
Median Size = 20.0 microns
Concentration = 1.0 mg/l
Percent
Grain Size (microns)

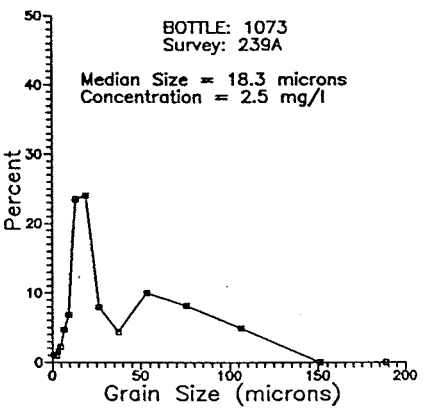
BOTTLE: 1073
Survey: 239A
Median Size = 18.3 microns
Concentration = 2.5 mg/l
Percent
Grain Size (microns)

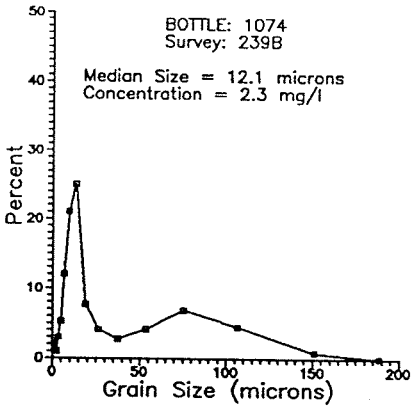
BOTTLE: 1074
Survey: 239B
Median Size = 12.1 microns
Concentration = 2.3 mg/l
Percent
Grain Size (microns)

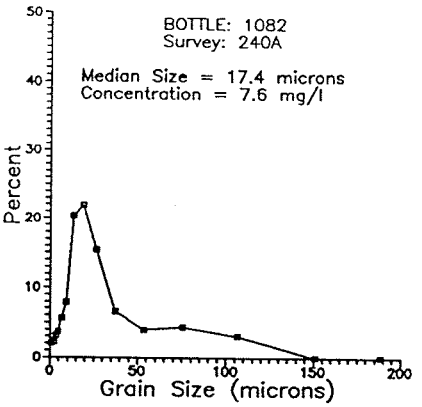
BOTTLE: 1082
Survey: 240A
Median Size = 17.4 microns
Concentration = 7.6 mg/l
Percent
Grain Size (microns)

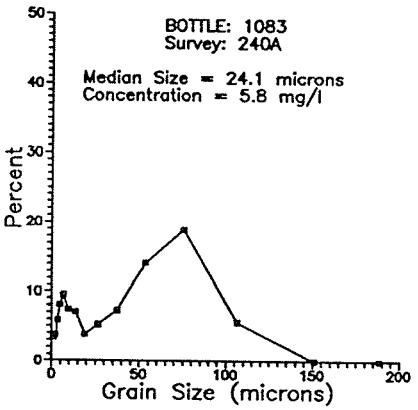
BOTTLE: 1083
Survey: 240A
Median Size = 24.1 microns
Concentration = 5.8 mg/l
Percent
Grain Size (microns)

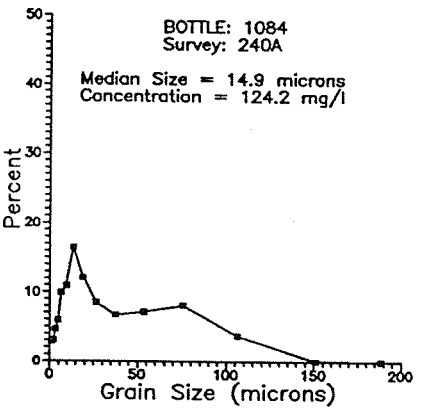
BOTTLE: 1084
Survey: 240A
Median Size = 14.9 microns
Concentration = 124.2 mg/l
Percent
Grain Size (microns)

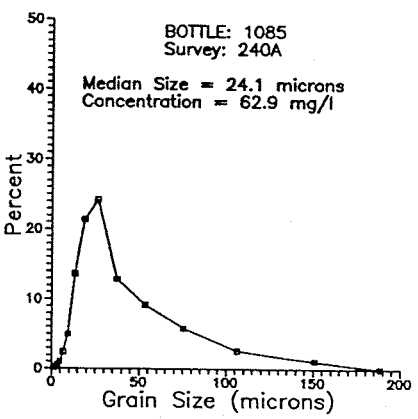
BOTTLE: 1085
Survey: 240A
Median Size = 24.1 microns
Concentration = 62.9 mg/l
Percent
Grain Size (microns)

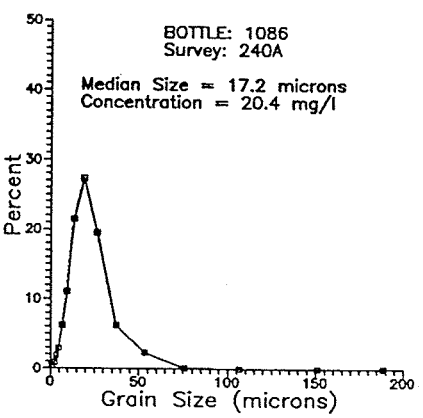
BOTTLE: 1086
Survey: 240A
Median Size = 17.2 microns
Concentration = 20.4 mg/l
Percent
Grain Size (microns)

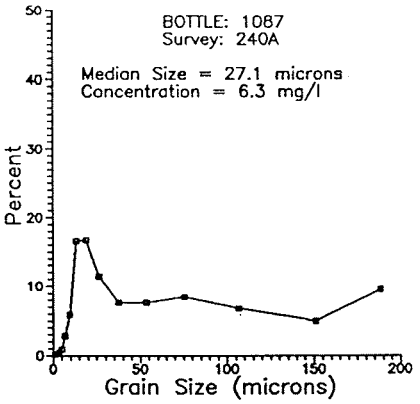
BOTTLE: 1087
Survey: 240A
Median Size = 27.1 microns
Concentration = 6.3 mg/l
Percent
Grain Size (microns)

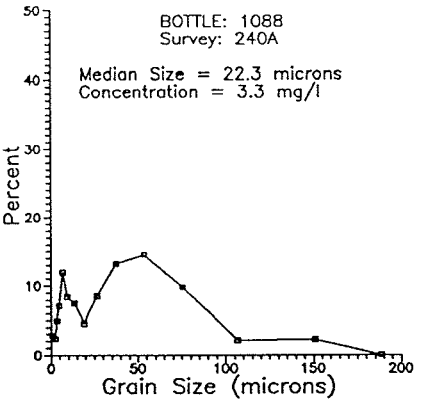
BOTTLE: 1088
Survey: 240A
Median Size = 22.3 microns
Concentration = 3.3 mg/l
Percent
Grain Size (microns)

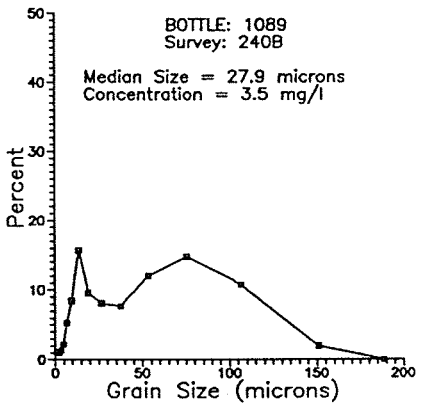
BOTTLE: 1089
Survey: 240B
Median Size = 27.9 microns
Concentration = 3.5 mg/l
Percent
Grain Size (microns)

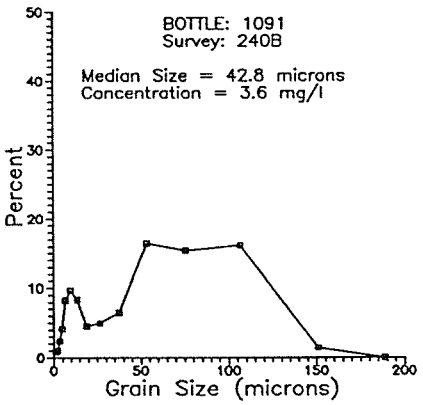
BOTTLE: 1091
Survey: 240B
Median Size = 42.8 microns
Concentration = 3.6 mg/l
Percent
Grain Size (microns)

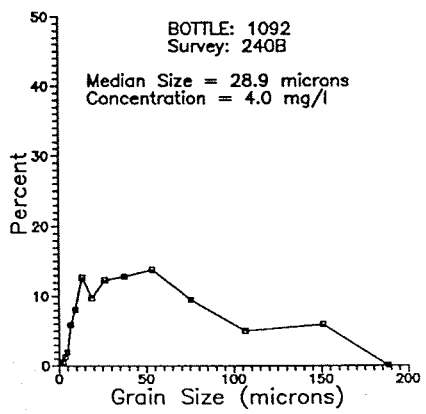
BOTTLE: 1092
Survey: 240B
Median Size = 28.9 microns
Concentration = 4.0 mg/l
Percent
Grain Size (microns)

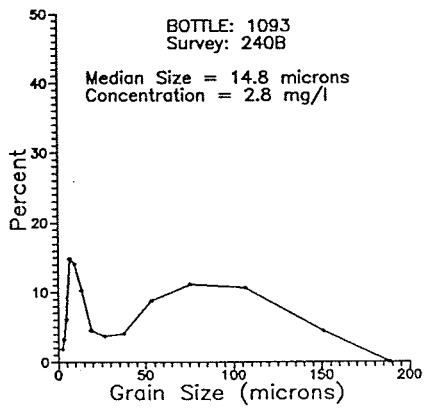
BOTTLE: 1093
Survey: 240B
Median Size = 14.8 microns
Concentration = 2.8 mg/l
Percent
Grain Size (microns)

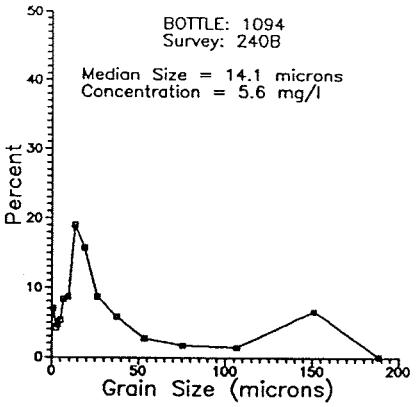
BOTTLE: 1094
Survey: 240B
Median Size = 14.1 microns
Concentration = 5.6 mg/l
Percent
Grain Size (microns)

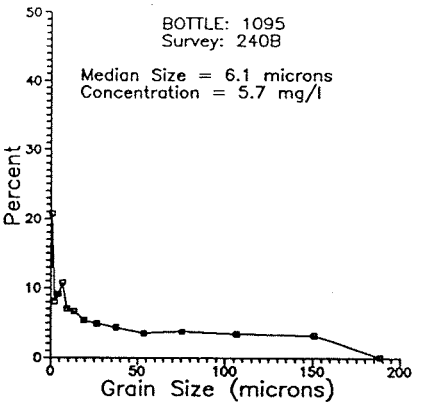
BOTTLE: 1095
Survey: 240B
Median Size = 6.1 microns
Concentration = 5.7 mg/l
Percent
Grain Size (microns)

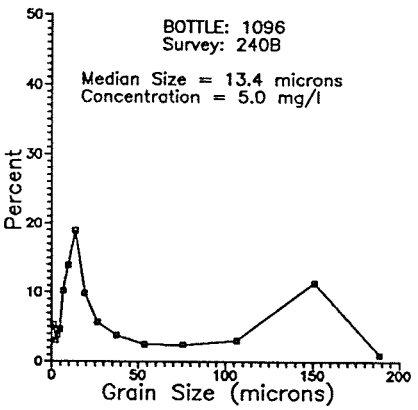
BOTTLE: 1096
Survey: 240B
Median Size = 13.4 microns
Concentration = 5.0 mg/l
Percent
Grain Size (microns)

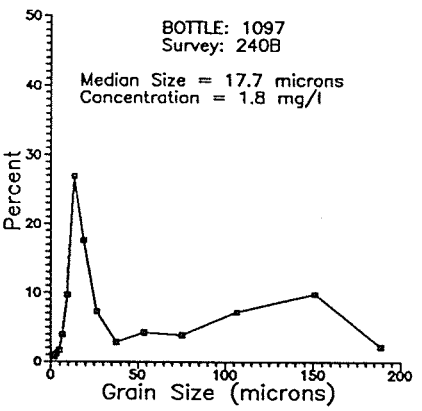
BOTTLE: 1097
Survey: 240B
Median Size = 17.7 microns
Concentration = 1.8 mg/l
Percent
Grain Size (microns)

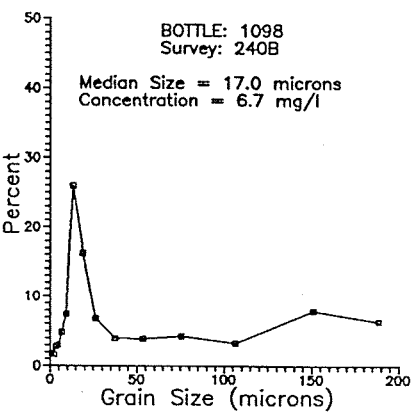
BOTTLE: 1098
Survey: 240B
Median Size = 17.0 microns
Concentration = 6.7 mg/l
Percent
Grain Size (microns)

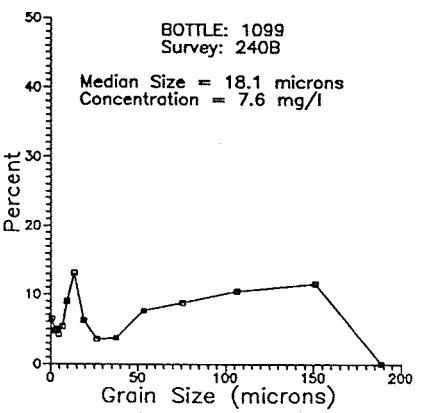
BOTTLE: 1099
Survey: 240B
Median Size = 18.1 microns
Concentration = 7.6 mg/l
Percent
Grain Size (microns)

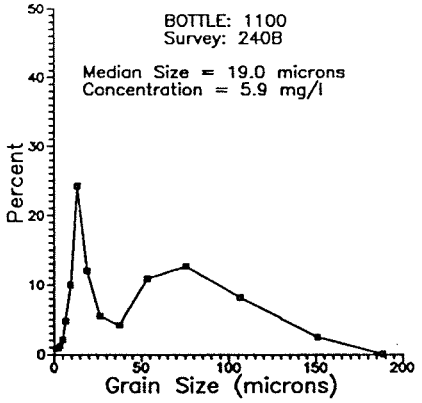
BOTTLE: 1100
Survey: 240B
Median Size = 19.0 microns
Concentration = 5.9 mg/l
Percent
Grain Size (microns)

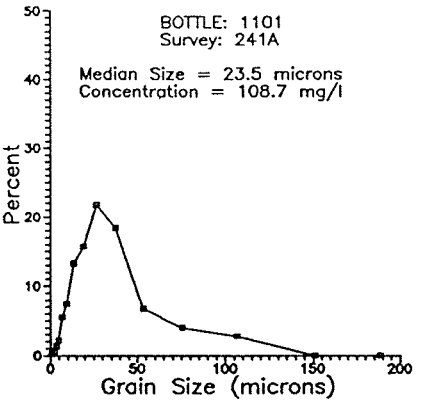
BOTTLE: 1101
Survey: 241A
Median Size = 23.5 microns
Concentration = 108.7 mg/l
Percent
Grain Size (microns)

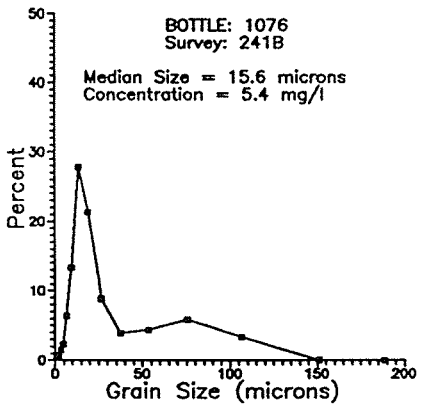
BOTTLE: 1076
Survey: 241B
Median Size = 15.6 microns
Concentration = 5.4 mg/l
Percent
Grain Size (microns)

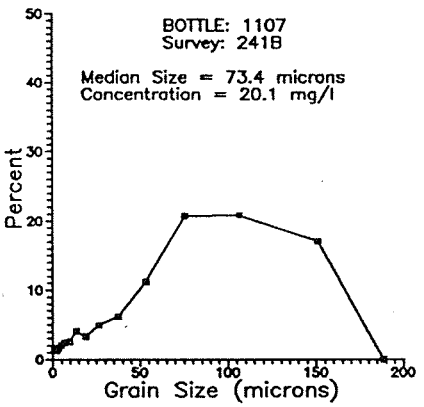
BOTTLE: 1107
Survey: 241B
Median Size = 73.4 microns
Concentration = 20.1 mg/l
Percent
Grain Size (microns)

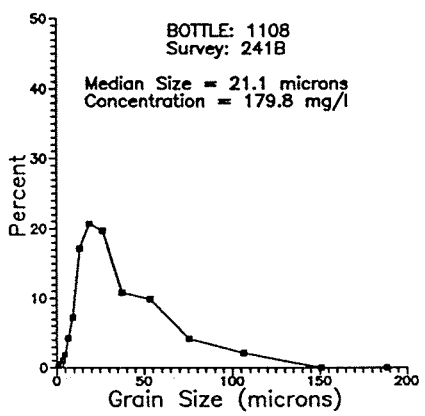
BOTTLE: 1108
Survey: 241B
Median Size = 21.1 microns
Concentration = 179.8 mg/l
Percent
Grain Size (microns)

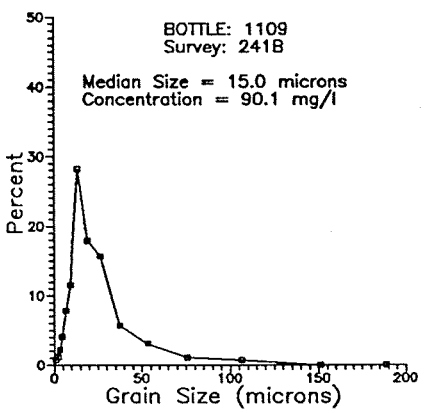
BOTTLE: 1109
Survey: 241B
Median Size = 15.0 microns
Concentration = 90.1 mg/l
Percent
Grain Size (microns)

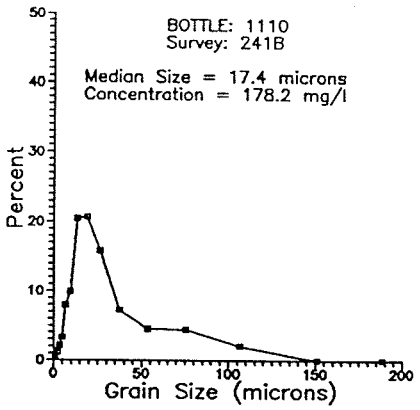
BOTTLE: 1110
Survey: 241B
Median Size = 17.4 microns
Concentration = 178.2 mg/l
Percent
Grain Size (microns)

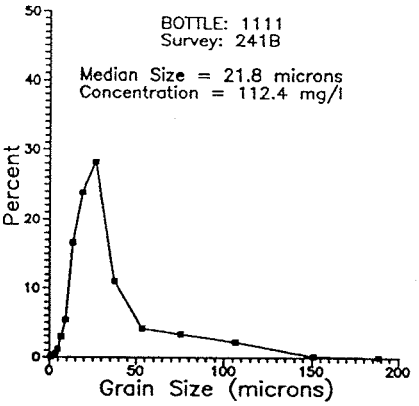
BOTTLE: 1111
Survey: 241B
Median Size = 21.8 microns
Concentration = 112.4 mg/l
Percent
Grain Size (microns)

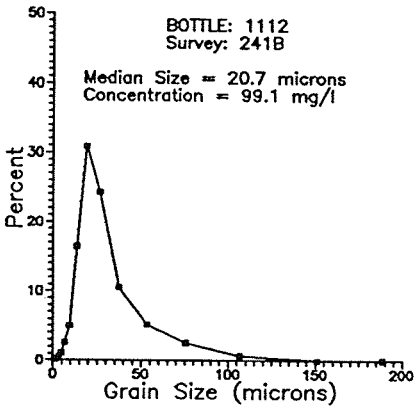
BOTTLE: 1112
Survey: 241B
Median Size = 20.7 microns
Concentration = 99.1 mg/l
Percent
Grain Size (microns)

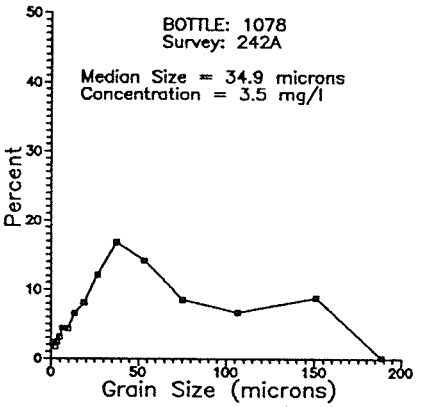
BOTTLE: 1078
Survey: 242A
Median Size = 34.9 microns
Concentration = 3.5 mg/l
Percent
Grain Size (microns)

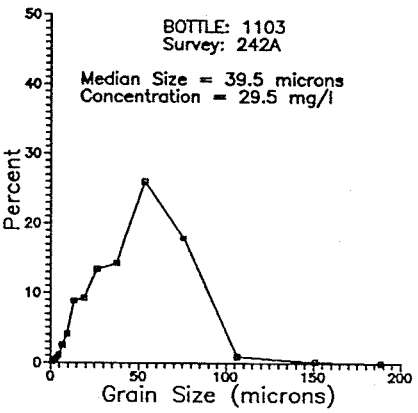
BOTTLE: 1103
Survey: 242A
Median Size = 39.5 microns
Concentration = 29.5 mg/l
Percent
Grain Size (microns)

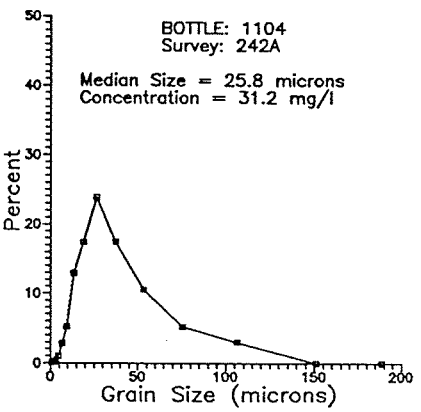
BOTTLE: 1104
Survey: 242A
Median Size = 25.8 microns
Concentration = 31.2 mg/l
Percent
Grain Size (microns)

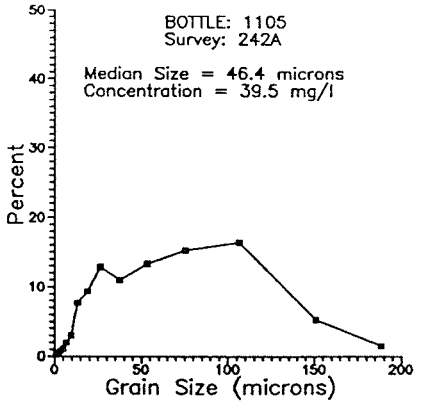
BOTTLE: 1105
Survey: 242A
Median Size = 46.4 microns
Concentration = 39.5 mg/l
Percent
Grain Size (microns)

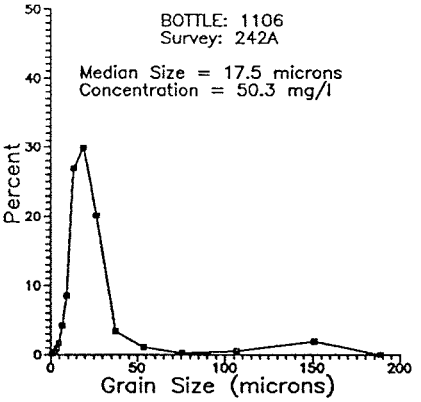
BOTTLE: 1106
Survey: 242A
Median Size = 17.5 microns
Concentration = 50.3 mg/l
Percent
Grain Size (microns)

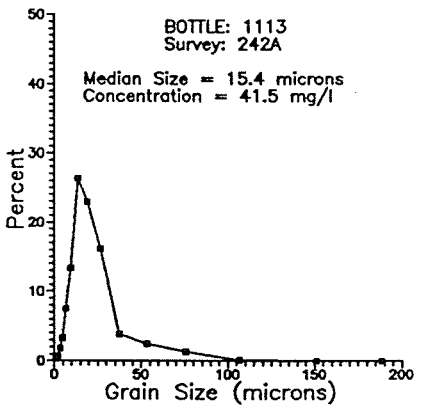
BOTTLE: 1113
Survey: 242A
Median Size = 15.4 microns
Concentration = 41.5 mg/l
Percent
Grain Size (microns)

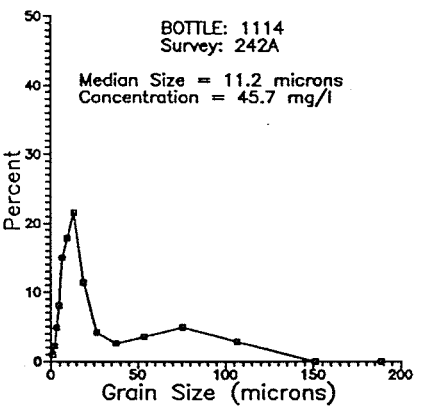
BOTTLE: 1114
Survey: 242A
Median Size = 11.2 microns
Concentration = 45.7 mg/l
Percent
Grain Size (microns)

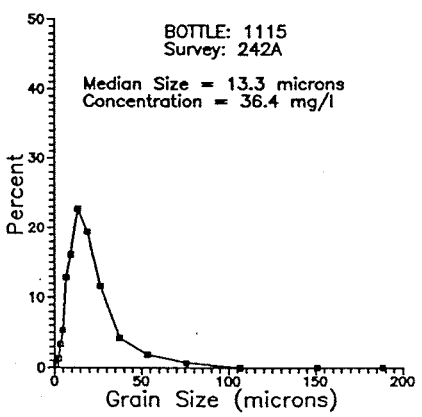
BOTTLE: 1115
Survey: 242A
Median Size = 13.3 microns
Concentration = 36.4 mg/l
Percent
Grain Size (microns)

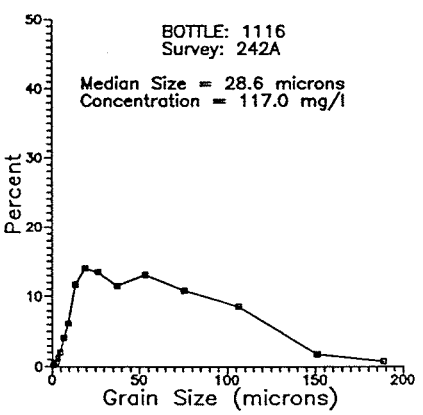
BOTTLE: 1116
Survey: 242A
Median Size = 28.6 microns
Concentration = 117.0 mg/l
Percent
Grain Size (microns)

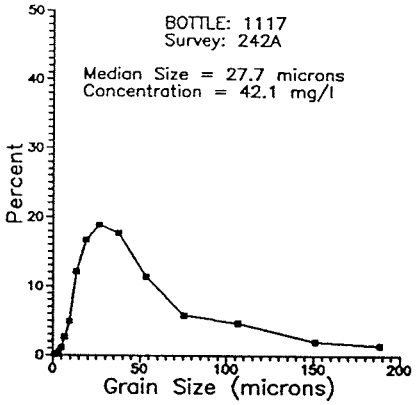
BOTTLE: 1117
Survey: 242A
Median Size = 27.7 microns
Concentration = 42.1 mg/l
Percent
Grain Size (microns)

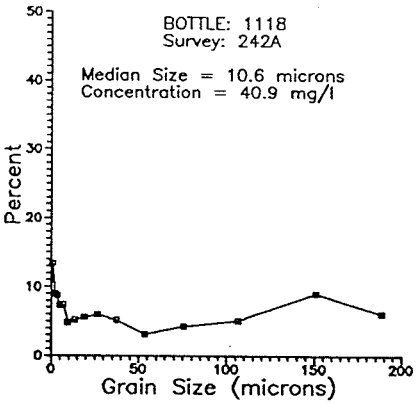
BOTTLE: 1118
Survey: 242A
Median Size = 10.6 microns
Concentration = 40.9 mg/l
Percent
Grain Size (microns)

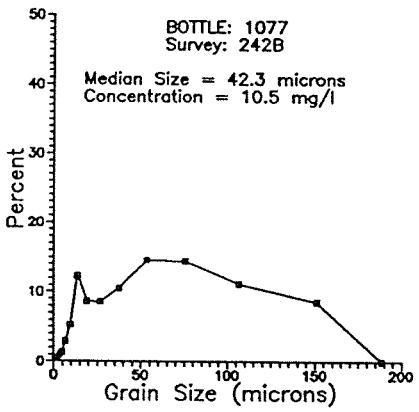
BOTTLE: 1077
Survey: 242B
Median Size = 42.3 microns
Concentration = 10.5 mg/l
Percent
Grain Size (microns)

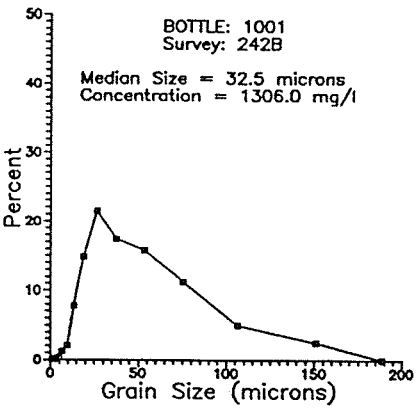
BOTTLE: 1001
Survey: 242B
Median Size = 32.5 microns
Concentration = 1306.0 mg/l
Percent
Grain Size (microns)

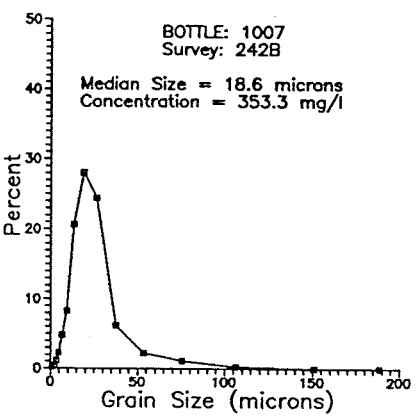
BOTTLE: 1007
Survey: 242B
Median Size = 18.6 microns
Concentration = 353.3 mg/l
Percent
Grain Size (microns)

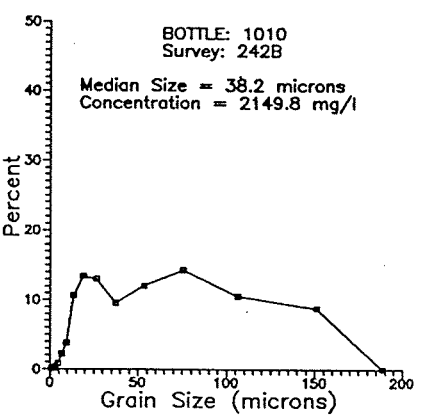
BOTTLE: 1010
Survey: 242B
Median Size = 38.2 microns
Concentration = 2149.8 mg/l
Percent
Grain Size (microns)

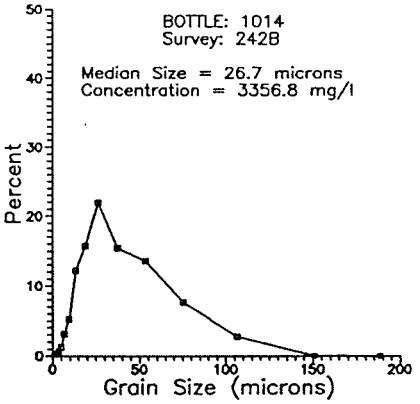
BOTTLE: 1014
Survey: 242B
Median Size = 26.7 microns
Concentration = 3356.8 mg/l
Percent
Grain Size (microns)

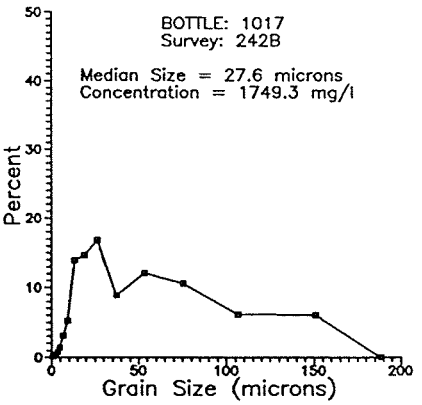
BOTTLE: 1017
Survey: 242B
Median Size = 27.6 microns
Concentration = 1749.3 mg/l
Percent
Grain Size (microns)

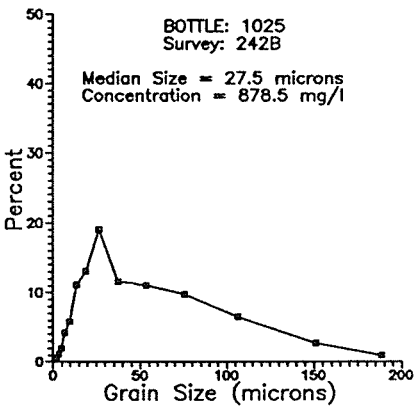
BOTTLE: 1025
Survey: 242B
Median Size = 27.5 microns
Concentration = 878.5 mg/l
Percent
Grain Size (microns)

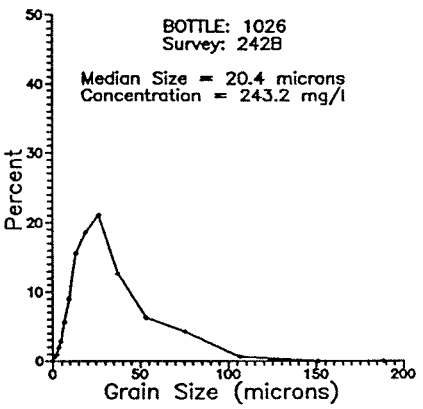
BOTTLE: 1026
Survey: 242B
Median Size = 20.4 microns
Concentration = 243.2 mg/l
Percent
Grain Size (microns)

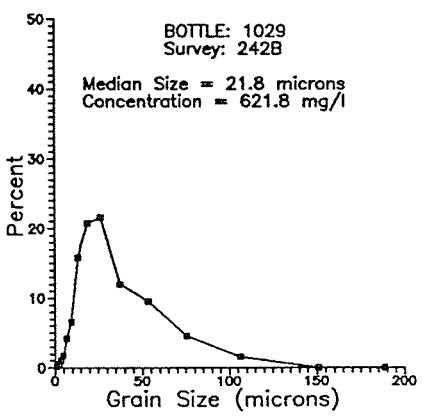
BOTTLE: 1029
Survey: 242B
Median Size = 21.8 microns
Concentration = 621.8 mg/l
Percent
Grain Size (microns)

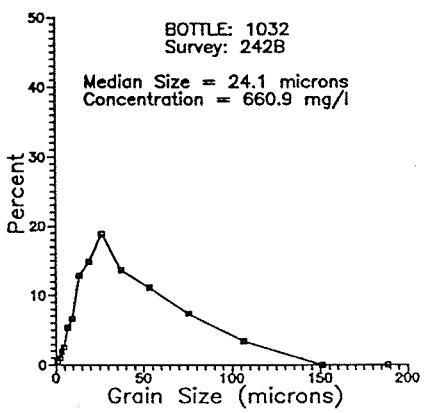
BOTTLE: 1032
Survey: 242B
Median Size = 24.1 microns
Concentration = 660.9 mg/l
Percent
Grain Size (microns)

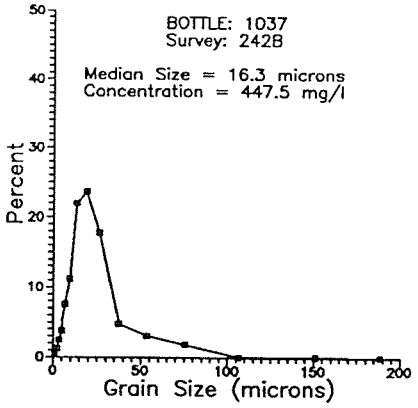
BOTTLE: 1037
Survey: 242B
Median Size = 16.3 microns
Concentration = 447.5 mg/l
Percent
Grain Size (microns)

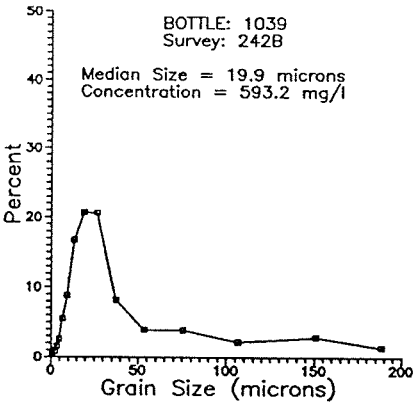
BOTTLE: 1039
Survey: 242B
Median Size = 19.9 microns
Concentration = 593.2 mg/l
Percent
Grain Size (microns)

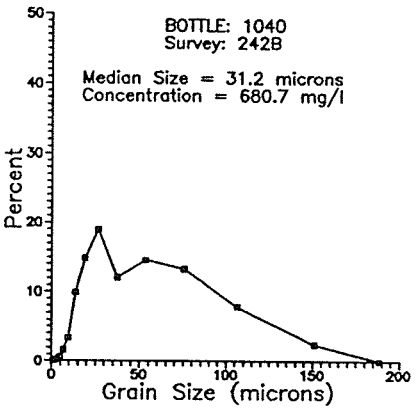
BOTTLE: 1040
Survey: 242B
Median Size = 31.2 microns
Concentration = 680.7 mg/l
Percent
Grain Size (microns)

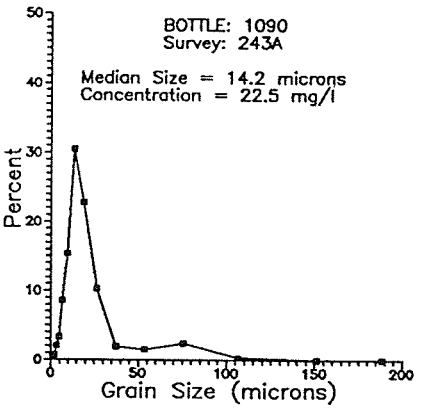
BOTTLE: 1090
Survey: 243A
Median Size = 14.2 microns
Concentration = 22.5 mg/l
Percent
Grain Size (microns)

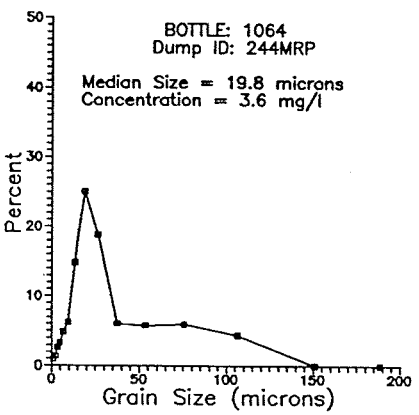
BOTTLE: 1064
Dump ID: 244MRP
Median Size = 19.8 microns
Concentration = 3.6 mg/l
Percent
Grain Size (microns)

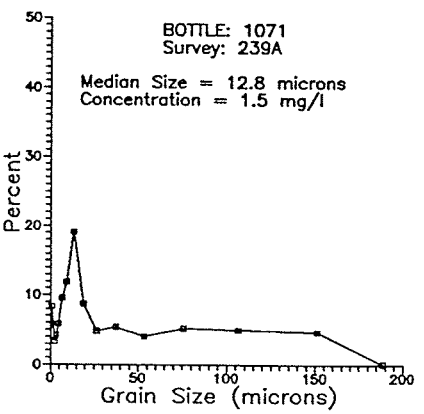
BOTTLE: 1071
Survey: 239A
Median Size = 12.8 microns
Concentration = 1.5 mg/l
Percent
Grain Size (microns)

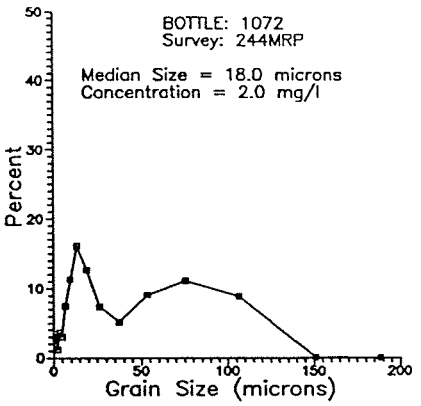
BOTTLE: 1072
Survey: 244MRP
Median Size = 18.0 microns
Concentration = 2.0 mg/l
Percent
Grain Size (microns)

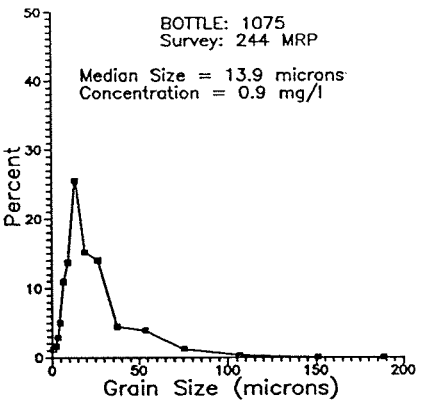
BOTTLE: 1075
Survey: 244 MRP
Median Size = 13.9 microns
Concentration = 0.9 mg/l
Percent
Grain Size (microns)

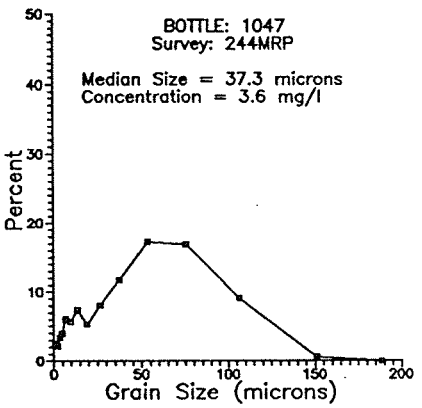
BOTTLE: 1047
Survey: 244MRP
Median Size = 37.3 microns
Concentration = 3.6 mg/l
Percent
Grain Size (microns)

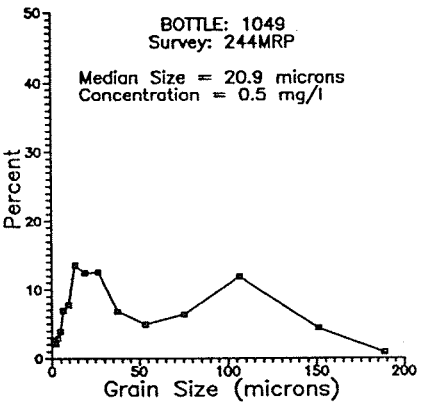
BOTTLE: 1049
Survey: 244MRP
Median Size = 20.9 microns
Concentration = 0.5 mg/l
Percent
Grain Size (microns)

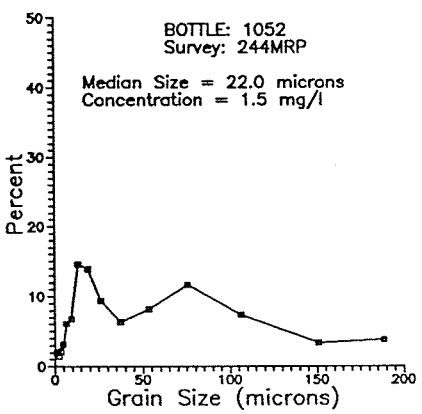
BOTTLE: 1052
Survey: 244MRP
Median Size = 22.0 microns
Concentration = 1.5 mg/l
Percent
Grain Size (microns)

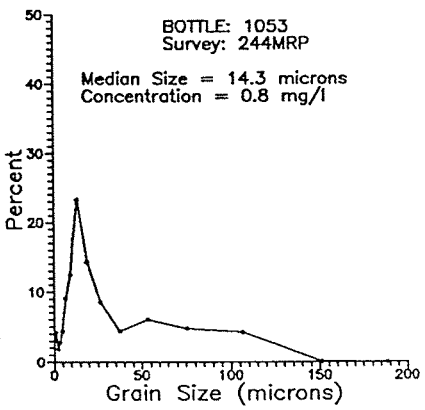
BOTTLE: 1053
Survey: 244MRP
Median Size = 14.3 microns
Concentration = 0.8 mg/l
Percent
Grain Size (microns)

5. MEASUREMENTS WITH AN ACOUSTIC DOPPLER CURRENT PROFILER (ADCP)

ATLE LOHRMANN, CHRISTOPHER A. HUMPHREY

RD Instruments
San Diego, California 92131

Contents

1. Introduction

Acoustic Doppler Current Profilers (ADCP) transmit short acoustic pulses along narrow beams at a known, fixed frequency (from a nominal 75 to 1,200 kHz, depending on the transducer). The ADCP listens to and processes the echoes from successive volumes (depth cells or bins) along the beams to determine by how much the frequency has changed. The difference in frequency between transmitted and reflected sound is proportional to the relative velocity between the ADCP and the scatterers in the water that produce the reflection (backscattering). This frequency change is called the Doppler shift. The ADCP uses an autocovariance method to compute the mean value (first moment) of the Doppler frequency, and the velocity of the scatterers is determined from this value. Data are output from the ADCP digitally and are displayed, recorded, and further processed on a microcomputer.

Sound is scattered by small particles of suspended sediment and zooplankton. These small particles tend to move with the water current, thus providing an estimate of the current velocity. Reflections from fish are infrequent and rarely affect the measurements.

The ADCP uses four beams to estimate current velocity. The standard configuration of each of these four beams is 30 deg relative to the vertical in 90-deg azimuth increments (Figure 5.1). Multiple beams are required because an ADCP measures only the velocity component parallel to the beam. Through range gating, i.e., analysis of the return signal in increments of time, it is possible to compute velocity (and backscatter) in a series of contiguous, discrete ranges along each beam. These ranges are called depth cells.

The depth cell size is determined by the durations of both the range gate and the transmit pulse length. The range gate and transmit pulse are normally set to be equal; their durations are equal to twice the spacing between depth cells (using the speed of sound to convert between length and time coordinates). The first ADCP depth cell is defined as the one closest to the ADCP, and successive bins are contiguous and partially overlapping.

The ADCP measures the velocity along each of the four beams and thus four different volumes in each depth cell. If one assumes that the current at any given depth is the same through all four beams (the homogeneous velocity assumption (RD Instruments (RDI) 1989)), then the three-dimensional (3-D) velocity vector may be computed using trigonometry. Note that any three of the four beams are sufficient to calculate the 3-D velocity vector, and the fourth beam is

redundant. This redundancy allows evaluation of the homogeneous velocity assumption and permits detection of other possible errors in data quality.

For the Mobile, Alabama, Dredging Research Program Field Data Collection Project (MFDCP), the standard configuration (Figure 5.1) was slightly modified. One of the ADCP beams was orientated at 0 deg relative to the vertical (see Figure 5.2). This orientation allowed for a more robust estimate of the vertical velocity and the acoustic backscatter of materials within the plume through the water column to the Gulf bottom. The geometry of the remaining three beams was such that they were pointed 30 deg relative to vertical: two of which were directed fore and aft (along the longitudinal ship axis) and one directed starboard (perpendicular to the longitudinal ship axis).

The fore and aft beams, when combined trigonometrically, provided an additional estimate of velocity and backscatter intensity vertically, as well as an estimate of the relative pitch of the ship (which may introduce errors in velocity estimates). The ADCP was also amplitude calibrated. This established a relationship between the sampled amplitude ("counts") and the backscatter intensity, expressed in decibels (dB). A more detailed description of the amplitude calibration procedure is given in a later section and in Appendix 5A.

The ADCP allows estimation of the ship velocity and direction by bottom tracking, which is performed by transmitting a longer acoustic pulse than that used for water velocity profiling. Bottom tracking is not constrained by the need to have high vertical resolution, and, therefore, longer pulses may be used. The longer pulse, combined with the fact that the bottom is a strong localized reflector, makes it possible for the ADCP to bottom track deeper than it can water track, resulting in a small short-term variance. Further discussion of bottom tracking is included in a later section.

A significant relation between the strength of the ADCP amplitude signal and the presence of sediment plumes was observed during the MFDCP. The analysis of the ADCP backscatter amplitude consisted of three parts: evaluation of the instrument itself, comparison of the amplitude data with the collected sediment concentration samples, and an attempt to model the backscatter.

In addition to the amplitude data, the data set from this field data collection project includes a time series of accurate ship position data from a miniranger navigation system (Chapter 3, this report). This unique opportunity to compare the ADCP Doppler current velocity measurements with an accurate reference was taken, and the results are included in this chapter. The current

velocity data were analyzed to obtain the mean velocity as well as to evaluate possible sources of error in the mean velocity measurement during each disposal event. An analysis of the plume dynamics during two of the events is included. Conclusions and recommendations are given at the end of this chapter.

2. ADCP System: Hardware and Software

Hardware

The ADCP used on the MFDCP cruise was a 1.2-MHz vessel-mounted (VM) system deployed off the side of the ship. An interface with the ship compass (Figure 5.3) allowed computation of average ship velocity (and thus the velocity of the ADCP). Table 5.1 lists some of the parameters encompassed by the data collection.

Software

The software used to process and display the current velocity and acoustic backscatter was a pilot version of RDI's transect program. This program, presently under development, produces a real-time visual picture of the processes being observed. The following is a list of the primary capabilities of this software:

- Recording and playback of raw data in real-time.
- Calculation and display of estimated range-gated backscattering levels from all four beams (using a time series of profiles to create a color contour plot for each beam).
- Calculation and display of estimated vertical and horizontal velocity structure from all four beams. The displayed data are then available to be spatially averaged by using the bottom tracking capability of the ADCP to determine the distance traveled by the ship.
- Rapid surveying of multiple transects, allowing sequential display of backscattering intensity within the plume over time.
- Integration of position data into the recorded data.

3. Measurement of Sediment Concentration

An analysis of the relationship between acoustical backscattering (scattering cross section) and sediment concentration contains four elements. Each is essential to the analysis. The first element concerns system calibration in the ADCP and how the numbers (or counts) reported by the instrument correspond to the strength of scattering from the particles inside the ensonified volume of water. The results of RDI's effort on this subject is reported in Appendix 5A. The second element is a model for the contribution of the individual particles to the total backscattering cross section, for which the particles are assumed to behave as Rayleigh scatterers. This assumption is reasonable given that the size of the particles ($\approx$0.01 mm) is much smaller than the acoustic wavelength of the instrument ($\approx$1.25 mm). The third element to tie the analysis together is a set of field data. During the MFDCP, more that 100 bottle water samples were collected and their contents analyzed for concentration (dry weight per volume) and particle size distribution. Of this data set, samples from seven disposal events were used in the analysis. The fourth element is an error analysis.

Calibration of ADCP for backscatter

Calibration of the ADCP involves range-dependent and range-independent contributions. The range dependency involves the effects of geometrical spreading and water absorption. This dependency was removed in the real-time display by adding terms describing absorption ($2\alpha R$) and geometrical spreading (20 log R) to the receiver output (R is the range to the scattering layer along the beam in meters, and α the coefficient of absorption in decibels/meter). The range-independent (and instrument-dependent) part of the calibration was carried out before the field project. In addition, the calibration was improved upon after the project as a result of insight gained in the electronic circuitry that constitutes the response function of the ADCP. The main parameters found through the calibration procedure are the source level of the ADCP, the directional response of the transducer, and the response of the automatic gain control (AGC). Of these parameters, the directional response of the transducer is modeled once for each frequency, and the source level is measured for each beam. The AGC has proved to be much harder to characterize, and the results presented rely as much on modeling of the (temperature-dependent) circuitry as on actual calibration measurements. A typical response curve for the receiver circuitry measured at 22 deg C is shown in Figure 5.4. As can be seen, the response is linear (in log space)

over a dynamic range of 80 dB. In Table 5.2, the system parameters referred to in Appendix 5A are shown for the 1.2-MHz ADCP used on the *R/V Pelican* during the MFDCP.

Comparison with particle concentration

The accuracy of the comparison between the scattering cross section derived from the ADCP measurements and the particle concentration derived from the bottle samples involves several issues that are presently unresolved or can only be crudely estimated. Of special interest is the issue of how closely the bottle samples represent the overall sediment plume concentration. Throughout the MFDCP, the ship was nearly stationary with respect to surface currents during bottle sampling, and strong stratification and shear (vertical variation of horizontal currents) were present. Temporal variation of plume dispersion was the dominant time scale. Concentration of the falling dredged material changed on a scale of seconds to tens of seconds, and it was impossible to sample in situ concentrations faster than this time variation (Chapter 4, this report). As a result, the spatial variability in bottle-sampled particle concentration was large. The concentrations measured in this experiment show variations of up to +/-50 percent over a 1-min period, and it is difficult to estimate the actual uncertainty in the individual measurements. Ideal field sampling would close several water bottles simultaneously; however, because of the type of closing mechanism implemented for the water sampling rosette, this was not possible. Sample bottles were held open at each depth for at least 15 to 30 sec, before closing. This length of time is adequate for hydraulic flushing, but probably exceeds the time of variation in ambient concentration. Thus, for comparison to ADCP backscatter intensity measurements, a rough estimate of the uncertainty in the particle concentration obtained by the water sampling would be +/-3 dB (equivalent backscatter units).

Error analysis

Based on our knowledge of the ADCP, the range of temperatures during the field project, and the variation observed from beam to beam, we estimate the accuracy of the backscattering cross-section to be +/-3 dB. In addition to this absolute error, the problem remains of temporal and spatial variation in the amplitude data.

A first attempt at comparing the 1-sec averaged amplitude data with the measured concentrations led to a large spread in the data. A quality check and analysis procedure was implemented to improve accuracy and estimate the size and nature of the variation in the acoustic data. For the comparison between the two data sets, it was necessary to assume that the amplitude data and bottle samples were representative of the same water mass.

Temporal variation. As a first attempt at calibration, the amplitude data (sampled at 5 to 8 Hz) were averaged over the 10-sec period before the time of closing of the bottles. There are two principal reasons for this. To obtain a stable estimate of the amplitude, it is first necessary to average out the variation in the amplitude data produced by Rayleigh scattering. Second, the bottle samples must necessarily have a relatively long flushing period after they have been lowered. It is assumed that over this longer averaging period, the two data sets would more likely represent a similar temporal average. Finally, the standard deviation of the amplitude over this averaging period is used as a measure for indicating the added effect of blockage of the beam pattern. Interference could occasionally happen when the data logger, used to measure conductivity (C), temperature (T), and depth (D) (CTD), and attached to a rosette sampling apparatus (Chapter 4) blocked the transmitted pulse for one or more of the beams. By excluding all average data with a standard deviation greater than +/-3 dB, most of highly scattered data points were excluded.

In summary, the acoustic data have much better temporal resolution than the bottle samples. Because of the large spatial and temporal variations in the concentration inside the plume, bottle samples provide a crude magnitude estimate of the processes in action. This limitation also makes a comparison with acoustic data difficult. An example of the temporal variation in the amplitude data can be seen in Figure 5.5. This plot indicates the maximum variation over the 28-sec period is nearly 15 dB. Another example can be seen in Figure 5.6, where Beam 2 is blocked by the rosette.

Vertical variation. The vertical variation over the 10-sec period was calculated to quantify the uncertainty in the data and to exclude data points influenced by the bottom. Data with a standard deviation greater than +/-3 dB were excluded. This method was effective in eliminating data points that were influenced by the bottom or were found to be in the shadow of the CTD rosette.

The backscatter amplitude data proved to be sensitive to vertical variation at the start of the plume descent. Such data points pertaining to rapid evolution of the plume were not included in the comparison between concentration and acoustic scattering. An example of both the temporal and vertical variation in the volume backscattering can be seen in Figure 5.7.

For Survey 240B, Figure 5.7 shows contours of the backscatter amplitude data (expressed in decibels) as a function of time (Greenwich Mean Time (GMT)) and range (m) along the vertically oriented beam (Beam 2). Tic marks on the time axis are separated by approximately 33 sec. For this vertically oriented beam, the slant range along the beam is equal to the vertical distance from the ADCP transducer. The bottom can be seen at a depth of 10 m, where the backscattering has

a global maximum of -40 dB. The *R/V Pelican* is beginning to move over the plume at 20:36:30 GMT, and the backscattering rises steeply from the background (-70 dB) to a maximum of -44 dB. The intensity then decreases to about -65 dB until the ship drifts back into the plume at approximately 20:42:45 GMT. This plume signal is much weaker than the first, as can be seen from the slanted -60-dB contour. Toward the end of the survey shown in the plot, the plume is strongly sheared.

Data comparison. In Figure 5.8, a scatter plot between the measured concentration and the volume backscatter after quality check and calibration is shown for seven of the surveys. Data points for each of the four beams have been plotted (generating apparent vertical lines in the scattergram), and each survey includes 2 to 11 samples. The data cover a dynamic range of 40 dB both in concentration and acoustic scattering.

It is difficult to determine a curve that best represents the data set. An overall view gives the impression of a nonlinear curve with a slope that decreases with increasing concentration. However, if the survey that covers the highest concentrations (Survey 242B) is removed from the data set, a linear curve constitutes a fairly good fit. The spread is largest for low concentrations. Because the data are shown in logarithmic units, this effect can be explained by assuming a fixed or a percentage error in the concentration data.

As a first attempt to compare the ADCP backscatter data and the concentration, the results are promising. With a standard deviation in both data sets of at least +/-3 dB, a deterministic curve could be fit to the data set such that the uncertainty in the concentration derived from acoustic measurements lies within one order of magnitude. For dynamical studies or studies over large spatial scales, this accuracy would provide a much enhanced capability to characterize plumes. However, additional comparisons of backscatter and concentration are required to estimate rigorous error bounds and understand more fully the relationship between these two measures.

4. Simple Models of the Acoustic Backscatter

Because particle size distributions of the water samples are available, it is possible to make a comparison of predictions from the simplest scattering models and the measured backscatter. It is usually assumed that the scattering behavior for sediments follows the Rayleigh scattering model, as has been demonstrated in the laboratory for spherical particles of varying size, where it is assumed that the particle size is much smaller than the wavelength of the acoustic pulse. If the

reflected angle is equal to the incident angle for the scattered sound, the Rayleigh scattering cross section (disregarding density and elasticity) can be written (constant density) (Rayleigh 1945),

$$\sigma = b k^4 \sum_{i=1}^{M} C_i a_i^3 \qquad C_i \sim N_i a_i^3 \tag{5.1}$$

where

σ = scattering cross section
b = empirical constant
k = acoustic wave number
C_i = concentration by weight of particles in size class i
a_i = radius of one particle in size class i of a total of M size classes
N_i = number of particles per unit volume in size class i

If the particle size distribution does not change (i.e., $N_i / \sum N_i$ = constant), the cross section is proportional to the total number of particles and hence to the particle concentration.

It is not possible to simplify the calculation by using the median or mean radius of the particles in the calculation and still be consistent with this scattering model. If only statistical parameters are available, the appropriate value to use for the "mean volume" in Equation 1 is:

$$a^3 = \frac{\sum C_i a_i^3}{C} \tag{5.2}$$

where a^3 is a weighted mean volume, C_i is the partial concentration associated with particles of radius a_i, and C is the total concentration.

Because the scattering cross section in this model depends on the 6th power of the radius, the scattering is heavily weighted toward the large particles. This weighting implies that knowledge of the size distribution becomes important for the relationship between acoustic scattering and concentration.

Based on the size distribution of the sediments collected with the water bottles, a scatter plot between the model prediction and the actual scattering is shown in Figure 5.9. This plot shows a larger spread than Figure 5.8, which corresponds to a 3rd-power scattering law. All power laws between 1 and 6 were tested for comparison, with a minimum spread obtained using the 3rd-power

law. Of interest also is the spread to be expected in a scatter plot between the acoustic signal and concentration if a 6th-power law is applied. Figure 5.8 shows the results based on the size distributions observed in the project. Comparison of the previous scattergram (Figure 5.8) reveals a similiarity in trend to the theoretical calibration curve (Figure 5.9). The spread is sufficiently small that knowledge of the backscattering strength is adequate to predict the concentration within one order of magnitude (see Figure 5.8).

In the data, there is neither support for the 6th-power scattering model nor evidence to refute the model. If the scattering model is correct, one might conclude that density variations and the effective scattering cross section of the individual particles must be taken into account to reduce the spread in the data.

5. Bottom Tracking and Navigation

The ADCP measures the Doppler shift of an emitted pulse. The source of the sound is the transducer element fixed to the transducer head. On a moving vessel, the transducer head moves with the vessel; thus, the Doppler shift is a vector combination of both the water current and the velocity of the vessel itself. In the following, this combined velocity is referred to as the "water velocity."

The purpose of the special ADCP mode called "bottom tracking" is to measure the motion of the vessel with respect to the bottom. The estimate of the vessel velocity is then subtracted from the water velocity to yield the current velocity. If the water is too deep or if it impossible to automatically detect the bottom on the basis of the acoustic echo, the velocity of the vessel will remain unknown, and the true current velocity cannot be calculated. In these cases, another way of determining the ship velocity must be found. One option is to use the time derivative of the position data. For ships operating in areas with full ocean depth, this is the most common method of deriving the vessel velocity.

Just as the position data can be used to measure the velocity of the ship, the bottom track data can be integrated to yield the position of the ship relative to a starting point (dead reckoning). This technique is used in volume transport measurements with the ADCP.

During the MFDCP, ADCP bottom tracking data and positioning data from a highly accurate Mini-Ranger navigation system were recorded. To determine errors and accuracy involved with

each of the methods described above, the recorded data were analyzed, and the results are reported in the following.

Bottom tracking

The bottom track pulse is distinguished from the water track pulse by processing that takes place within the ADCP. Instead of processing the echo at fixed range gates, the processing is configured to locate steep gradients in the echo strength, thereby measuring the Doppler shift of the echo from the bottom and area in the vicinity of the bottom. Whereas the water track transmit pulse usually needs to be short to retain vertical resolution, the bottom track transmit pulse is usually long. This long pulse is required to reduce the single ping variance of the Doppler shift; also, the sound beam must ensonify the bottom over the entire beam to avoid changing the effective beam angle. Based on previous calibration projects, this long pulse illuminating the bottom will produce an accurate and stable estimate of ship velocity.

Analysis of bottom track and navigation data

The ADCP provides ship velocity measurements, whereas navigation data provide an estimate of ship position. By integrating the ADCP bottom track data, a relative ship position can be determined and compared with navigation data. Similarly, differentiation of navigation data yields relative ship velocity, which can be compared with ACDP bottom tracking velocity. Before a direct comparison of the two data sets could be performed, the data had to be corrected for three systematic errors.

1. The transducer was mounted somewhat irregularly on a pipe over the side of the *R/V Pelican*, and the error in the installation angle (referred to as transducer misalignment) had to be determined. The misalignment was assumed to be equal to the difference between the mean of the direction of course from the bottom track velocity and the mean of the direction of course based on navigation data. These angles, expressed in degrees, are given in Table 5.3.
2. For precise comparison, ADCP data must be corrected for the speed of sound. The nominal conversion factor between the recorded Doppler shift and engineering units is based on the value 1536 m/sec for the speed of sound (defined by the conditions: T = 26 deg C, and 35 ppt salinity). For the bottom track data set collected during the MFDCP, the speed of sound was taken to be equal to this value.
3. The navigation data have to be checked for quality. The ship was stationary during microwave positioning checks, during which time no tracking checks were possible. Positions were recorded every 2 sec. Rotating the transceiver antenna affected reliability of the positioning, as did the position of the ship (there were some shadow zones). The task of checking the quality of the navigation data was carried out by staff of Evans-Hamilton, Inc., and the analyzed data were judged to be quite reasonable (Chapter 3, this report).

Comparisons of ACDP bottom track data to the navigation data were performed for seven transects to estimate errors and accuracy of each method and to create a postprocessing template for additional event processing. Unweighted least squares fits were computed for the following: ship position (from navigation data) and ship velocity estimated from the integrated ADCP data (bottom track velocity); ADCP ship velocity and ship velocity estimated from ship position; and ship heading computed from integrated ADCP bottom track data and from navigation data. The results of these analyses are tabulated in Tables 5.4 through 5.7.

In general, the two methods (ADCP and navigation) exhibited a high linear correlation. The data were unweighted because errors in each measurement method were assumed to be uniform over all measurements. Plots of ADCP and navigation-determined tracks versus time were made for both position and velocity to determine variation as a function of time. Data pairs were aligned to within one second in accordance with the 1-sec standard for accuracy between the different clocks used in the project. In the following, all velocity time series plots are a function of elapsed time in minutes (0 min corresponding to the start time of the survey).

Before comparison of position data, the ADCP bottom tracking data (recorded in beam coordinates) were converted to north and east components of the true ship velocity using the heading information and transducer misalignment correction. The velocity components were converted to relative north and east position components by integration with respect to time. The data were converted to feet in accordance with the coordinate system used by the Mini-Ranger positioning system, referenced to the Alabama State Plane Coordinate System (ASPCS).

Before comparison of the velocity data, the ADCP bottom track velocity components were converted to east and north components, and the navigation data were converted to velocity by differentiation with respect to time. The total velocity from each source was then computed and compared. Results of this analysis are discussed next.

Bottom track data. Data measured by the ADCP using bottom tracking were recorded at 2-1/2-sec intervals and saved in separate files for each survey in ASCII format (ADCP bottom tracking data file name: ADCP####.BTM (the four-character string #### corresponds to a survey number)). The data format for each line of the file is [HR:MN:SC VX VY HEADING], where:

HR:MN:SC = Eight-character string corresponding to the local hour, minute, and second of each velocity measurement

VX = Component of velocity perpendicular to the main axis of the ship (positive starboard) in units of 0.125 cm/sec.

VY = Component of velocity along the main axis of the ship (positive forward) in units of 0.8 cm/sec.

HEADING = Ship heading measured in degrees from north.

Navigation data. Navigation data for the *R/V Pelican* provided ship position and were recorded at 2-sec intervals and saved in separate files in ASCII format for each survey (navigation data file name: EDT#### (the four character string #### corresponds to a survey number)). The data format for each line of the file is [HR:MN:SC EP NP], where:

HR:MN:SC = Eight-character string corresponding to the local hour, minute, and second of each position measurement

EP = East (easting) position in feet

NP = North (northing) position in feet

Plots of the ship tracks from the navigation (Mini-Ranger) system for surveys covered in this chapter are shown in Figures 5.11 through 5.17 at the end of the chapter. The ADCP data were converted to feet and referenced to the ASPCS.

The results of intercalibration of ship velocity, position, and heading from ADCP bottom tracking and navigation data are presented for Surveys 237A, 238A, 238B, 239A, 239B, 241A, and 242A.

Ship direction. The direction of the ship velocity as reported by the ADCP combined with the heading data was compared with the direction of the velocity vector derived by differentiating the northern and eastern components of position (from navigation data). The velocity time series plots (Figures 5.18-5.31) suggest that while the ship is turning (sustained low mean ship speed), computation of ship heading from position data may be unreliable.

Scatter plots of ship heading computed from ADCP bottom track and navigation data are shown in Figures 5.32, 5.33, 5.34, 5.35, 5.36, 5.37, and 5.38. The linear regression between the two

sources of ship heading are tabulated in Table 5.4 and demonstrates a high correlation for the events processed.

Ship speed. Results of the linear regression analysis are given in Table 5.5. The scatter plot of ADCP bottom track speed as a function of speed calculated with the navigation data is shown in Figures 5.39, 5.40, 5.41, 5.42, 5.43, 5.44, and 5.45. The data show high correlation for most of the surveys. Although the time series plots (Figures 5.18, 5.20, 5.22, 5.26, 5.28, and 5.30) show noise in both sets of velocity data, the Mini-Ranger navigation data show larger variance in ship velocity. This analysis suggests that ship velocity measurements derived from navigation data may be less accurate than ADCP bottom track velocity measurements.

Ship position. Times series plots for the estimates of ship position from the ADCP bottom track data and the navigation data are shown in Figures 5.46 through 5.52. Linear regression between the north and east position estimates for the events considered also exhibited high linear correlation, as shown in Tables 5.6 and 5.7. The large value and uncertainty for the offset results from the difference between the ADCP position and the origin of the navigation grid.

An offset bias was added to the ADCP position data to align the data at the initial point in the time series. This offset bias is equivalent to aligning ADCP data to the navigation coordinate grid. Note that both the navigation and ADCP position data are relatively free of high-frequency noise.

This analysis indicates ADCP bottom track velocity data, integrated to compute position, provide stable and accurate position information comparable with position data obtained from land-based navigational sources.

Results from individual events. Results of the intercalibration of navigation and bottom track data are presented in Tables 5.4 through 5.7. Scatter plots and time series plots are also presented in Figures 5.11 through 5.52.

6. Current Velocity

Measurements of current structure (velocity and direction) in the area around the dredged material placement site are shown in Figures 5.53 through 5.68. These plots show little horizontal variation in the current velocity. Synthesis of current structure data was achieved by first subtracting the velocity of the ship from the collected current velocity data. For each depth bin, the current velocity was then averaged over the entire event. The small horizontal variation in the current structure near the disposal sites was disregarded. Depth bins within 2 m of the bottom

were rejected from analysis. The vertical variation shows a relatively weak shear in some events, with typical current speeds of 30 cm/sec near the surface and 10 cm/sec near the bottom. Because of the small horizontal variation, the data have been synthesized into one vertical profile from each survey.

It was observed during the data collection that the direction and magnitude of the measured current (as illustrated with current sticks on the computer monitor) exhibited a weak dependency on the speed of the ship. It became clear that there was a coupling between the two parameters, and an analysis to quantify the interaction of the current and ship speed was undertaken.

The problem is caused by the influence of the ship on the flow field below the hull of the ship. Conceptually, the ship can be thought of as "pulling" the water along in the direction of its motion. This action leads to a net apparent current in the direction of the travel of the ship. The effect has not been previously reported among ADCP users, and the result was therefore surprising. Research on this phenomenon is presently being conducted. Most likely, the effect was particularly strong during the MFDCP because of the shallow water (compared with the keel depth and displacement of the ship) and because the ADCP was mounted off the side of the ship.

The analysis of the coupling was achieved by linear regression between each of the components of the current velocity and the ship velocity. The influence of the ship motion on the undisturbed current field is stronger near the surface (2 to 3 percent of ship speed) and decays toward the bottom, and it is stronger in shallower water than in deeper water. The error is large enough that the current data need to be corrected before they can be used to characterize the undisturbed flow field. There is no effect on the bottom track measurements because the bottom is unperturbed by the ship motion. Typical results of the linear regression data collected are shown in Table 5.8 (shallow depth, Survey 242A) and Table 5.9 (medium depth, Survey 238B).

7. Vertical Velocity, Backscattering, and Internal Waves

The ADCP provides two independent estimates of the vertical current velocity. One estimate is derived directly from the vertical beam, and the other is derived from a linear combination of the fore and aft ADCP beams (Beams 3 and 4) directed 30 deg from the vertical. Comparison of backscattering amplitude to vertical velocity measurements, examination of plume dispersion, and the generation of internal waves were performed using time series plots and contour plots as a function of depth and time (or space).

Survey 240B

During Survey 240B, the ship entered the plume at a speed of 2 m/sec and then slowly drifted through the plume sideways with a speed of 0.2 to 0.3 m/sec. Figure 5.69 shows the backscattering for the vertically oriented beam (Beam 2) in depth cell 2 (4.3 m). The first part of the plot (starting at 150 sec) shows that the plume had very high initial concentration and is probably confined to a very small area. After 320 sec, a central plateau appears with an interval of slightly lower backscattering with only small temporal variations. The plume at this time appears to be spread over a large area, and material is well mixed. At an elapsed time of 800 sec, the ship has drifted out of the plume, and the backscattering amplitude returns to the value it had before plume entry (-80 dB).

Figure 5.70 is also from Survey 240B and shows plots of forward and transverse ship velocity along with the bottom track and water velocities in bin 2 (vertical beam). Note that the bottom track and the water track velocities have been multiplied by a factor of 10 to aid visual comparison. Two observations can be made from this figure. One is that the ship speed is small during the time the *R/V Pelican* drifted through the plume and, consequentially, the parameters in the figure (to first order) represent a single point in the horizontal. The other is that the water track velocity along the vertical beam is greater than the bottom track velocity. This latter observation is important because it rules out the possibility that the vertical velocities are artifacts of vertical misalignment in the transducer installation.

There are three mechanisms by which vertical velocities could be introduced given conditions during the field data collection. The first is the fall speed of the particles through the water. The fall speed of individual particles is expected to be of order 1 to 5 cm/sec for the first 10 min after the initial placement of the material (after the descent of the collective body of material immediately after release). The second mechanism is the existence or generation of internal waves. The third mechanism is the generation of potential flow around the vessel that disturbs the background flow field. The strong peak in vertical current seen in Figure 5.71 (-10 cm/sec) at elapsed time of 150 sec can be explained only as generated by this potential flow field. The effect is particularly severe at this time because the ship is making a sharp turn and partially yawing (transverse motion).

Figures 5.71 and 5.72 show the two independent estimates of the vertical current velocity within a temporal subset of the previous figures. The subset corresponds to the time when the ship is drifting through the plume. This correspondence allows for maximum dynamic range in the plot

and rules out the possibility of significant interference by the potential flow. Figure 5.71 shows data from the vertical beam (Beam 2), and Figure 5.72 shows combined data from Beams 3 and 4. Both figures show the vertical current velocity from bins 2 and 5 along with the bottom track velocity. The current velocity is equivalent to the water velocity minus the bottom track velocity shown in Figure 5.70. As expected, the vertical current for bins 2 and 5 is generally of the same shape, with larger negative velocities for the deeper bin 5. The bottom track velocity is close to zero. Although the two figures show much of the same structure, the differences between the two estimates of the vertical velocity imply that the horizontal distance between the sampling volumes for the three beams is important. From these figures, it appears that the vertical current is dominated by the propagation of internal waves that have an amplitude of 5 to 10 cm/sec. This domination is unfortunate, because it makes direct measurement of the fall velocities difficult.

The first contour plot (Figure 5.73) shows backscatter amplitude as a function of depth and time. The temporal range is a subset of that used in Figures 5.69 through 5.72. The spacing of contour lines over time gives an indication of plume dispersion. The initial closely packed contour lines indicate a denser scattering field and the presence of a plume structure. The later widely spaced contour lines indicate dispersion and settling of the dredged material.

The second contour plot (Figure 5.74) shows the vertical current from the vertically oriented beam (Beam 2) as a function of depth and time. The temporal range is identical to that used in Figure 5.73. The relatively high velocities in the interval from 150 to 350 sec show the presence of the released dredged material moving rapidly downward through the vertical water column. Again, the large velocities after the initial placement are believed to be a manifestation of an internal wave propagating away from the area.

Survey 238B

Instead of examining the temporal variation as the ship drifts into the plume, Survey 238B was analyzed from the perspective of temporal change of the plume taken as a whole. The plume was traversed several times after the initial placement, and each transect (although taking 3 to 5 min) can be seen as representing the state of the plume at a given averaged elapsed time. From a dynamical point of view, the transverse sampling method is a more powerful type of presentation if the aim is to understand development of the plume.

To assure that the presentation was as correct as possible, all the position data were projected onto a straight line representing a suitable cross section of the plume. This projection ensures that

variation in the ship speed or changes in the angle of the transect do not distort the horizontal image of the plume. The line runs in the direction from 225 to 75 deg (positive) true north.

The first plot (Figure 5.75) shows the backscattering (in relative units) from bin 3 (depth 5.3 m) for each of the five transects. The first transect (marked 1) shows the highest concentration of scattering material and a narrow horizontal baseline. Subsequent transects (marked 2, 3, 4, and 5) show lower backscatter amplitude and larger horizontal extent. The last phenomenon is even more pronounced in the data from bin 6 (Figure 5.76), where the whole plume shifts over to the positive side of the plot. The reason is that the plume material is being advected by the average horizontal current. The strong eastward current in the bottom layer during this event explains both why the bottom layer is shifted more than the top layer and why the bottom layer of the plume moves toward the positive side of the plot (toward 75 deg).

Figure 5.77 illustrates the observed vertical velocity during the first 2-1/2 transects that were made across the plume. The internal wave believed to be generated at the time of the placement propagates out from the placement site and produces a relatively large vertical velocity. The maximum velocity is observed in bin 3 (depth 5.3 m). The density gradient at this level is of order two sigma-theta units per meter (1 sigma-theta unit is approximately equal to 1 kg/m^3). For a two-layered fluid, the wave may be regarded as propagating freely on the interface, following the standard dispersion relation with reduced gravity.

The wavelength λ of the interface wave is of order 100 m, and the wave has propagated 350 m from the time of the first transect until the ship passed over the wave the second time. The propagation velocity (group speed) c_g of the wave is,

$$c_g = \sqrt{\frac{g'}{k}} \tag{5.3}$$

where

g' = $g(\rho_1-\rho_2/\rho_2)$,

ρ_1 = density of the upper layer

ρ_2 = density of the lower layer

k = $2\pi/\lambda$ (λ = wavelength)

The reduced gravity g' is $2\cdot10^{-3}$ m/sec^2, and c_g = 0.56 m/sec is obtained, indicating the wave will take 630 sec to propagate 350 m. By comparison, the time between the initial positive peak in the vertical velocity and the negative peak observed at the end of the second transect was 580 sec.

It thus appears that a simple two-layer model can explain the propagation well within the uncertainty in the density gradient, the propagation distance, and the wavelength.

The contour plots in Figures 5.78 through 5.81 show the development of the backscattering values for the four first transects. The plume material is behaving as expected, falling as a narrow downward jet of material at the outset, then evolving into an upside-down mushroom-shaped cloud. The material spreads out from the bottom cloud in elapsed time (as seen in successive Figures 5.78 through 5.81). Simultaneously, the concentration in the main jet is reduced, and the whole plume is advected with the horizontal current. Small internal waves can be seen to propagate on top of the expanding mushroom-shaped cloud.

The vertical velocity component (Figures 5.82 to 5.84) shows the rapid evolution of internal waves in the first few minutes after placement. There is a maximum in the vertical velocity at the point of maximum density gradient. After the first transect was completed, the vertical velocity field became quite noisy (except for the trailing edge of initial wave seen in the right-hand corner of pass 2). The upward movement of the cloud, the small internal waves generated by the upward motion near the bottom, and the falling particles in the initial jet all disturb the total field enough to make the vertical velocity measurement obscure after the initial pass. The times for each transect after the data sampling was initialized (21:55:38) were:

	sec
Pass 1 (from right to left):	0 - 330
Pass 2 (from left to right):	467 - 740
Pass 3 (from right to left):	852 - 1132
Pass 4 (from left to right):	1,357 - 1,627

8. Conclusions and Recommendations

Bottom track

Comparison of the bottom tracking data and navigation data shows, in general, good correspondence. During the first phase of each placement event, the bottom track data are influenced by the high backscatter in the water. There also are some spikes in the navigation data that have not been filtered out, and there are some small problems related to correct estimation of integration times. However, for the purpose of this initial study, bottom tracking data have been shown to be adequate both as a measure of the ship speed and as a tool for navigation when position devices are unavailable.

Current velocity

The current velocities were relatively weak during the MFDCP, and one surprise was encountered in analysis of the data. This previously unreported phenomenon was the apparent interference of the ship on the current field, which could amount to 3 percent of the ship speed. There are two alternatives for avoiding this problem. One is to correct the data with a software procedure that accounts for the presence of the ship, and the other is to use ships smaller than the *R/V Pelican* in shallow-water areas.

Sediment concentration

Two independent results in this chapter point toward the feasibility of using acoustic backscatter as a tool for determining sediment concentration. One is the comparison with the bottle sample data, which shows that for the MFDCP data set, the concentration can be found within an order of magnitude from the measured volume backscattering. The other result is the qualitative correspondence between the contour plot of the plume transects and knowledge of plume dynamics. Although not pointing directly to the relationship between backscatter and concentration, it is difficult to believe that the backscatter is a poor measure of the concentration from examination of the contour plots.

The next step in the application of acoustic instrumentation is measurement of suspended sediments in the controlled laboratory environment. In the laboratory, the particle size, distribution, and type can be controlled, and uncertainty in the acoustic measurements reduced to a minimum. An experiment to relate the volume backscatter and the sediment concentrations for several size classes and different types of particles might also be conducted. This experiment would provide valuable information about the limitation and applicability of the measurement technique and potentially lead to the routine application of acoustic instrumentation in this area. Such a firm development in instrumentation would be of great benefit in the measurement of particulates in pollution studies (e.g., sewage), which is a situation acoustically similar to the measurement of sediment.

References

Rayleigh, J.W.S. 1945. *Theory of Sound*, Vol. 2, Dover Publications, Inc., New York.

RD Instruments. 1989. "Acoustic Doppler Current Profilers, Principles of Operation: A Practical Primer", San Diego, CA.

Table 5.1

ADCP Characteristics for the MFDCP

Parameter	Value
ADCP model	RD-DR1200 direct-reading ADCP
Frequency	1,228 kHz
Depth cell size	1 m
Measurement ensemble size	28 pings (+/-3 pings)
Measurement ensemble duration	3 sec
Single-ping measurement error	13 cm/sec
Measurement bias	0.5 to 1.0 cm/sec
Ensemble measurement error	2.5 cm/sec
ADCP transducer depth	1.8 m
ADCP beam width	1.5 deg
Transducer side-lobe level	-55 dB

Table 5.2

ADCP System Configuration for Amplitude Calibration

System Configuration

Property	Value
ADCP frequency	1,200 Hz
Ks	5,650,000.0
ADCP input voltage	110.0 VAC
Chassis temperature	30.0 deg C
Salinity	28.0 ppt
Depth of the transducer	1.8 m
Sound velocity at transducer depth	1,538.3 m/sec
Water absorbtion coefficient (α)	0.474
Blanking	0.5 m
Pulse length	1.0 m
Depth cell length	1.0 m

Beam Configuration

Parameter	Beam 1	Beam 2	Beam 3	Beam 4
K2	9.520	10.630	9.530	10.270
Kc	0.428	0.428	0.428	0.428
K1	47.428	51.829	46.424	43.593
Nc	28.400	28.400	30.500	26.300
ϕ*, deg	30	0	30	30

* ϕ : Beam angle measured from vertical.

Table 5.3

Transducer Misalignment

Survey	237A	238A	238B	239A	239B	241A	242A	243A
Angle (deg)	6.78	8.69	8.51	10.62	10.27	9.48	3.38	4.78

Table 5.4

Ship Heading Linear Regression (ADCP = m · Navigation + b)

Survey	m*	Uncertainty in m	b	Uncertainty in b	r
237A	0.99	+/- 0.01	8.99	+/- 28.57	0.988
238A	0.96	+/- 0.01	16.35	+/- 43.68	0.962
238B	0.96	+/- 0.01	16.06	+/- 29.77	0.987
239A	0.98	+/- 0.01	14.89	+/- 23.08	0.991
239B	0.96	+/- 0.01	16.15	+/- 27.14	0.982
241A	0.98	+/- 0.01	13.86	+/- 28.20	0.979
242A	0.98	+/- 0.01	4.51	+/- 44.30	0.978

* m = slope, b = offset, and r = linear correlation coefficient.

Table 5.5

Ship Speed Linear Regression (ADCP = m · Navigation + b)

Survey	m	Uncertainty in m	b	Uncertainty in b	r
237A	0.96	+/- 0.01	9.11	+/- 53.24	0.965
238A	0.92	+/- 0.01	3.57	+/- 67.75	0.924
238B	0.98	+/- 0.02	4.53	+/- 93.95	0.890
239A	0.96	+/- 0.01	4.61	+/- 68.85	0.950
239B	0.99	+/- 0.01	1.65	+/- 42.54	0.970
241A	0.99	+/- 0.03	4.73	+/-175.44	0.740
242A	0.95	+/- 0.01	15.46	+/- 53.79	0.950

Table 5.6

Northing Ship Position Linear Regression (ADCP = m · Navigation + b)

Survey	m	Uncertainty in m	b	Uncertainty in b	r
237A	0.97	+/- 0.00	-296,704.33	+/- 1,859.94	0.998
238A	1.00	+/- 0.00	-305,618.34	+/- 31,395.63	0.995
238B	1.00	+/- 0.01	-304,539.37	+/- 41,934.60	0.991
239A	0.99	+/- 0.00	-300,020.71	+/- 13,534.91	0.999
239B	0.99	+/- 0.00	-301,881.06	+/- 6,158.94	0.999
241A	0.97	+/- 0.00	8534.83	+/- 18,085.04	0.998
242A	1.01	+/- 0.00	-316,114.49	+/- 14,447.30	0.998

Table 5.7

Easting Ship Position Linear Regression (ADCP = m · Navigation + b)

Survey	m	Uncertainty in m	b	Uncertainty in b	r
237A	0.98	+/- 0.01	-53,719.42	+/- 6,862.43	0.992
238A	0.97	+/- 0.01	-54,025.98	+/- 7,135.21	0.992
238B	0.99	+/- 0.00	-56,788.45	+/- 1,535.90	0.999
239A	0.97	+/- 0.00	-54,886.85	+/- 5,479.97	0.995
239B	0.99	+/- 0.00	-55,713.50	+/- 4,481.23	0.997
241A	0.99	+/- 0.01	922.92	+/- 7,732.47	0.992
242A	1.18	+/- 0.01	-70,314.49	+/- 11,000.29	0.988

Table 5.8

Linear Regression Between Ship Speed and Current Speed (Survey 242A)

	$U_c = A_u U_s + B_u$		$V_c = A_v V_s + B_v$	
Depth, m	A_u	r	A_v	r
3	0.037	0.77	0.030	0.33
4	0.038	0.77	0.033	0.37
5	0.045	0.74	0.027	0.24
6	0.031	0.62	0.020	0.18
7	0.032	0.63	0.014	0.16

Table 5.9

Linear Regression Between Ship Speed and Current Speed (Survey 238B)

	$U_c = A_u U_s + B_u$		$V_c = A_v V_s + B_v$	
Depth, m	A_u	r	A_v	r
4	0.023	0.49	0.019	0.29
5	0.027	0.47	0.021	0.26
6	0.018	0.32	0.017	0.23
7	0.016	0.34	0.012	0.15
8	0.013	0.29	0.004	0.06
9	0.011	0.26	0.006	0.08

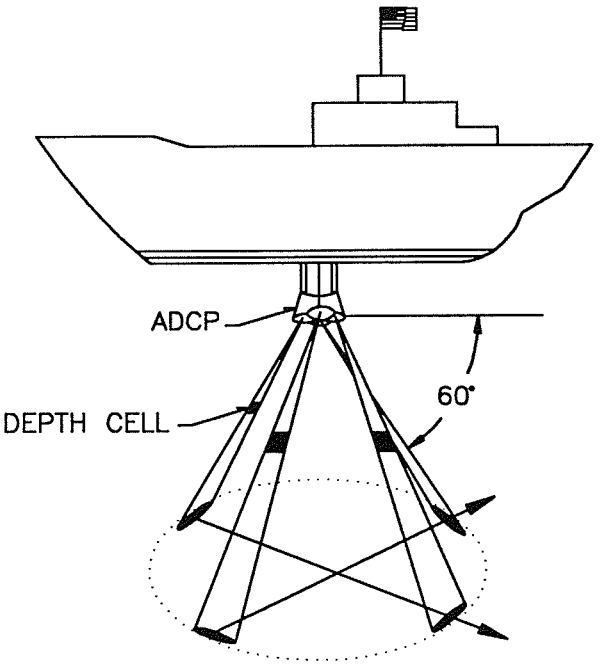

Figure 5.1. Standard ADCP beam configuration.

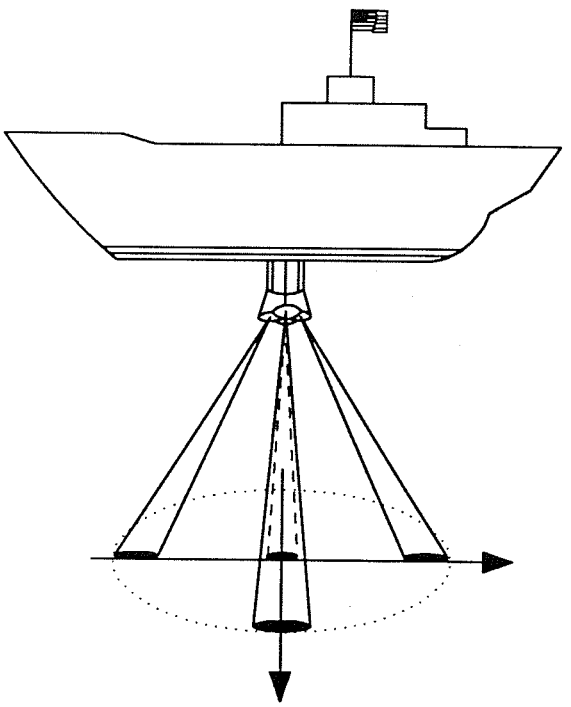

Figure 5.2. ADCP beam configuration used during the MFDCP.

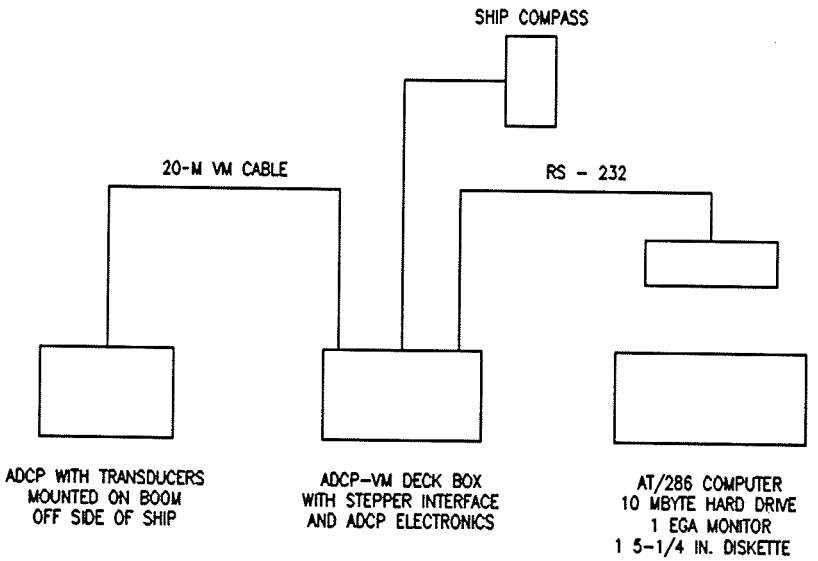

Figure 5.3. ADCP hardware configuration on the *R/V Pelican*.

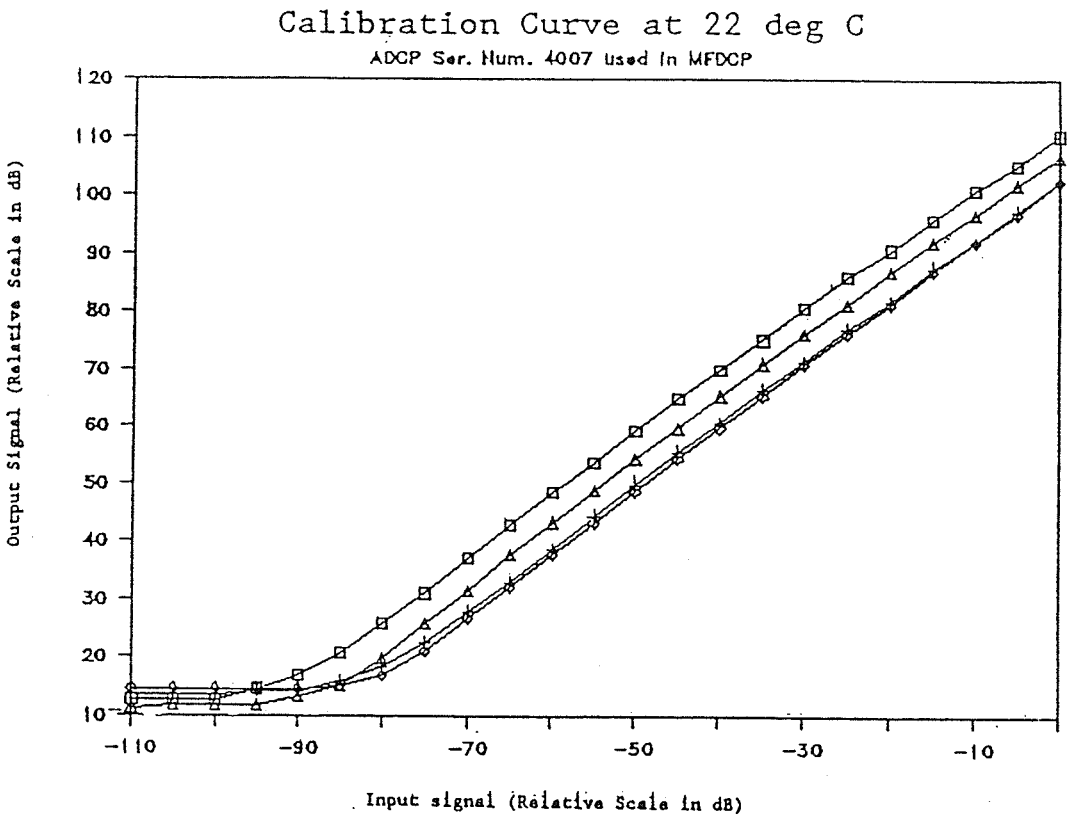

Figure 5.4. Response of ADCP receiver circuitry measured at 22 deg C.

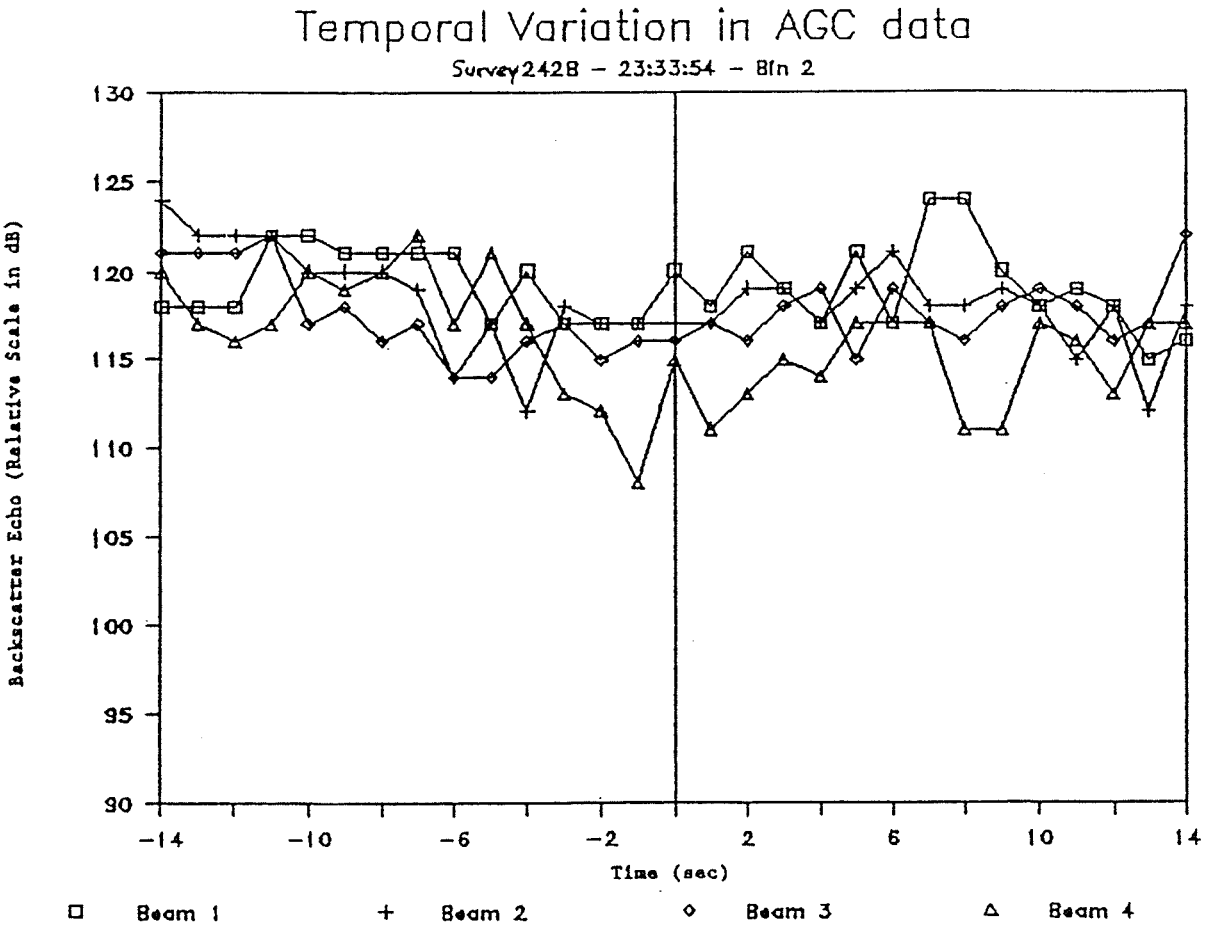

Figure 5.5. Temporal variation of ADCP amplitude (Backscatter Echo) for bin 2 of all four ADCP beams for a 28-sec period.

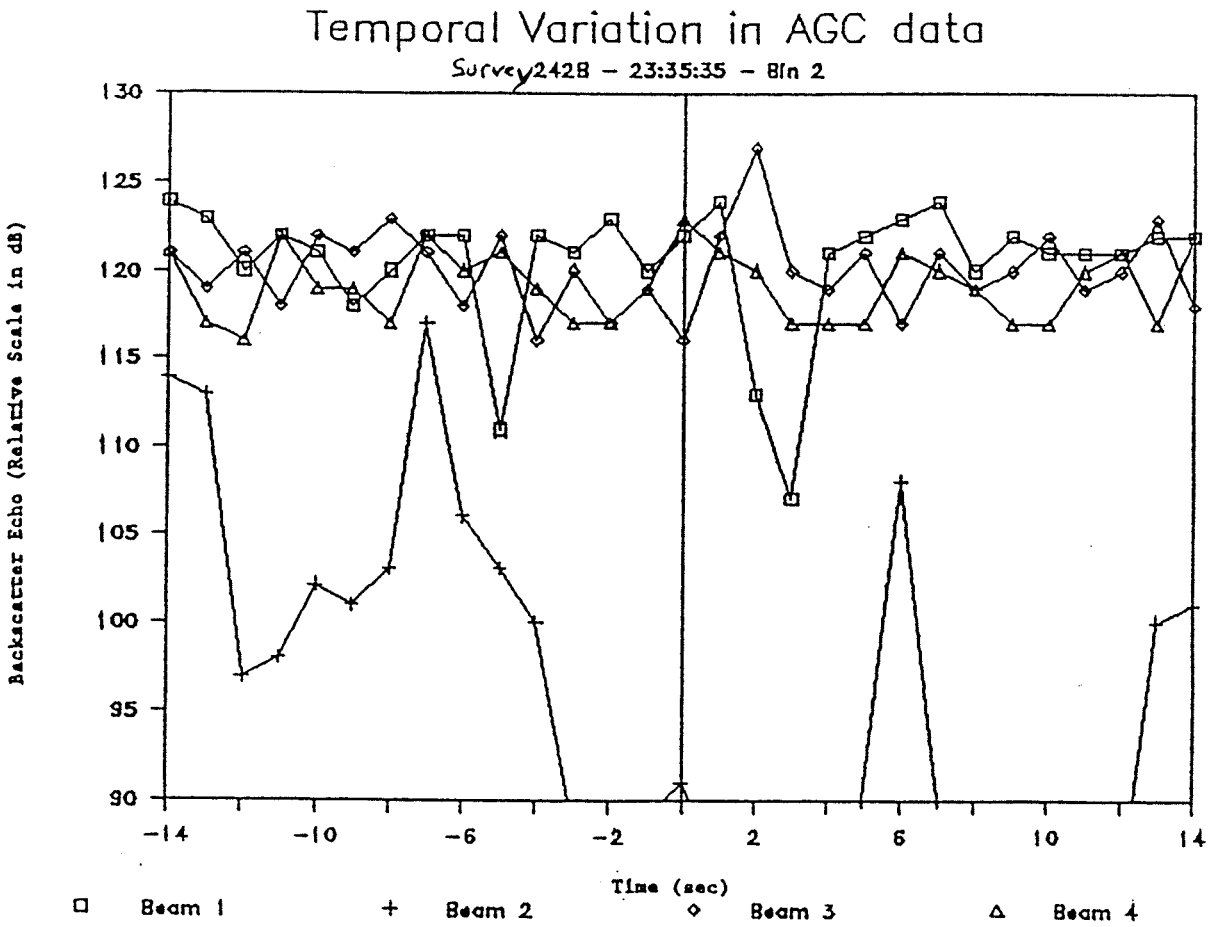

Figure 5.6. Temporal variation of ADCP amplitude (Backscatter Echo) for bin 2 of all four ADCP beams for a 28-sec period. Beam 2 (the vertical beam labeled with "+") is in the shadow of the CTD rosette.

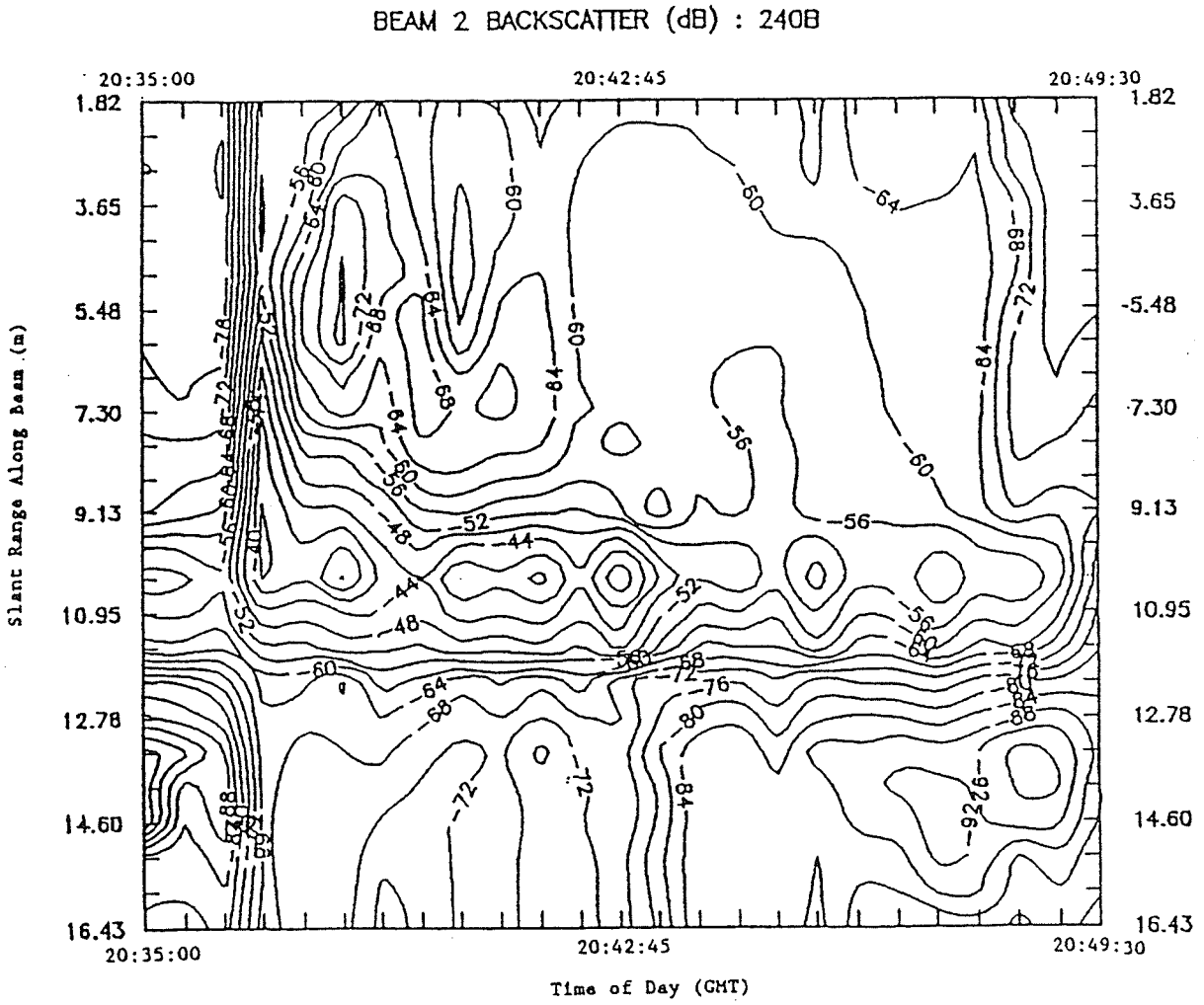

Figure 5.7. Contour plot of backscatter amplitude data in decibels as a function of time and slant range along Beam 2 (m). For this vertically oriented beam, slant range is equal to distance from the transducer.

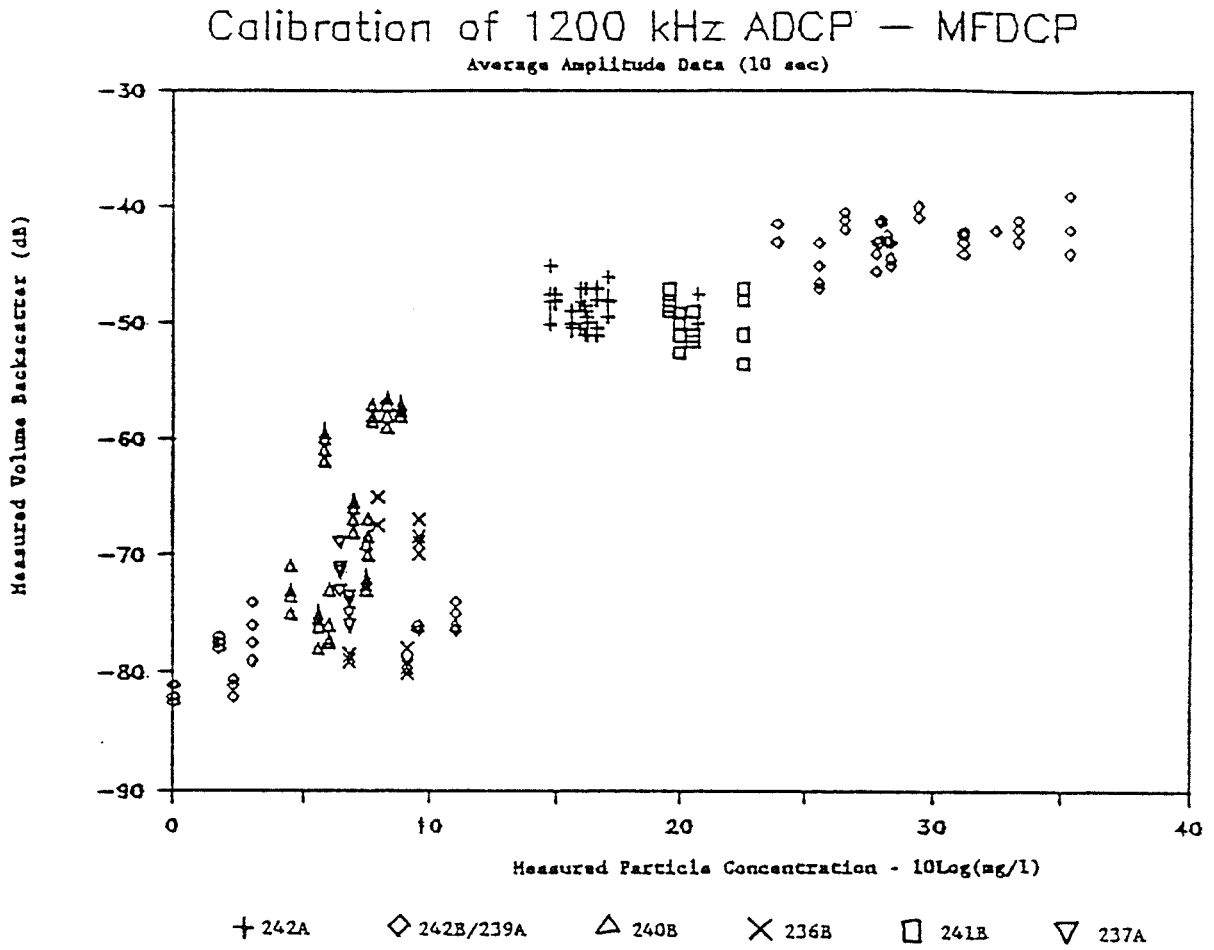

Figure 5.8. Scatter plot between measured particle concentration and the volume backscatter, after quality check and calibration, for seven release surveys. Data for all four beams have been included, generating apparent vertical lines in the scattergram.

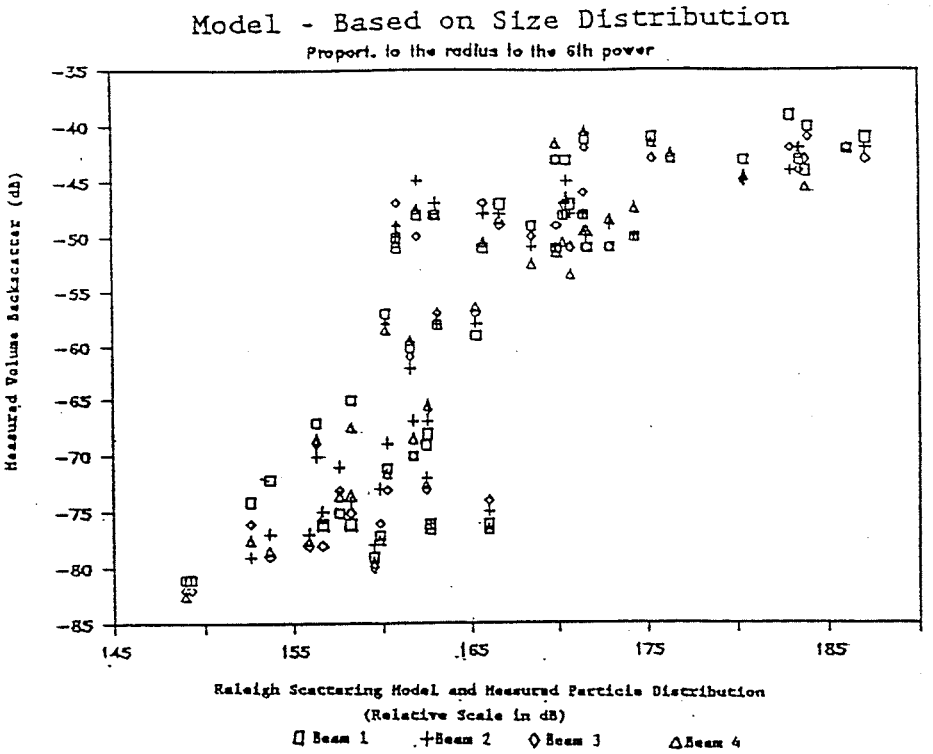

Figure 5.9. Measured volume backscatter and Rayleigh scattering model.

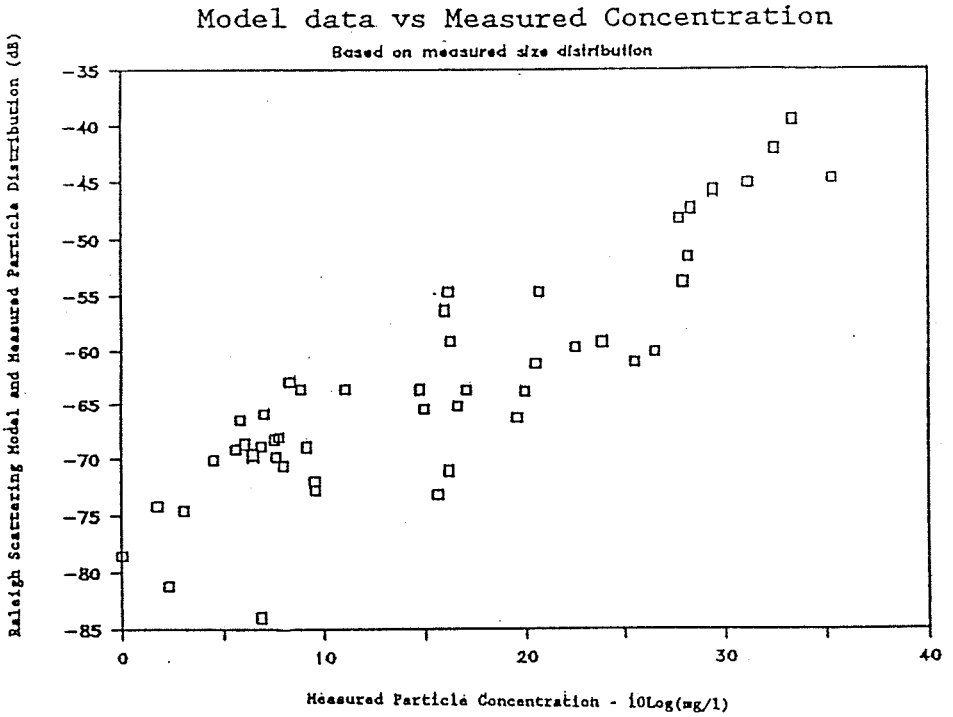

Figure 5.10. Rayleigh scattering model and measured particle concentration.

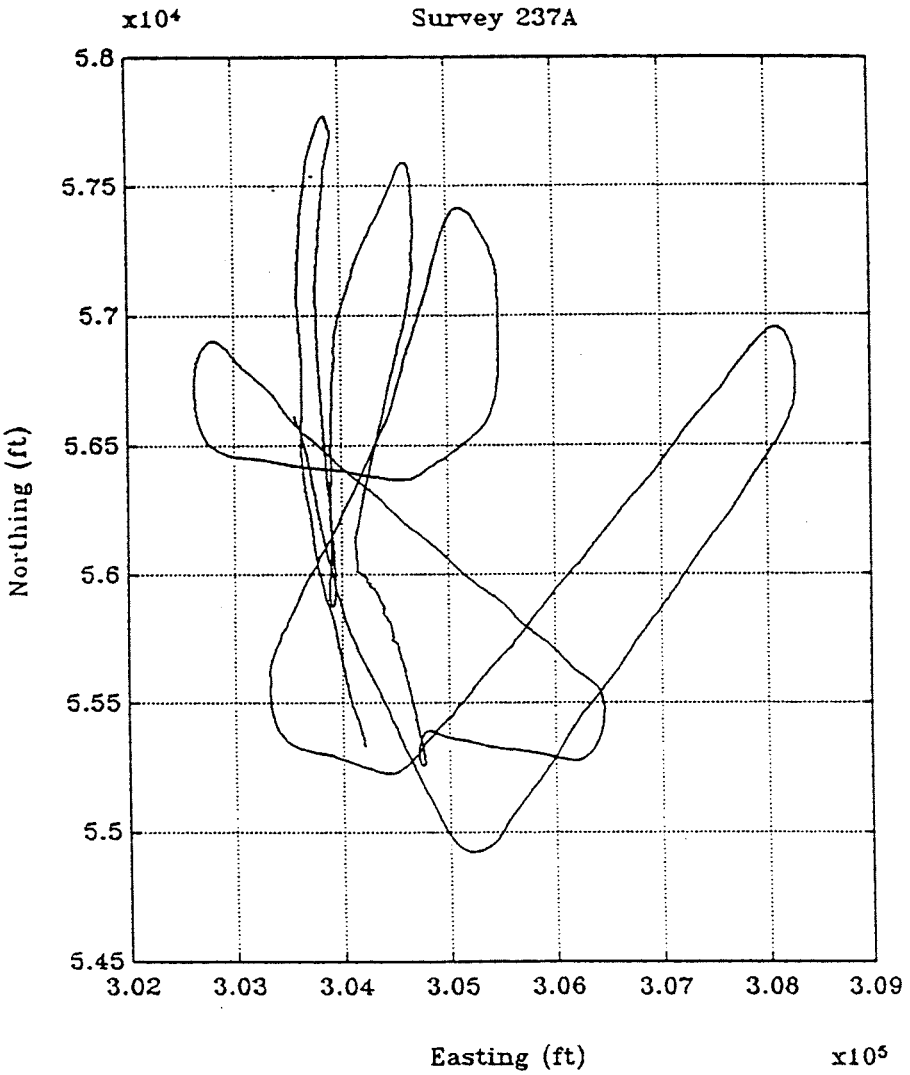

Figure 5.11. Survey 237A: ship tracks from navigation (Mini-Ranger) data.

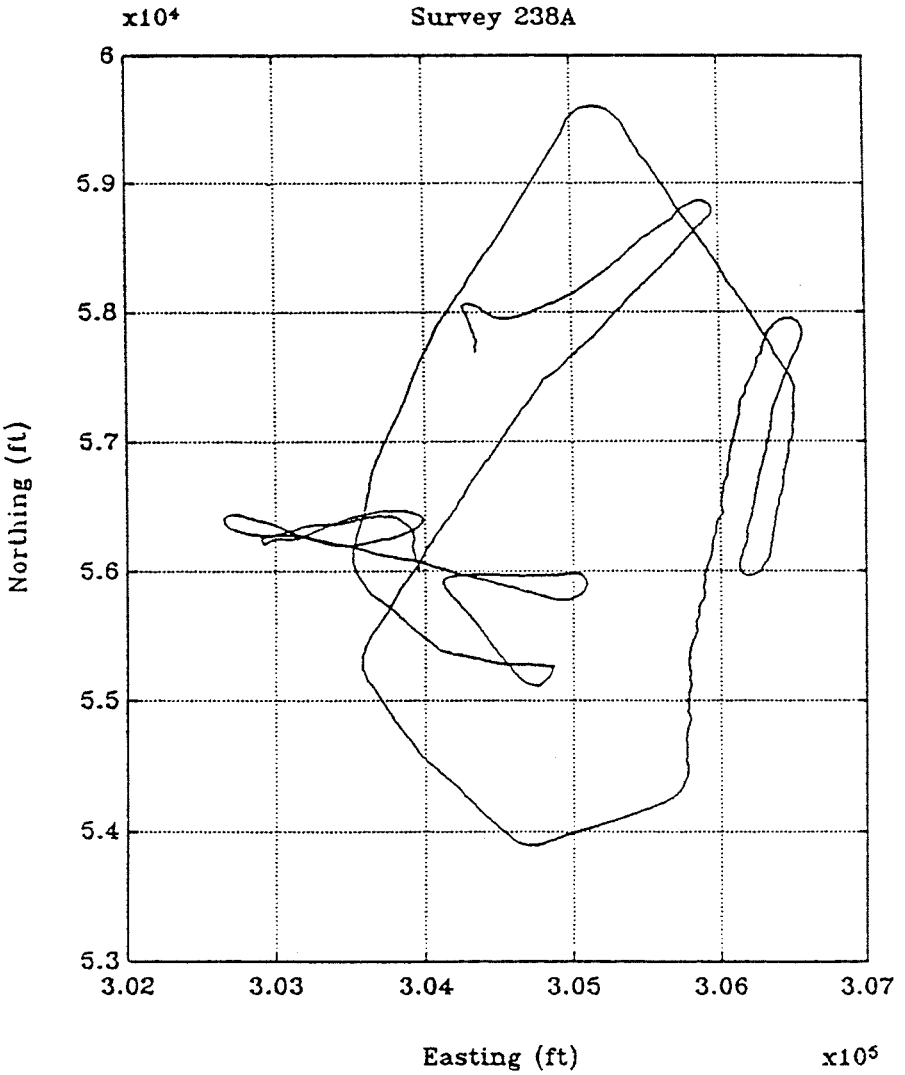

Figure 5.12. Survey 238A: ship tracks from navigation (Mini-Ranger) data.

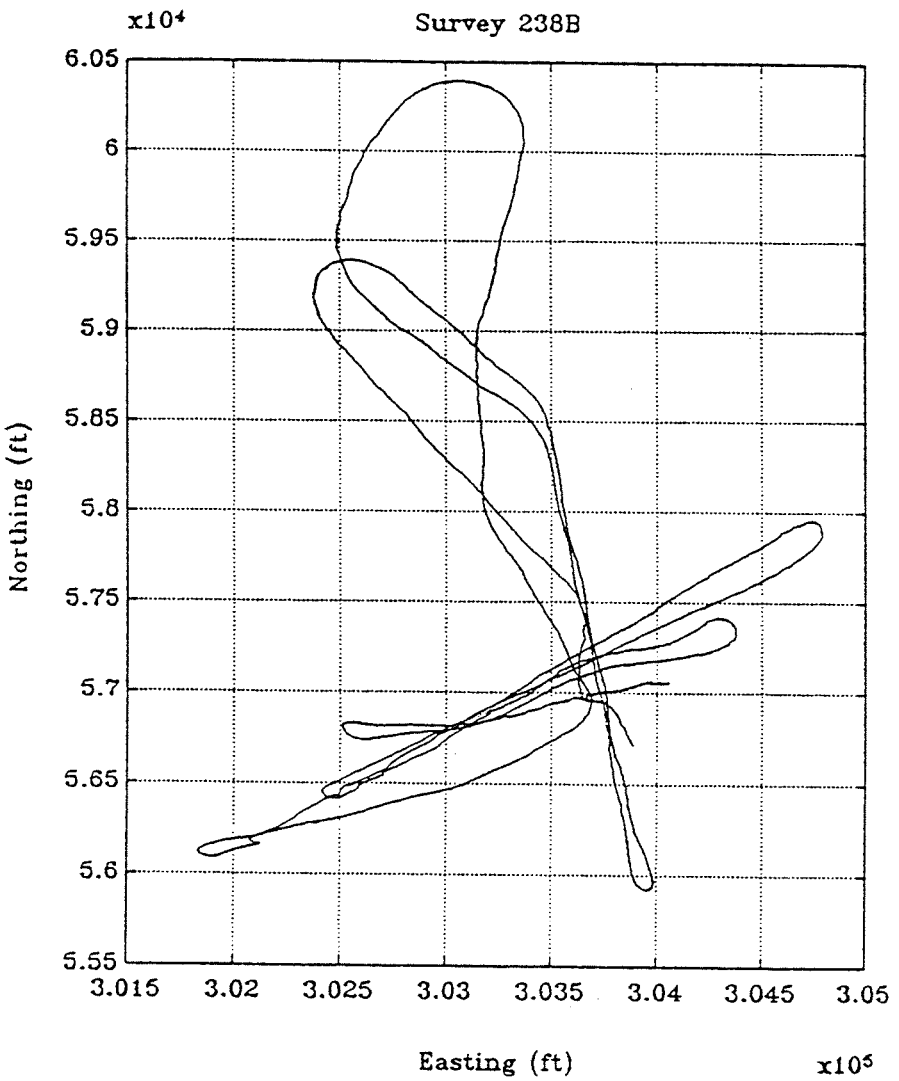

Figure 5.13. Survey 238B: ship tracks from navigation (Mini-Ranger) data.

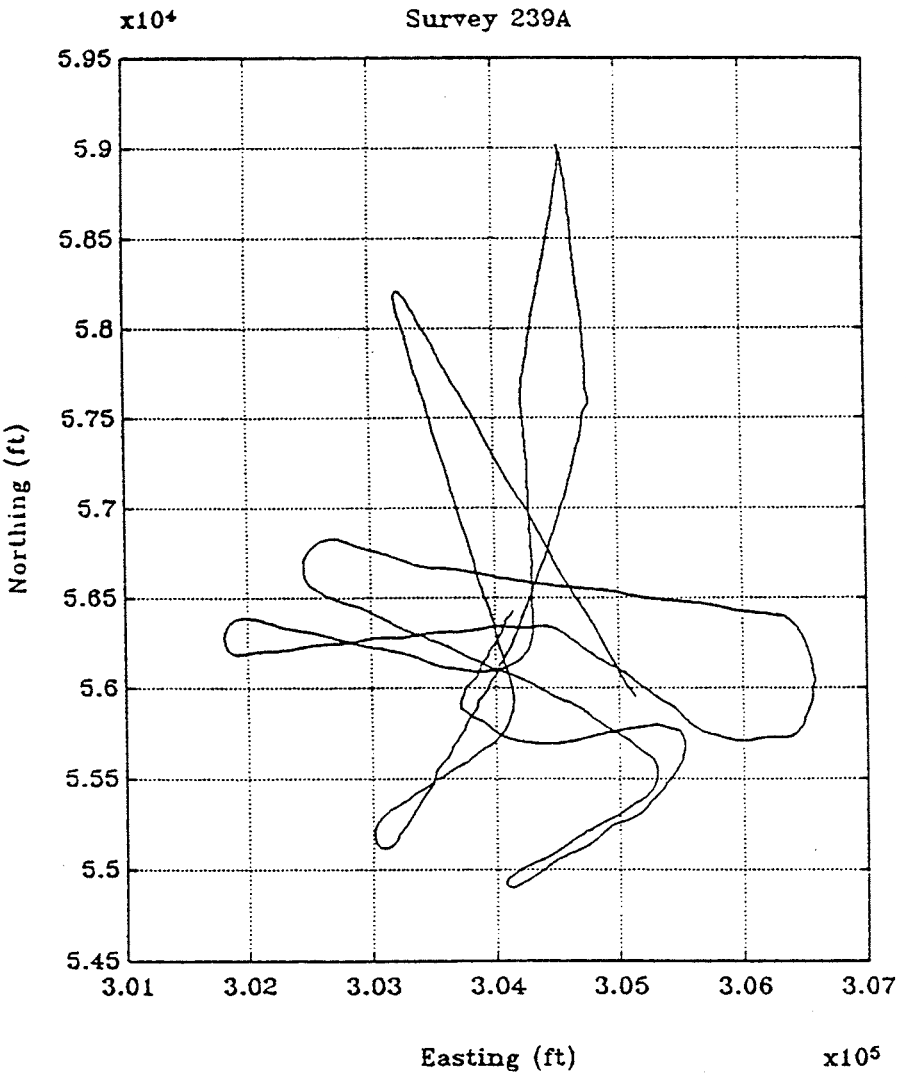

Figure 5.14. Survey 239A: ship tracks from navigation (Mini-Ranger) data.

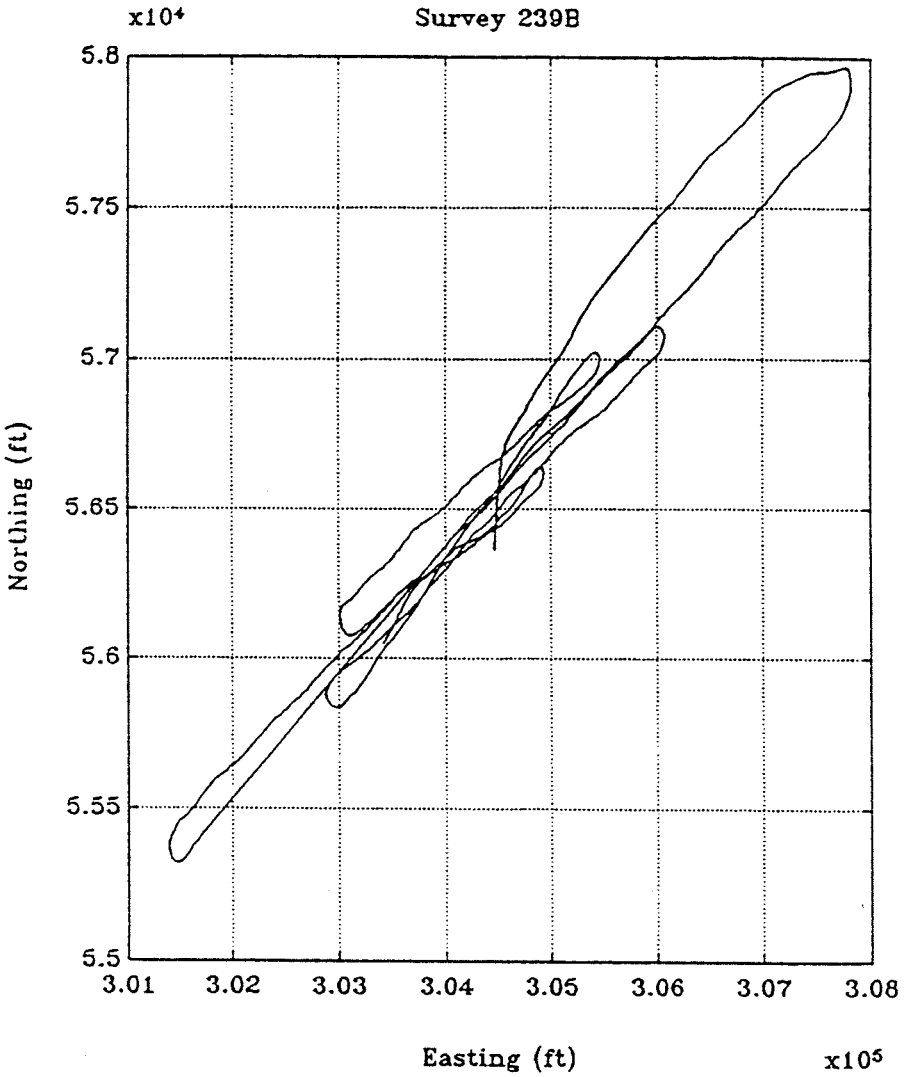

Figure 5.15. Survey 239B: ship tracks from navigation (Mini-Ranger) data.

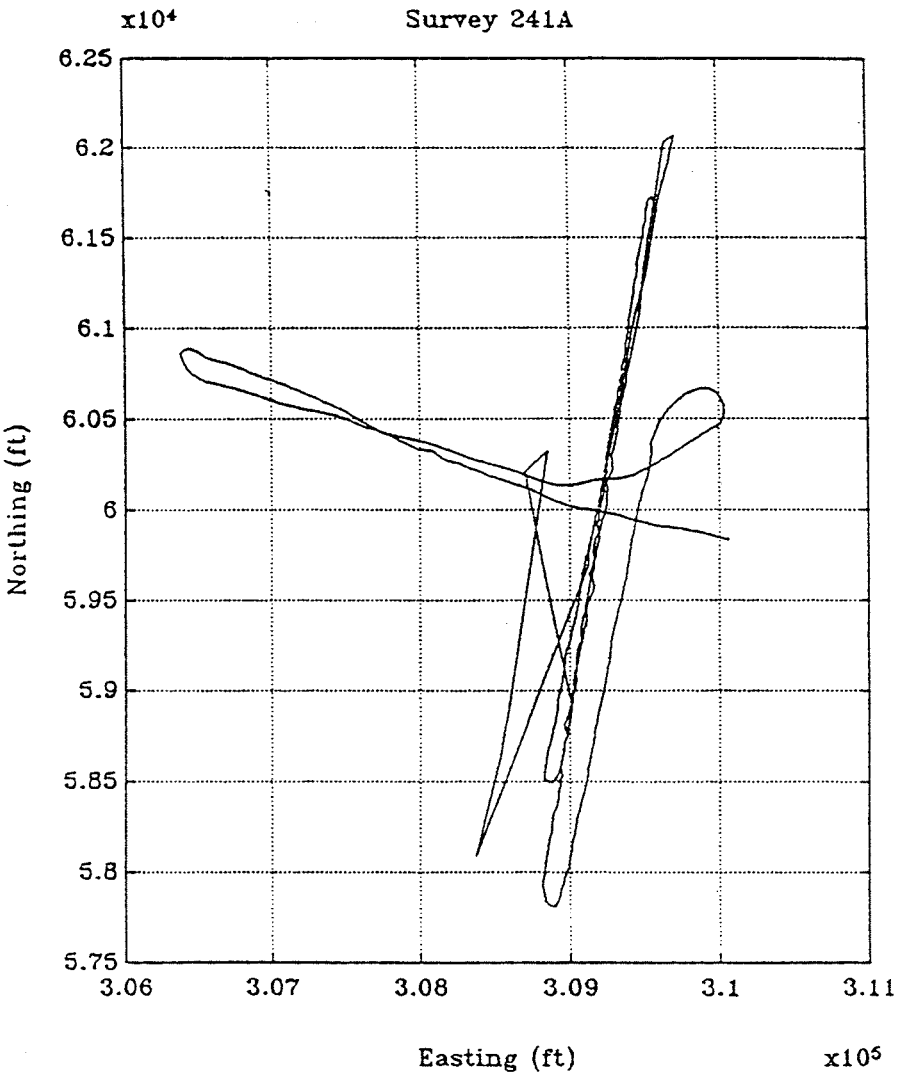

Figure 5.16. Survey 241A: ship tracks from navigation (Mini-Ranger) data.

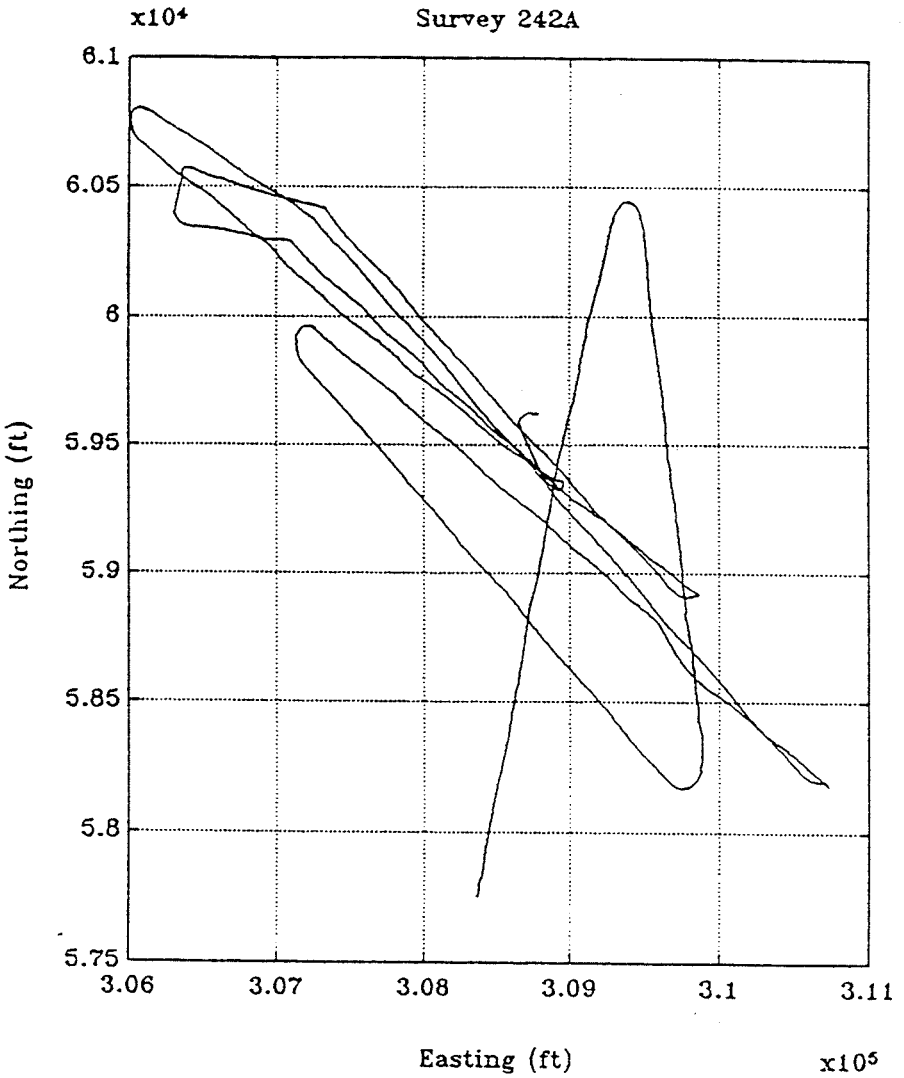

Figure 5.17. Survey 242A: ship tracks from navigation (Mini-Ranger) data.

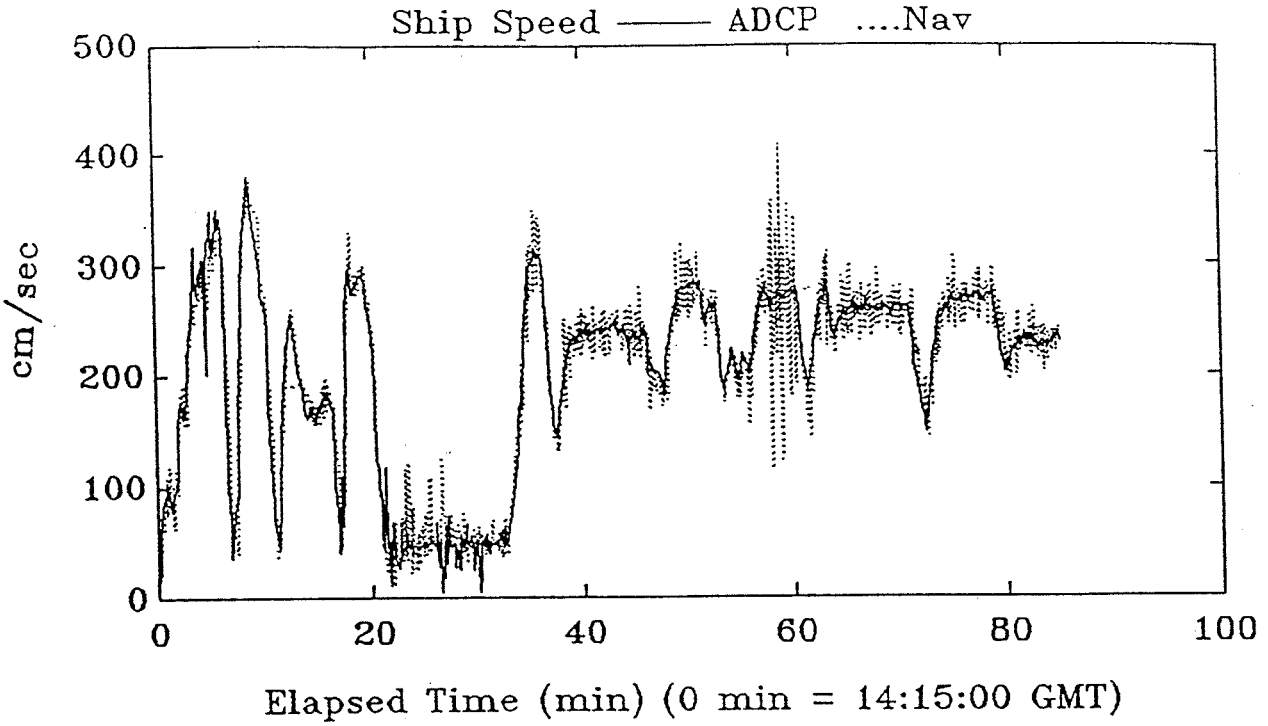

Figure 5.18. Survey 237A: time series of ship speed data.

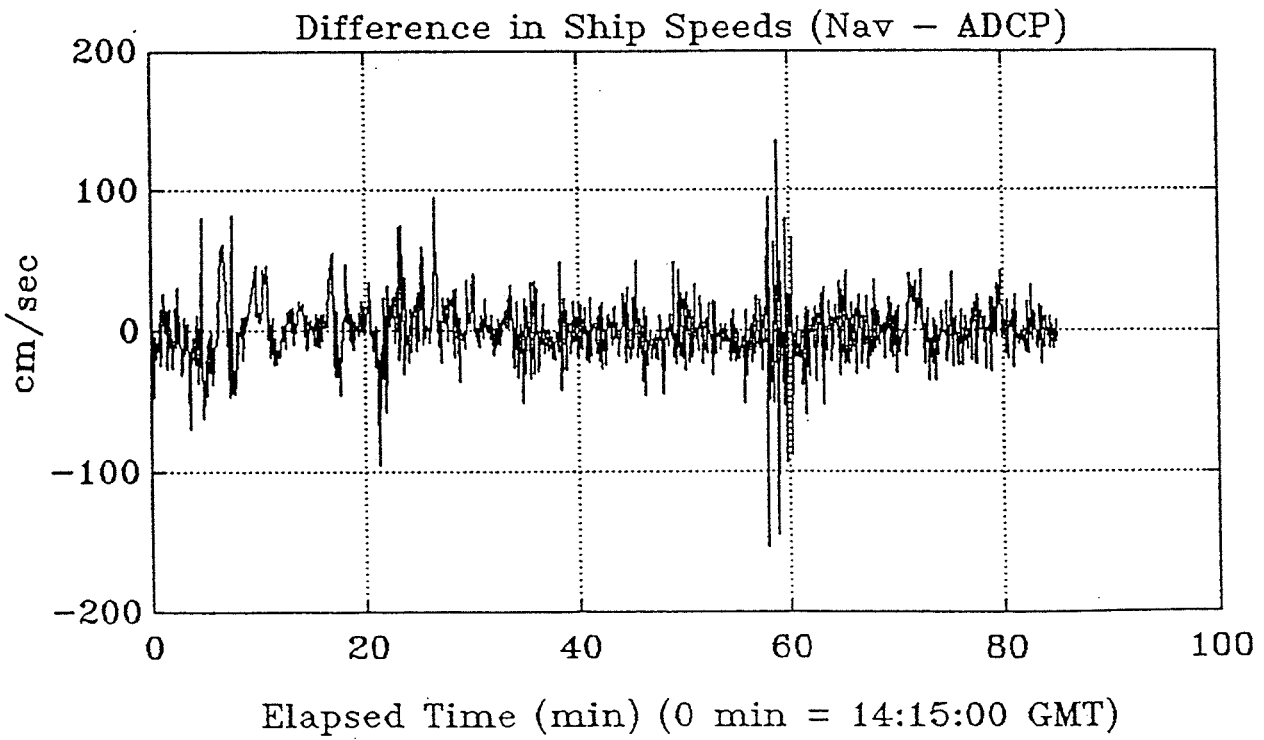

Figure 5.19. Survey 237A: time series of the difference in ship speed.

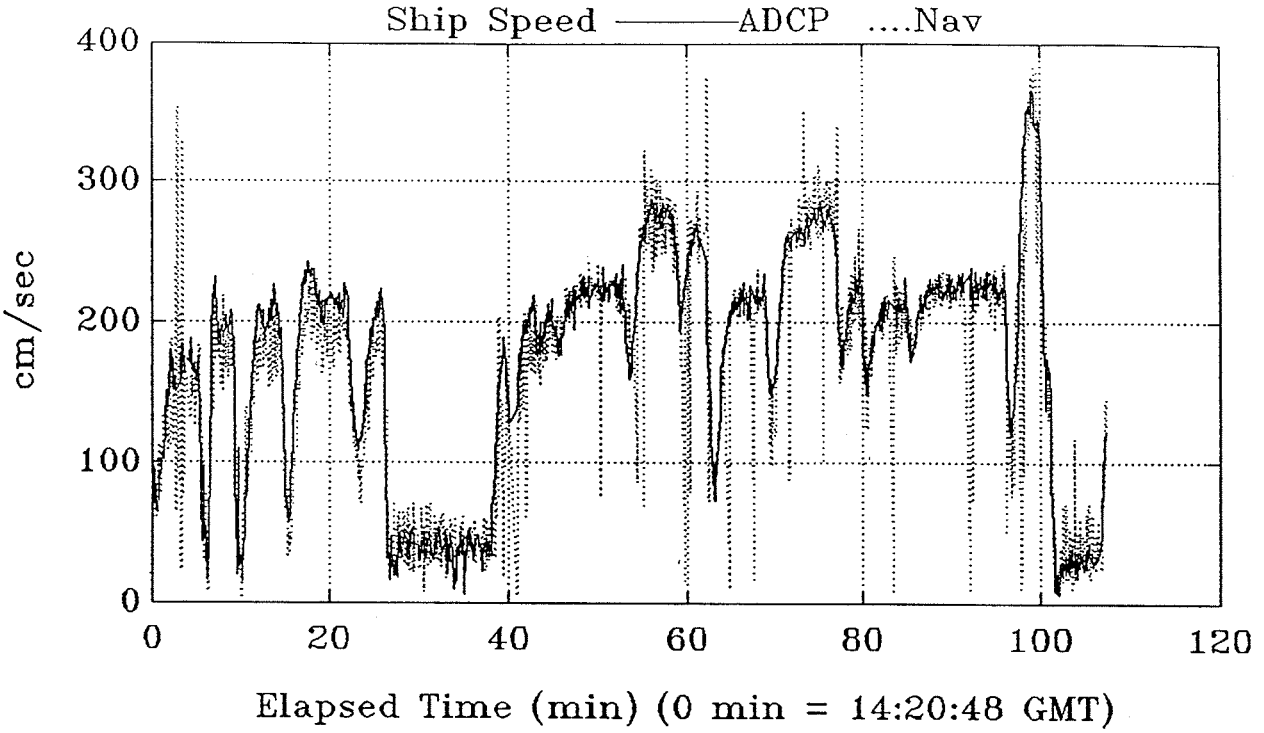

Figure 5.20. Survey 238A: time series of ship speed data.

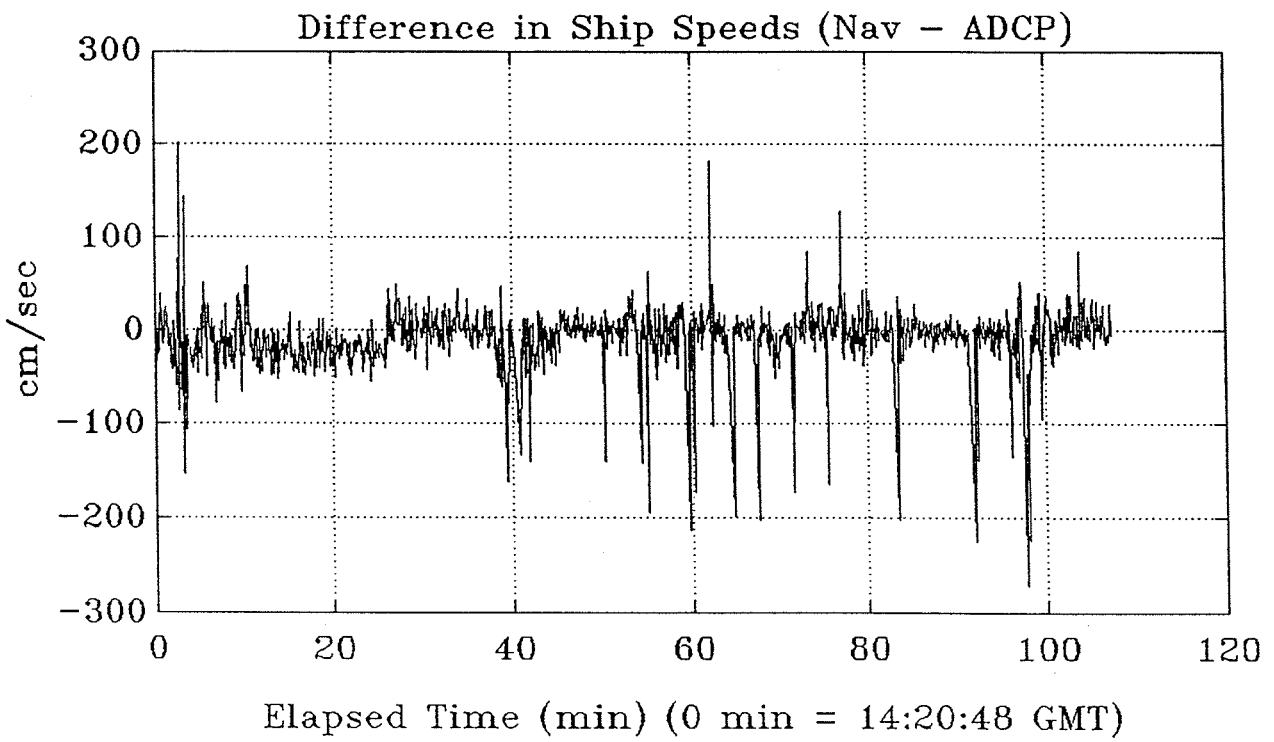

Figure 5.21. Survey 238A: time series of the difference in ship speed.

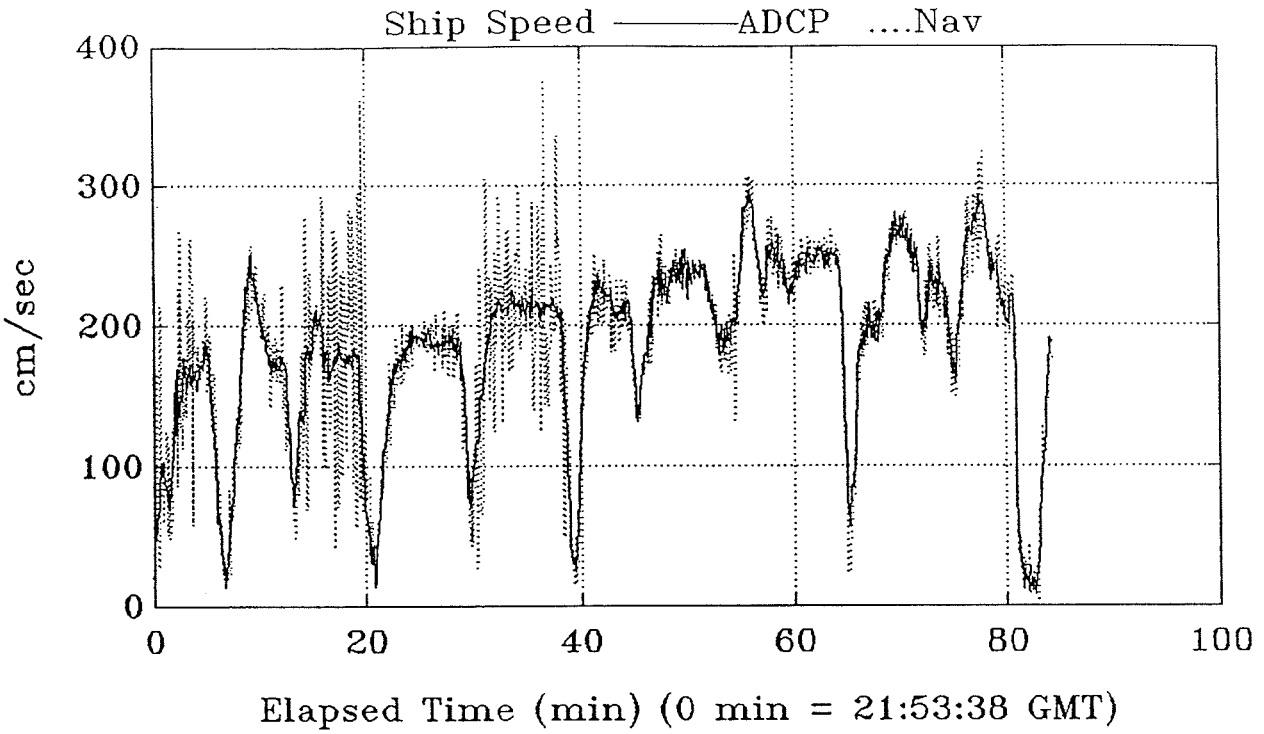

Figure 5.22. Survey 238B: time series of ship speed data.

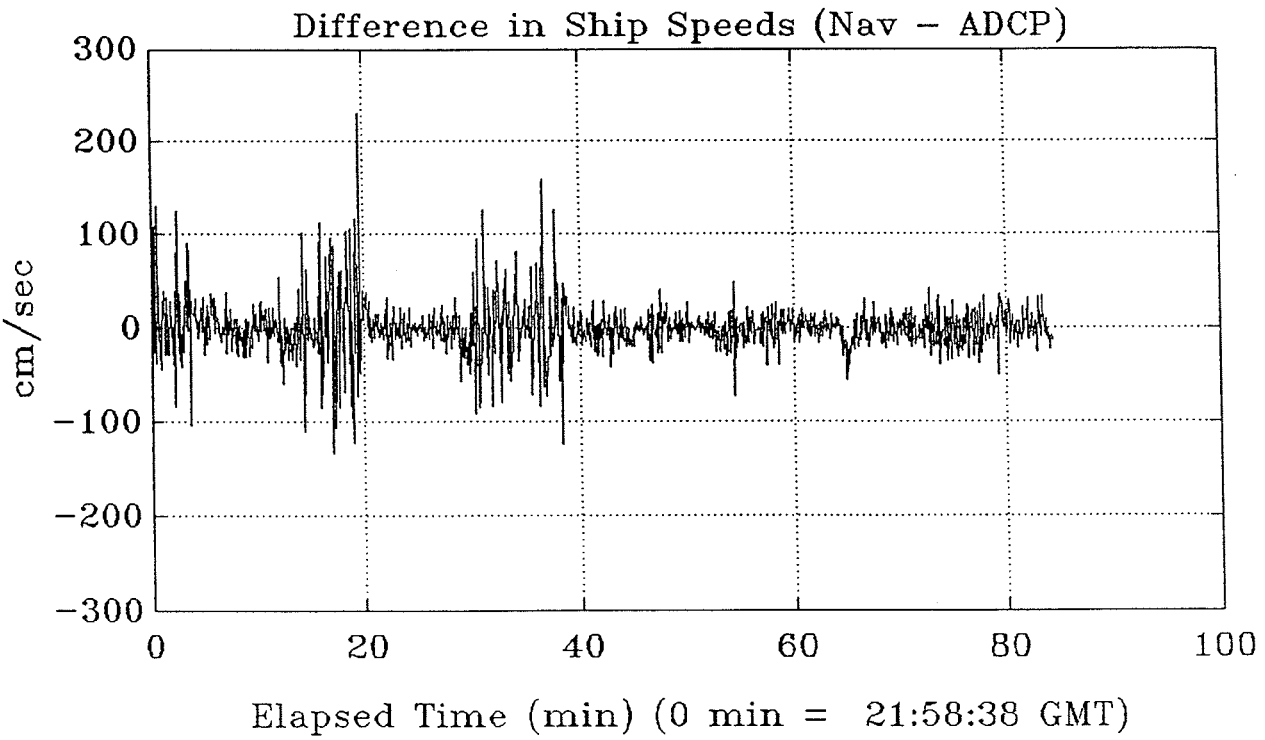

Figure 5.23. Survey 238B: time series of the difference in ship speed.

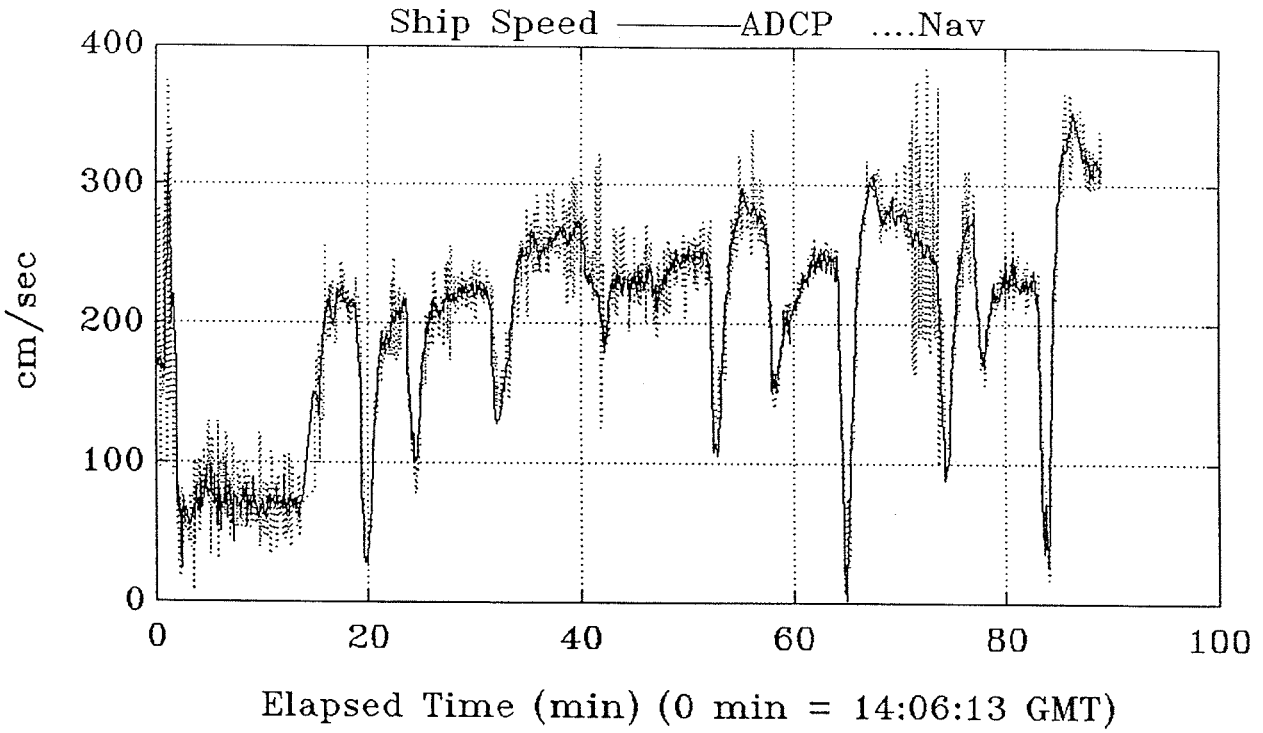

Figure 5.24. Survey 239A: time series of ship speed data.

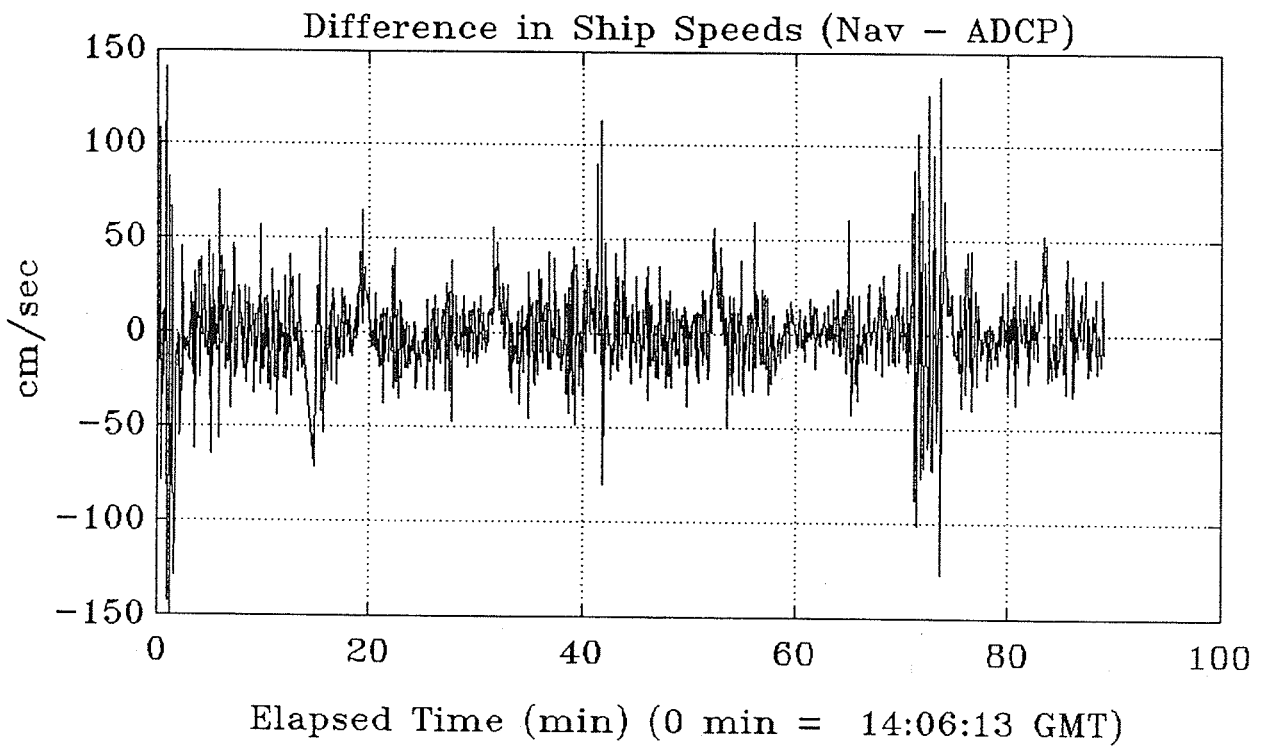

Figure 5.25. Survey 239A: time series of the difference in ship speed.

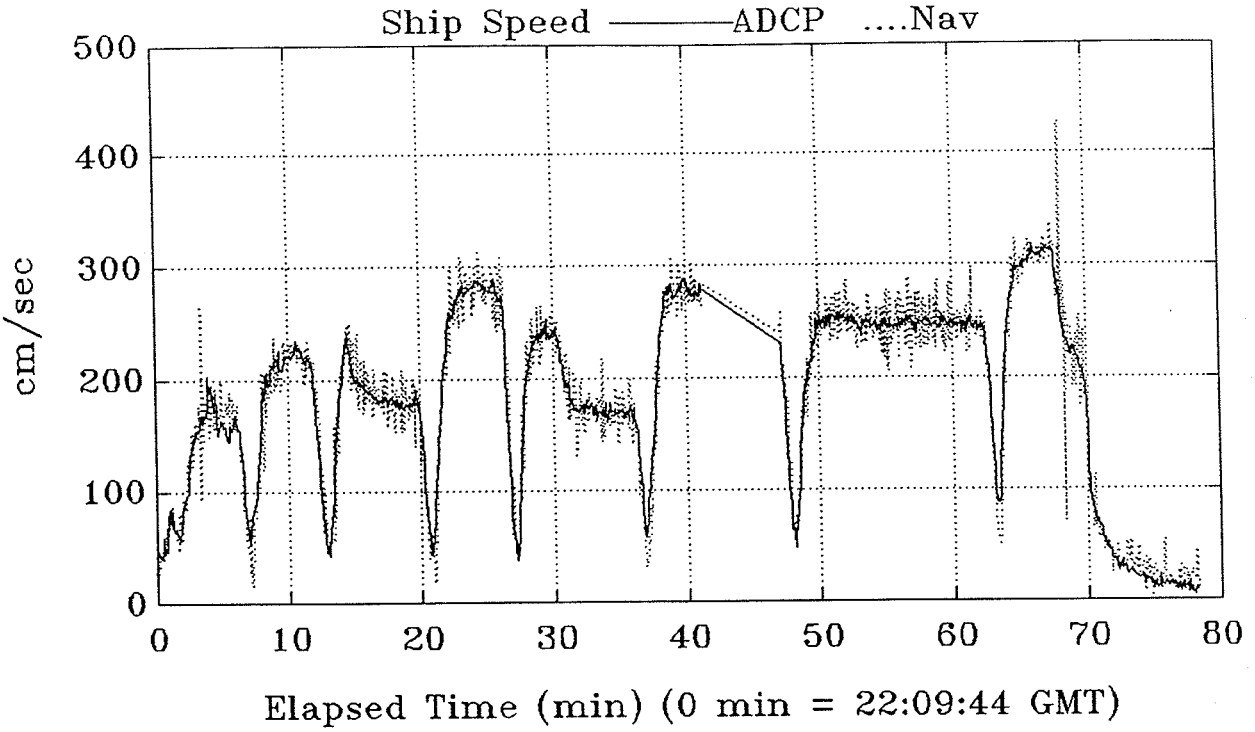

Figure 5.26. Survey 239B: time series of ship speed data.

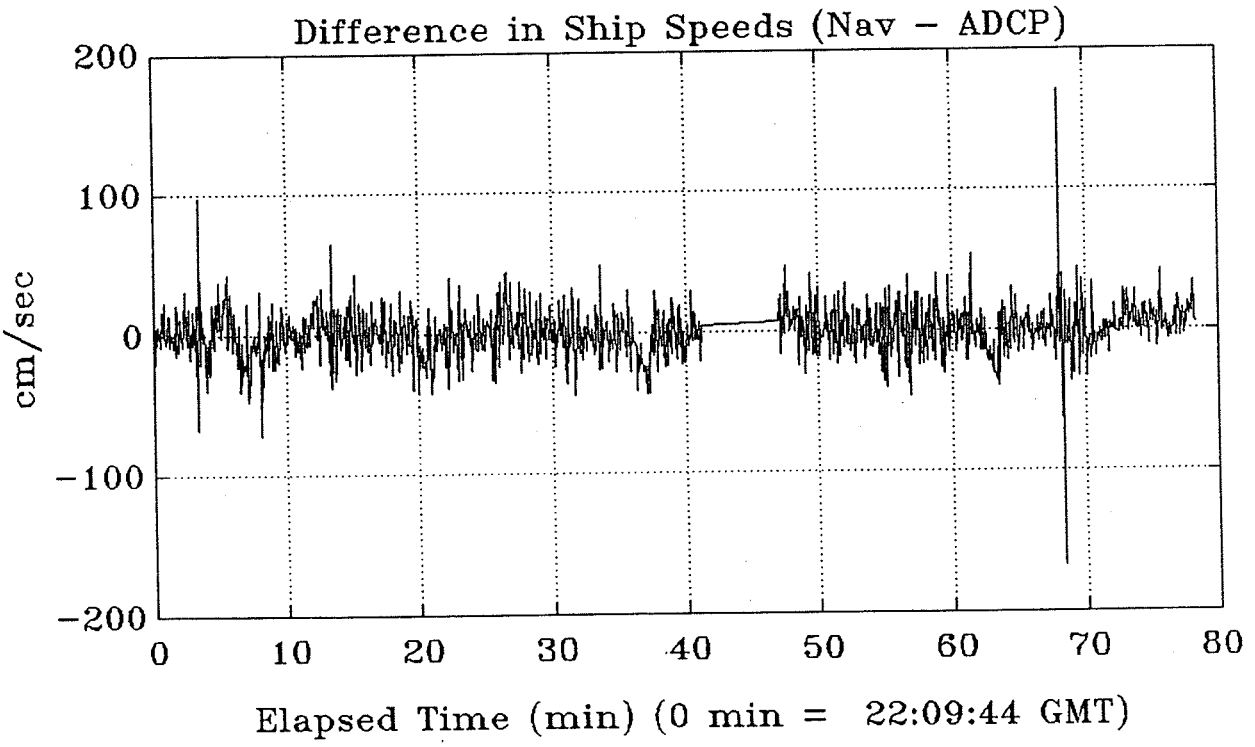

Figure 5.27. Survey 239B: time series of the difference in ship speed.

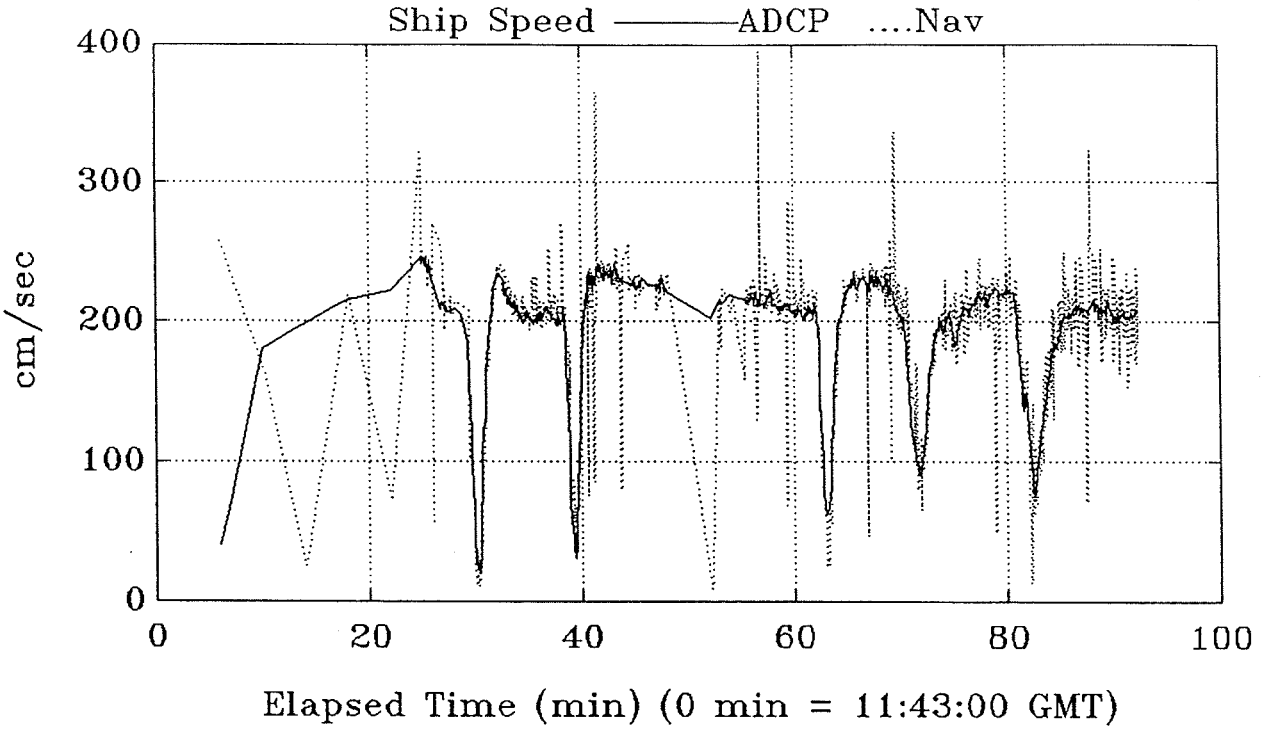

Figure 5.28. Survey 241A: time series of ship speed data.

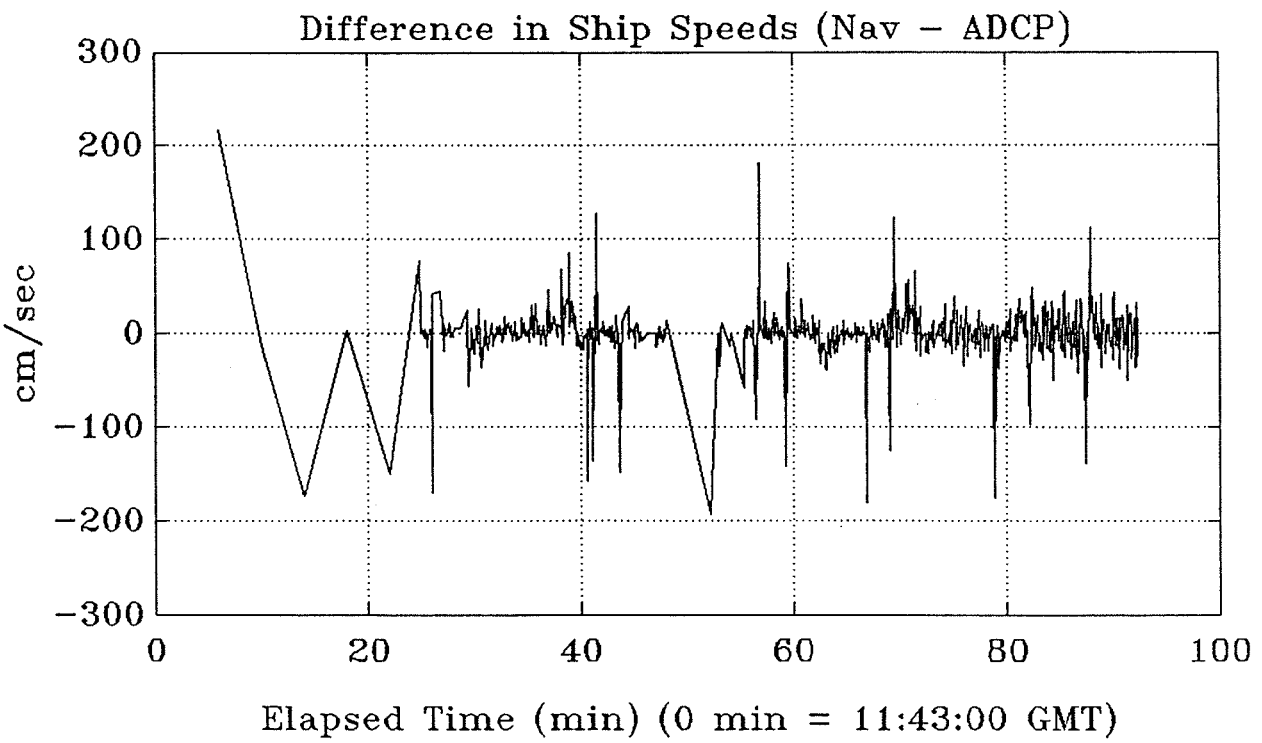

Figure 5.29. Survey 241A: time series of the difference in ship speed.

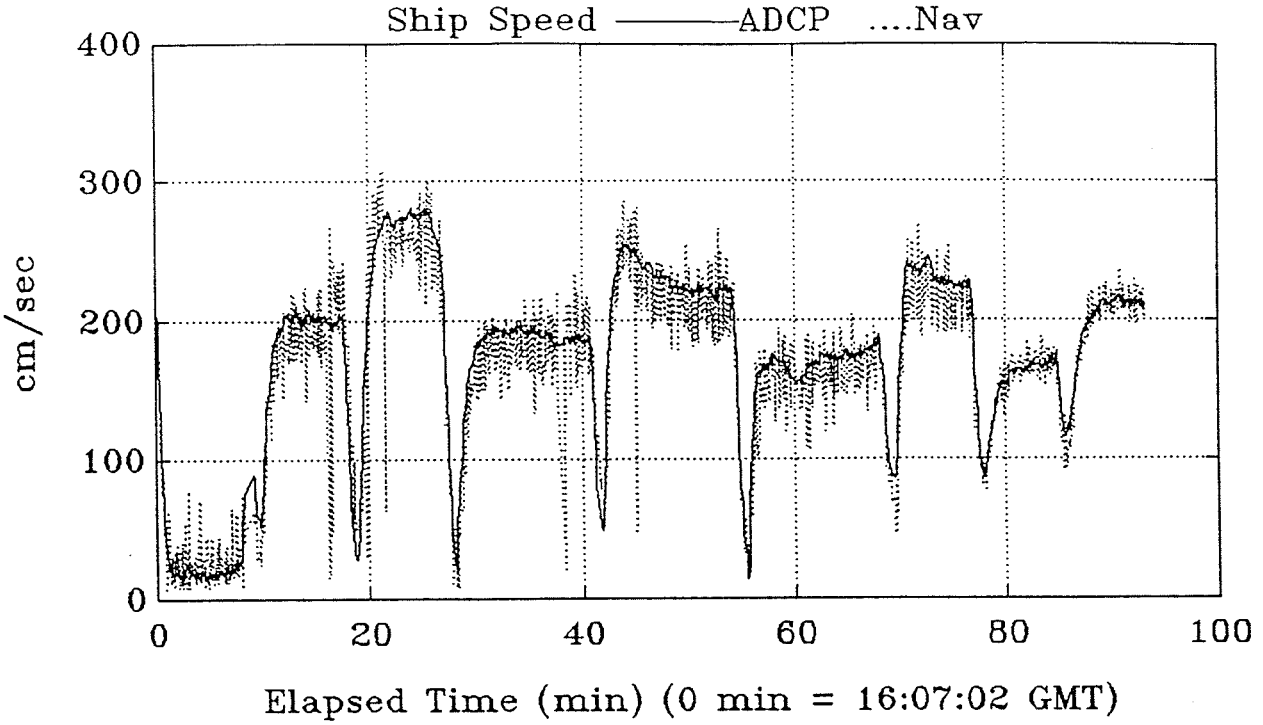

Figure 5.30. Survey 242A: time series of ship speed data.

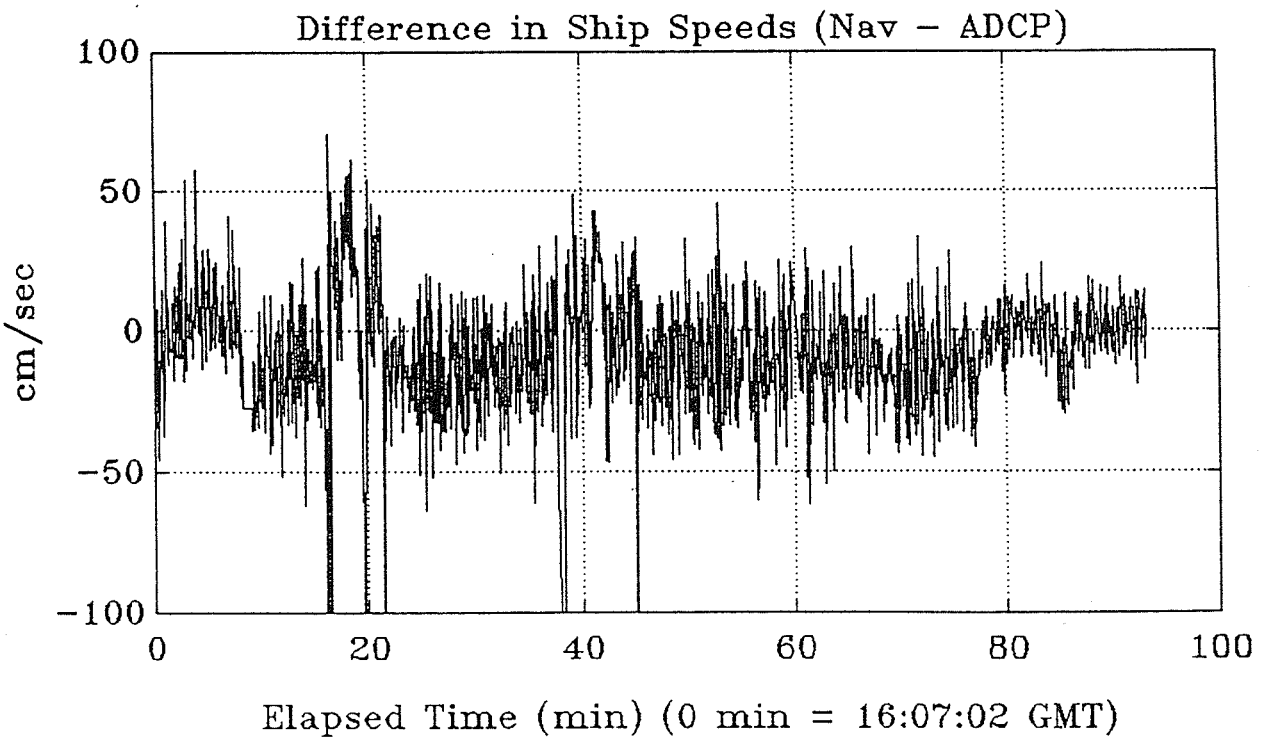

Figure 5.31. Survey 242A: time series of the difference in ship speed.

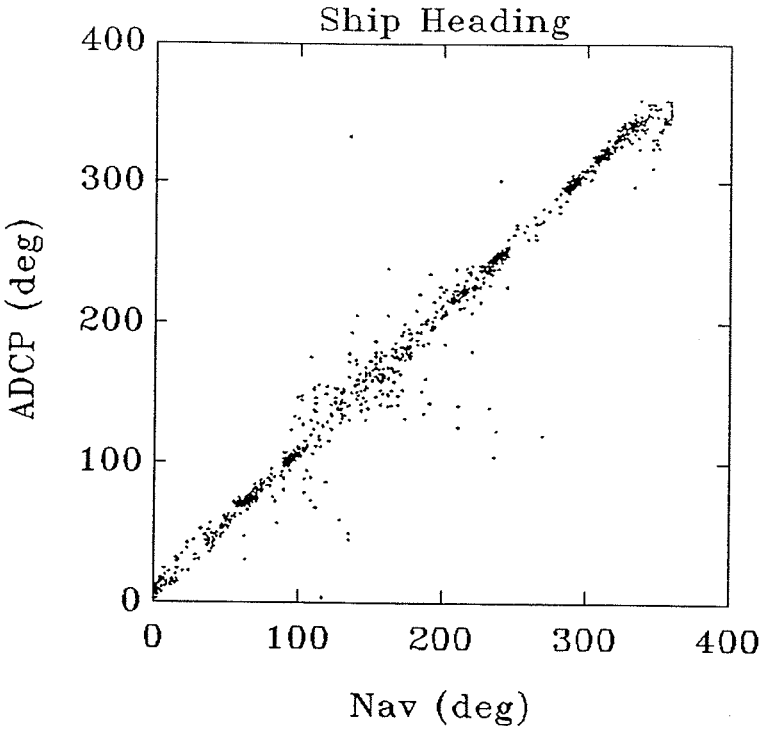

Figure 5.32. Survey 237A: comparison plot of ship heading.

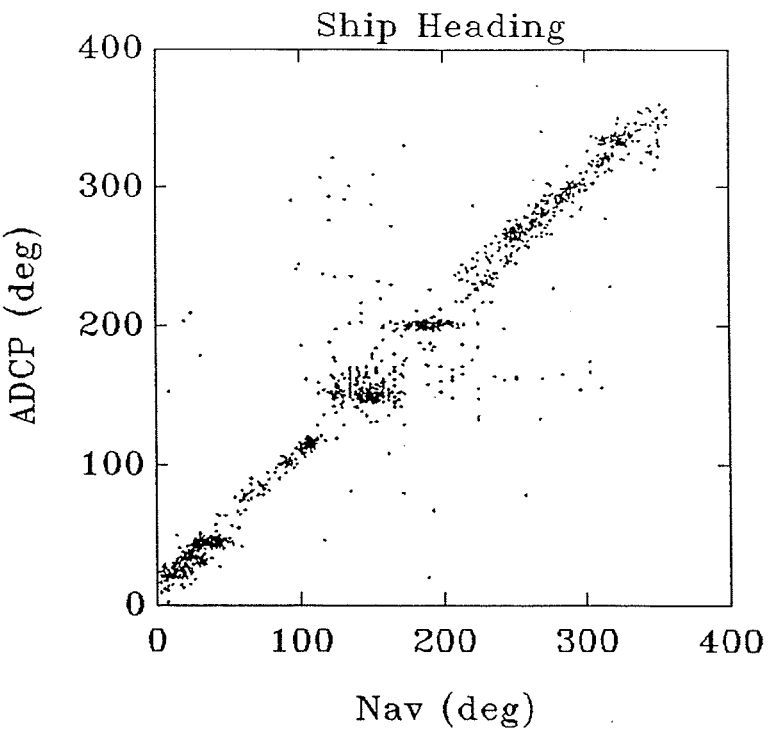

Figure 5.33. Survey 238A: comparison plot of ship heading.

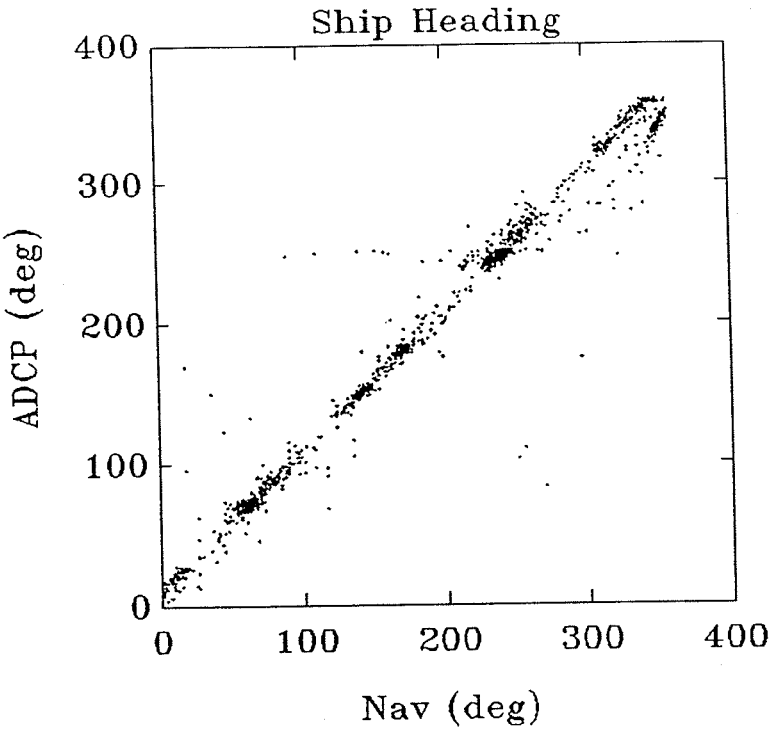

Figure 5.34. Survey 238B: comparison plot of ship heading.

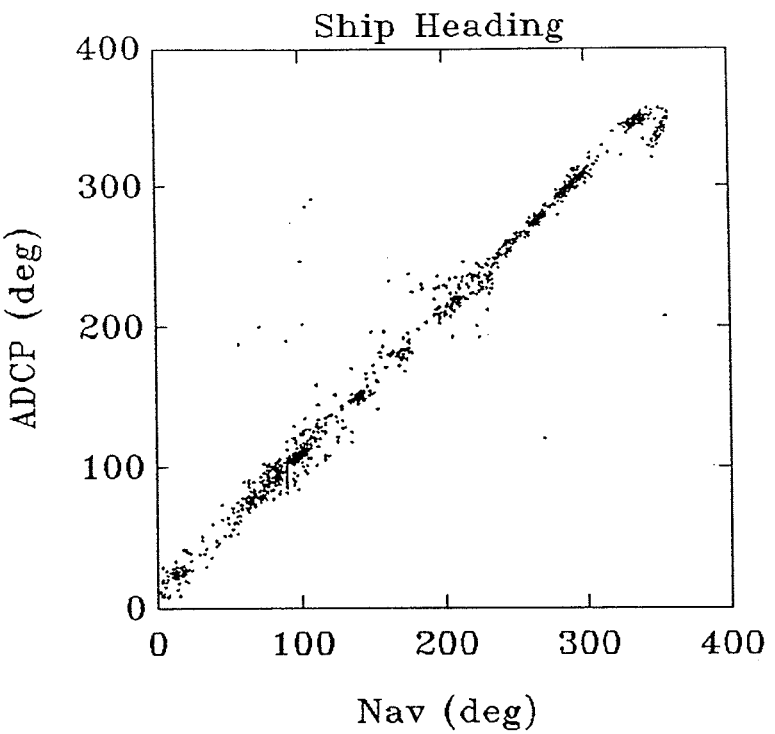

Figure 5.35. Survey 239A: comparison plot of ship heading.

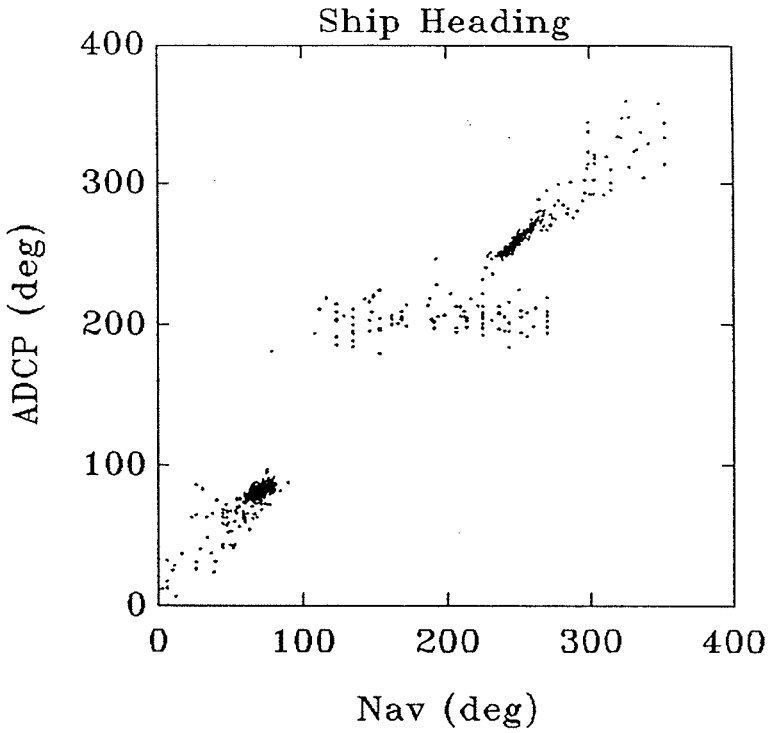

Figure 5.36. Survey 239B: comparison plot of ship heading.

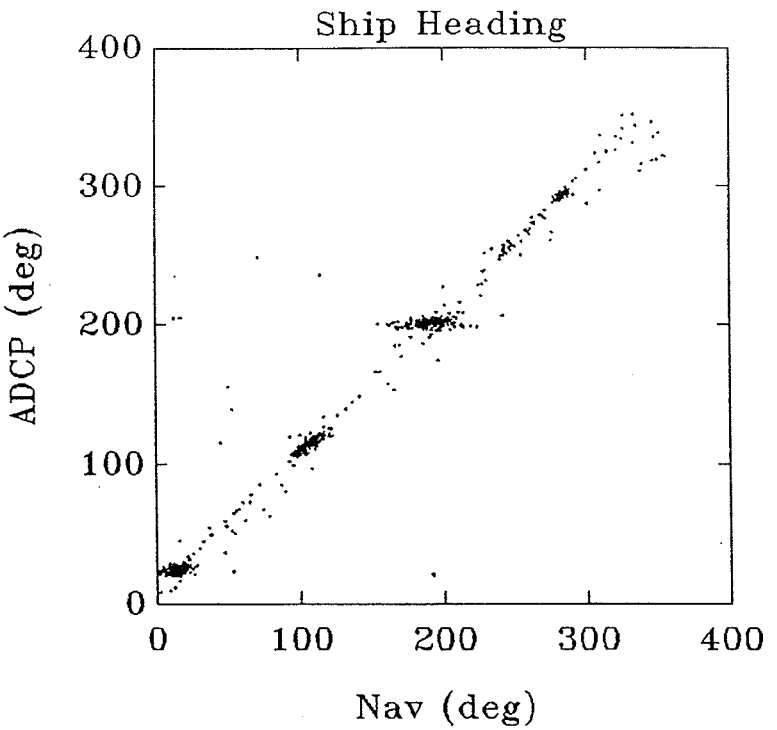

Figure 5.37. Survey 241A: comparison plot of ship heading.

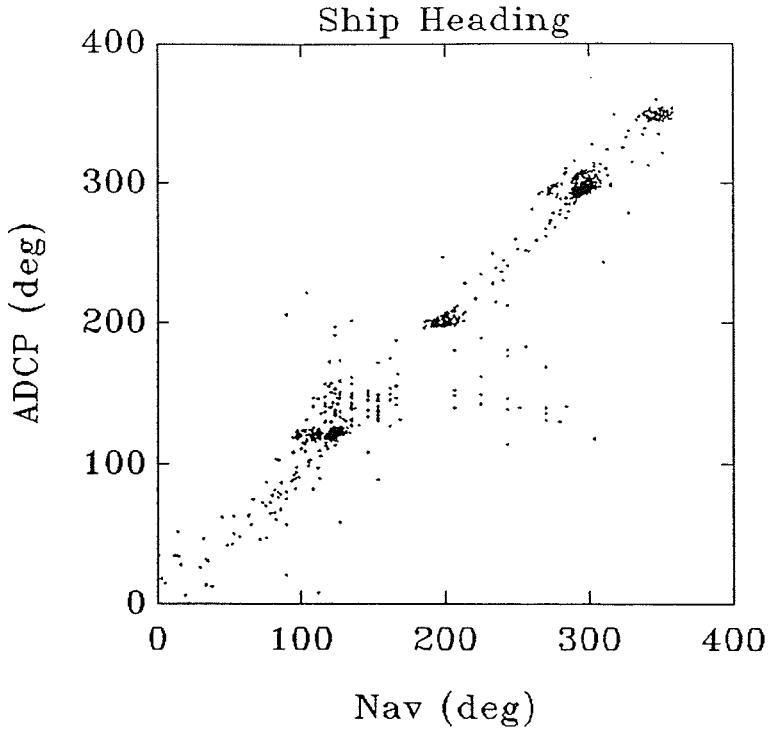

Figure 5.38. Survey 242A: comparison plot of ship heading.

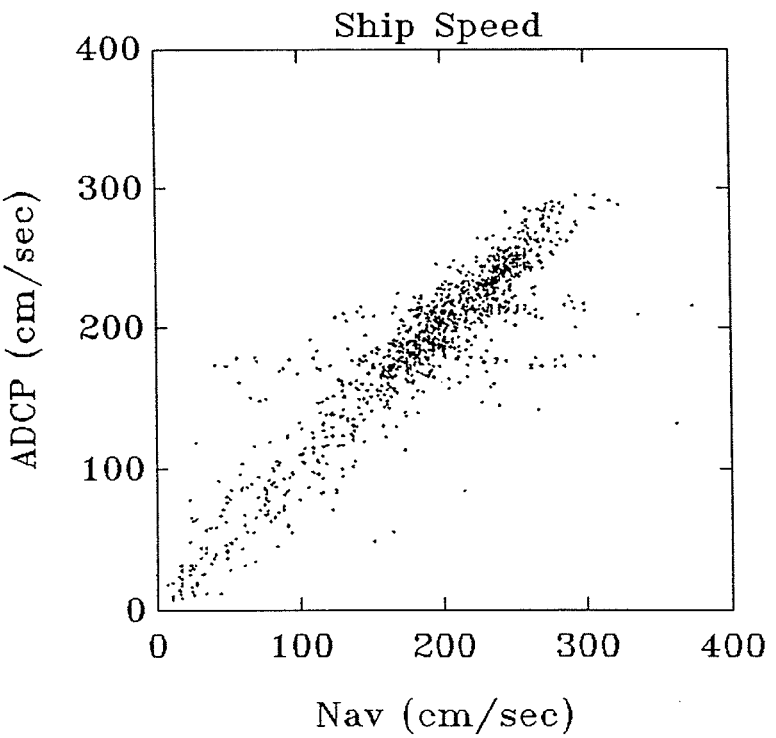

Figure 5.39. Survey 237A: comparison plot of ship speed.

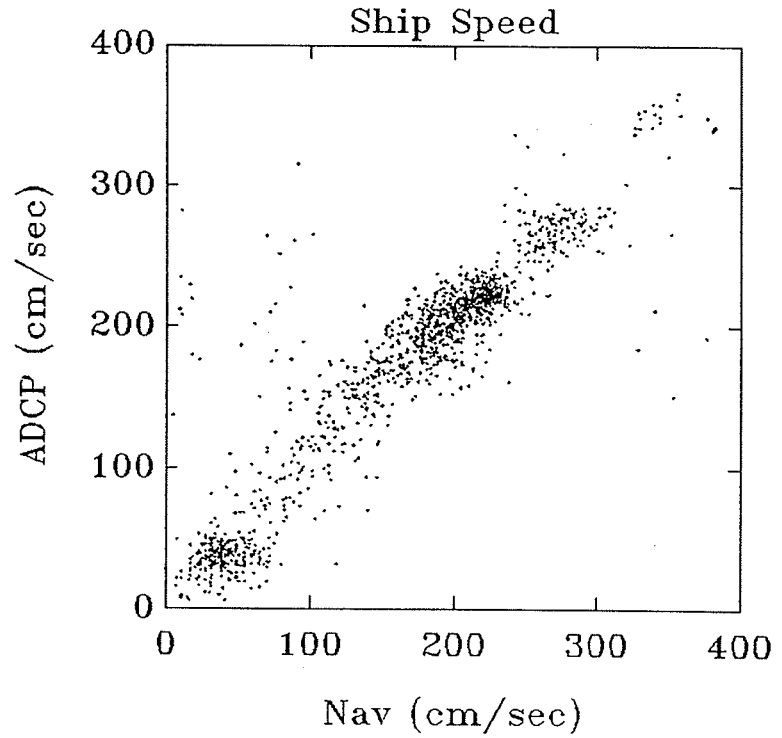

Figure 5.40. Survey 238A: comparison plot of ship speed.

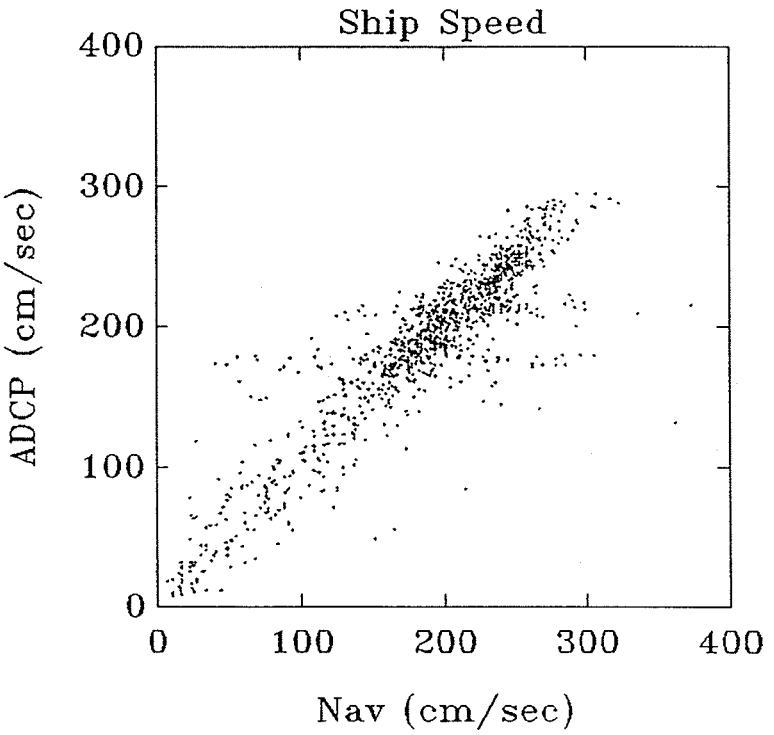

Figure 5.41. Survey 238B: comparison plot of ship speed.

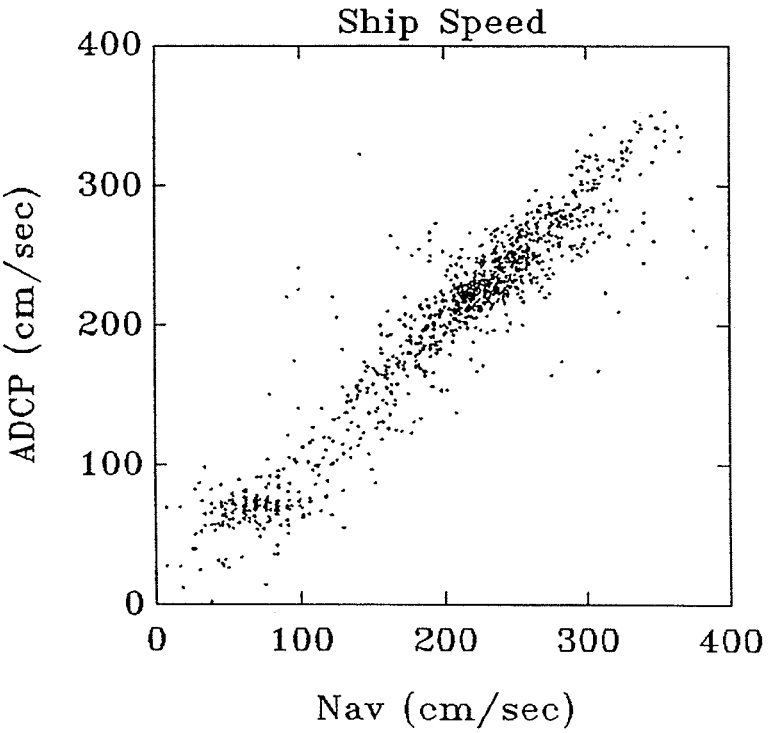

Figure 5.42. Survey 239A: comparison plot of ship speed.

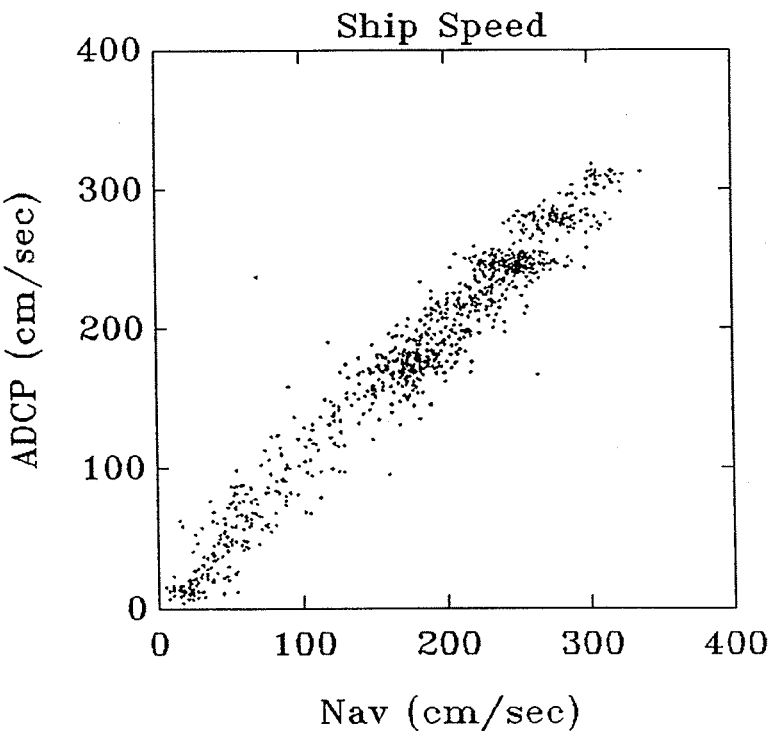

Figure 5.43. Survey 239B: comparison plot of ship speed.

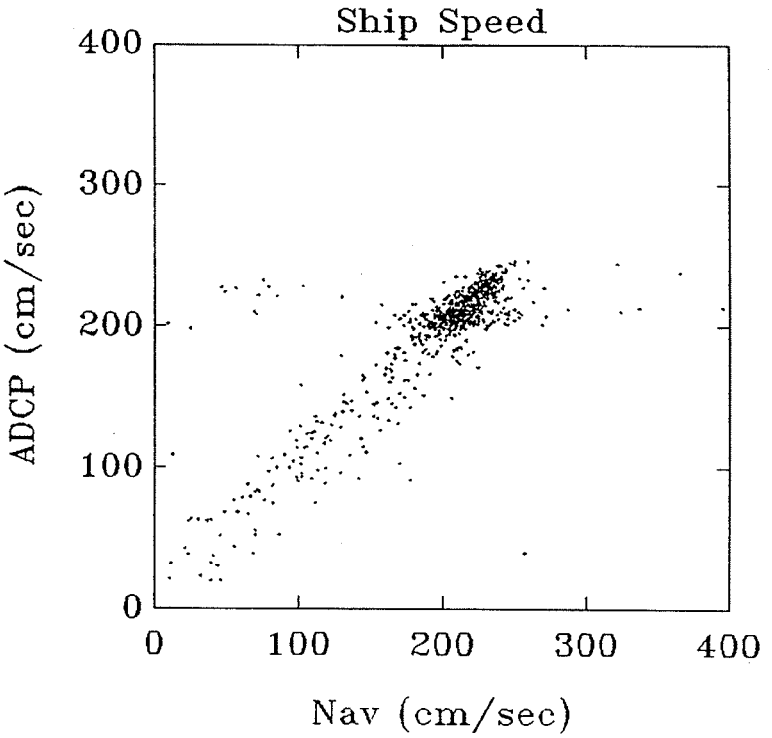

Figure 5.44. Survey 241A: comparison plot of ship speed.

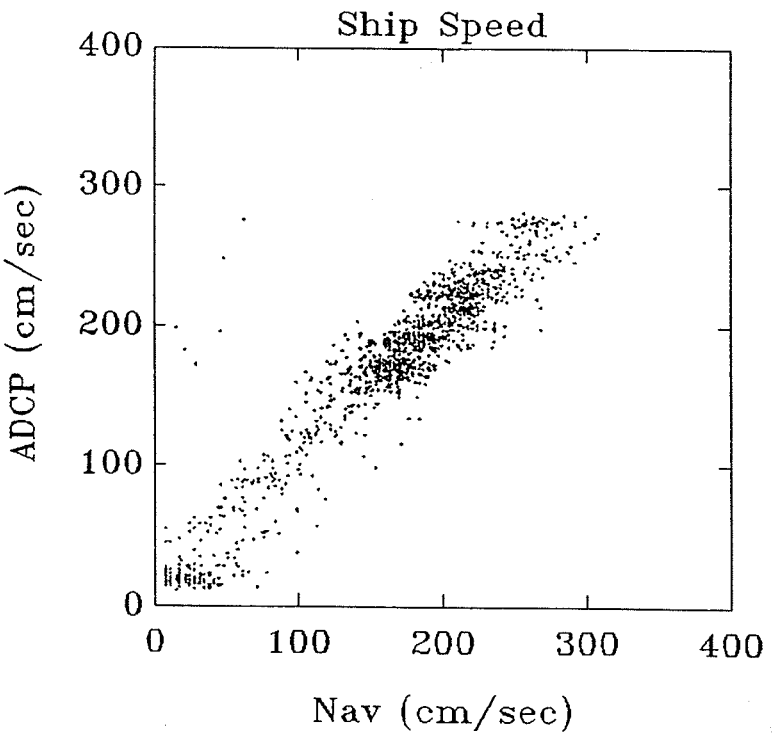

Figure 5.45. Survey 242A: comparison plot of ship speed.

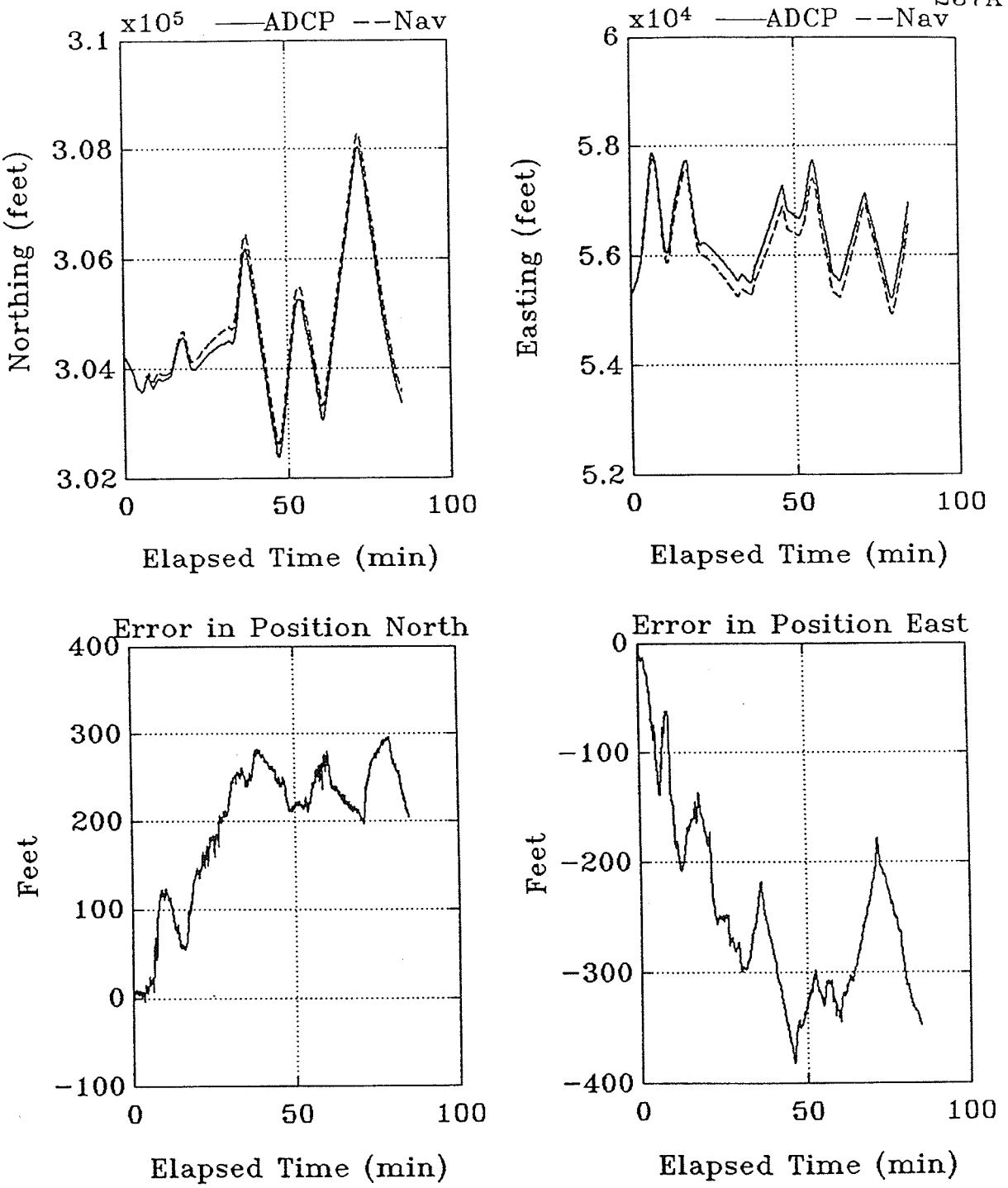

Figure 5.46. Survey 237A: time series for the estimates of ship position from the ADCP bottom track data and the navigation data. Clockwise from upper left: (a) North ship position (ADCP solid line, Navigation dashed); (b) East ship position (ADCP solid line, Navigation dashed); (c) Error in north position estimates (Navigation - ADCP); (d) Error in east position estimate (Navigation - ADCP). Elapsed time is given in minutes from the start of the survey (0 min = 14:15:00 GMT).

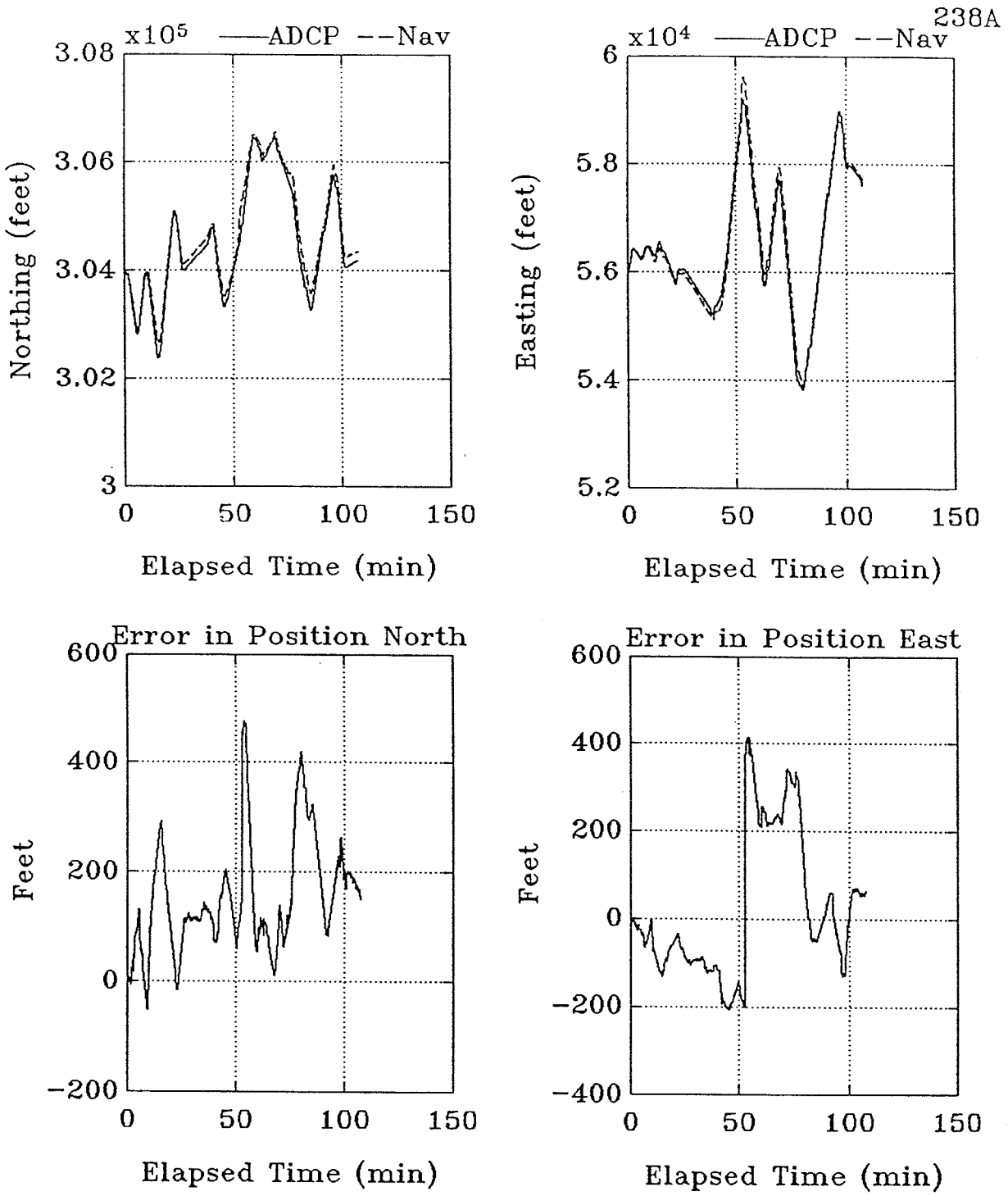

Figure 5.47. Survey 238A: time series for the estimates of ship position from the ADCP bottom track data and the navigation data. Clockwise from upper left: (a) North ship position (ADCP solid line, Navigation dashed); (b) East ship position (ADCP solid line, Navigation dashed); (c) Error in north position estimates (Navigation - ADCP); (d) Error in east position estimate (Navigation - ADCP). Elapsed time is given in minutes from the start of the survey (0 min = 14:20:48 GMT).

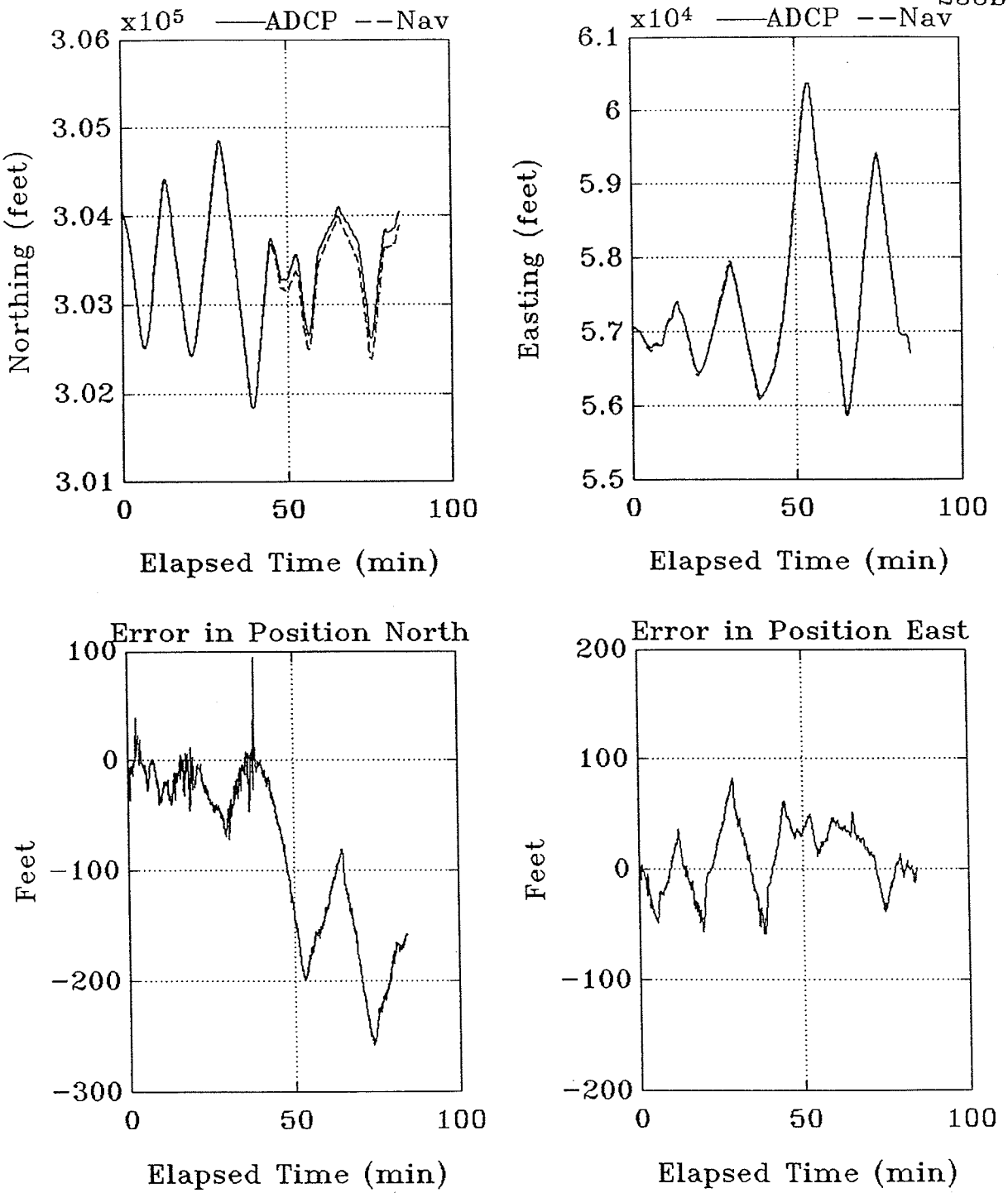

Figure 5.48. Survey 238B: time series for the estimates of ship position from the ADCP bottom track data and the navigation data. Clockwise from upper left: (a) North ship position (ADCP solid line, Navigation dashed); (b) East ship position (ADCP solid line, Navigation dashed); (c) Error in north position estimates (Navigation - ADCP); (d) Error in east position estimate (Navigation - ADCP). Elapsed time is given in minutes from the start of the survey (0 min = 21:53:38 GMT).

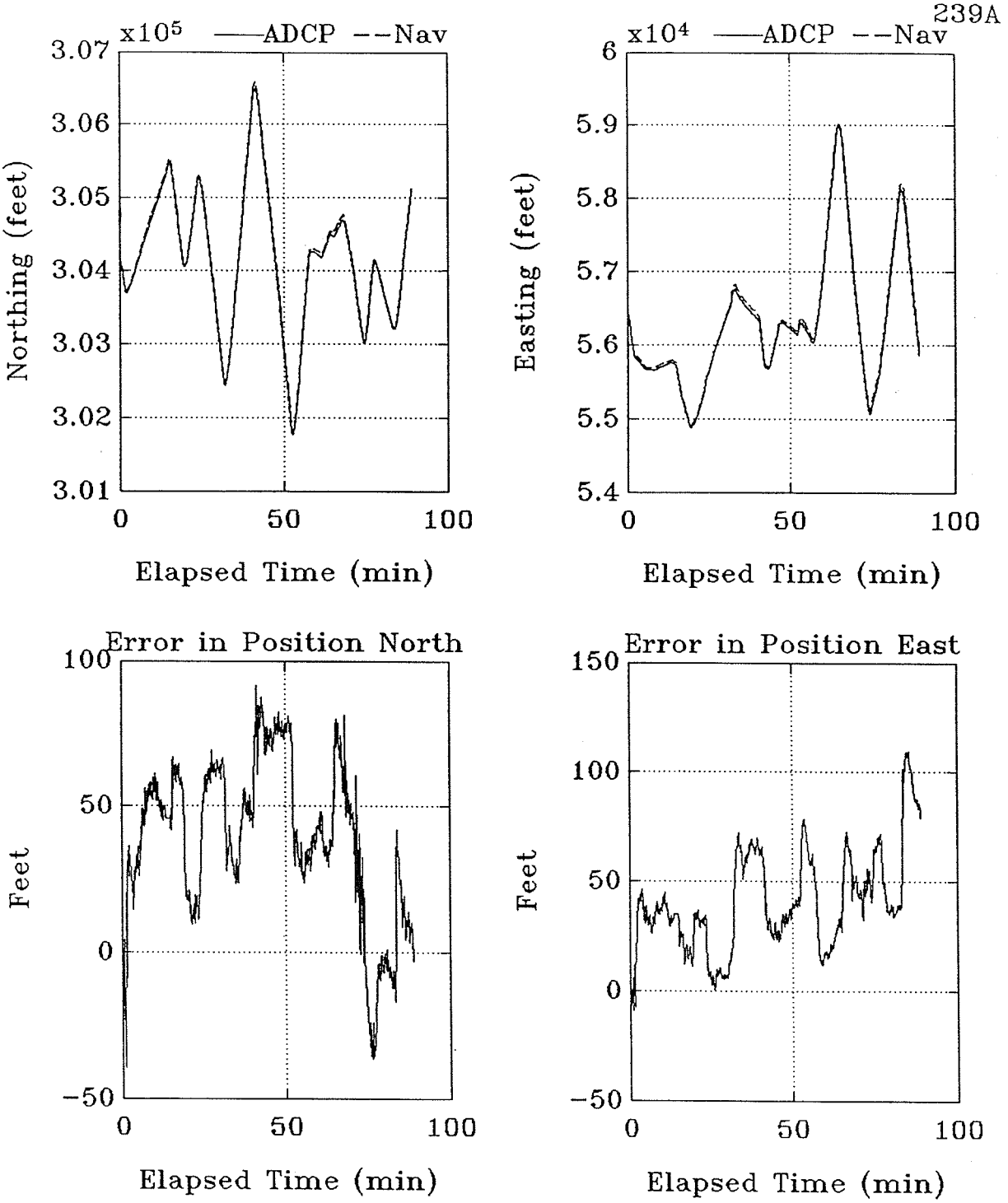

Figure 5.49. Survey 239A: time series for the estimates of ship position from the ADCP bottom track data and the navigation data. Clockwise from upper left: (a) North ship position (ADCP solid line, Navigation dashed); (b) East ship position (ADCP solid line, Navigation dashed); (c) Error in north position estimates (Navigation - ADCP); (d) Error in east position estimate (Navigation - ADCP). Elapsed time is given in minutes from the start of the survey (0 min = 14:06:13 GMT).

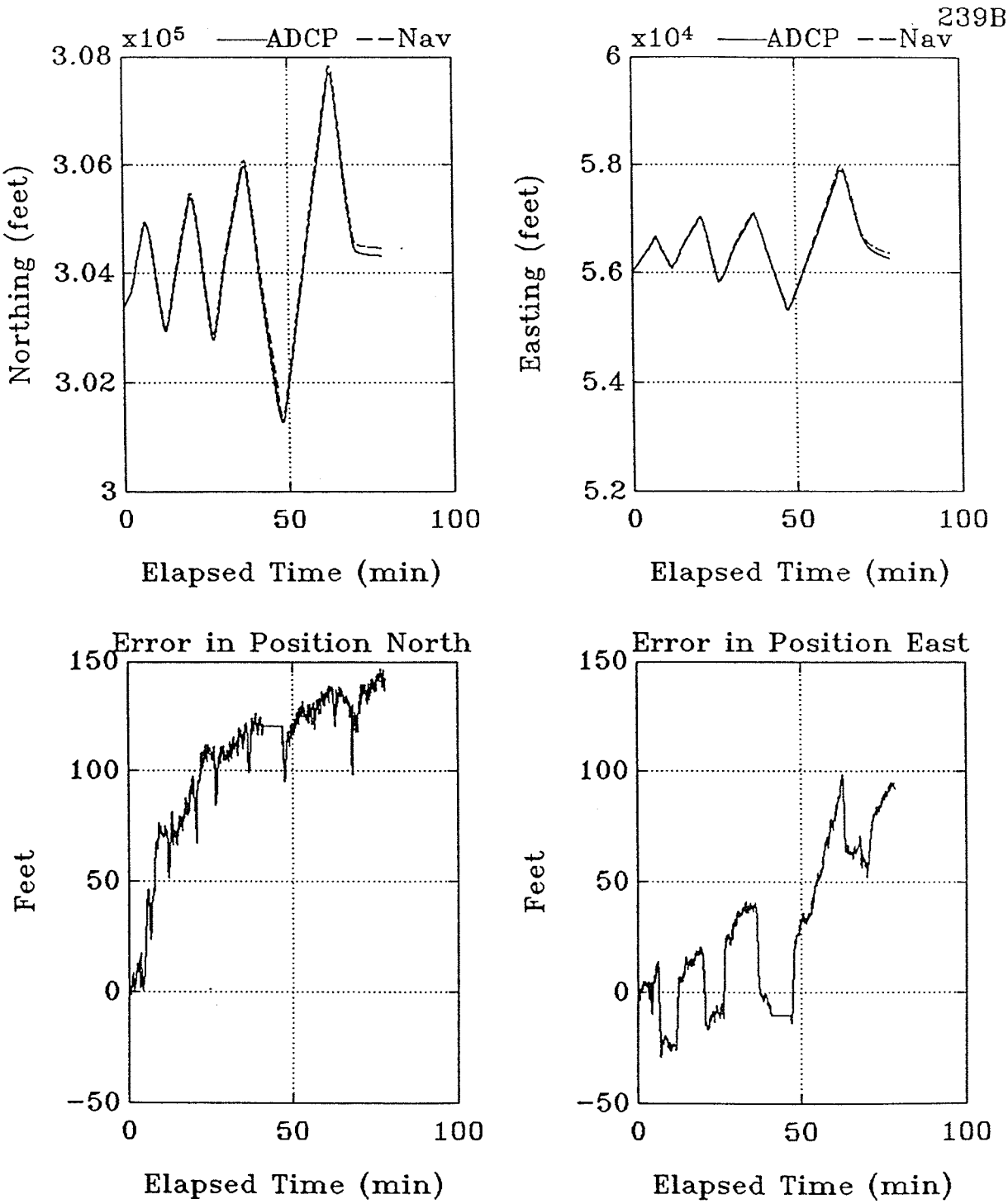

Figure 5.50. Survey 239B: time series for the estimates of ship position from the ADCP bottom track data and the navigation data. Clockwise from upper left: (a) North ship position (ADCP solid line, Navigation dashed); (b) East ship position (ADCP solid line, Navigation dashed); (c) Error in north position estimates (Navigation - ADCP); (d) Error in east position estimate (Navigation - ADCP). Elapsed time is given in minutes from the start of the survey (0 min = 22:09:44 GMT).

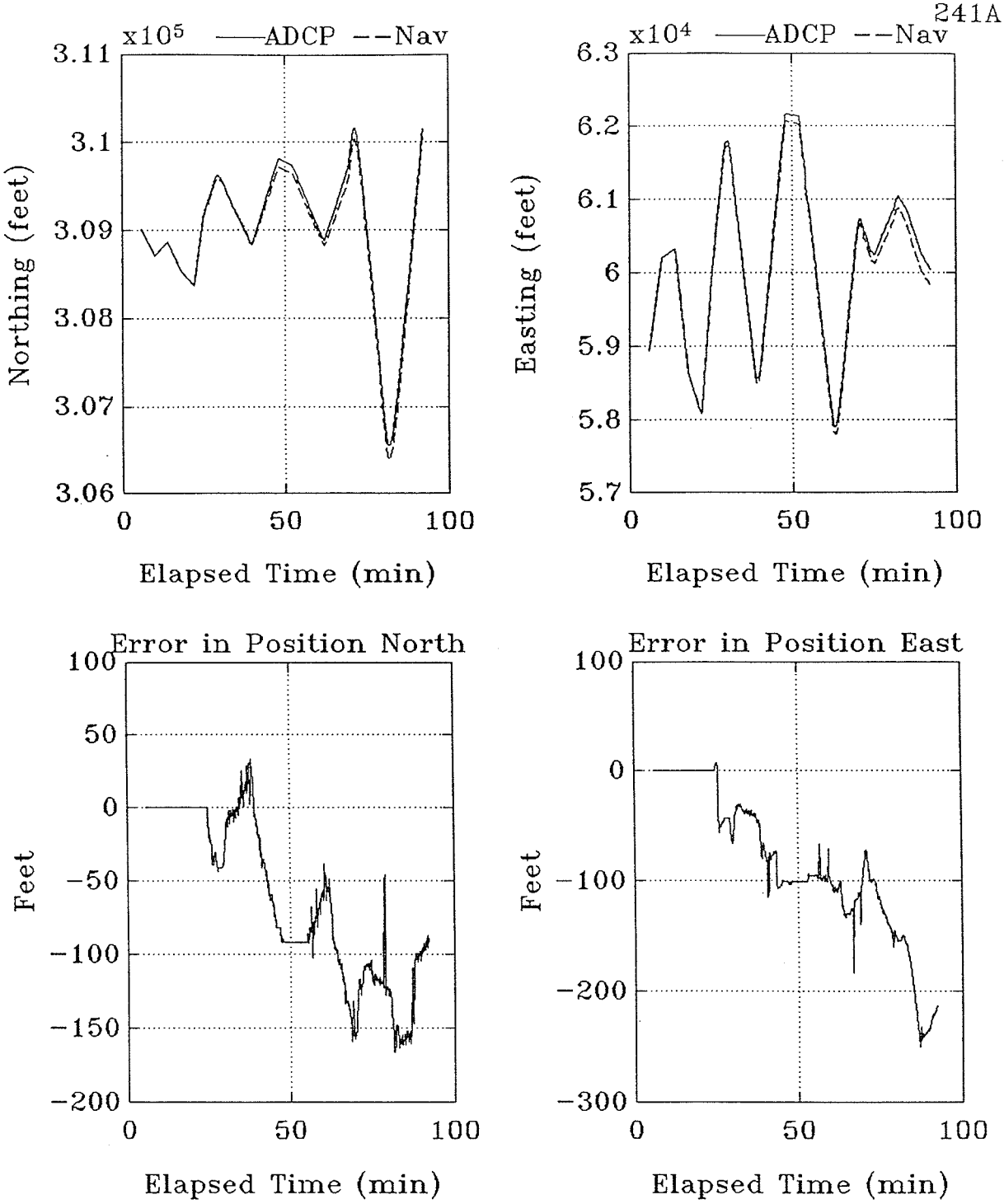

Figure 5.51. Survey 241A: time series for the estimates of ship position from the ADCP bottom track data and the navigation data. Clockwise from upper left: (a) North ship position (ADCP solid line, Navigation dashed); (b) East ship position (ADCP solid line, Navigation dashed); (c) Error in north position estimates (Navigation - ADCP); (d) Error in east position estimate (Navigation - ADCP). Elapsed time is given in minutes from the start of the survey (0 min = 11:43:00 GMT).

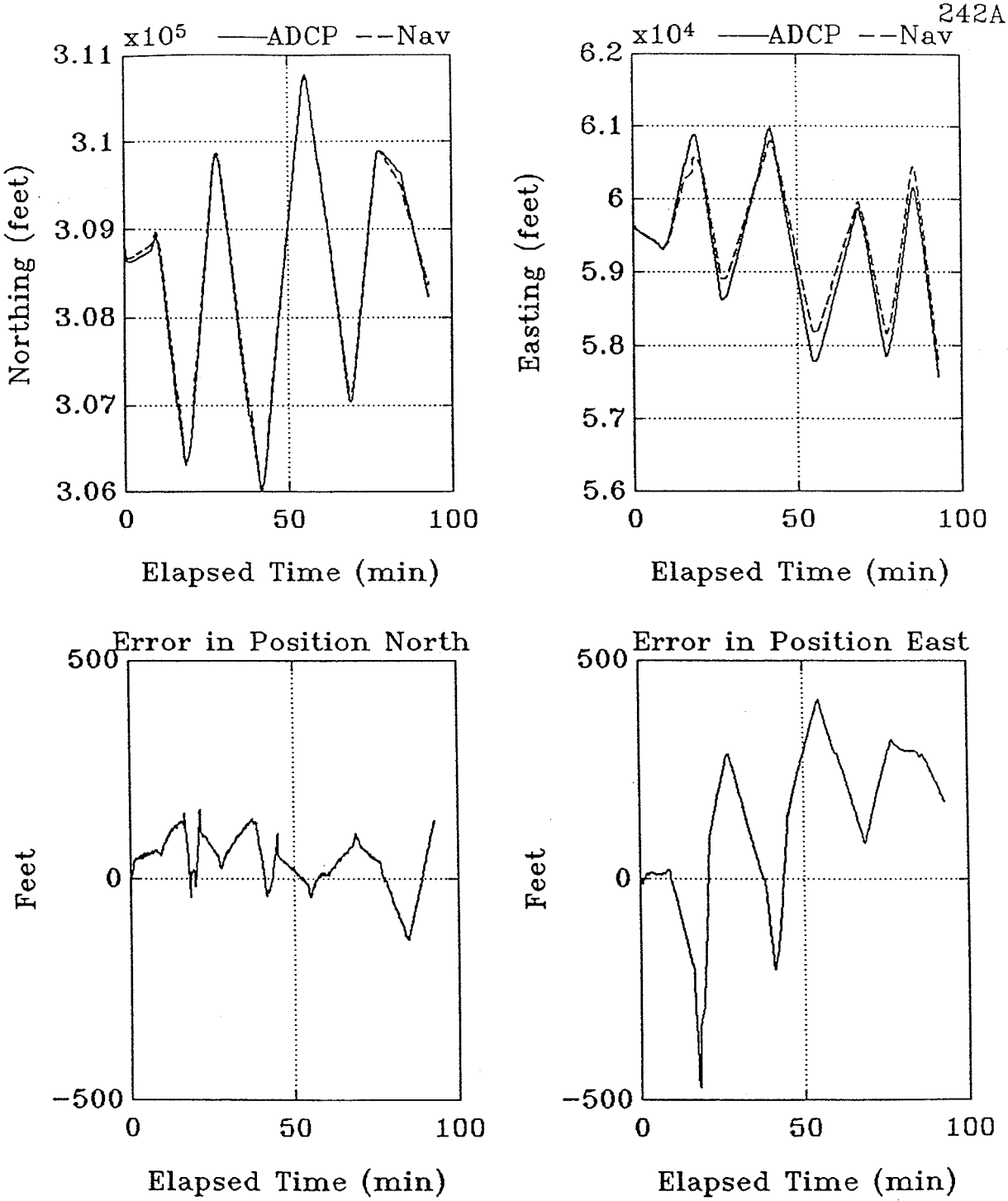

Figure 5.52. Survey 242A: time series for the estimates of ship position from the ADCP bottom track data and the navigation data. Clockwise from upper left: (a) North ship position (ADCP solid line, Navigation dashed); (b) East ship position (ADCP solid line, Navigation dashed); (c) Error in north position estimates (Navigation - ADCP); (d) Error in east position estimate (Navigation - ADCP). Elapsed time is given in minutes from the start of the survey (0 min = 16:07:02 GMT).

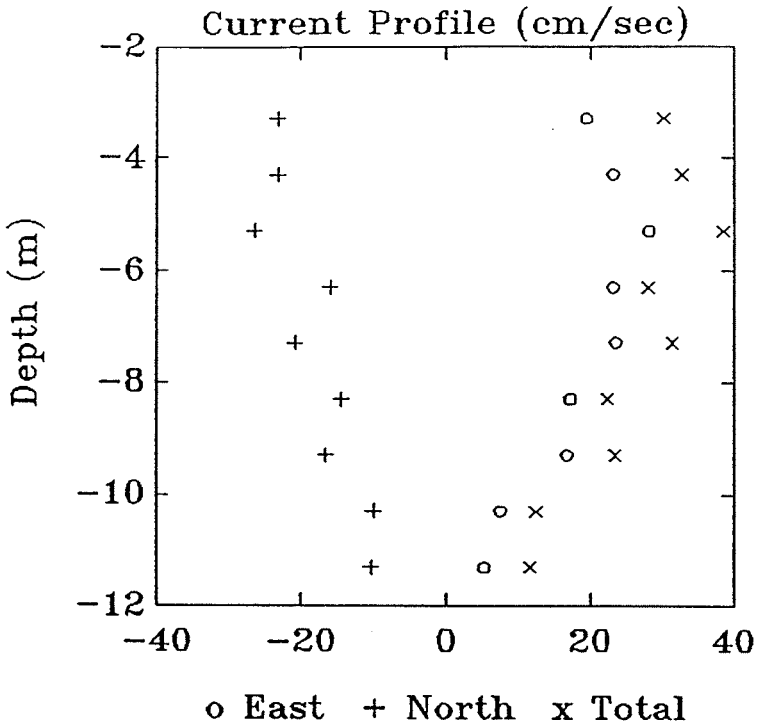

Figure 5.53. Survey 237A: vertical current profile.

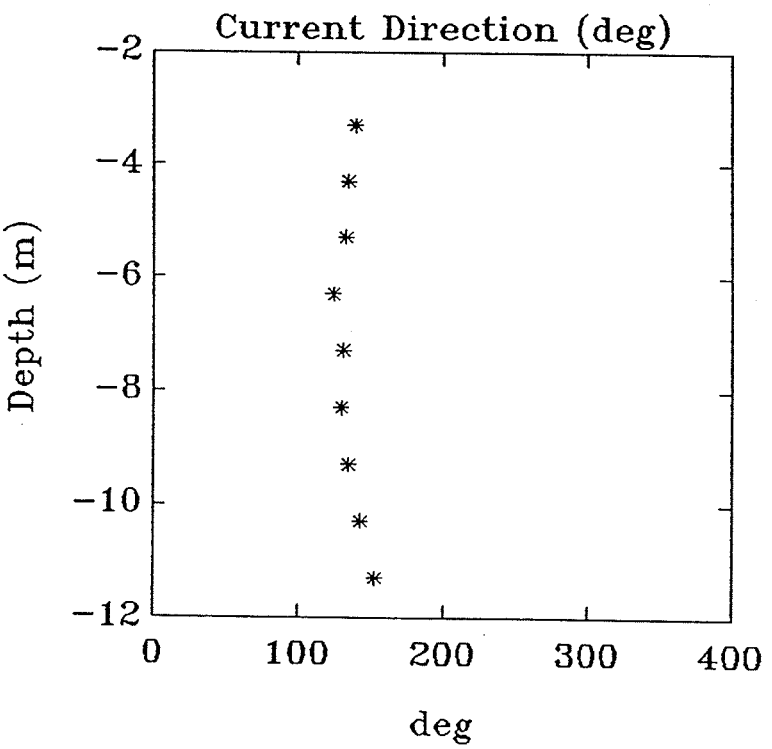

Figure 5.54. Survey 237A: current direction (degrees from north).

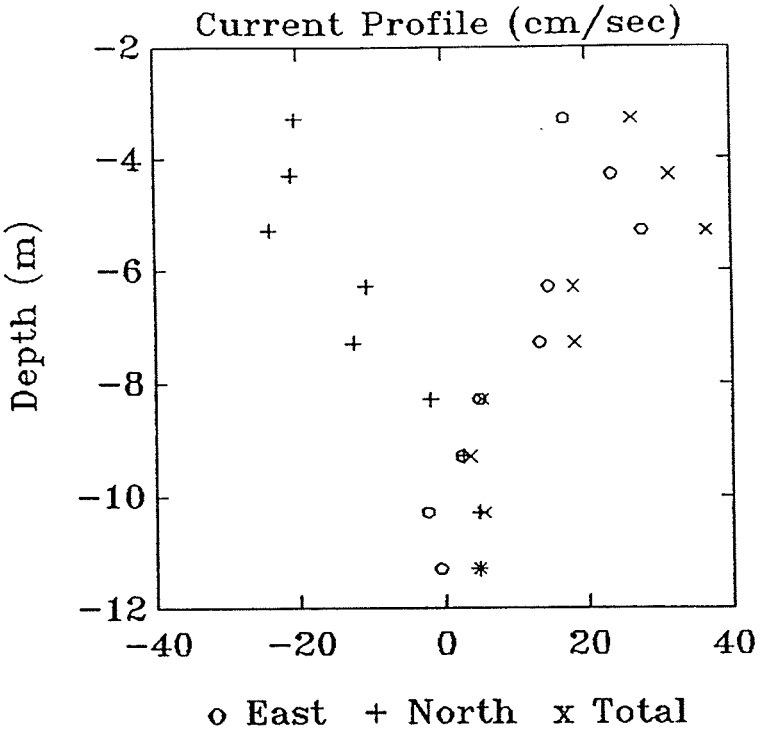

Figure 5.55. Survey 238A: vertical current profile.

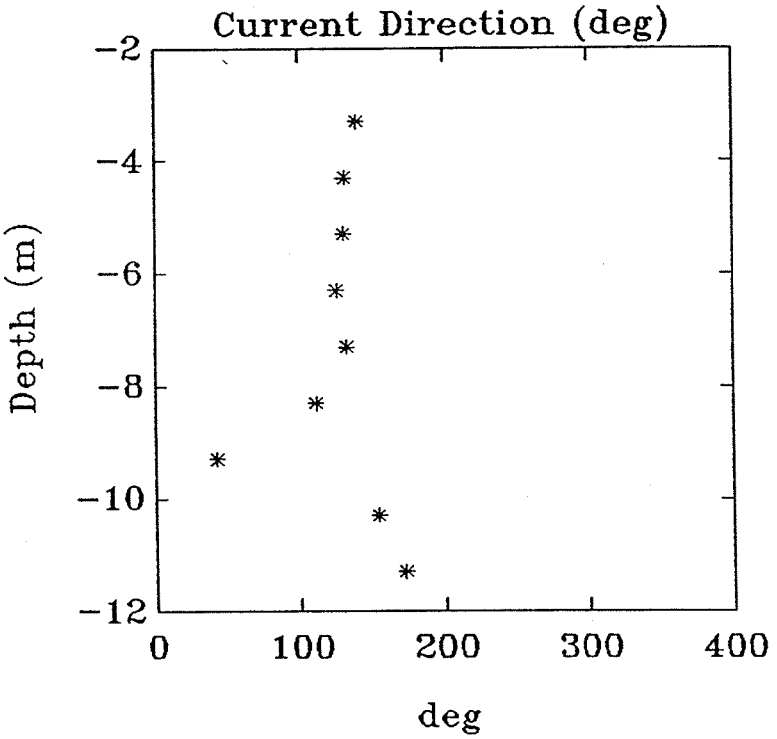

Figure 5.56. Survey 238A: current direction (degrees from north).

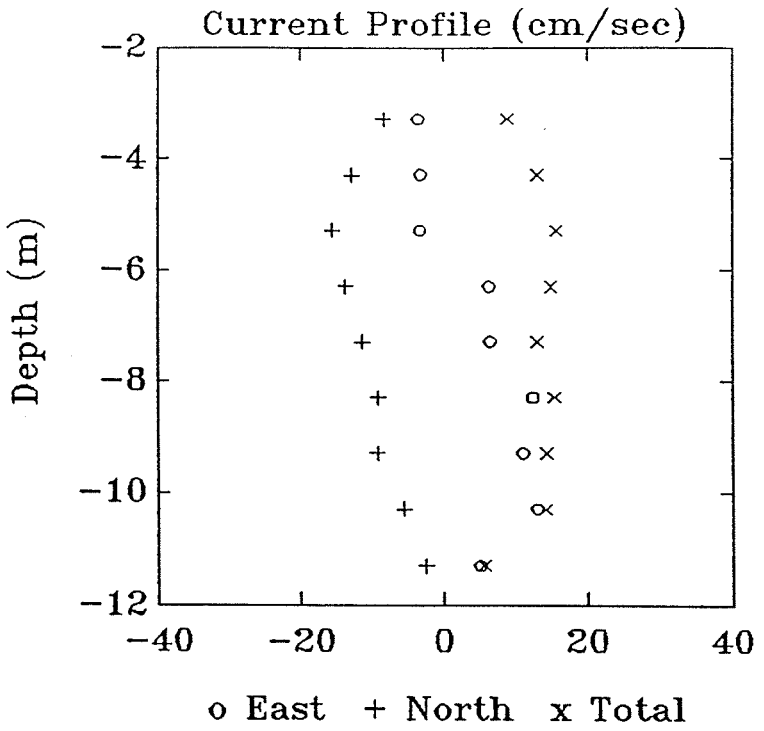

Figure 5.57. Survey 238B: vertical current profile.

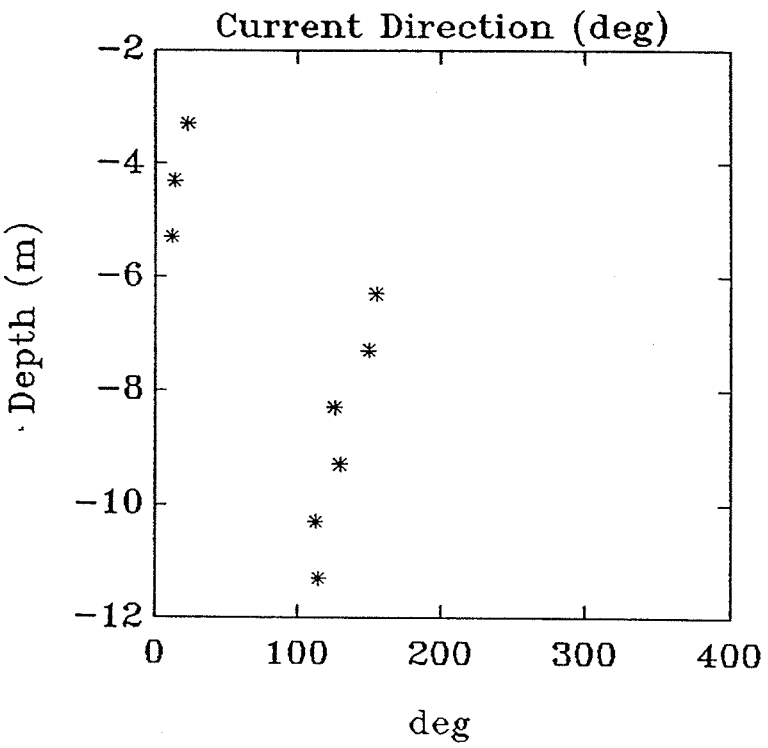

Figure 5.58. Survey 238B: current direction (degrees from north).

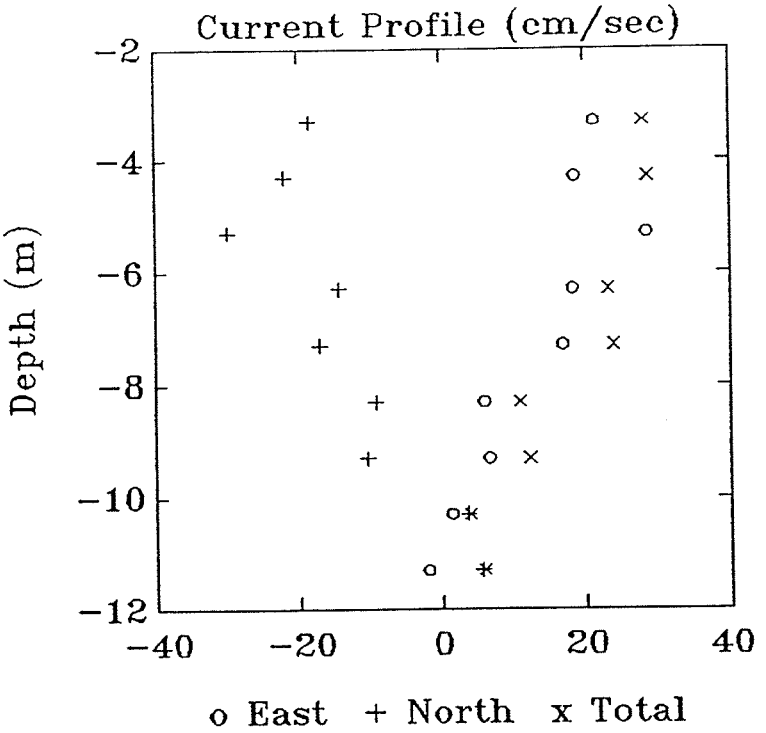

Figure 5.59. Survey 239A: vertical current profile.

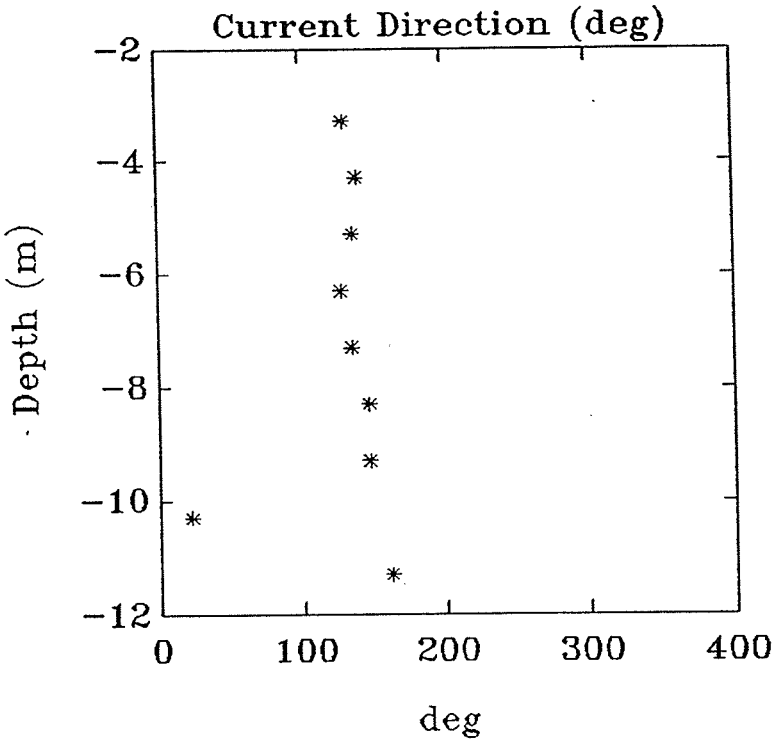

Figure 5.60. Survey 239A: current direction (degrees from north).

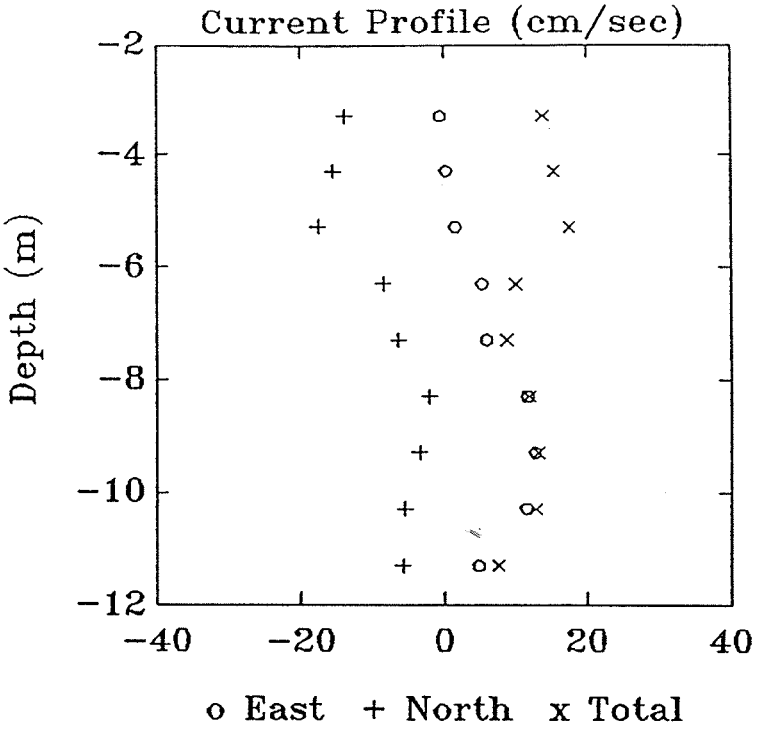

Figure 5.61. Survey 239B: vertical current profile.

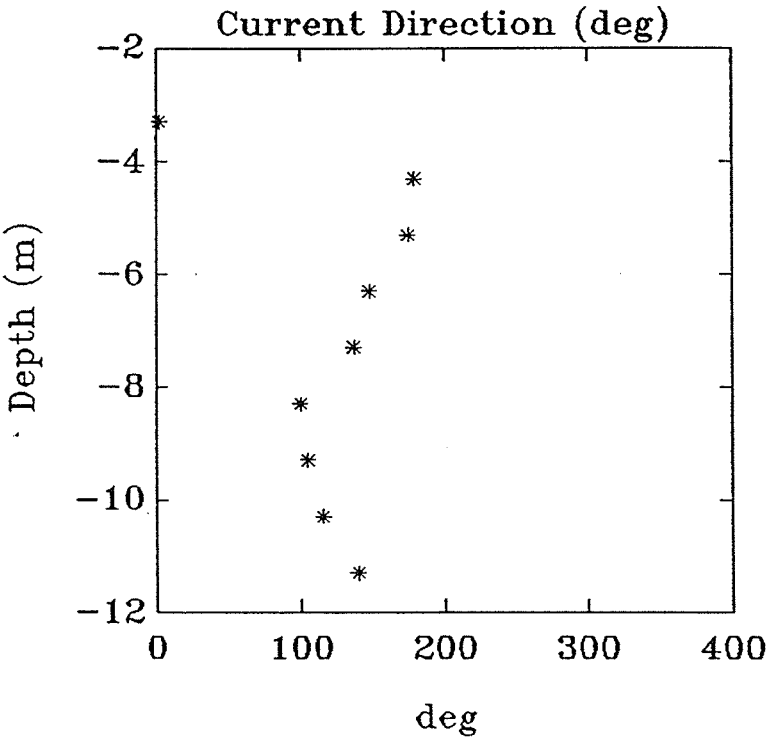

Figure 5.62. Survey 239B: current direction (degrees from north).

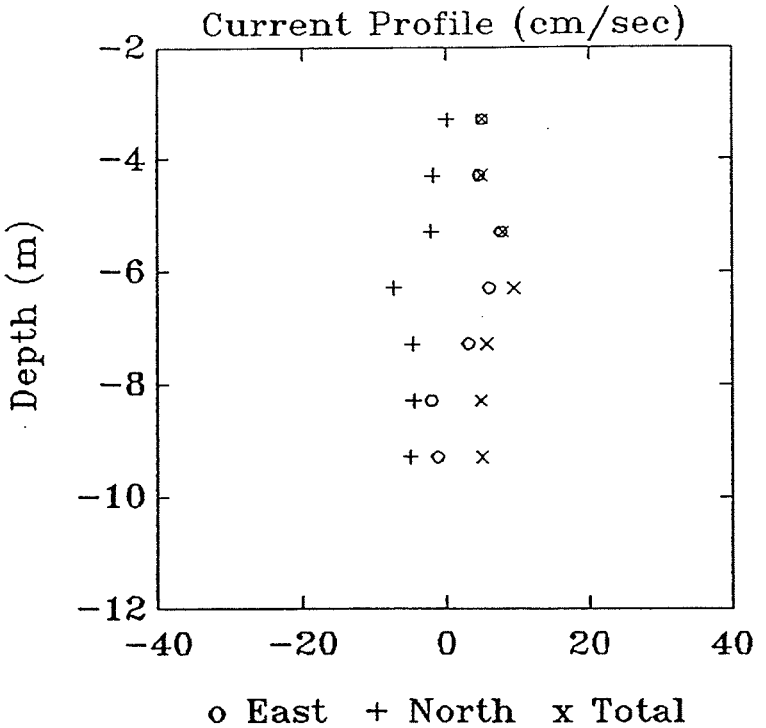

Figure 5.63. Survey 241A: vertical current profile.

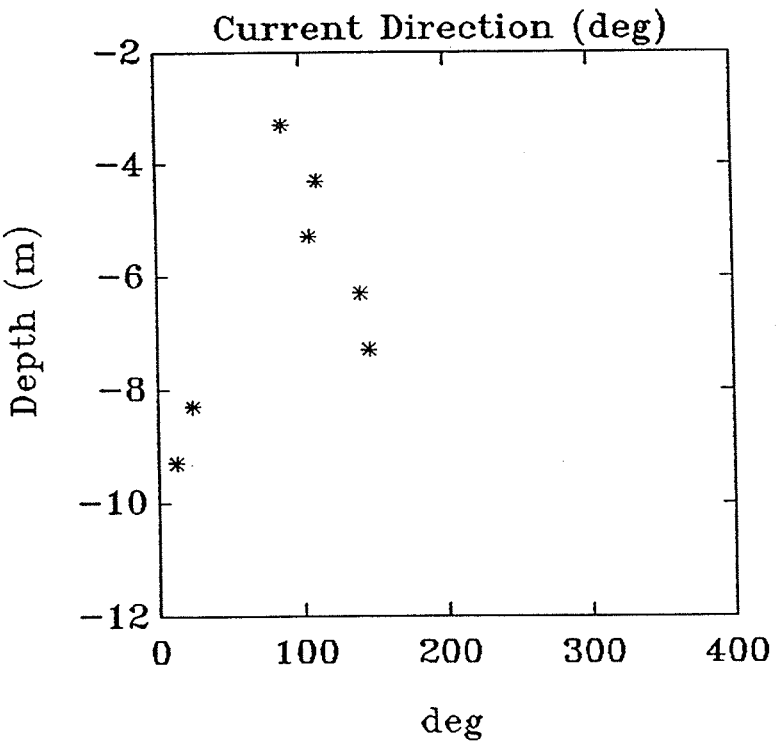

Figure 5.64. Survey 241A: current direction (degrees from north).

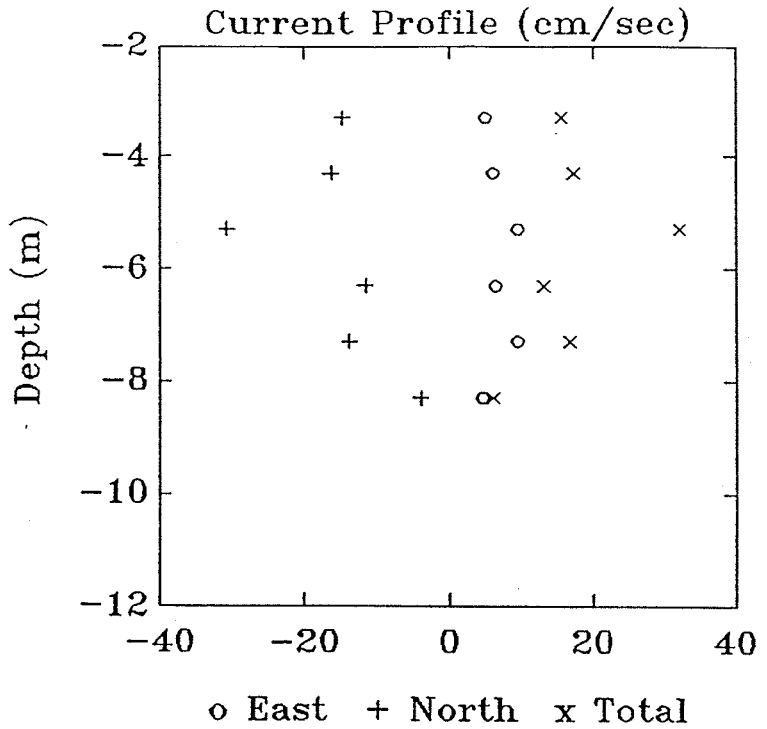

Figure 5.65. Survey 242A: vertical current profile.

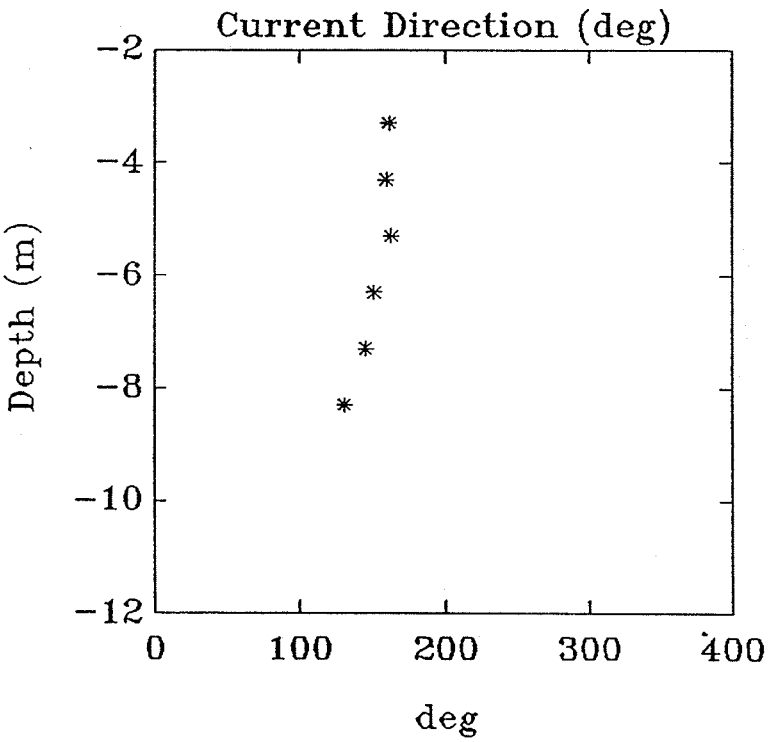

Figure 5.66. Survey 242A: current direction (degrees from north).

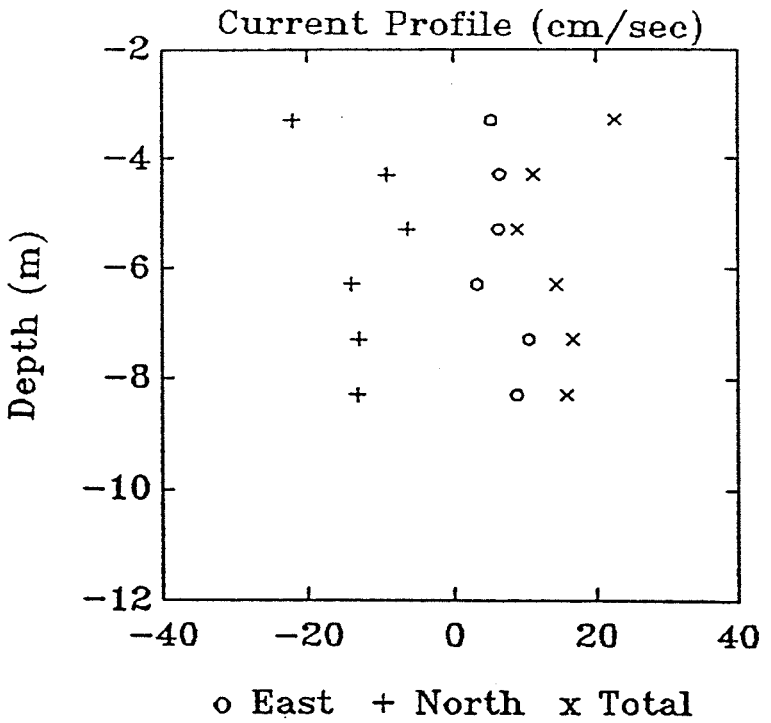

Figure 5.67. Survey 243A: vertical current profile.

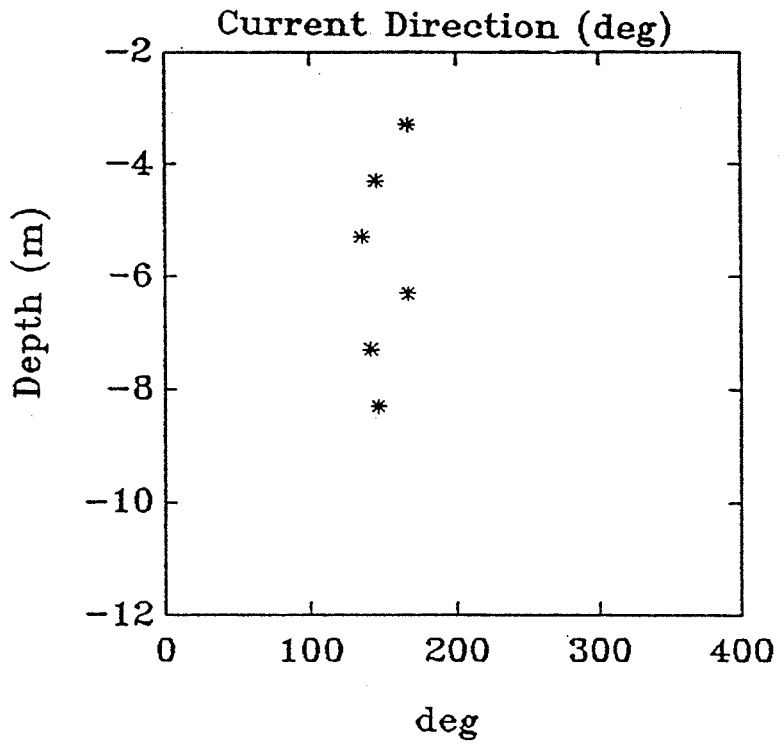

Figure 5.68. Survey 243A: current direction (degrees from north).

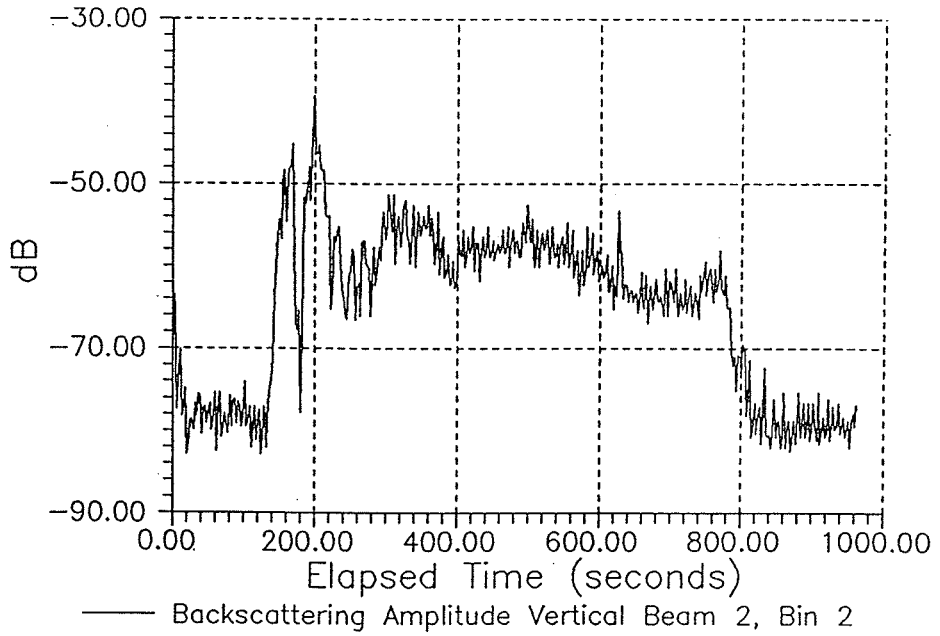

Figure 5.69. Backscattered amplitude data received by the ADCP bin 2 (4.45 m), Beam 2 (vertical beam) as the *R/V Pelican* passed through the plume. Backscattering level of -75 to -80 dB corresponds to the background level.

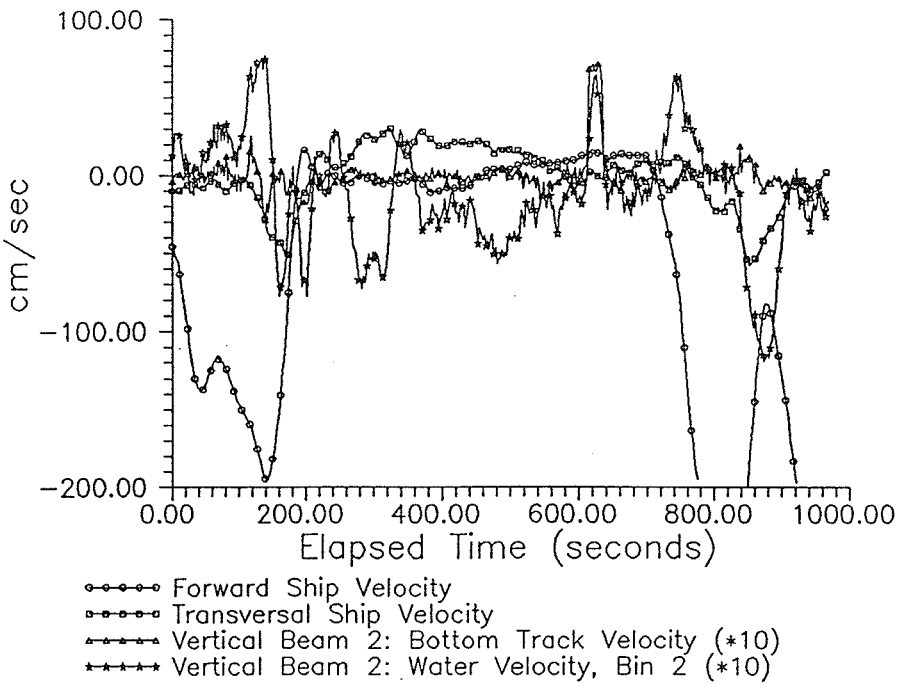

Figure 5.70. Forward velocity and transverse velocity of the bottom relative to the ship in addition to the water track velocity observed along the vertical beam. Vertical velocities have been multiplied by a factor of 10.

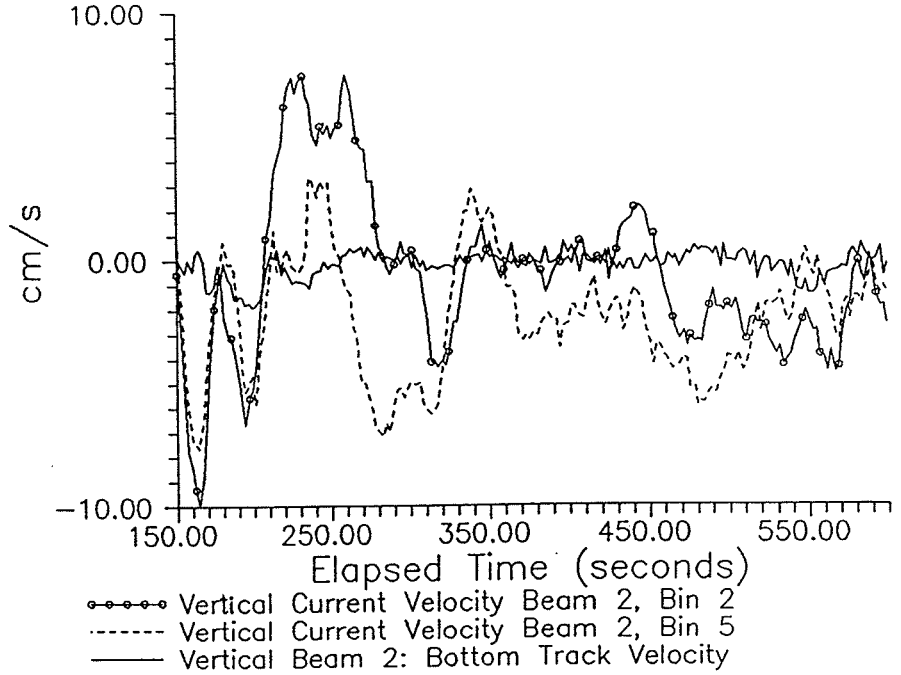

Figure 5.71. Subset of Figure 5.70 when the boat drifted through the plume. The lines depict the bottom track velocity and the vertical current velocity from bins 2 and 5 calculated from the vertical beam (Beam 2).

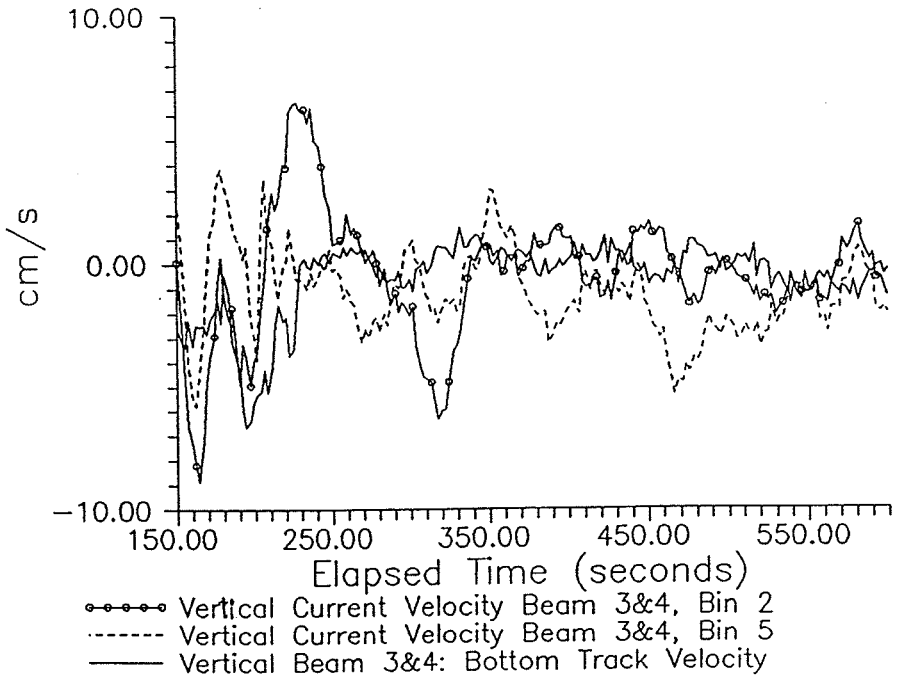

Figure 5.72. Subset of Figure 5.70 when the boat drifted through the plume. The lines depict the bottom track velocity and the vertical current velocity from bins 2 and 5 calculated from Beams 3 and 4 (pointing in the direction of the ship).

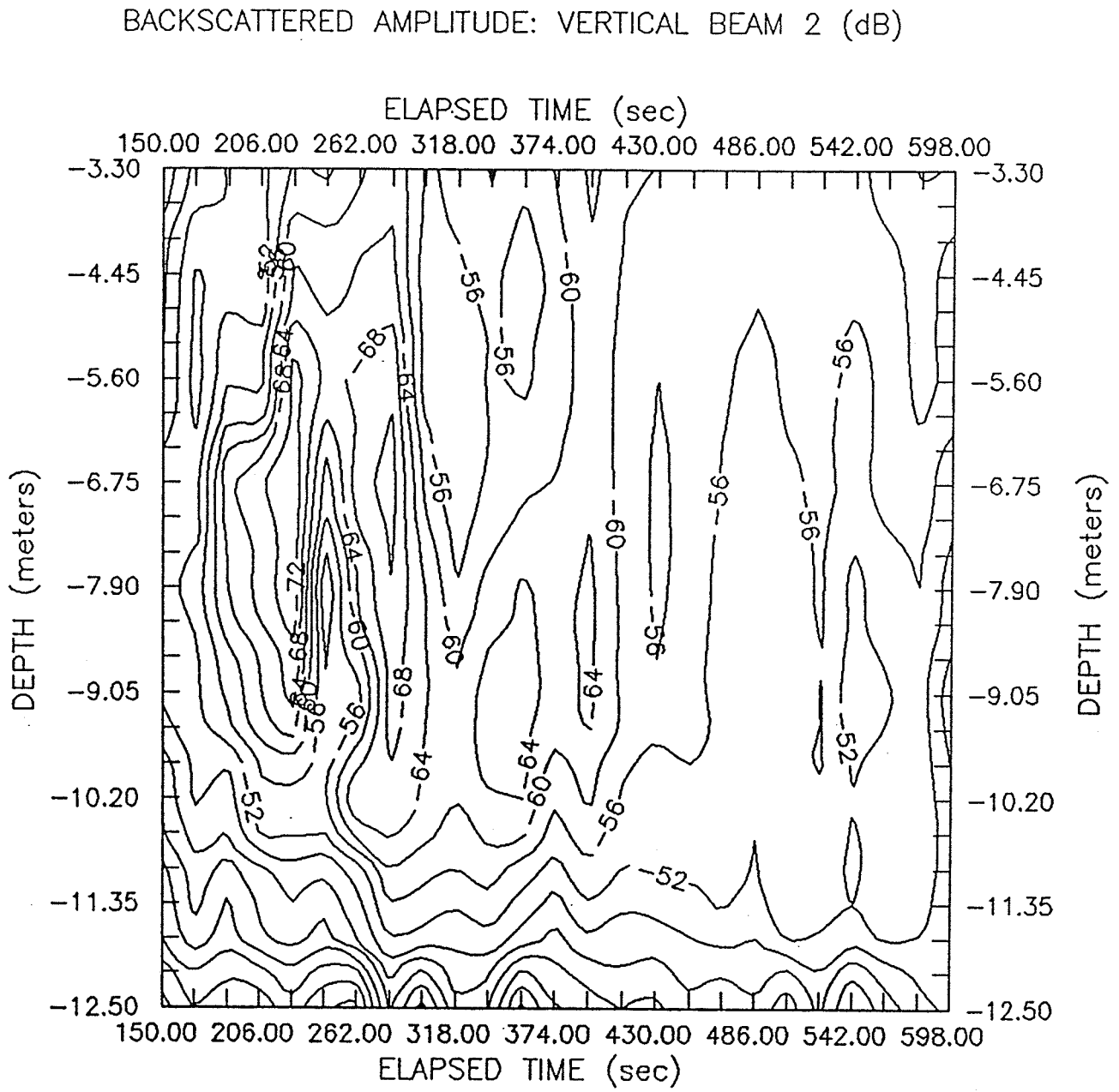

Figure 5.73. Variation in backscattering (from vertical Beam 2) as the *R/V Pelican* drifts through the plume. Temporal subset is same as in Figures 5.71 and 5.72.

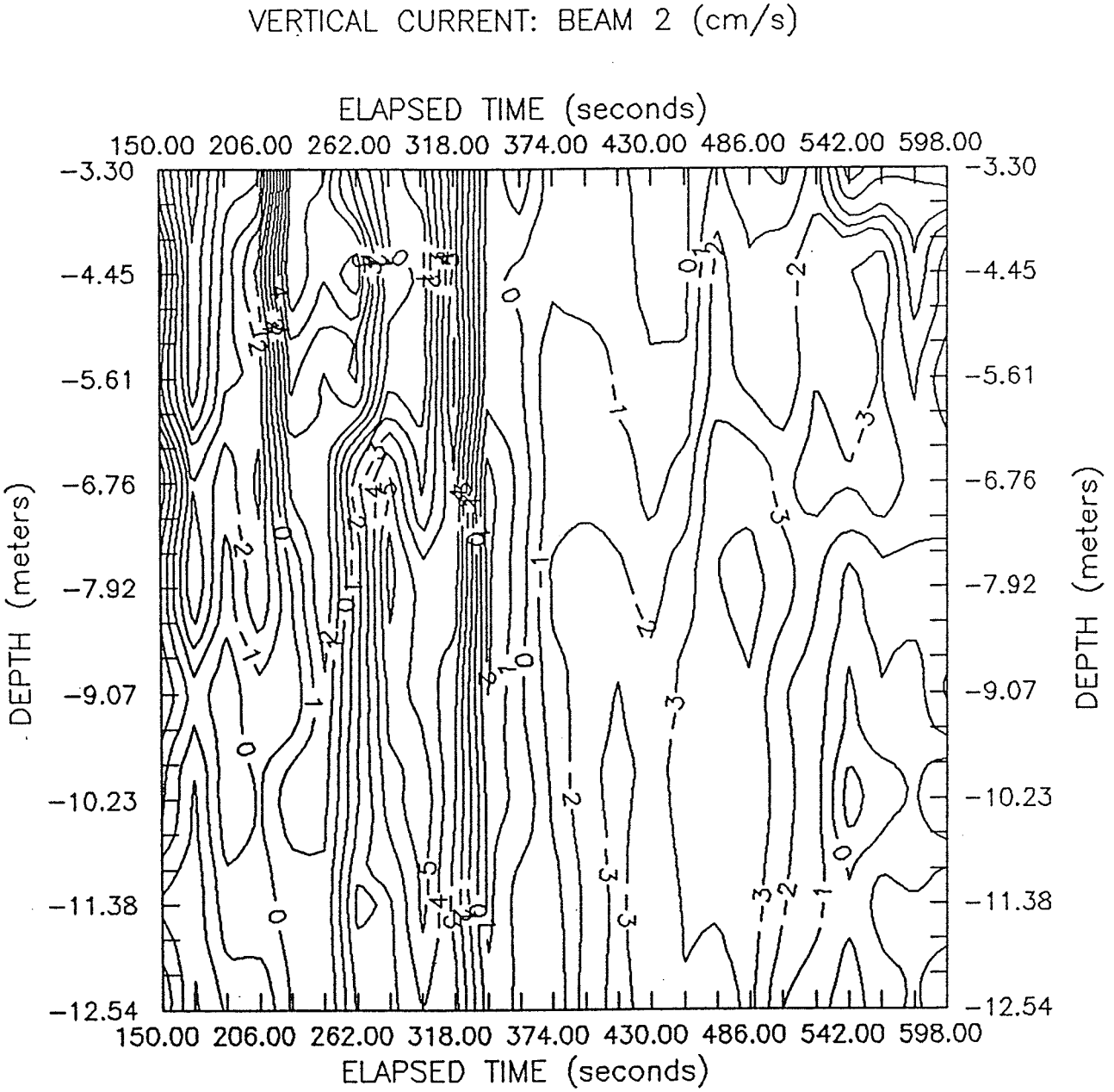

Figure 5.74. Variation vertical current velocity (from vertical Beam 2) as the *R/V Pelican* drifts through the plume. Temporal subset is the same as in Figures 5.71 and 5.72.

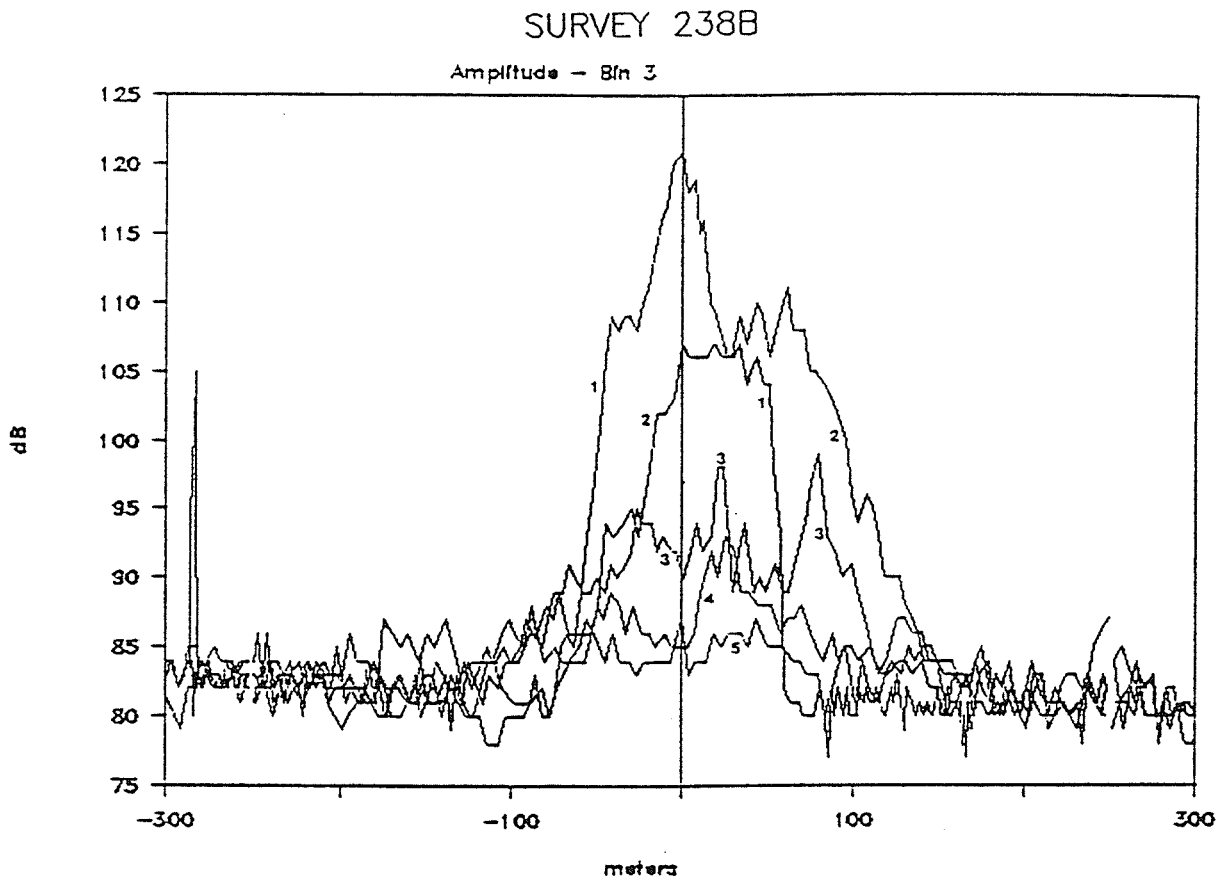

Figure 5.75. Survey 238B: amplitude data collected along five transects. The amplitude is in decibels (relative units) and is taken from bin 3 (5.3 m) along Beam 2 (vertical beam).

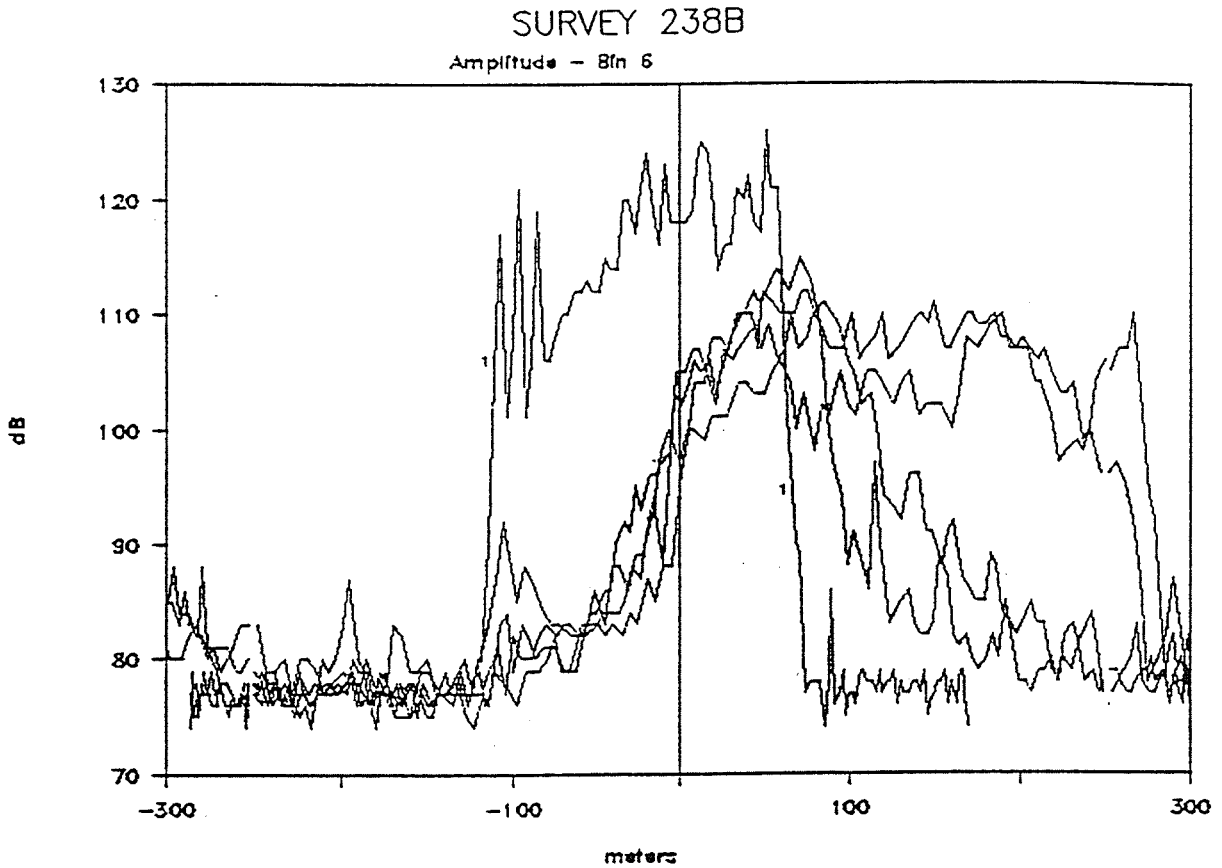

Figure 5.76. Survey 238B: amplitude data collected along five transects. The amplitude in decibels (relative units) is taken from bin 6 (8.3 m) along Beam 2 (vertical beam).

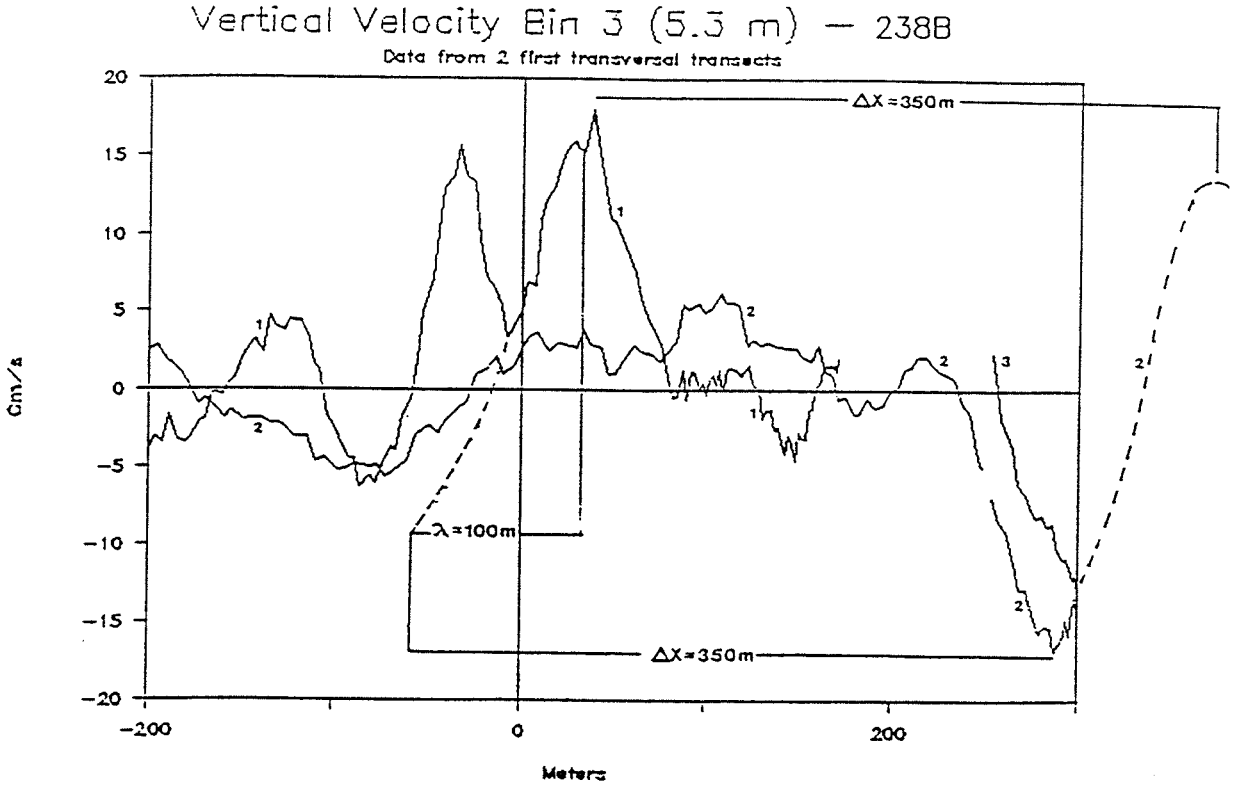

Figure 5.77. Survey 238B: vertical velocity collected 5.3 m below the surface along the first two transects. Note internal waves generated during the first transect have traveled to the edge of the plot at the end of the second transect.

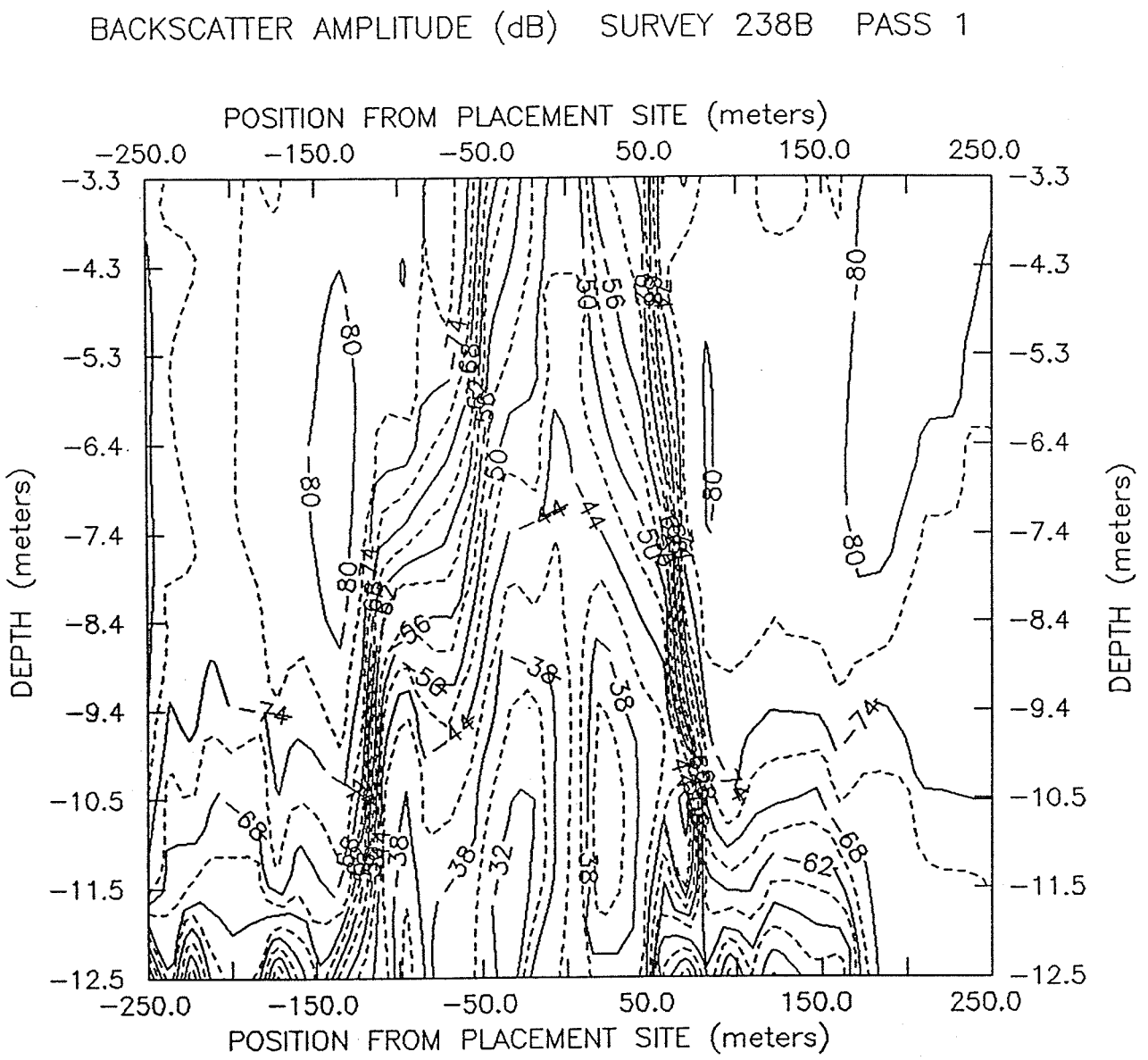

Figure 5.78. Survey 238B: contour plot showing the variation of the backscattering strength as a function of horizontal distance from the placement site during the first transect across the plume. The data have been projected onto a section that runs in the direction from 225 to 75 deg (positive) true north.

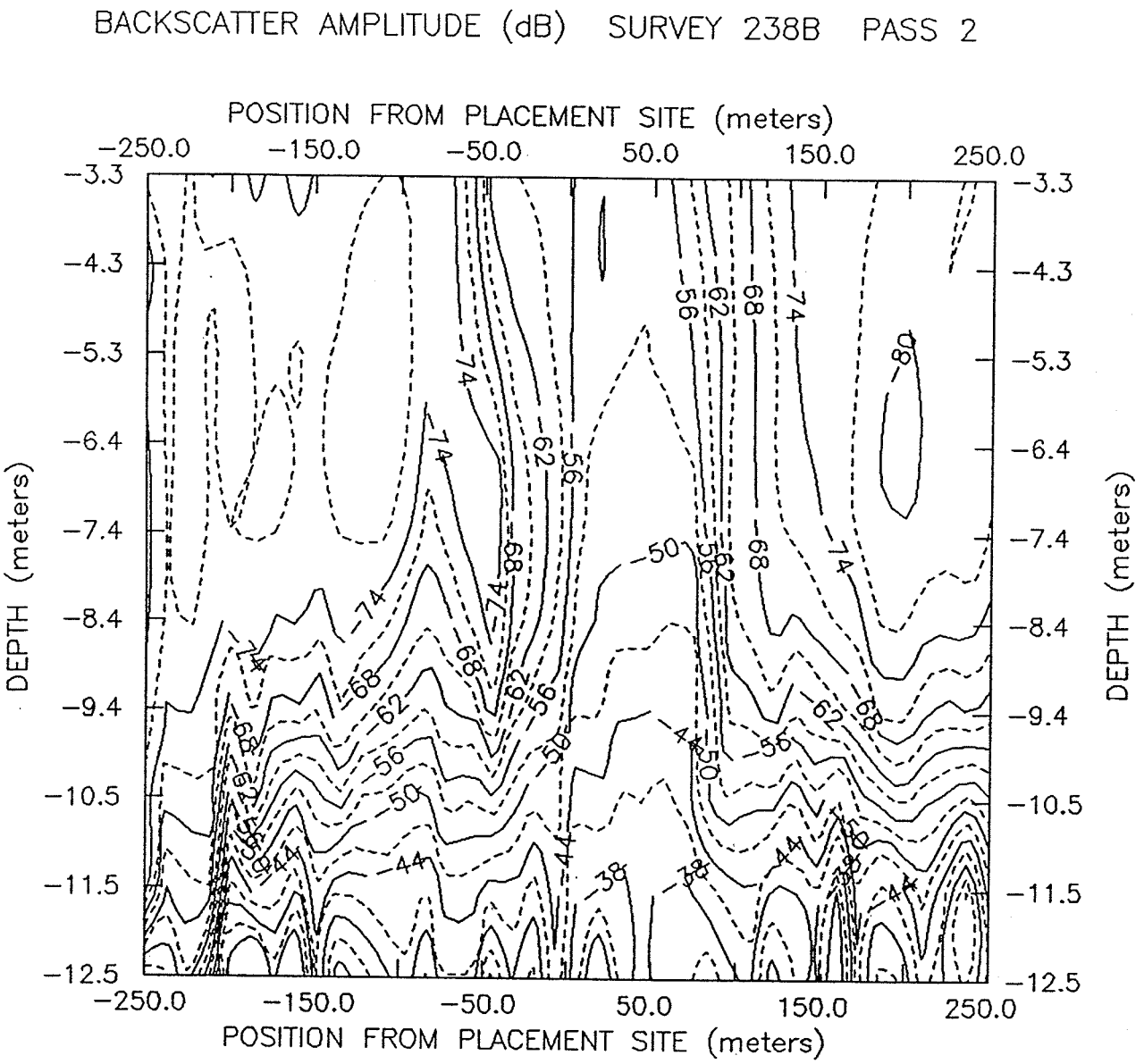

Figure 5.79. Survey 238B: contour plot showing the variation of the backscattering strength as a function of horizontal distance from the placement site during the second transect across the plume. Same projection as Figure 5.78.

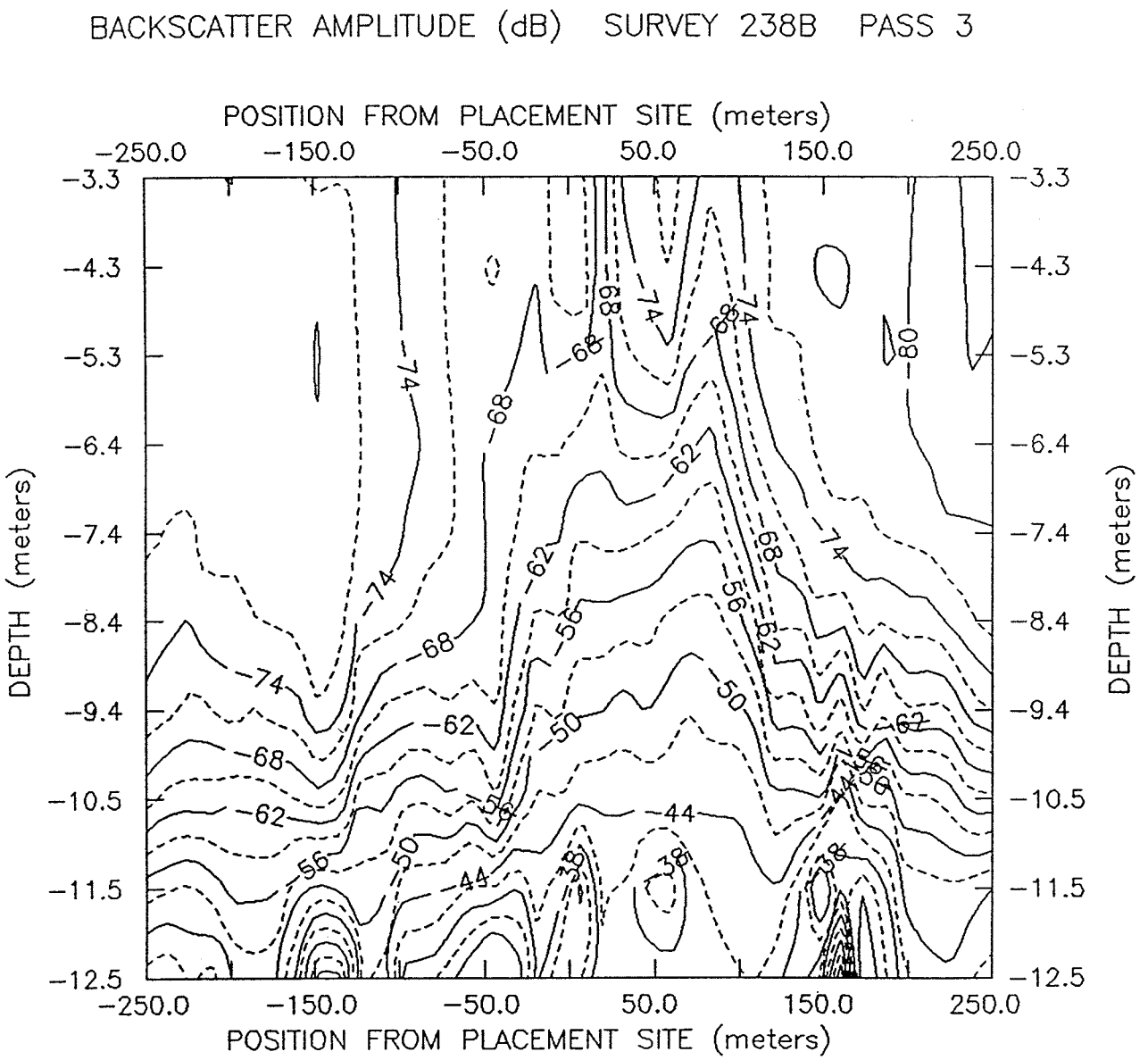

Figure 5.80. Survey 238B: contour plot showing the variation of the backscattering strength as a function of horizontal distance from the placement site during the third transect across the plume. Same projection as Figure 5.78.

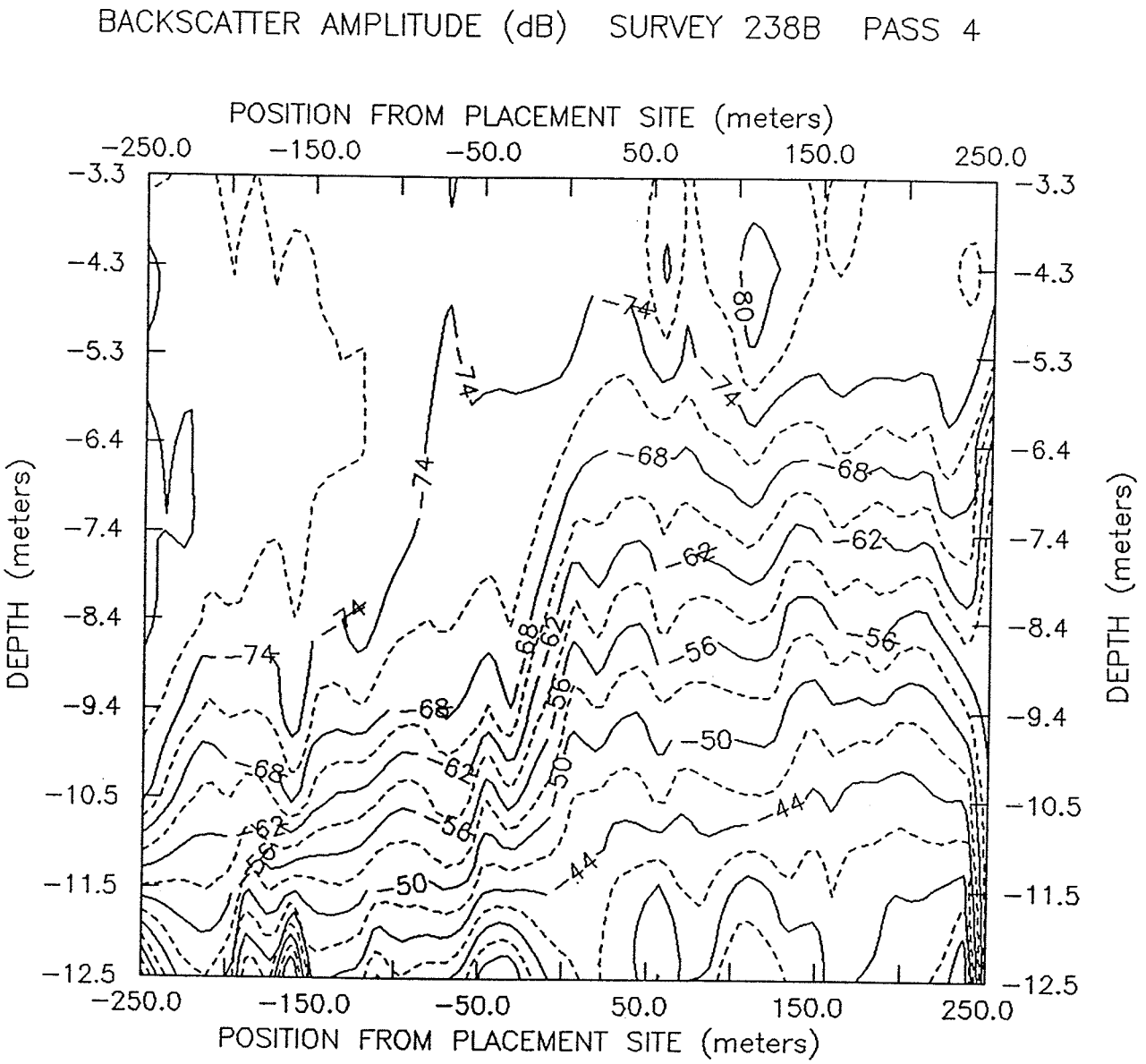

Figure 5.81. Survey 238B: contour plot showing the variation of the backscattering strength as a function of horizontal distance from the placement site during the fourth transect across the plume. Same projection as Figure 5.78.

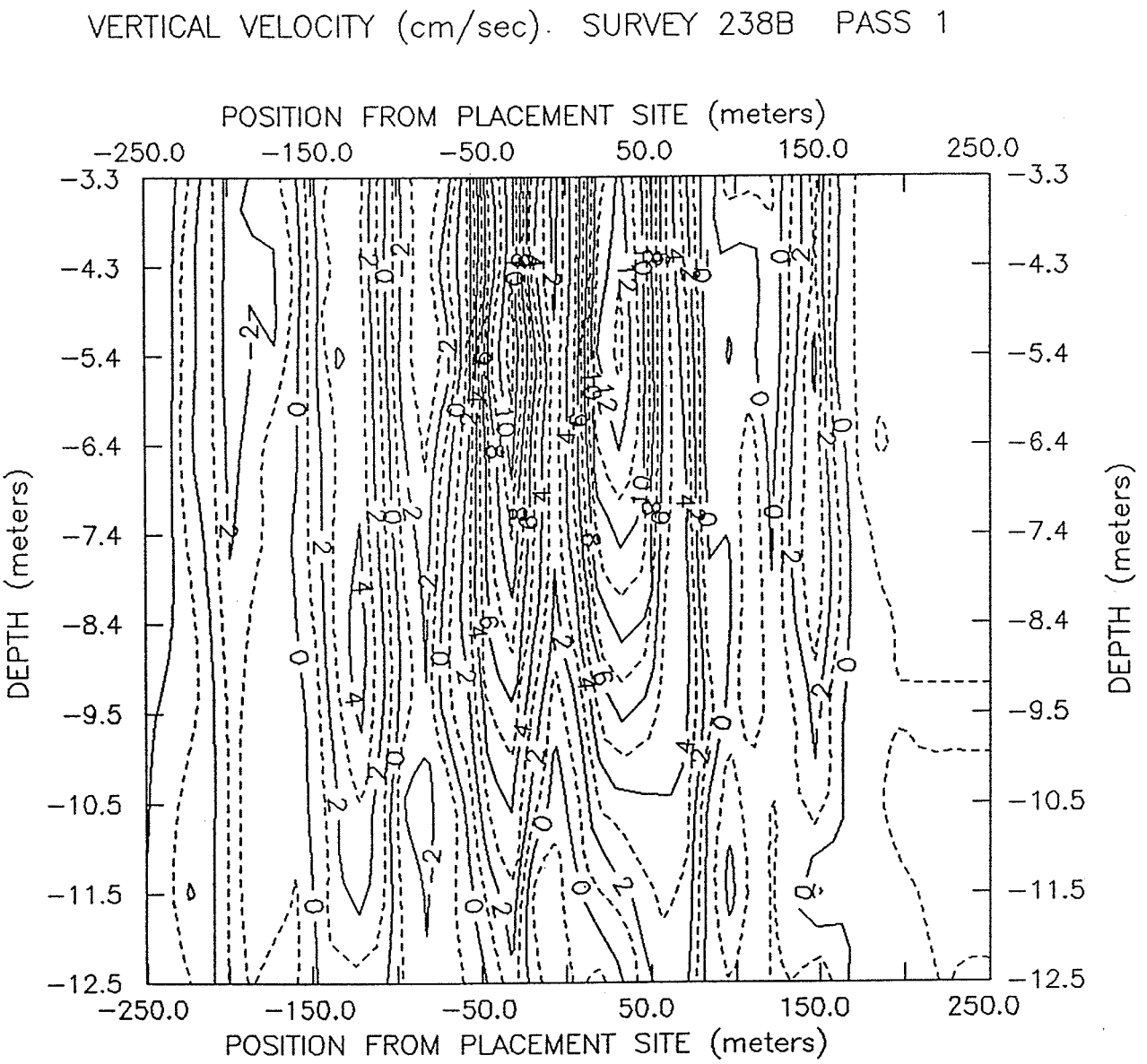

Figure 5.82. Survey 238B: contour plot showing the variation of the vertical velocity as a function of horizontal distance from the placement site during the first transect across the plume. Same projection as Figure 5.78.

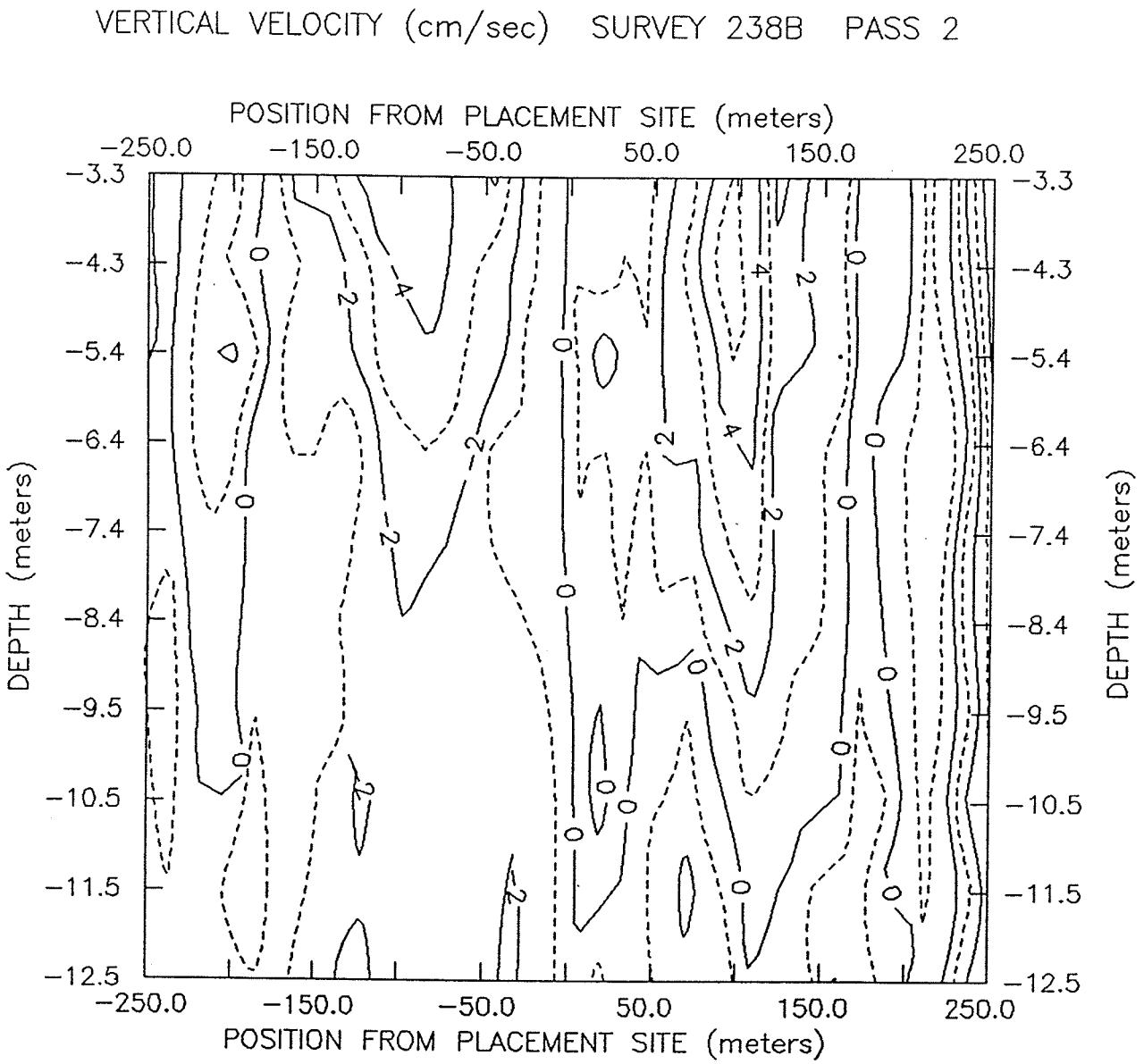

Figure 5.83. Survey 238B: contour plot showing the variation of the vertical velocity as a function of horizontal distance from the placement site during the second transect across the plume. Same projection as Figure 5.78.

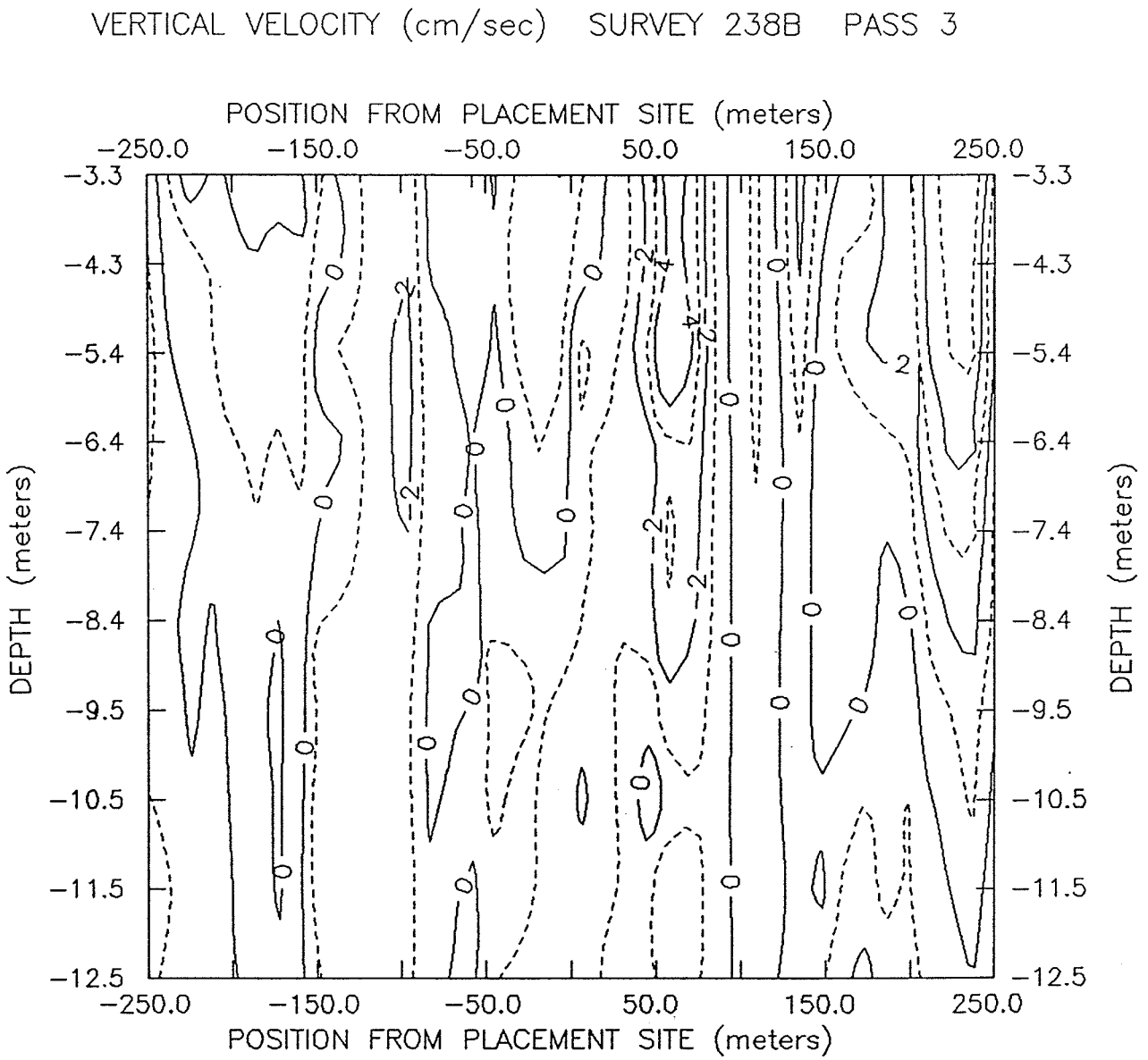

Figure 5.84. Survey 238B: contour plot showing variation of vertical velocity as a function of horizontal distance from placement site during third transect across the plume. Same projection as Figure 5.78.

Appendix 5A: Beam Amplitude Calibration

(RDI Technical Bulletin ADCP-89-04)

Introduction

This appendix describes how to perform a beam amplitude calibration on an RD Instruments (RDI) Acoustic Doppler Current Profiler (ADCP) to obtain absolute backscatter strength. Descriptions of the parameters involved in the calibration and derivation of the backscatter coefficient equation are also included. In this appendix the different ADCP models are labeled as follows: "VM" refers to the vessel-mounted ADCP; "SC" refers to the self-contained ADCP; and "DR" refers to the direct read ADCP.

An Overview of Measuring Backscatter Strength and Echo Amplitude

An uncalibrated RDI ADCP can measure relative backscatter strength at different ranges along each acoustic beam. The measurement is relative because it allows only comparison of backscatter strength from one discrete range cell to the backscatter strength from other range cells along the same acoustic beam. A beam amplitude calibration must be done on the ADCP to obtain absolute backscatter strength so that measurements can be compared with other beams or with other ADCPs. Once the ADCP is calibrated, one can compute absolute backscatter (+/-3 dB) using ADCP calibration data and known (or assumed) values for speed of sound, geometric spreading, and absorption. An ADCP calibration has three tests:

1. Test 1 - The power each transducer beam puts into the water at a specific supply voltage level is measured. This measurement is used to calculate the acoustic energy in the water.
2. Test 2 - The noise factor of the ADCP is determined. The noise factor is a measure of how much worse an actual receiver is as compared with a perfect receiver.
3. Test 3 - The conversion factor from the ADCP's echo amplitude measurement (in counts) to power (in decibels) is determined. Since echo amplitude is not linear with temperature, the slope is determined at three temperatures. The three temperatures (over the range of 0 to 40 deg C) are chosen depending on the expected operating environment.

The temperature at the ADCP's electronics chassis contributes the most to the echo amplitude slope changes. The temperature of the transducer head and beams have very little effect. Therefore, the temperature of the electronics during deployment must be known. The temperature is easily found for DR and SC ADCPs because the transducer has a thermistor that measures the temperature of the water at the transducer head. If the ADCP is completely submerged, this temperature will be nearly the same as in the ADCP's electronics chassis. Since

the VM-ADCP electronics chassis is separated from the transducer, the temperature of the chassis must be measured. The rack-mounted ADCP chassis often has higher temperatures than the room; therefore, the chassis should have a temperature measurement device.

Backscatter Coefficient Equation

This section describes the Backscatter Coefficient Equation (S_v). The following tabulation lists a description of each term within the equation and explains how it is obtained. Derivation of the Backscatter Coefficient Equation is included in a later section of this appendix. The Backscatter Coefficient Equation is for a single beam:

$$S_v = 10 \log \left[\frac{4.47 * 10^{-20} K2\, Ks\, T (10^{Kc(Ec-Nc)/10} - 1) R^2}{c\, L\, K1\, 10^{-2\alpha R/10}} \right] \qquad (5A.1)$$

Term	Description
S_v	Backscatter Coefficient (decibels)
K2	System Noise Factor - This is the factory-measured noise factor of the ADCP. An Amplitude Calibration Sheet (furnished with the ADCP) lists this value or each beam of the ADCP as a ratio. This ratio is the reference noise floor for the ADCP system.
Ks	Fixed Value Based on System Frequency - This value is the ratio of the ADCP system's IF (or AGC) bandwidth, B, to the square of the transducer's diameter, d. Therefore, *Ks* = B/d2 and is equal to:

Ks	ADCP Frequency, kHz
1.09 * 105	75
4.17 * 105	150
7.69 * 105	300
1.56 * 106	600
5.65 * 106	1200

T	Temperature (degree kelvins) - The temperature of the transducer.

(Continued)

(Continued)

Term	Description

Kc Slope of Echo Amplitude Curve - This number is given on the Amplitude Calibration Sheet (supplied) for each beam at three separate temperatures. With a Beam Amplitude Calibration, the user is also provided the echo amplitude curves for each beam. *Kc* must be chosen for the temperature closest to the actual temperature of the ADCP electronics chassis. In most cases, the temperature measured by DR and SC-ADCPs at the transducer will be close to the temperature of the chassis. For VM-ADCPs, the temperature of the chassis will have to be measured.

Ec Total Echo Amplitude Counts - Echo amplitude data are output for each beam at each depth cell (bin) location. The depth cell and beam of interest will need to be chosen for analysis.

Nc Noise (Echo Amplitude Counts with no signal present) - This value is the number of Echo Amplitude Counts of the noise floor. Do this test to determine noise floor counts.

NOTE: This test should be done at the site where backscatter measurements will be taken. If this is not possible, the user can still do this test by taking the following precautions:

(1) The electronics chassis must be at the same temperature it will be at the measurement site. This is due to the variability of measured echo amplitude with temperature.

(2) DR or VM users operating on a vessel must stop the boat while the test is being done. The boat motion causes flow noise. Flow noise will cause a bias in the measurement of the noise floor and make the calculation of true backscatter strengths impossible.

(3) The user should make sure there is no other equipment running that may generate a signal that the ADCP could receive. This interference will cause a bias in the measurement of the noise floor.

c Speed of Sound - This factor is the speed of sound at the scattering layer being measured. The user must calculate this number. It should take into account changes in salinity, temperature, and depth.

L Transmit Pulse Length in meters

*K*1 Power into the Water - This value scales the acoustic power into the water at a given supply voltage. RDI provides *K*1*a* for each beam on an Amplitude Calibration Sheet. The user must scale *K*1*a* for the supply voltage during the deployment. As supply voltage levels change, so will the power into the water. *K*1*a* is measured at 40 VDC for all systems. Choose the appropriate formula from the three that follow to correct the *K*1*a* value.

(Continued)

(Continued)

Term — Description

SC users:

$$K1 = \left[\frac{V2 - 5.76}{34.24}\right]^2 * K1a \qquad (5A.2)$$

where:

$V2$ = (Counts from high volts in leader data) * (0.17)

NOTE: Remember that $K1$ needs to be scaled periodically, because the supply voltage is from batteries and battery voltage decreases as deployment time progresses.

DR users:

$$K1 = \left[\frac{(ACrms * 1.397) - 6.3}{35.1}\right]^2 * K1a \qquad (5A.3)$$

where

ACrms = Measured RMS AC voltage at the ADCP. Using an ACrms Voltmeter, measure the voltage at pins 19 and 20 of the ADCP connector when not plugged into the pressure case. This is done so any voltage loss through the cable can be ignored. For systems operating at 220 AC volts, divide the *ACrms* by two before entering it in the formula.

VM users:

$$K1 = \left[\frac{(ACrms * 1.397) - 4.27}{37.14}\right]^2 * K1a \qquad (5A.4)$$

where

ACrms = Measured RMS AC voltage at the ADCP. Using an ACrms Voltmeter, measure the voltage at the AC receptacle that the ADCP will be plugged into. For systems operating at 220 AC volts, divide the *ACrms* by two before entering it in the formula.

(Continued)

(Concluded)

Term	Description
α	Absorption Coefficient (in water) in decibels/meter - The user must provide this measurement. This value accounts for the loss in echo strength through attenuation in the water.
R	Slant Range - This value is the range to the scattering layer along the beam in meters. Use the following formula to calculate the value of R.

$$R = \left[\frac{BK + \left| \frac{PL - BL}{2} \right| + (N * BL) + \frac{PL}{4}}{Cos\theta} \right] * \frac{c}{1475.1} \qquad (5A.5)$$

where

BK = blank beyond transmit, m

PL = transmit pulse length, m

BL = depth cell length, m

N = depth cell number of the scattering layer being measured

Θ = angle of transducer beams to vertical, usually 30 deg

c = weighted average of the speed of sound between the transducer and depth cell of interest. The ADCP has a default speed of sound of 1,475.1 m/sec. This term corrects for speeds of sound other than 1,475.1 m/sec.

Derivation of the Backscatter Coefficient Equation

The Sonar Equation - The following equation presents Signal-to-Noise (S/N) ratio as a function of backscatter, range, and other ADCP parameters.

$$\frac{S}{N} = \frac{PE}{4\pi}\,\frac{G}{R^2}\,10^{-\alpha R/10}\,\frac{\pi[R\phi]^2}{4}\,\frac{ct}{2}\,\frac{10^{S_v/10}}{R^2}\,10^{-\alpha R/10}\,\frac{Gk^2}{4\pi}\,E\,\frac{1}{KTBF} \qquad (5A.6)$$

Term: 1 2 3 4 5 6 7 8 9 10

where

S/N = signal-to-noise ratio
P = electrical power to transducer, W
E = transducer efficiency
G = transducer gain or directivity
R = range to scatterers along the beam, m
α = water absorption, dB/m
ϕ = effective two-way beam width, rad
c = speed of sound, m/sec
t = transmit pulse length, sec
S_v = backscatter coefficient (dB)
k = wavelength of transmitter, m
K = Boltzmann's constant, J/deg K
T = temperature, deg K
B = noise bandwidth, Hz
F = receiver noise factor

The following tabulation describes each term in Equation 5A.6:

Term	Description
1	Power density of a spherically spreading pulse on the surface of 1-m sphere
2	Corrects for directivity of the transducer and adjusts for range (one-way)
3	Corrects for absorption of the out-going pulse
4	Instantaneous ensonified area of water
5	Instantaneous ensonified depth of water
4 * 5	Gives instantaneous ensonified volume of water
6	Corrects for backscatter strength and adjusts for range (one-way)
7	Corrects backscattered signal for absorption
8	Capture area of the transducer
9	Corrects for transducer efficiency
1 to 9	Give signal power (S)
10	Noise power (N)

For a circular piston $G = (\pi d/k)^2$ and $\phi^2 = (4k/\sqrt{2}\pi d)^2$, where d is the transducer diameter. Substituting for G and ϕ^2 and combining terms:

$$\frac{S}{N} = \frac{PE\ \pi ct}{4\pi R^2}\ 10^{S_v/10}\ 10^{-2\alpha R/10}\ \frac{\pi d^2 E}{4}\ \frac{1}{KTBF} \tag{5A.7}$$

and

$$S_v = 10 \log \left[\frac{5.09 S/N\ R^2\ KTBF}{PE\ ct\ 10^{-2\alpha R/10}\ d^2\ E} \right] \tag{5A.8}$$

Defining the term PE as $K1$ - power into the water, the term F/E as $K2$ - system noise factor, and the term $Ks = B/d^2$ - system dependent parameters, we obtain

$$S_v = 10 \log \left[\frac{5.09 S/N\ R^2\ KT\ Ks\ K2}{K1\ ct\ 10^{-2\alpha R/10}} \right] \tag{5A.9}$$

Substituting $K = 1.38\ 10^{-23}$ J/deg K, and $t = 0.00157L$, where L is the transmit length in meters

$$S_v = 10 \log \left[\frac{4.47 * 10^{-20} \, S/N \, R^2 \, T \, Ks \, K2}{K1 \, cL \, 10^{-2\alpha R/10}} \right] \quad (5A.10)$$

The term S/N can be determined from the ADCP AGC output.

Now define Ec as counts representing S+N power, Nc as counts representing N power (no signal present), and Kc as the conversion factor decibels/count, as follows

$$Ec = 10\log(S+N)/Kc \quad (in\ counts) \quad (5A.11)$$

$$S+N = 10^{KcEc/10} \quad (5A.12)$$

$$S = 10^{KcEc/10} - N \quad (5A.13)$$

$$N = 10^{KcNc/10} \quad (5A.14)$$

$$S/N = 10^{Kc(Ec-Nc)/10} - 1 \quad (5A.15)$$

Finally, substituting Equation 5A.15 into Equation 5A.10:

$$S_v = 10 \log \left[\frac{4.47 * 10^{-20} \, (10^{Kc(Ec-Nc)/10} - 1) \, R^2 \, T \, Ks \, K2}{K1 \, cL \, 10^{-2\alpha R/10}} \right] \quad (5A.16)$$

6. SEDIMENT PLUME MEASUREMENTS WITH AN ACOUSTIC CONCENTRATION PROFILER

W. PAUL DAMMANN, JOHN R. PRONI

Atlantic Oceanographic and Meteorological Laboratories,
National Oceanic and Atmospheric Administration
Miami, Florida 33149

Contents

1. Introduction

In August 1989, the U.S. Army Corps of Engineers conducted a series of dredged material discharge studies off Mobile Bay, Alabama, called the Mobile Field Data Collection Project (MFDCP). The objectives of the MFDCP included (a) measurement of discharge sediment plume concentration distributions, (b) measurement and analysis of physical processes affecting distribution and transport of discharged material, and (c) evaluation of acoustical methods for the study of concentration distributions and material transport. One important instrument used in the studies was the Acoustic Concentration Profiler (ACP). The ACP was operated by personnel from the National Oceanic and Atmospheric Administration (NOAA), Atlantic Oceanographic and Meteorological Laboratories (AOML), Ocean Acoustics Division, located in Miami, Florida. Of the eighteen discharge events monitored during the MFDCP (Chapter 1, this report), eight have been selected for analysis. These are denoted as plume Surveys 237A, 238A, 238B, 239A, 239B, 241A, 242A, and 243A. In addition, a shallow-water berm survey performed on Julian day 238 is analyzed.

The MFDCP produced a rich data set on discharge plume characteristics, concentrations, transport, and movement and on acoustical methodologies for the study of such features and processes. In addition to the principal objectives listed in the preceding paragraph, several subobjectives may be noted. These include (a) identifying and measuring, where possible, any discharge parameters or processes for which formerly only poor estimates, or only laboratory estimates, are available for use in numerical plume models; (b) examination of at least some of the processes whereby dredged material might potentially be transported out of the placement site; (c) development of initial thoughts for the evolution of an acoustical device for real-discharge-time or post-discharge-time monitoring of dredged material placement and retention; and (d) identification of any processes that are not yet included in existing numerical plume dynamics numerical simulation models.

2. Background

The AOML has carried out acoustical studies on dredged material discharges in various locations including Lake Ontario, the New York Bight, and the Miami deepwater dump site (for example, Proni et al. 1989). These studies together with the MFDCP have revealed or confirmed many plume characteristics and processes. A key point to recognize about acoustical methodologies is that a great deal may be learned about dredged material discharges even if the relationship between the plume material scattered acoustical intensity and plume concentration is only specified in a statistical sense. It is sufficient in many circumstances to assume only that the scattered sound intensity is proportional to the concentration or the mean concentration plus a small random concentration component. In acoustical Doppler systems, for instance, the main assumption is that enough scattering is present to produce a plume-related echo. However, a calibration research effort and development program for acoustical devices for making concentration measurement is greatly needed.

3. Equipment and Procedures

The ACP used during the MFDCP consisted of a Datasonics model DFT-210 dual-channel acoustic transceiver with internal preamplifier (pre-amp) enhancements, operating at 20 and 200 kHz. The transducers were mounted in a streamline towbody aimed vertically downward and towed at a constant depth of 1 m below the surface of the water approximately 15 ft outboard of the vessel's starboard beam at a location a few feet forward of amidships. Two Raytheon digital chart recorders were used to record echographs from the DFT-210. The receiver output was recorded simultaneously with an IRIG-B time code and synchronizing pulses on standard VHS video cassette tapes using two JVC video tape recorders and a Sony audio signal processor, and separately onto two Sharp digital audio tape (DAT) recorders. The time code was generated by a Systron Donner time code generator and frequency multiplexed with a 1-msec 15-kHz key pulse. The system configuration is diagrammed in Figure 6.1, and the towbody configuration is shown in Figure 6.2.

Upon arrival at the placement site each operating day, the ACP towbody was deployed and remained in the water as described for the entire working day. Each morning, the time code generator was synchronized to universal time by radio monitoring of station WWV at 5, 10, 15, or

20 MHz. New tapes were loaded into all of the tape recorders approximately 30 min prior to each survey. Data recording began when the tug was within 5 min of arriving at the placement site. The transceiver transmitted pulses of 0.1-msec duration at both frequencies simultaneously every 0.250 sec throughout each survey. The equipment remained active until all transects were completed and water samples obtained. Receiver pre-amp gains were adjusted between transects to increase the overall dynamic range of the recorded data set. Table 6.1 shows the start time and elapsed times of the ACP tape records during the MFDCP.

The data recorded on the DATs were processed as follows. The time code channel was monitored by a time code reader to find areas of specific interest on the tapes. The 10-kHz double side band signal was played back into a band pass filter that removed 60-cycle noise and provided anti-aliasing protection for the following stage, which consisted of an analog demodulator. The demodulator output was further filtered and amplified for input to a 12-bit analog to digital (A/D) converter interfaced to an IBM-AT compatible computer. Synchronizing pulses multiplexed with the time code were used to initiate A/D sampling bursts. Each burst consisted of 128 samples taken at equal time/depth intervals within a pulse, and the range to the last sample was used to determine the necessary sample rate such that,

$$sample\ rate = 127\ \frac{c}{(2 \cdot range)} \tag{6.1}$$

where c is the speed of sound in seawater (1,500 m/sec), and the range was 13 m. Entering these values into Equation 6.1 yields a sampling rate of 7,327 samples per second used for digitizing all data included herein.

The digitized data consist of a series of records each containing 128 16-bit integer words. Each consecutive 2-byte integer represents a root-mean-square (rms) voltage V_{rms} at the output of the receiver accurate to 12 bits. The integer values range from 0 to 4,095 and are linearly proportional to V_{rms} such that:

$$V_{rms} = \frac{Integer}{4{,}095} \tag{6.2}$$

The time difference t between data points is equal to the reciprocal of the sampling frequency f_s, and the depth Z associated with each point is given by,

$$Z = \frac{ct}{2} \tag{6.3}$$

where

$$t = \frac{n}{f_s} \qquad (f_s = 7{,}327\text{sec}^{-1}) \tag{6.4}$$

and n is the index of the 2-byte integer.

The voltage V_{rms} at the input of the A/D converter is proportional to the rms plane wave sound pressure P_{rms} present at a reference location 1 m from the face of the transducer. This relationship is,

$$20Log_{10}\,(V_{rms}) = RR + RL + G \tag{6.5}$$

where RR is the receiving response of the transducer given in decibels referenced to 1 volt per micropascal (dB reference to 1V/1μPa), RL is the reverberation level given by,

$$RL = 20Log_{10}\,(P_{rms}) \tag{6.6}$$

and is expressed in dB reference to 1μPa, and the value G is the overall system gain expressed in decibels such that:

$$G = 20Log_{10}\left(\frac{V_{input}}{V_{output}}\right); \quad V_{output} \neq 0 \tag{6.7}$$

For a cloud of particulate scatterers such as a sediment plume, the reverberation level is given by,

$$RL = SL - 20Log_{10}(r) - 2\alpha r + S_v + 10Log_{10}\left(\frac{c\tau\psi}{2}\right) \quad (6.8)$$

where SL is the source level (dB reference to 1μPa/V), r is range in meters, α is the absorption coefficient in decibels per meter, S_v is the volume scattering strength in decibels, τ is the transmitted pulse duration in seconds, and ψ is the equivalent solid angle of a uniform beam containing the same integrated power as the actual transmitted beam and is given in steradians. For further information on decibel units, refer to Urick (1975). Also, for more information on scattering strength, refer to Clay and Medwin (1977).

Combining Equations 6.5 and 6.8 gives the relation used to calculate volume scattering strength:

$$S_v = 20Log_{10}(V_{rms}) - RR - G - SL + 20Log_{10}(r) + 2\alpha r - 10Log_{10}\left(\frac{C\tau\psi}{2}\right) \quad (6.9)$$

For conical beam transducers such as those used in the ACP,

$$10Log_{10}\left(\frac{c\tau\psi}{2}\right) = 10Log_{10}\left(\frac{c\tau\theta}{2}\right) - 31.6 \quad (6.9a)$$

where θ is the angle between the reference axis of the transducer, and the first point on the beam diagram at a level of -3 dB referenced to the axis level (Urick 1975). A more complete derivation of the theoretical background for these procedures is presented in Appendix 6A.

4. Analysis and Results

The first 3 min of each of the eight placement surveys selected for detailed analysis were processed to provide contour plots of volume reflection coefficient as a function of depth and distance. In addition to each contour plot, a series of graphs was plotted at 1-m intervals to give reflection coefficients as a function of horizontal distance across the plume. These plots corresponding to the eight selected surveys are available from the authors of this chapter and from the DRP Technical Area 1 Manager, Dr. Nicholas C. Kraus, WES. An additional five 3-min transects were plotted for Survey 239B in order to provide a total of five transects across the plume. A short narrative of each survey follows.

Survey 237A

This plume was monitored using a longitudinal track (along the major axis of the plume). The placement occurred at the deep in approximately 14 m of water. At depths between zero and 6 m, background scattering was slight and patchy, and it was one to two orders of magnitude less than at depths greater that 6 m. The plume was first detected by both systems at about 14:18:30 GMT. The plume dominated the upper water column over the first 40 m traversed into the plume, and the plume material filled the entire water column beyond that distance. The 20-kHz system appears to have been overcome by attenuation inside the plume during the initial stages, and the 200-kHz system was also affected, but not as severely. During the first 2 min inside the plume, the 200-kHz system showed little variation in scattering throughout the water column, and, as scattering diminished, the plume became more patchy.

Survey 238A

This is the first of the transverse monitoring operations chosen for analysis. The placement occurred in about 14 m of water at the deep site. Background scattering was slight and patchy above 10 m and clear below. Both the 20- and 200-kHz systems detected a large bottom surge while approaching the plume; the leading edge appeared to be 2 to 3 m high, and the horizontal extent was at least 20 m at 14:24:10 GMT (more about this feature is discussed under Survey 239B). Attenuation was again extremely severe at 20-kHz and significant at 200-kHz.

Survey 238B

This was another transverse operation at the deep site at approximately 14-m depth. Background scattering was slight and patchy above 5 m. A bottom surge is clearly seen upon entry and exit of the plume on both the 20- and 200-kHz records. The plume boundaries are visible, although 20-kHz attenuation is severe inside the plume and 200-kHz attenuation is notable.

Survey 239A

This survey was a transverse-monitored placement at the deep site in approximately 13 m of water. The background scattering was moderate above 6 m. Bottom surge and plume boundaries were recorded on both systems. Attenuation is again severe at 20-kHz and significant at 200-kHz in the midsection of the plume.

Survey 239B

This operation used transverse monitoring, and seven transects were performed at the deep site in about 14 m of water. The background scattering was slight and patchy above 5 m. Survey 239B contains several features of dredged material discharges that were not observed

before the MFDCP. This data set has been selected for a more extensive discussion because of these features.

Examination of Survey 239B reveals novel features that have been clearly identified for the first time during the MFDCP. This survey also illustrates the increase in data interpretation capability when more than one acoustical frequency is used to obtain data simultaneously on dredged material discharges. Figures 6.3 through 6.7 are color contour plots of the 200-kHz reflection coefficient for consecutive ship passes over the discharge plume. The data in these figures indicate the existence of the following features:

1. A bottom surge is created with a tall leading edge, and the surge is detected both upon entering and exiting the plume.
2. The effect of the bottom manifests itself upon the movement of the plume and becomes evident at about the 8-m depth horizon. This depth horizon is located approximately 5 m above the bottom, and the nominal bottom depth is 13 m. The effect of the bottom upon the dynamical plume behavior is manifested as a large change in the slope of the outer plume boundary.
3. A gross apparent inhomogeneity is observed in the plume structure in the initial two passes; the authors hypothesize that this inhomogeneity is the result of a region of bubbles intertwined with the discharged dredged particulate material.
4. Over time, the plume seems to separate into two distinct lobes settling at different rates.
5. A strong current shear effect acts to horizontally separate the upper and lower water column portions of the plume over the duration of the survey.

To evaluate the validity of the bubble hypothesis advanced in 3 above, a comparison of the 200-and 20-kHz data was made for consecutive ship passes over the discharge plume. Figure 6.8 shows the reflection coefficients at 6-m depth for the 20-kHz (top) and 200-kHz (bottom) signals for transect number 1 (22:13 to 22:16 GMT). The gap seen on the 20-kHz record, extending from approximately 105 to 118 m, appears as a sharp dip in the 200-kHz record at about 115 m. Figure 6.9 shows reflection coefficients for both frequencies at 6 m for the second pass through the plume (22:17:30 - 22:20:30 GMT); the gap seen in the 20-kHz record extending from about 150 to 160 m is not evident on the 200-kHz record. Figure 6.10 shows similar data for the third pass through the plume (22:25 - 22:28 GMT). No gaps appear evident in either record at this time. This type of frequency-dependent absorption that is transient in nature lends support to the hypothesis of a dispersing cloud of bubbles present in the water column. It is important to note that immediately following many of the releases, the surface of the water was visually observed to effervesce as if air had been entrained in the discharged material and was released

upon immersion. The contour plot shown in Figure 6.11 shows the 20-kHz reflection coefficients for the second transect. The feature over the horizontal distance extending from 150 to 160 m is the same feature seen as a gap in Figure 6.9. Notice that, over the horizontal extent of that feature, from a depth of 4 to 6 m, the signal level steadily drops at a rate in excess of the surrounding plume. This drop in signal level is indicative of a region of localized excess absorption that extends to a depth of at least 6 m, implying that the hypothesized bubble cloud extends to at least that depth.

Subsequent passes through Survey 239B reveal both the horizontal dispersion of the plume material and current shear effects upon the dispersing plume. A portion of the water column may act as a "ceiling" for plume material below it (~8 m), while another portion (~5 m) acts as a "floor" for dispersing plume material above it.

Other important features such as internal waves and midwater surge fronts are also evident in these data, but detailed discussion of such is beyond the scope of this report.

Survey 241A

This survey consisted of a release in the shallow-water site in approximately 10 m of water followed by transverse monitoring. The plume boundaries are clear on both the 20- and 200-kHz records. Bottom surge is not as evident upon entering the plume, but is more clearly seen upon exiting. Absorption is high in the middle of the plume, with the 20-kHz signal again being more greatly affected.

Survey 242A

This survey occurred at the shallow site in about 10 m of water. Background scattering was very low. In this survey the ship entered the discharge plume and remained there for a period in excess of 10 min. The 200-kHz signal color contour plot of reflection coefficients for the first 3 min of the time period 16:06 to 16:09 is shown in Figure 6.12. Line contour plots and depth interval plots corresponding to the color contour plot are found in Appendix 6B. An expansion of the plume width with depth is clearly evident as the *R/V Pelican* entered the discharge plume. An apparently buoyant area of return is seen to overlie the initial plume expansion slope; this area could be bubbles. An incipient bottom surge is also visible. Note that for a vertical increment Δz of 2 m, a horizontal increment Δx of about 10 m is observed, yielding an estimate for the entrainment coefficient ϵ of $\Delta z/\Delta x = 0.2$. Figure 6.13 shows the reflection coefficients for the 7- and 8-m depth horizons for the 200-kHz acoustical system. It is possible to obtain an estimate of ϵ from these figures by dividing the depth difference of 1 m by the horizontal displacement of the

10^{-9} iso-reflection line of 5 m. Figure 6.14 is a line contour plot of the 20-kHz signal data corresponding to the same time period as in Figure 6.12. It may readily be seen that the suspected bubble feature discussed above coincides with a region of heavy absorption of the 20-kHz sound. This absorption of the 20-kHz sound further supports the bubble hypothesis.

Survey 242A provides sufficient acoustical, concentration, and transmissivity data to make rough estimates of confidence limits for measurements of the three data types. Using concentration estimates C_i provided from the samples gathered during Survey 242A (Chapter 4, this report), one obtains a mean concentration C_{avg} of 47.4 mg/ℓ, a standard deviation in concentration σ_c of 25.2 mg/ℓ, and a coefficient of variation $\sigma_c/C_{avg} = 0.53$. For the acoustical data set, using first-approximation acoustical processing, the average scattering coefficient (Appendix 6A) $R_{avg} = 7 \cdot 10^{-7}$, the standard deviation in the reflection is $\sigma_a = 6 \cdot 10^{-7}$, and $\sigma_a/R_{avg} = 0.9$. For the optical transmissivity data set, $\%T_{avg} = 42.5$, $\sigma_t = 15.4$, and $\sigma_t/\%T_{avg} = 0.36$. All three data sets are, therefore, properly dispersed in a statistical sense.

Survey 243A

This operation consisted of transverse sampling at the shallow site in approximately 10 m of water. Background scatter was slight. This survey showed clear signs of a bottom surge upon entry and less so upon exit. There was clearly strong absorption at 20 kHz in the midsection of the plume, with significant absorption at 200 kHz as well.

Shallow-Water Berm Survey

The 200- and 20-kHz data were recorded from 17:57 to 19:57 GMT on Julian Day 237. The 200-kHz system detected a weak background with no significant change in structure over the course of the survey. The 20-kHz system detected weak background scattering with an apparent increase in scattering from fish schools in the shallower portions of the survey. From these data it is concluded that there were no notable sand suspension events along either the shallower or deeper regions during the period of the survey.

Summary

The eight plume surveys analyzed show striking similarity in the overall make-up of plume features. Nearly all of the surveys showed evidence of horizontally propagating bottom surges during the first 5 min after release of the material. At least one edge of each plume showed a measurable growth in the horizontal width of the plume with increasing depth. Significantly greater absorption occurred in the upper water column for the 20-kHz signal than for the 200-kHz signal in the main body of each plume during the early stages of the survey.

Signal Comparison

Comparisons of acoustic scattering strength with concentrations measured from water bottle samples were performed on five discharge events (Surveys 240A, 240B, 241B, 242A, and 242B). These surveys were used because the in situ samples were taken at constant depth throughout each survey, reducing the number of degrees of freedom in the data from each survey, and the data contained a wide range of concentration values with which to compare. Table 6.2 lists the 20- and 200-kHz scattering strengths with the respective times, depths, and measured concentrations for the above five surveys. Figures 6.14 and 6.15 show the 20- and 200-kHz volume scattering strength (S_v) plotted against concentration for the five surveys. The wide dynamic range of values makes visualization of the correlation between S_v and concentration difficult if the values are plotted on a linear scale. Figures 6.16 and 6.17 show the same data plotted in decibel and log form. Plotted in this fashion, it becomes evident that from the 200-kHz data, there is a direct relationship between mean scattering strength and mean concentration from each survey at that frequency. At the time the samples were taken, the 20-kHz echoes were contaminated by echoes from the sampling rosette which resulted in the apparent lack of sensitivity of the 20-kHz data at that time to changes in concentration.

5. Conclusions

The MFDCP provided a rich data set on dredged material discharges for evaluating acoustic instruments that measure discharge plumes and particulate transport. Data were obtained on many key plume parameters including those of basic importance in numerical plume modeling. One example of these type of data is field measurement of the turbulent entrainment parameter. Numerical models may now be compared with a complete field data set on dispersion; this complete data set includes plume concentration, relative plume concentration, plume particulate distribution parameters, ambient density profiles, ambient current profiles, and meteorological parameters. The objectives of the ACP component of this general study have been achieved. Numerous discharge plume profiles of high quality using 20- and 200-kHz signals were obtained. These data may now be intercompared with other acoustical and nonacoustical data. Initial calibration curves have been obtained, and the effects of bubbles on acoustic echoes have been observed.

6. Discussion and Recommendations

The MFDCP yielded a unique data set and can surely be regarded as the most careful, extensive, and complete dredged material discharge study to date. From the point of view of evaluation of the applicability of acoustical methodologies to the study of dredged material discharges, the MFDCP was a pioneering effort. NOAA has now performed five cooperative acoustical studies of dredged material discharges with the U.S. Army Engineer Waterways Experiment Station. These studies are as follows;

1. Lake Ontario Discharge Study (1976).
2. New York Bight Discharge Study (1977).
3. James River Discharge Study (1982).
4. MFDCP (1989-present).
5. Miami Harbor Discharge Study (1990).

The data from these studies form a powerful set for research and model evaluation purposes.

It is now clear that the detection of dredged material discharge plumes can be accomplished acoustically. The essential remaining task is calibration of acoustical systems. In a strict sense, calibration of an acoustical system means establishment of a relationship whereby the scattered acoustical intensity is directly interpretable in terms of the concentration of the particulate load giving rise to the scattering. Attempts have been made both in the laboratory "and in the field" to establish a calibration of sorts. In the laboratory, measurements may be made using relatively homogeneous and well-defined particulate samples, particles of fixed size distribution and of fixed physical character (e.g., size, rigidity, elasticity, and shape). In the field, the situation is highly inhomogeneous and variable. Indeed, it must be borne in mind that, in evaluating the utility of acoustical devices, all other measurement approaches for plume particulate concentrations suffer from similar or worse problems than does acoustics. In particular, bottle samples, transmissivity, radioactivity, and other methods have method-specific measurement problems compounded by the natural spatial variability of the plume.

The MFDCP has provided information on the field calibration of the 20- and 200-kHz ACP systems. Data from the MFDCP have clearly shown the presence of bubble clouds intertwined with dredged material discharge plumes. The 20-kHz system performance is much

more affected by the presence of the bubbles; thus, the field calibration data of the 20-kHz system is much more variable than the 200-kHz system.

The following is a set of recommendations for analysis and future work.

Plume Analysis

The discharge surveys should be analyzed for the provision of data on parameters used in and basic to the operation of existing Corps numerical models of discharge plumes. For example, preliminary analysis of MFDCP acoustical data has yielded an estimate of about 0.2 for the turbulent entrainment coefficient. This coefficient could be computed for most of the discharge surveys.

Numerical simulation models should be run for the MFDCP discharge surveys. Comparison of model predictions with this extensive data set would be most interesting and valuable for model validation.

The influence of the ocean bottom on the flow and dynamics of discharge plumes should be carefully analyzed. It is clear from the MFDCP data that the influence of the bottom on flow dynamics of the plume extends to meters above the bottom.

A careful analysis of the effect of water column density profile characteristics and ambient current characteristics upon the passive dispersion phase of the plume discharge should be made. The existence of vertical shear and dispersion floor and ceiling effects has been indicated in the MFDCP data.

Acoustical System Analysis

Future analysis of MFDCP data should continue investigating differences between the 20- and 200-kHz data. A calibration effort should be undertaken for multiple acoustical frequencies as it is likely that a final design acoustical system for real-time monitoring and research will use multiple frequencies.

Intercomparison of ACP and Acoustic Doppler Current Profiler (ADCP) data should be made. The ADCP operated at a frequency of 1.2 MHz, thus providing yet a third frequency to compare with 20- and 200-kHz data.

A refined detailed analysis of acoustical data and concentration samples should be made.

The preceding is but a portion of the analysis which may be made with the MFDCP data.

References

Clay, C. S., and Medwin, H. 1977. *Acoustical Oceanography: Principles and Applications*, John Wiley & Sons, New York.

Proni, J. R., Dammann, W. P., Craynock, J. F., and Fergen, R. 1989. "Oceanic Wastewater Outfall Characteristics Measured Acoustically," *Eighth International Ocean Disposal Symposium*, Dubrovnik, Yugoslavia.

Urick, R. J. 1975. *Principles of Underwater Sound for Engineers*, McGraw-Hill, New York.

Table 6.1

ACP Recording Times, GMT*

Survey Number	Start Time	Elapsed Time, min	Tape Number
236A	00:16	113	N236A001
236B	14:39	121	N236B001
237A	14:00	110	N237A001
237B	22:10	122	N237B001
238A	14:05	117	N238A001
238B	21:45	95	N238B001
239A	13:42	122	N239A001
239B	22:00	122	N239B001
240A	13:25	122	N240A001
240B	20:32	122	N240B001
241A	11:40	107	N241A001
241B	18:39	112	N241B001
242A	15:58	105	N242A001
242B	23:15	121	N242B001
243A	18:00	61	N243A001

* Greenwich Mean Time.

Table 6.2

Scattering Strengths and Water Bottle Concentrations

Survey Number	Time GMT	200-kHz S_v	20-kHz S_v	Depth m	Concentration mg/ℓ
240A	13:42:11	-71.3	-52.6	10.7	124.2
240A	13:42:26	-74.6	-49.9	10.7	62.9
240A	13:42:44	-78.8	-50.5	10.7	20.4
240A	13:44:16	-56.7	-39.5	4.3	6.3
240A	13:45:44	-67.9	-58.5	1.3	3.3
240B	20:39:44	-111.0	-51.3	9.8	3.6
240B	20:39:59	-101.0	-48.9	9.8	4.0
240B	20:40:17	-116.0	-51.1	9.8	2.8
240B	20:40:58	-112.0	-39.6	9.8	5.6
240B	20:41:36	-88.3	-37.5	9.8	5.7
240B	20:41:54	-85.2	-37.7	9.8	5.0
240B	20:42:53	-83.6	-34.4	8.8	1.8
240B	20:43:45	-78.7	-34.6	9.8	6.7
240B	20:44:05	-87.4	-35.4	9.8	7.6
240B	20:44:56	-90.8	-44.7	9.8	5.9
241B	18:52:34	-68.2	-44.6	5.5	2.1
241B	18:53:42	-68.9	-50.7	5.6	179.8
241B	18:58:21	-65.4	-49.0	5.6	90.1
241B	18:58:47	-65.8	-47.6	5.5	178.2
241B	18:59:04	-66.6	-48.4	5.6	112.4
241B	18:59:24	-68.0	-52.8	5.5	99.1
242A	16:08:37	-56.8	-53.9	7.2	29.5
242A	16:09:07	-57.9	-50.0	7.2	31.2
242A	16:09:39	-59.8	-46.1	7.2	39.5
242A	16:09:56	-61.9	-50.6	7.2	50.3

(Continued)

Table 6.2 (Concluded)

Survey Number	Time GMT	200-kHz S_v	20-kHz S_v	Depth m	Concentration mg/ℓ
242A	16:10:12	-65.3	-52.3	7.2	41.5
242A	16:10:29	-62.6	-51.9	7.2	45.7
242A	16:11:05	-64.2	-51.6	7.2	36.4
242A	16:11:44	-66.2	-48.4	7.2	117.0
242A	16:12:12	-69.5	-51.4	7.2	42.1
242A	16:12:29	-70.9	-54.9	7.2	40.9
242B	23:33:37	-57.9	-68.0	5.0	1306.0
242B	23:33:54	-56.4	-79.3	4.8	353.3
242B	23:34:11	-59.0	-66.3	5.0	2149.8
242B	23:34:29	-61.5	-50.9	4.9	3356.8
242B	23:35:03	-55.9	-41.6	3.8	1749.3
242B	23:35:22	-55.8	-61.3	3.9	878.5
242B	23:35:44	-52.3	-55.2	3.9	243.2
242B	23:36:00	-56.2	-43.2	3.9	621.8
242B	23:36:15	-55.5	-37.7	3.8	660.9
242B	23:36:33	-60.6	-37.4	3.8	447.5
242B	23:36:50	-63.4	-44.4	3.8	593.2
242B	23:37:08	-59.4	-41.8	3.8	680.7

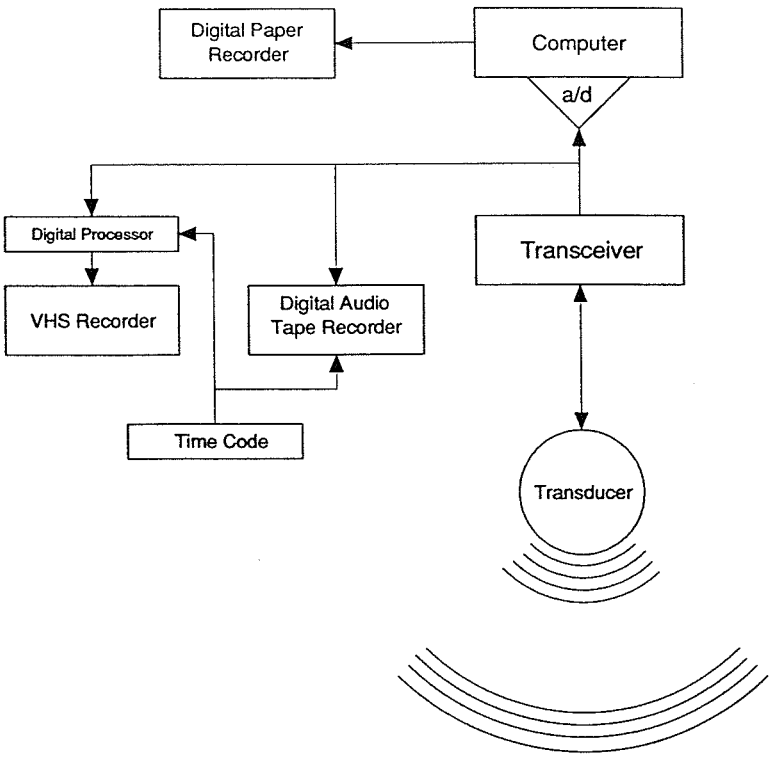

Figure 6.1. ACP system diagram.

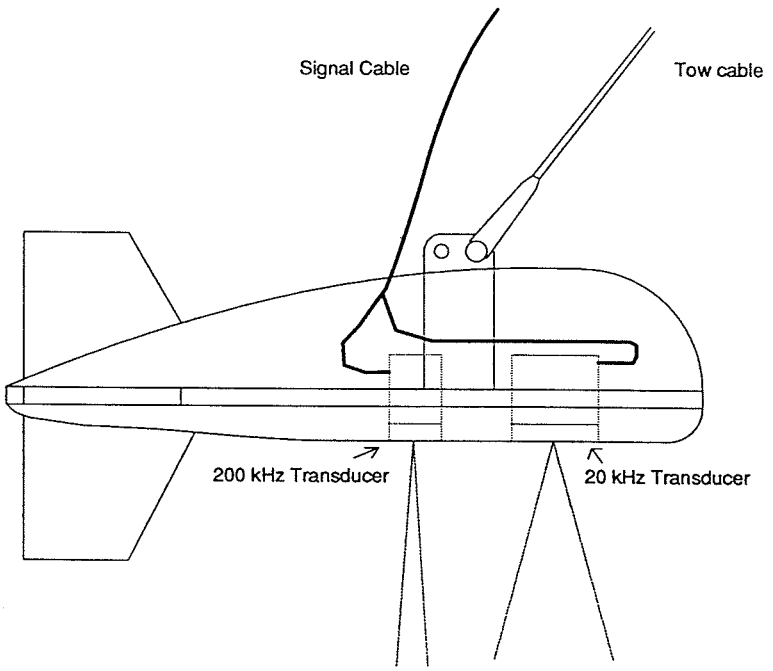

Figure 6.2. ACP towbody configuration.

KEY

Color codes for acoustic backscatter intensity (dB) in Figures 6.3 to 6.7 and Figure 6.12.

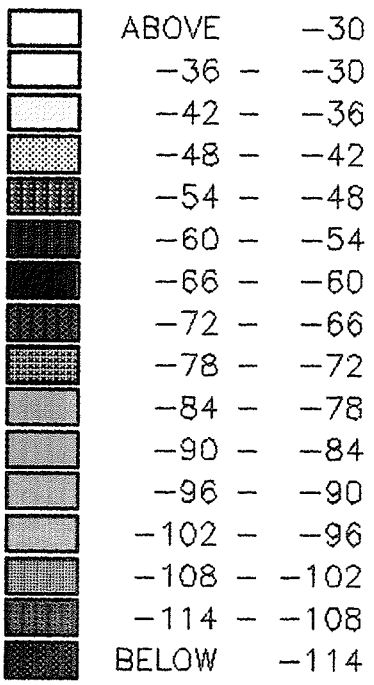

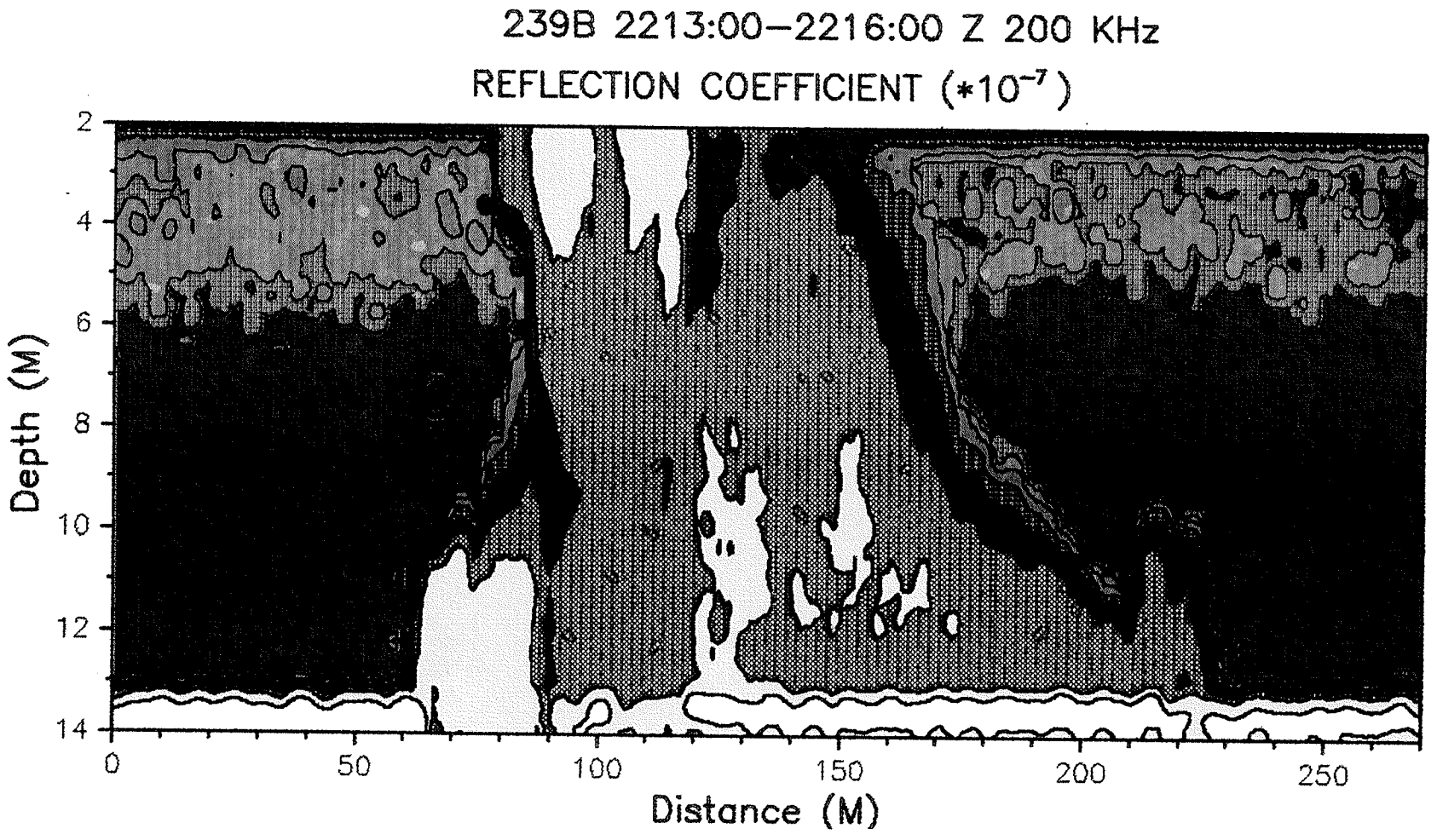

Figure 6.3. Survey 239B 200-kHz S_v Pass 1.

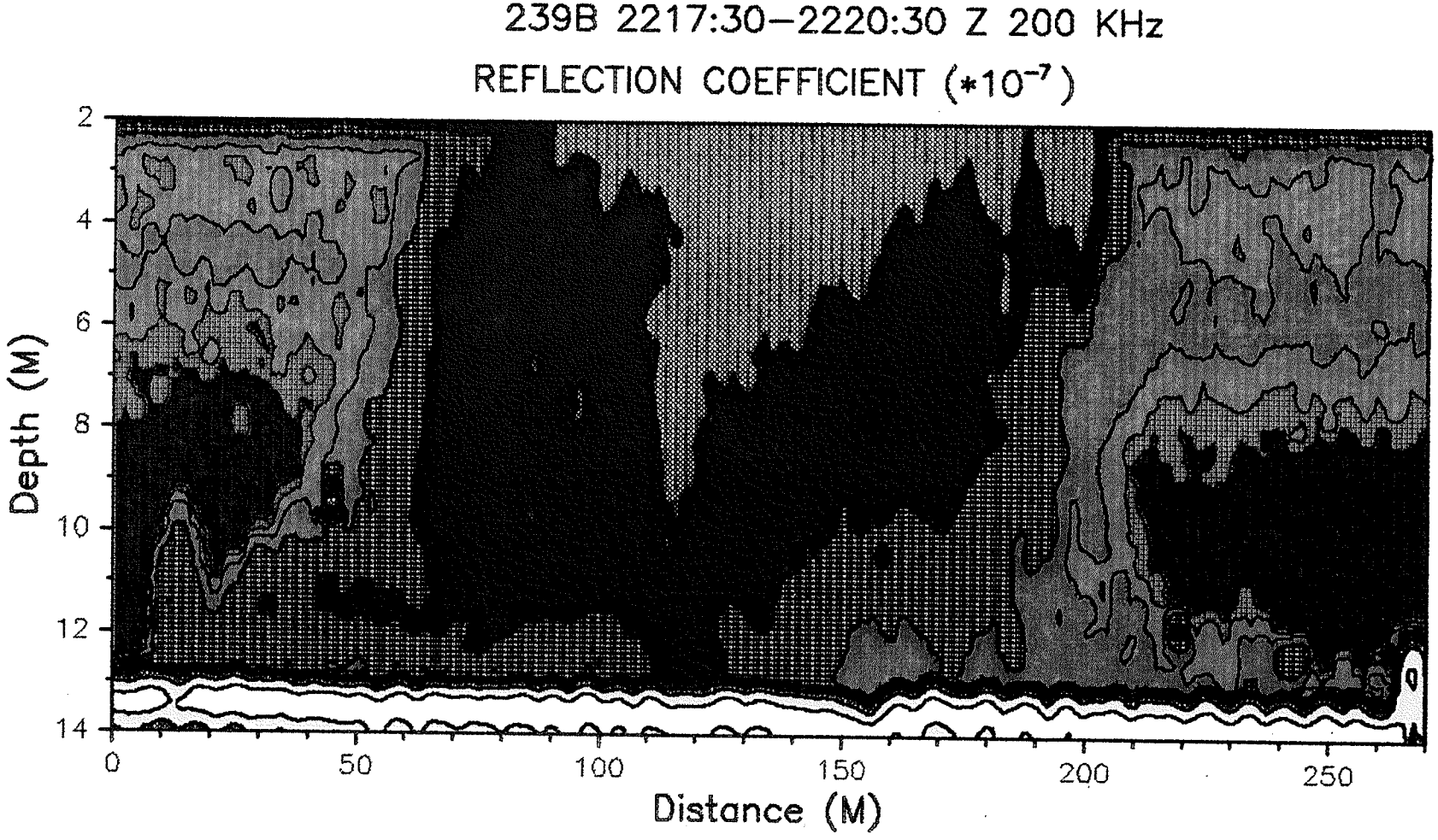

Figure 6.4. Survey 239B 200-kHz S_v Pass 2.

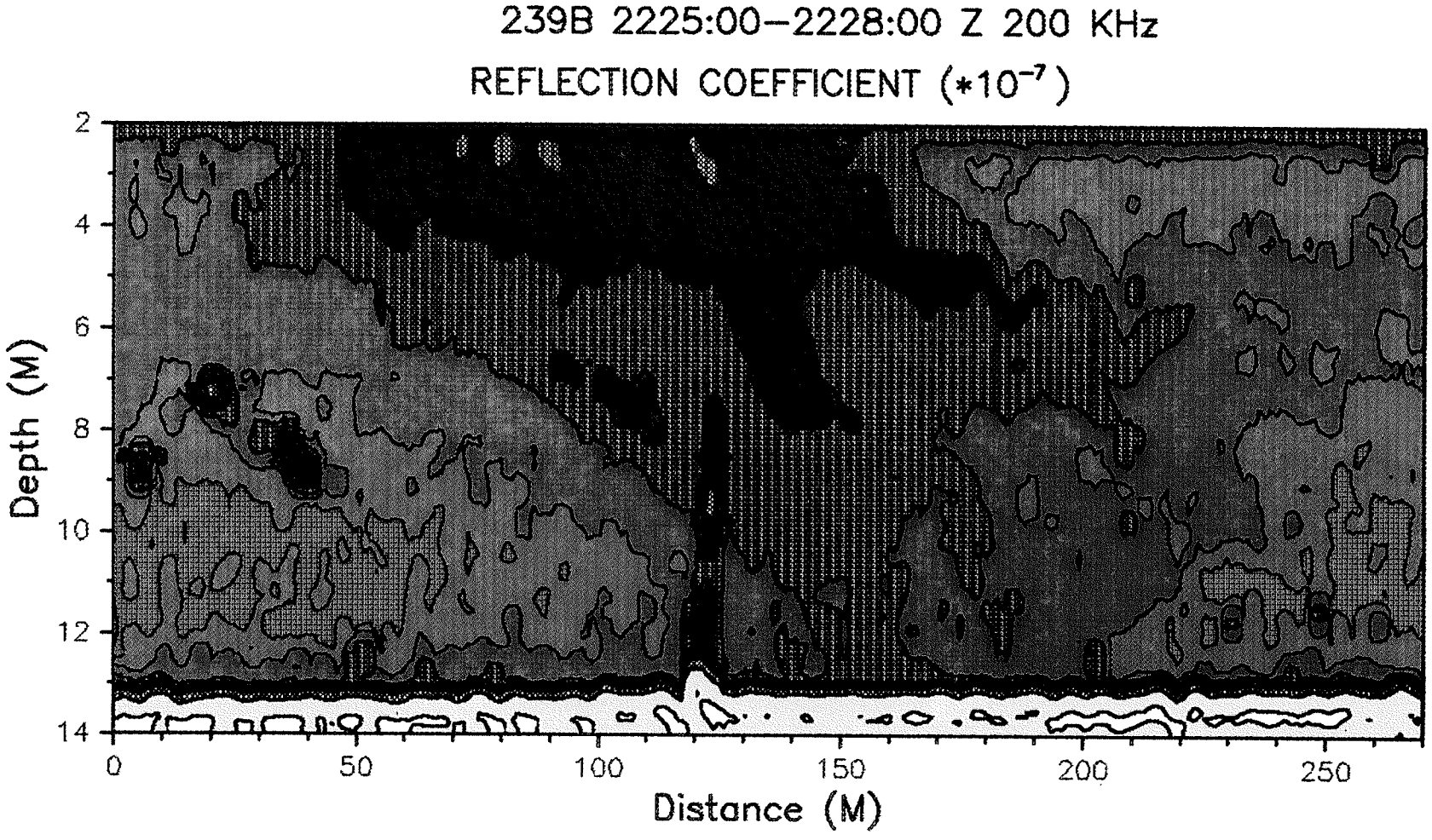

Figure 6.5. Survey 239B 200-kHz S_v Pass 3.

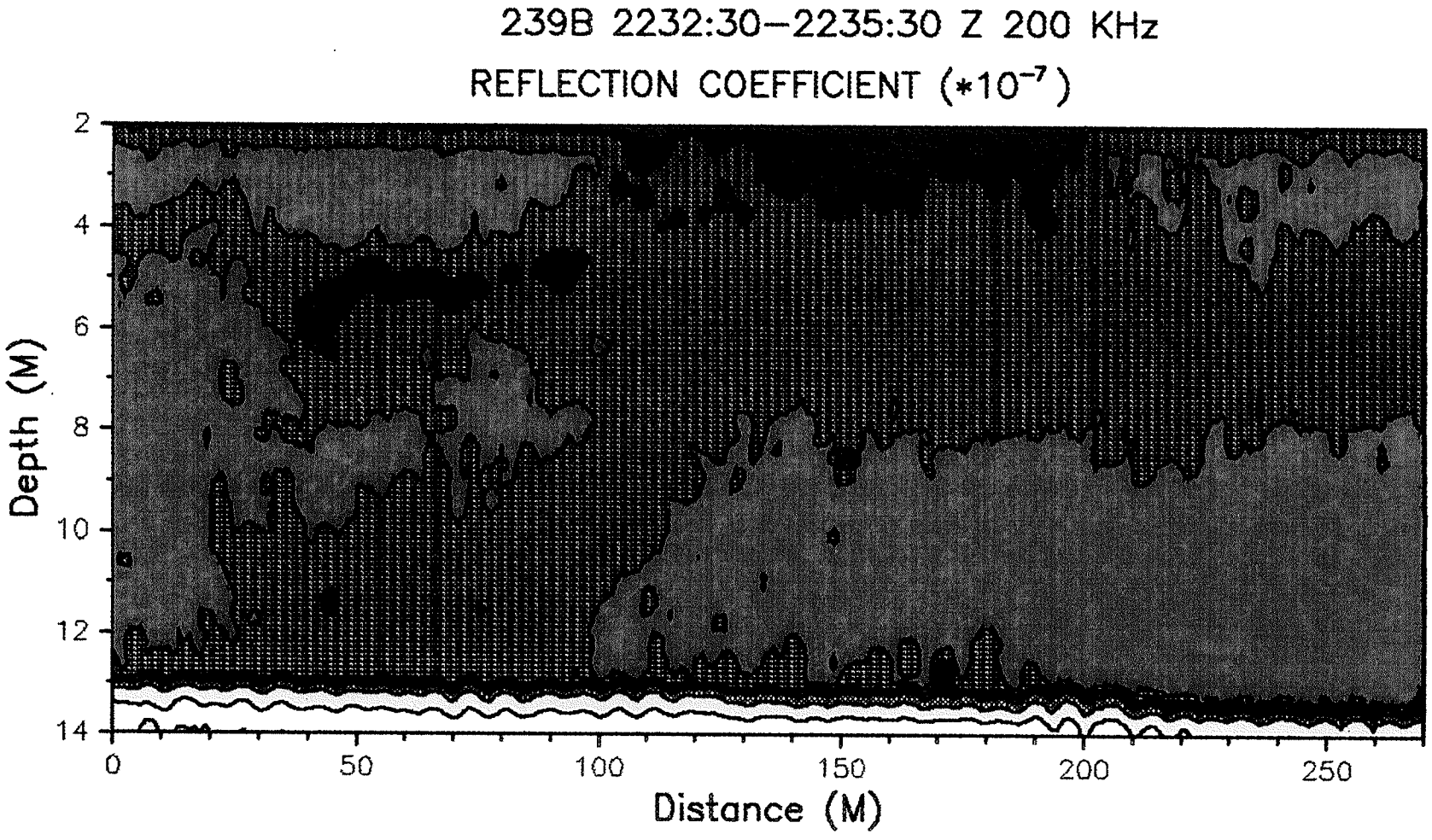

Figure 6.6. Survey 239B 200-kHz S_v Pass 4.

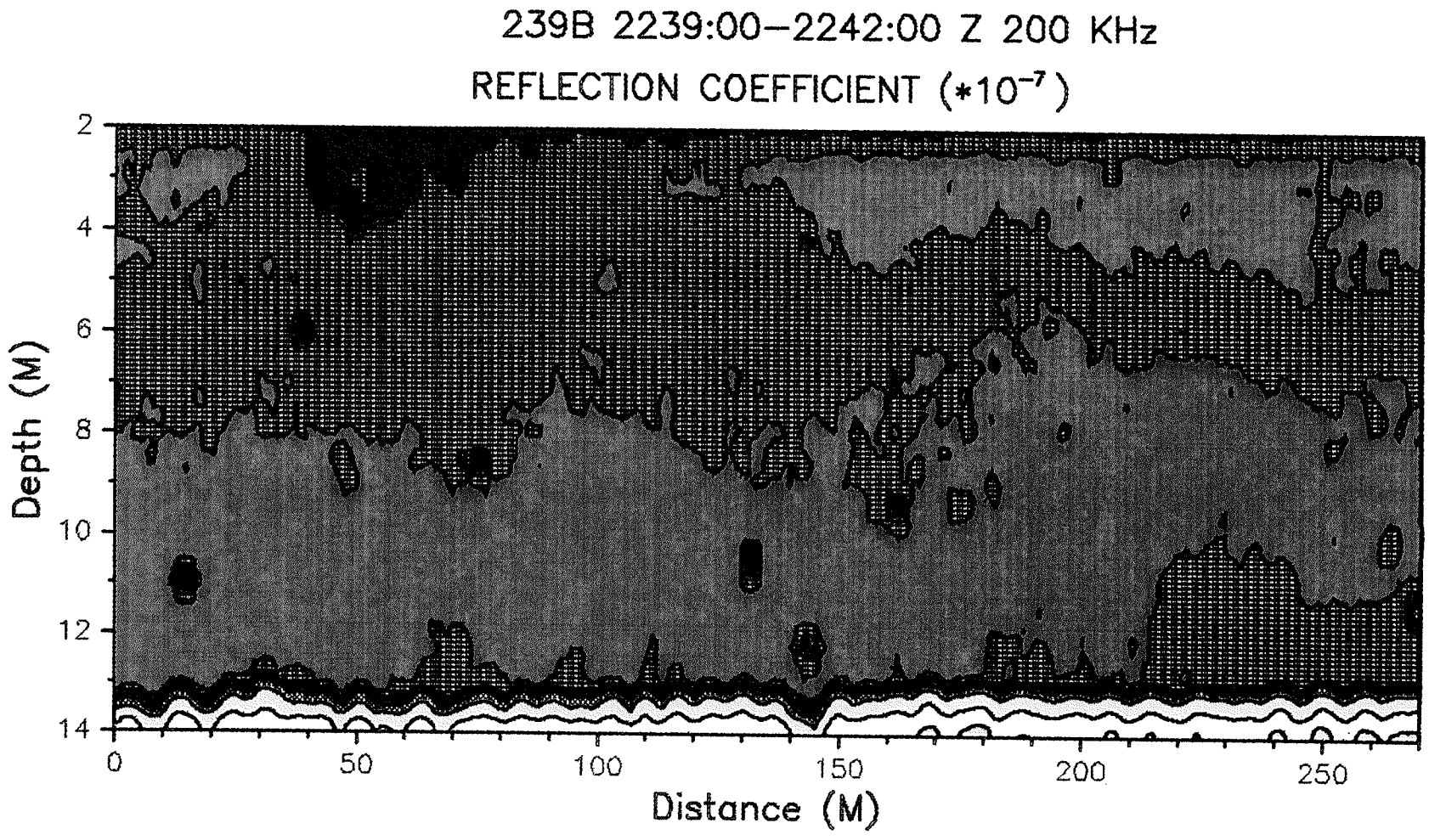

Figure 6.7. Survey 239B 200-kHz S_v Pass 5.

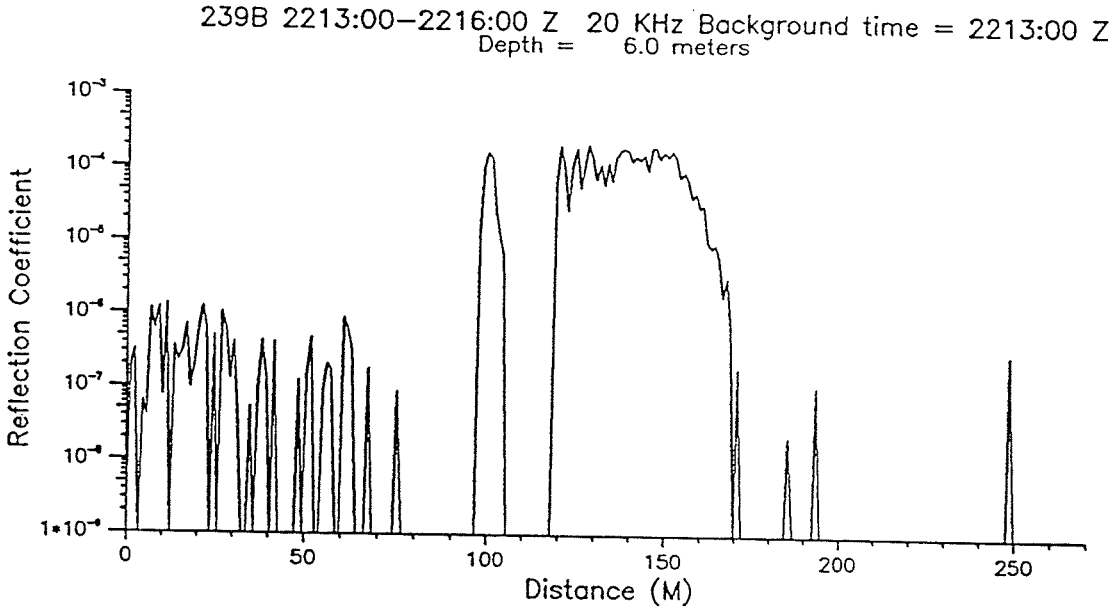

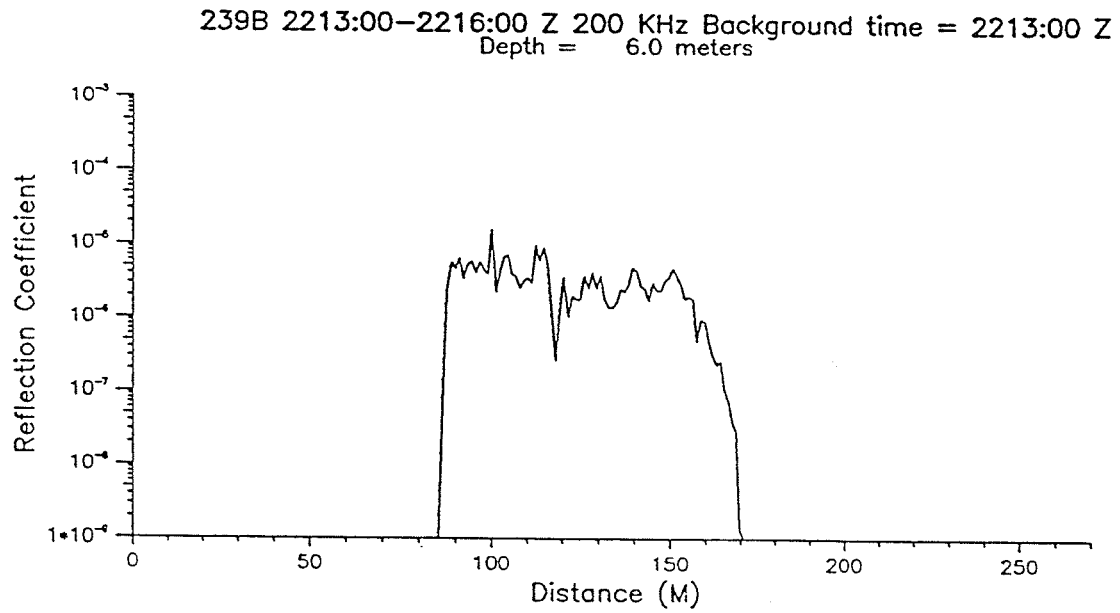

Figure 6.8. 239B 6 m S_{ν}, Pass 1.

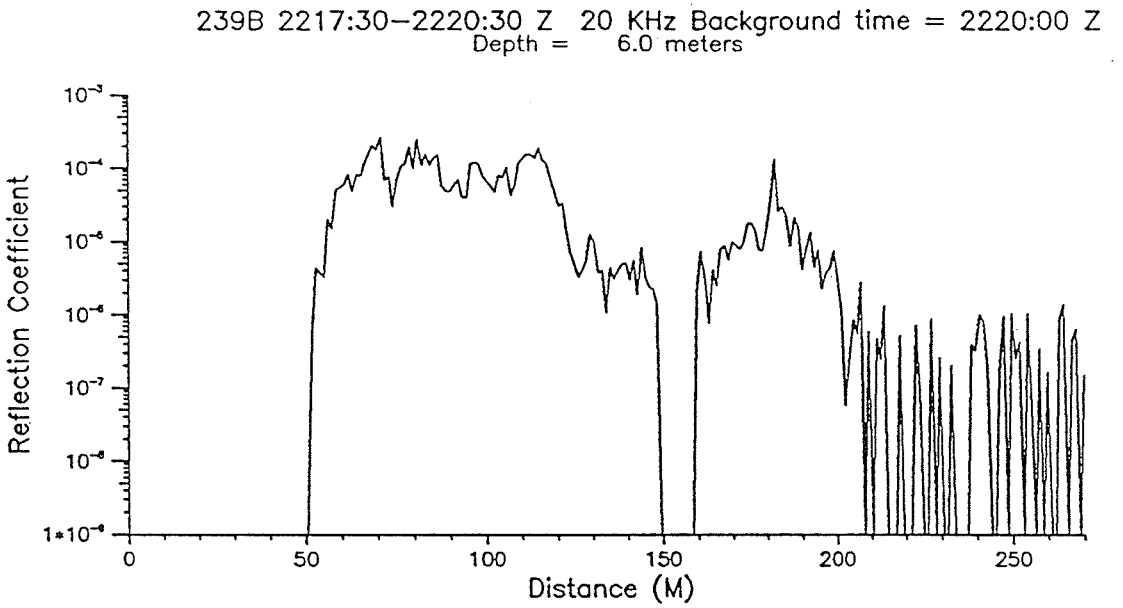

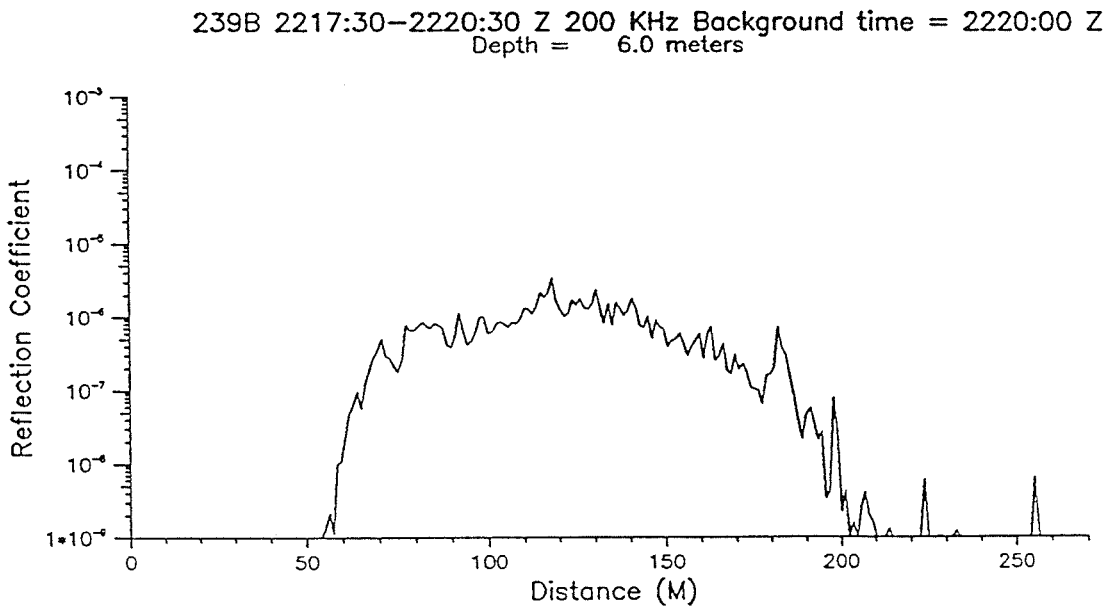

Figure 6.9. 239B 6 m $S_{\nu\nu}$, Pass 2.

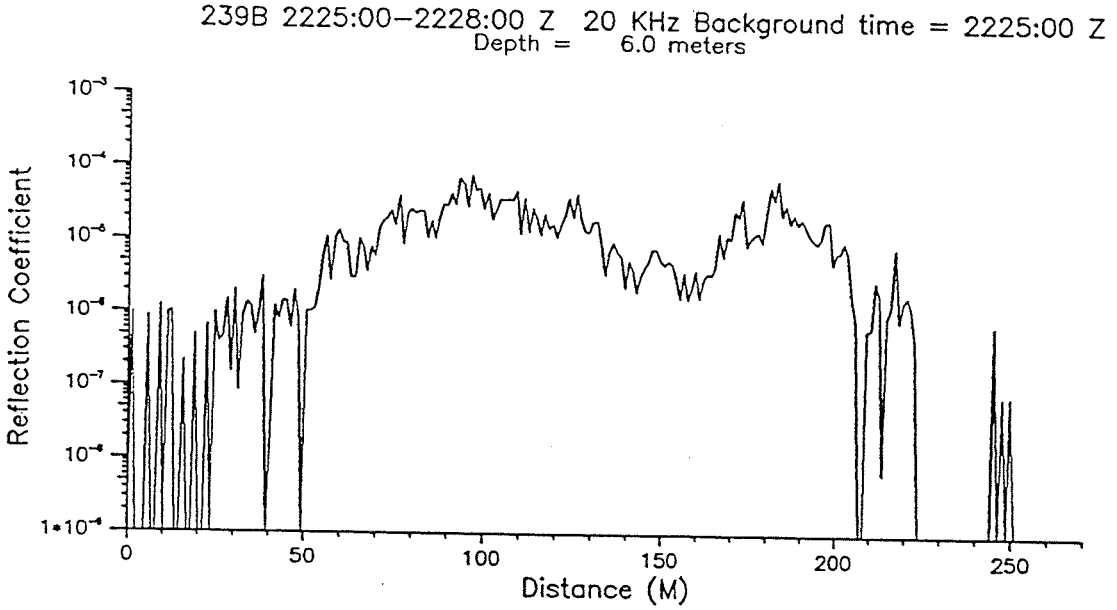

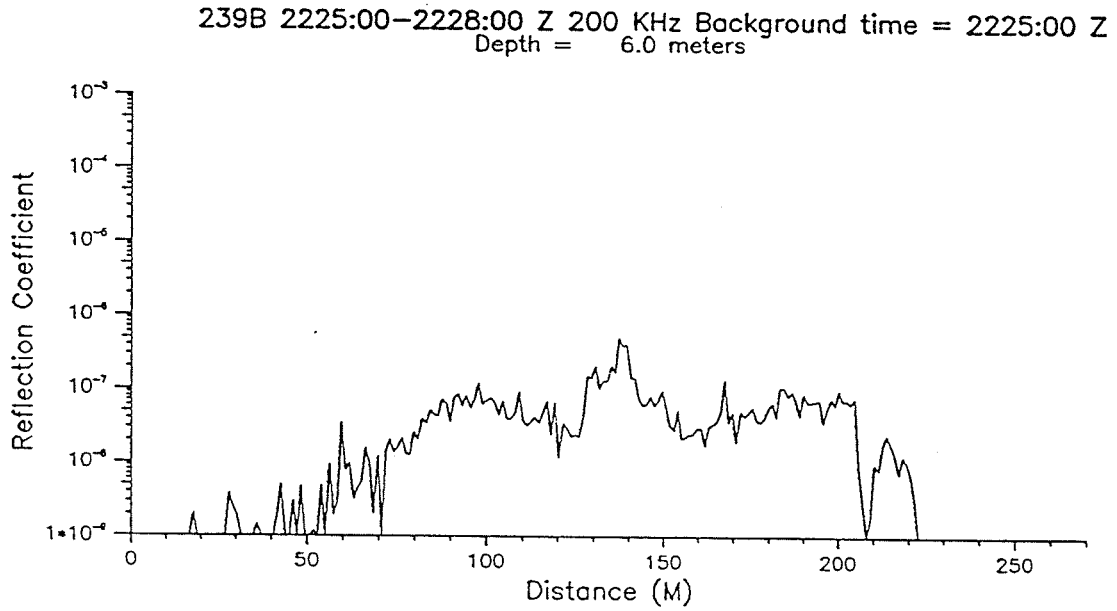

Figure 6.10. 239B 6 m $S_{\nu\nu}$ Pass 3.

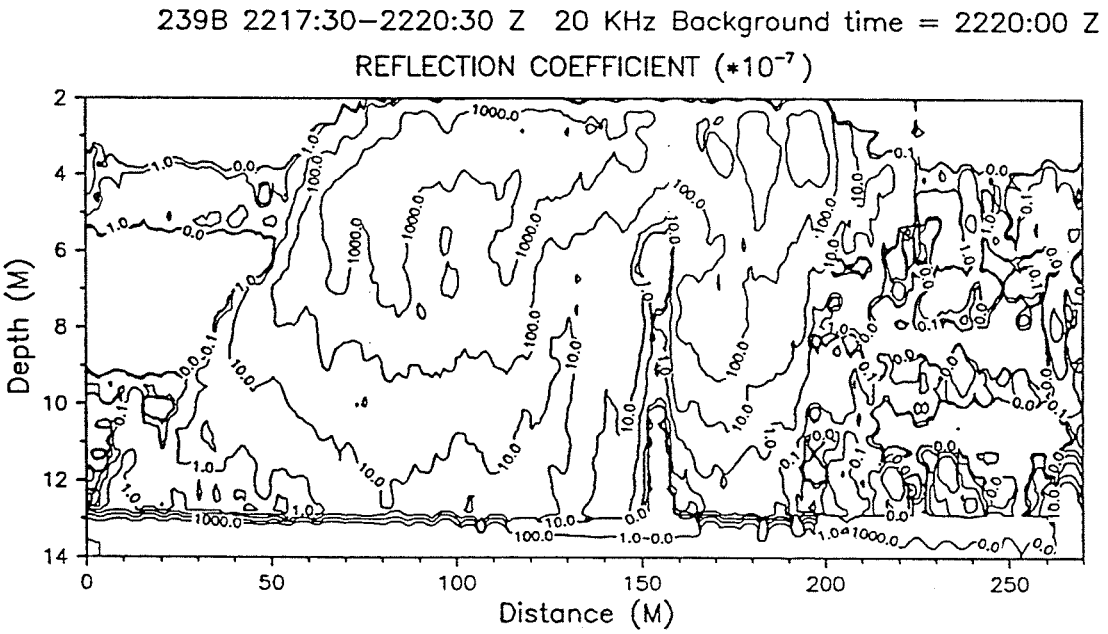

Figure 6.11. Survey 239B 20-kHz S_v Pass 2.

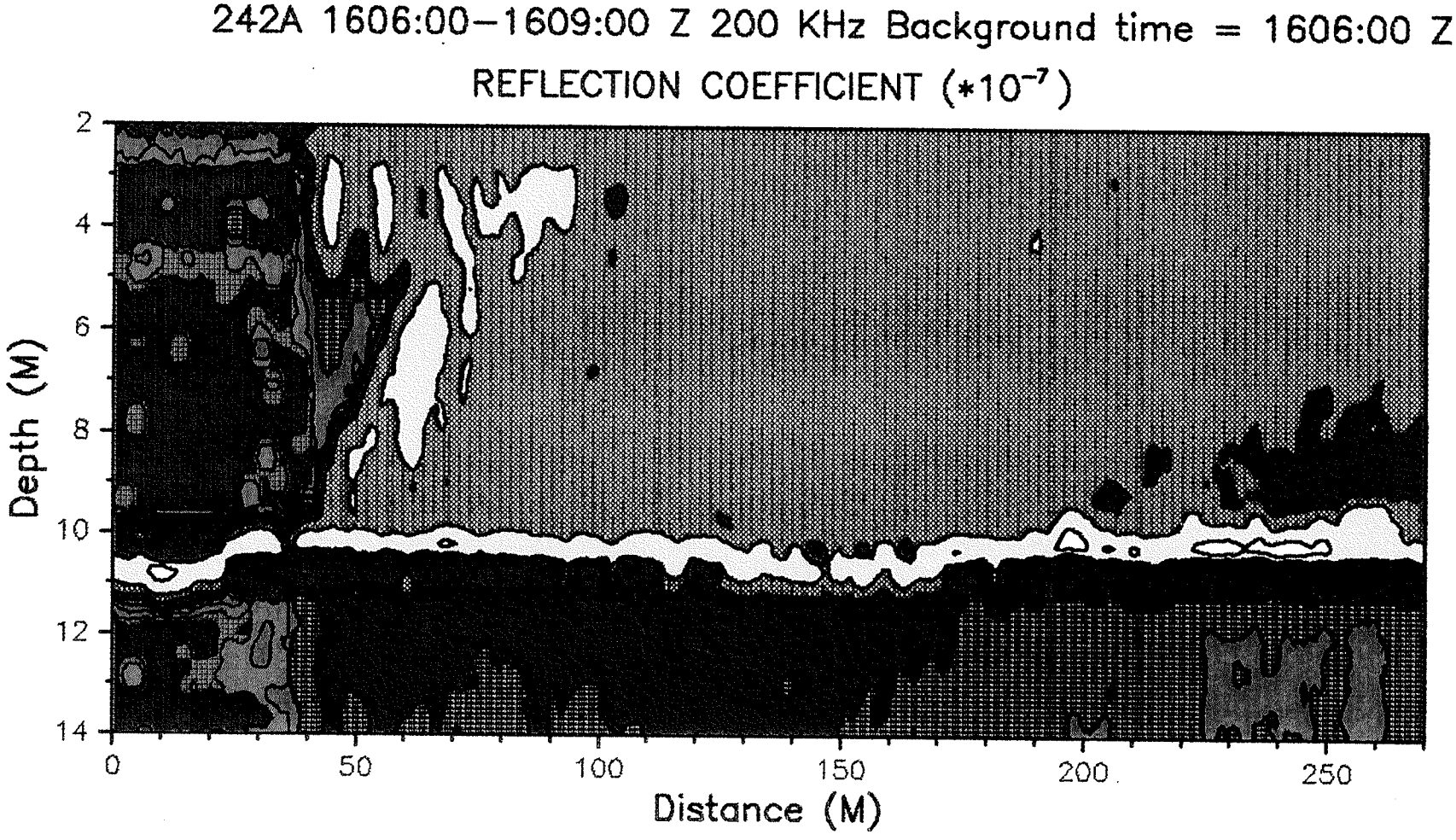

Figure 6.12. Survey 242A 200-kHz S_v Pass 1.

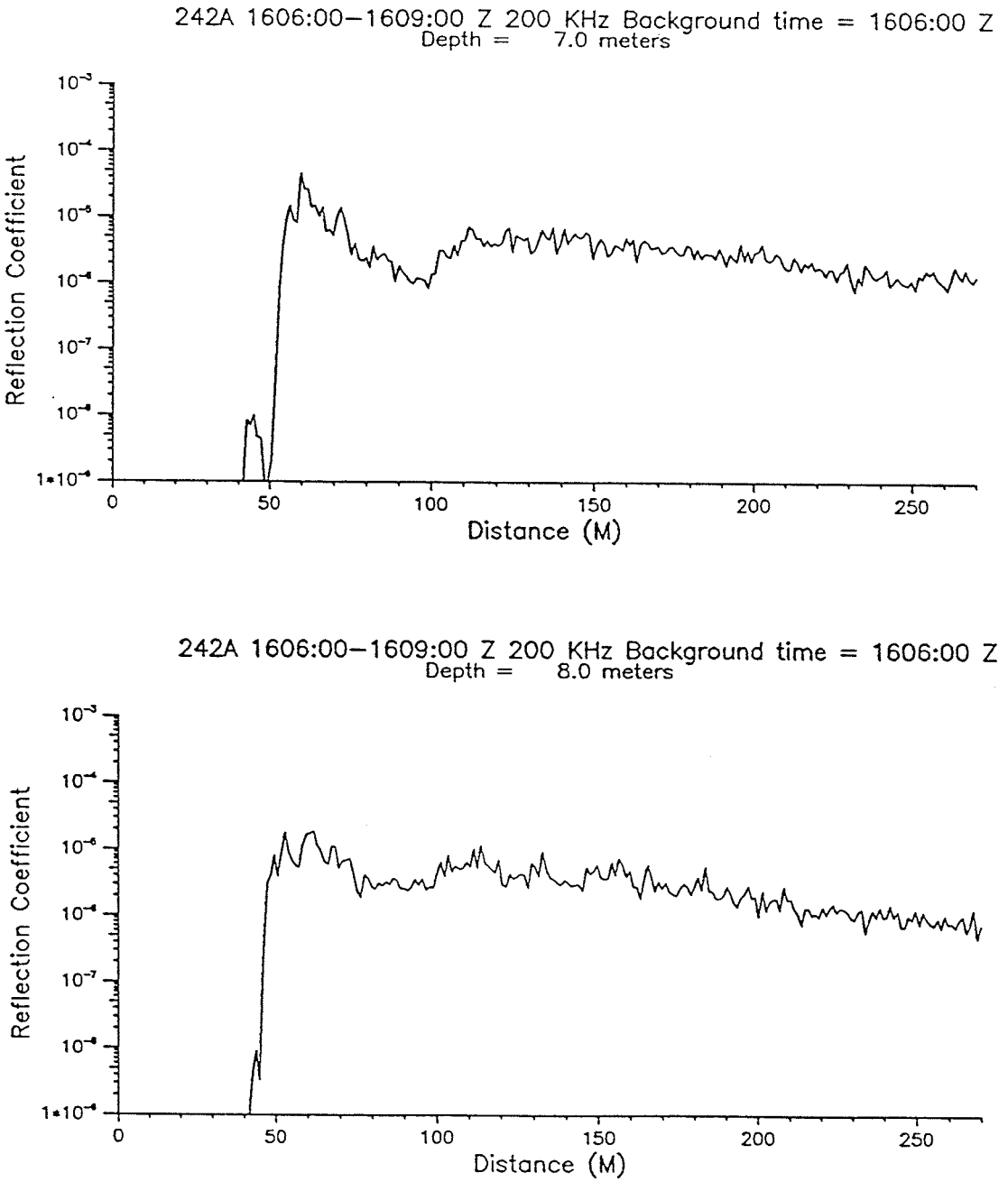

Figure 6.13. Survey 242A 200-kHz 7 and 8 m S_v.

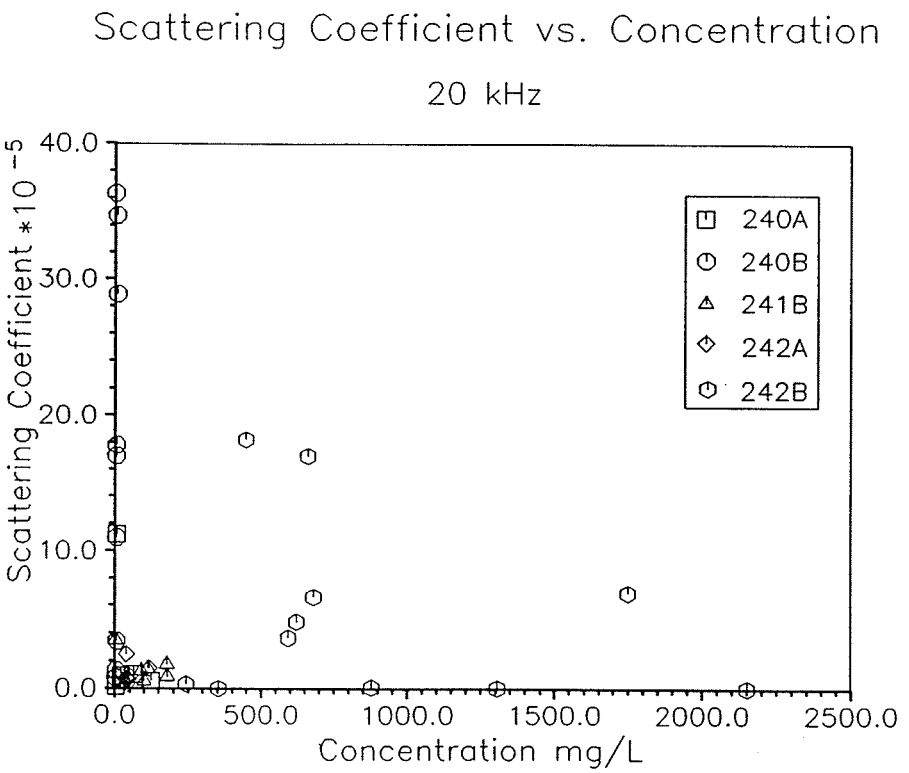

Figure 6.14. 20-kHz S_v versus concentration.

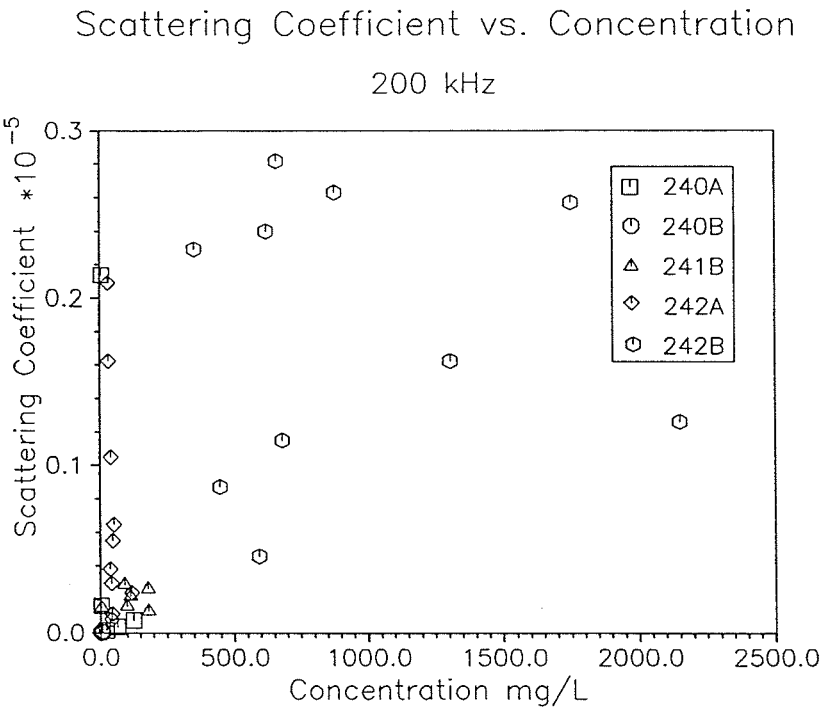

Figure 6.15. 200-kHz S_v versus concentration.

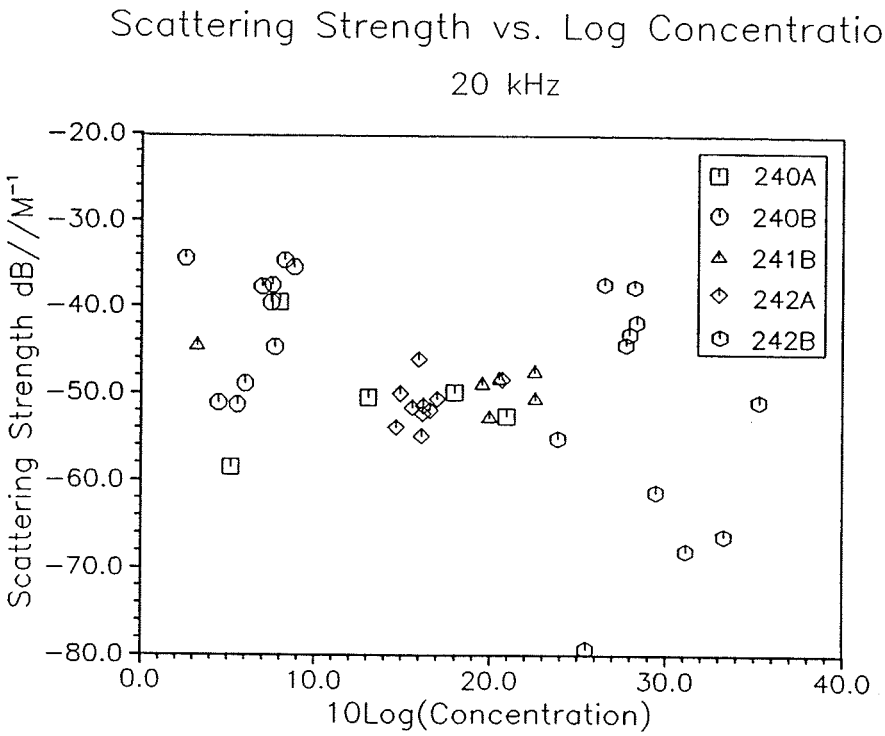

Figure 6.16. 20-kHz S_v versus log concentration.

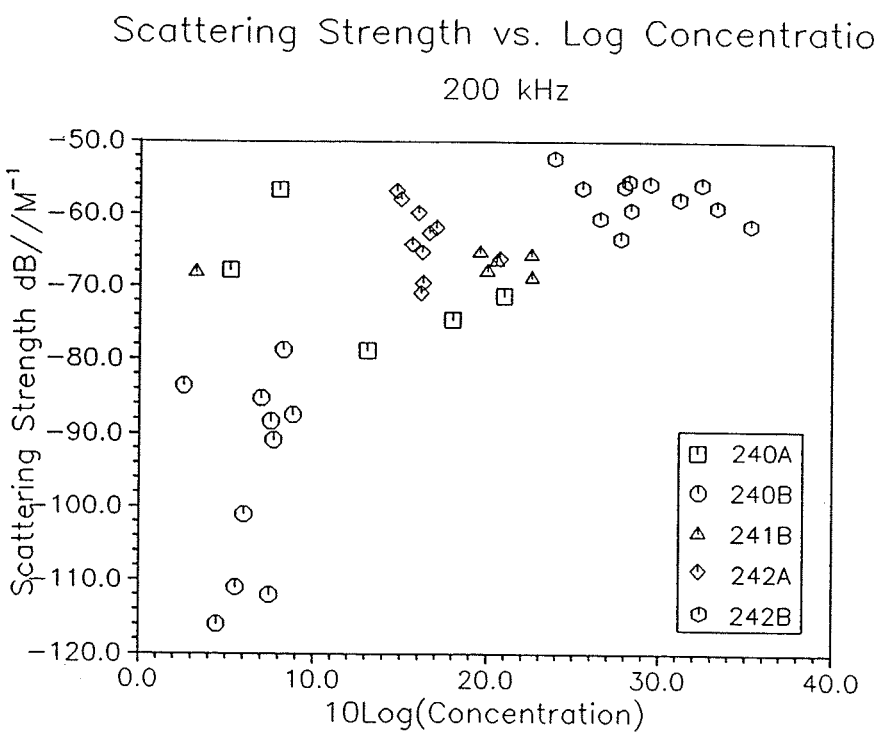

Figure 6.17. 200-kHz S_v versus log concentration.

Appendix 6A: Theoretical Background

Scattering Coefficient

The scattering coefficient R is the ratio of the scattered acoustic intensity I_s measured at a distance of 1 m from the center of the scattering volume in the direction of the transducer to the incident plane wave intensity I_i referenced to the same 1-m range,

$$R = \frac{I_s}{I_i} \tag{6A.1}$$

where the plane wave intensity is given by,

$$I = \frac{p^2}{\rho c} \tag{6A.2}$$

in which ρ is the mass density of seawater (1.024 kg/m^3).

The scattering strength S_v is the decibel equivalent of the scattering coefficient such that:

$$S_v = 10Log_{10}\,(R) \tag{6A.3}$$

In acoustically measuring particulate concentration, the approach taken is to relate particulate concentration to acoustic cross-section-per-unit volume s_v. Clay and Medwin (1977)* assert that,

$$s_v = \Sigma\, N_i \sigma_{bsi} \tag{6A.4}$$

where N_i is the number of particles per unit volume in the ith size class, and σ_{bsi} is the backscattering cross section (m^2) of those particles. The scattering coefficient is proportional to the cross-section-per-unit volume such that the scattering strength is given by:

$$S_v = 10Log_{10}\,(s_v r_1) \tag{6A.5}$$

where r_1 is the reference distance of 1 m.

For particles of similar shape and orientation in any given size class in a plume of scatterers, the backscattering cross-section-per-unit particle volume κ_i at orientation (θ, ϕ) is given by:

$$\kappa_i\,(\theta,\phi) = \frac{\sigma_{bsi}}{v_i} \tag{6A.6}$$

---

* See References at the end of main text.

where v_i is the volume of a particle of size class i. For a large number of particles oriented randomly, the mean backscattering cross-section-per-unit particle volume is given by,

$$\bar{\kappa}_i = N_i^{-1} \sum_{j=1}^{N_i} \kappa_i (\theta_j, \phi_j) \tag{6A.7}$$

Further, defining the probability density of orientations within the plume for particles of size class i as $p_i(\theta, \phi)$ gives,

$$\bar{\kappa}_i = \int_0^{\Pi} \int_0^{2\Pi} p_i \kappa_i \, d\theta \, d\phi \tag{6A.8}$$

and

$$S_v = \Sigma N_i \bar{\kappa}_i v_i = N \bar{\kappa} \bar{v} \tag{6A.9}$$

where $N = \sum N_i$.

The mass m_i of a particle of size class i is given by,

$$m_i = \bar{\rho}_i v_i \tag{6A.10}$$

where $\bar{\rho}_i$ is the mean density of a particle of size class i. The mass concentration C of particles in a fluid volume is given by,

$$C = \Sigma N_i m_i = \Sigma N_i \bar{\rho} v_i = N \bar{\rho} \bar{v} \tag{6A.11}$$

where C is in units of mass per unit volume. Dividing Equation 6A.11 by Equation 6A.9 yields,

$$C = \frac{S_v \bar{\rho}}{\bar{\kappa}} = A S_v = \frac{AR}{r_1} \tag{6A.12}$$

where A is an empirical coefficient of proportionality with units of mass per unit area.

Dilution Ratio

The dilution ratio δ between two scattering volumes with different concentrations C_1 and C_2 can be calculated from ratios of scattering coefficients R_1 and R_2 measured directly from the two volumes using the equation,

$$\delta_{21} = \frac{C_2}{C_1} = \frac{R_2}{R_1} \tag{6A.13}$$

Entrainment Coefficient

One key model parameter is the turbulent entrainment coefficient ϵ. An approximate argument may be constructed such that ϵ is directly measurable from real-time acoustical data. In particular, it may be shown that,

$$\epsilon = \frac{da(z)}{dz} \tag{6A.14}$$

where a is the radius of the descending discharge plume at depth z. The quantity ϵ may be read directly, even from simple acoustical real-time paper records. Thus it will be of interest in future data analysis to compute ϵ for the eight discharge surveys selected for in-depth review. Because an excellent database was gathered in the Mobile Field Data Collection Project in addition to the acoustical data, interesting interdata types of analyses may be performed in the future. For example, in Survey 242A the research vessel entered the discharge plume and remained there for more than 10 min. Conductivity, temperature, depth, transmissivity, and concentration were simultaneously measured by in situ water sampling.